Mechanical studies of the inner ear's tectorial membrane

Wei Dong

Department of Physiology

University of Bristol

December 2001

A dissertation submitted to the University of Bristol in accordance with the requirements of the degree of Doctor of Philosophy in the Faculty of Science

(49515 words)

Abstract

The tectorial membrane is a gelatinous structure overlying the sensory cells in cochlea. Both the strategic location and the internal structure of this membrane suggest that it plays a key role in delivering sound stimuli to the hair cells, but exactly how the membrane performs this role is not clear. To investigate the mechanics of the tectorial membrane, interferometric measurements of the tectorial membrane's responses to sound have been made in the apical turn of the guinea-pigs cochlea *in vivo* and *post mortem*. A three-dimensional (3-D) reconstruction technique was developed using an interferometer system combined with a two-axis goniometer, which detects vibrations in three orthogonal directions by using different viewing angles. Gold-coated polystyrene microbeads firmly attached to the tectorial membrane were found to move along nearly straight lines in three-dimensional space both *in vivo* and *post mortem*. The transverse motion of the observed points was nearly perpendicular to the reticular lamina and the radial motion is along the direction of the fibers of the tectorial membrane. The tectorial membrane responds to sound in a similar way to other structures in the cochlear partition. There is no obvious evidence to support the idea that the tectorial membrane resonates to form a second filter inside the cochlea.

Experimental measurements show that opening of the cochlea may cause several effects to the cochlear mechanics. Rupturing of the Reissner's membrane results in a loss of strong baseline position shifts and compressive nonlinearity in sound-evoked response of the cochlear partition. However, the basic tuning properties of the partition remain unchanged.

Dedication and acknowledgements

I would like to acknowledge Defeating Deafness for funding this project and University of Bristol for providing the ORS award. The work described in this dissertation was undertaken in the Physiology Department between Oct. 1998 and Oct. 2001. It is with great pleasure that I acknowledge the companionship of members of the department during these three years.

My foremost thanks go to Dr. Nigel P. Cooper to whom I am forever indebted for his dedicated supervision. With tireless enthusiasm he has inspired, guided and supported the development of this work. I am also grateful to Prof. Matthew. C. Holley for his generous guidance in cell culture and staining of tectorial membrane, and also for the immense personal support he offered as second supervisor.

I wish to convey my warmest appreciation to Dr. D. N. Sheppard, Dr. M. N. Rivolta, Dr. D. Davies, Mrs. D. Rivolta and Mr. M. Fitzgerald who provided valuable advice, technical support and will be remembered as very good friends. I would like to thank the whole Hearing Group who provided me with unforgettable social life to help overcome my loneliness away from my family.

And finally, I would like to thank the enduring support from all my family and friends, especially my husband and daughter.

To Shuyang , Yi, Mum and Dad .....

Author's Declaration

I declare that the work in this dissertation was carried out in accordance with the Regulations of the university of Bristol. The work is original except where indicated by special reference in the text and no part of the dissertation has been submitted for any other degree. Any views expressed in the dissertation are those of the author and in no way represent those of the University of Bristol. The dissertation has not been presented to any other University for examination either in the United Kingdom or overseas.

Signed: Wei Dong Date: 21.3.02

Table of Contents

Abbreviations

AOM	acoustic-optic modulator
3-D	three-dimensional
BF	best frequency
BM	basilar membrane
C	Claudius
CAP	compound action potential
CF	characteristic frequency
CM	cochlear microphonic
cPSTH	compound post-stimulus time histogram
D	Deiter's
dB	decibels
FAR	Faraday rotator
FFT	Fast Fourier Transfer
HC	Hensen's cell
HWP	half wave plate
Hz	Hertz
IHCs	inner hair cells
IP	inner pillar
L	lens
M	mirror
KM	Kimura's membrane
MET	mechanoelectrical transduction
MN	marginal net
Mo	modiolus
N/m^2	Newtons/metre^2
OHCs	outer hair cells
OP	outer pillar
Pa	Pascals
PBS	polarizing beam-splitter
PD	photodetector
PG	proteoglycan
PH	pinhole
RM	Reissner's membrane
RMS	square root of the mean of the squared pressure
SM	scala media
SP	summating potential
Sp.L	spiral ligament
SPL	sound pressure levels
ST	scala tympani
St.V	stria vascularies
SV	scala vestibuli
TM	tectorial membrane

List of Table

List of Figures

Chapter 1 General Introduction

1.1 Preface

The tectorial membrane is a gelatinous structure, which rests on top of the sensory hair cells in the inner ear (Steel 1983). Both the strategic location and the internal structure of this membrane suggest that it plays a key role in cochlear micromechanics.

The principal mechanical function of TM is believed to be the excitation of the hair cells by radial deflection of hair cell stereocilia as a result of shearing motion between the reticular lamina and the tectorial membrane. The outer hair cells (OHCs), central element in the organ of Corti, which sit in between the basilar membrane and the tectorial membrane, can inject mechanical energy into the organ of Corti by axial contraction and elongation of its cell body (Brownell et al. 1985; Zenner et al. 1985). Therefore, the hearing organ achieves its extreme sensitivity with an active and compressive nonlinear amplification process in three-dimensional space.

However, how the TM performs its function is still uncertain. Due to technically difficult access to the tectorial membrane directly from the scala vestibuli and also because of its transparency, and its extreme sensitivity to its ionic environment, experimental evidence on TM's mechanics is sparse and inconclusive.

The tectorial membrane can only be directly approached from the apex of the cochlea *in vivo*, although even this approach may cause many concerns. These include how normal the function of the cochlea is during the approach to the tectorial membrane, what effects might be caused by shaving a hole in the cochlear wall at the apex, and how the rupture of the Reissner's membrane affects the function of the cochlea.

The present thesis is intended to contribute to an understanding of the mechanisms of the cochlea *in vivo* by concentrating on the function of the tectorial membrane during sound delivery to the cochlea. It will provide basic experimental data for all of the above questions.

1.2 Outline of thesis

This thesis contains nine chapters arranged systematically to build up an understanding of the tectorial membrane's motion in 3-dimensional space in the apical turn of the cochlea *in vivo*.

Chapter 1 gives a brief overview of the peripheral auditory system, including the external, middle and inner ear's anatomy and physiology. It also compares the mechanics and physiology of the basal and apical cochlea.

Chapter 2 introduces the tectorial membrane in historical context both in structure and function.

Chapter 3 describes the methods used in this thesis, including the animal model, sound generation system, laser interferomety, goniometry, measurement of sound-evoked round window potentials, analysis of fast and slow waves and the 3-dimensional reconstruction.

Chapter 4 describes the assessment of cochlear condition across a wide range of frequency using round window potentials. Measurements made include the cochlear microphonic potentials, compound action potentials and the threshold of compound action potential.

Chapter 5 discusses the mechanical effects of sealing the opening of the cochlea. It provides responses from sealed and unsealed cochleae to pure tone pips and clicks. 'Fast' and 'slow' response components are shown to interact to produce a notch in the tuning curve, which is an artifact of the opening of the cochlea.

Chapter 6 discusses the effects of rupturing Reissner's membrane. It illustrates strong baseline position shifts and compressive nonlinearity when the Reissner's membrane is intact, but not when it is ruptured.

Chapter 7 describes the basic response pattern of the tectorial membrane.

Chapter 8 describes the tectorial membrane's motion in 3-dimensional space, based on the 3-dimensional reconstruction technique and mechanical recordings from tectorial membrane *in vivo* and *post mortem.*

Chapter 9 provides a summary and conclusion to the thesis, and aims to portray an overall understanding of the mechanism of the apical turn and the vibration of the tectorial membrane *in vivo.*

1.3 The use of an animal model to study the tectorial membrane

In order to investigate the function of the tectorial membrane in cochlear micromechanics, guinea pigs were used throughout the experiments instead of human beings. This is because this investigation may cause permanent hearing damage due to the direct approach to the organ of Corti. The guinea pig is one of the well-established animal models and is widely used in auditory research. Its cochlea has 4 turns, with its basilar membrane of 18.8 mm unrolled length (Echteleler 1994). Its peripheral auditory system is similar to humans. Guinea pigs have very good hearing, ranging from 54 Hz to 45 kHz (Heffner et al. 1971; Evans 1972). The apical turn of the guinea-pig cochlea is reasonably accessible due to its relatively thin wall, although this involves invasive surgery. Therefore, it is possible to make direct measurements from its apical turn and moreover, results could be compared with previous studies performed on guinea pigs, to yield a better understanding of the peripheral system.

1.4 Fundamentals of sound transmission

Sound, a kind of travelling pressure wave, can propagate through any elastic medium such as air, water and so on. The fundamental physical descriptors of a sound wave are its frequency and its intensity or amplitude. The frequency of a pure tone is the number of cycles or complete oscillations of condensation and rarefaction in one second. The unit of measurement is the Hertz (Hz). The intensity of the sound wave is the amount of power transmitted through a unit area of space. The amplitude of a pure tone is the magnitude of the movements produced, which has the subjective correlate of loudness.

The intensity of a sound wave is usually expressed in logarithmic units known as decibels (dB). The decibel notation always expresses the ratio between two intensities as described below:

$$\text{Number of dB} = 10 \log_{10} (\text{sound intensity/reference intensity})$$
$$= 20 \log_{10} (\text{sound pressure/reference pressure})$$

A common reference pressure is 2×10^{-5} N/m^2 RMS, or 20 μPascals RMS, which is close to the lowest sound pressure that can be detected by man.

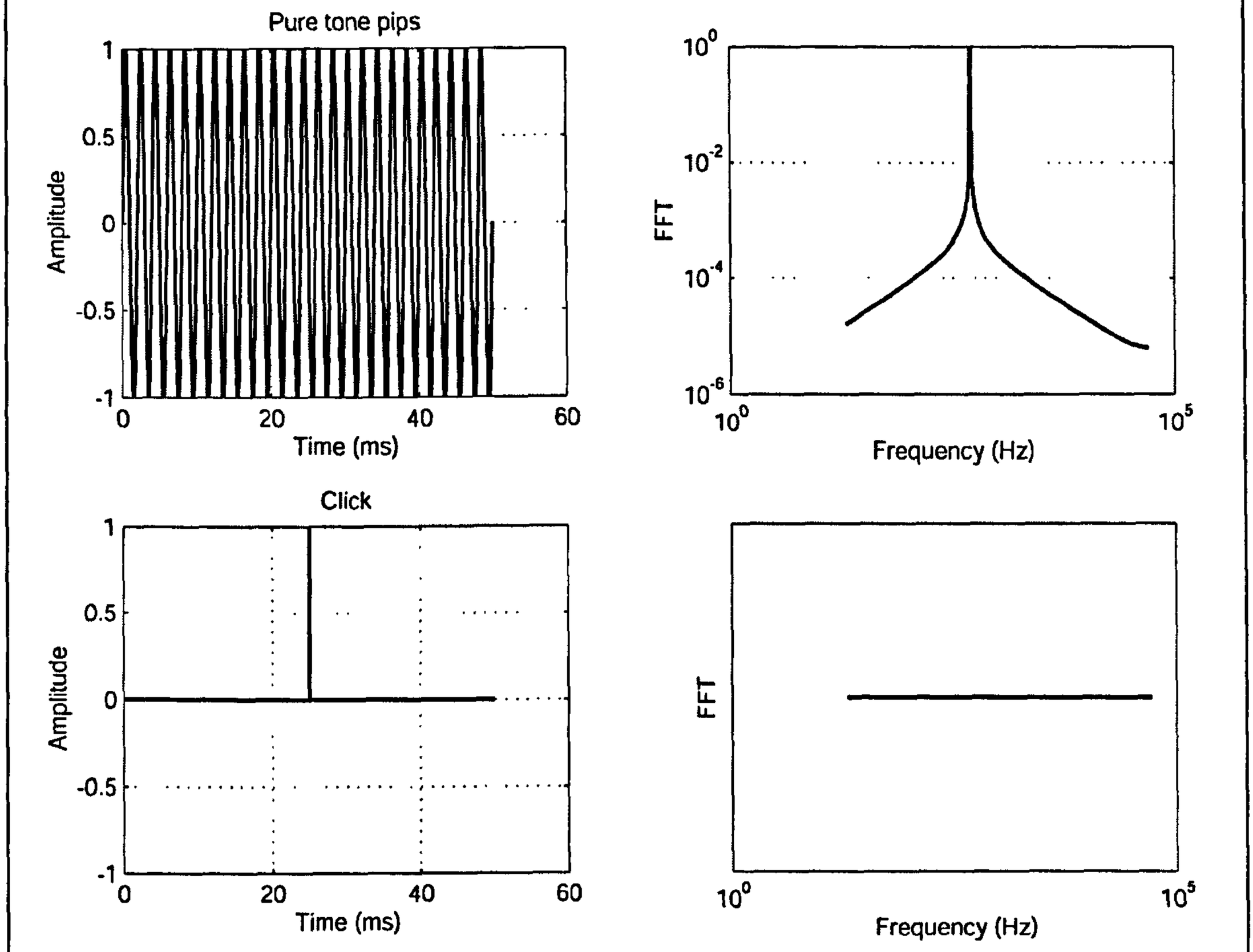

Figure 1-1 Sound waves in the time and frequency domain. Left panels show the waveform of sinusoidal and click stimuli in the time domain. Right panels show their Fast Fourier Transfer (FFT) results in the frequency domain.

Sound waves can be described in both the time and frequency domains. Sinusoidal and click waveforms in the time domain are shown in Fig. 1-1 (left) and their fast Fourier Transform (FFT) analyses (right). A simple sinusoid, which lasts for an infinite time, has a Fourier transform represented by a single vertical line, corresponding to the frequency of the sinusoid. Theoretically, a click is a waveform that can be turned on for an infinitesimal time, leading to an infinite spread of its spectrum across frequency, which is inversely related to the click's duration. As is shown in the figure, the spectrum of a click covers all frequencies equally. In practice, a click will of course last for a finite time, and this is associated with an upper frequency limit to the spectrum.

1.5 An introduction to the peripheral auditory system

Before delving into the details of auditory transduction mechanisms, it is worthwhile to describe the peripheral auditory systems.

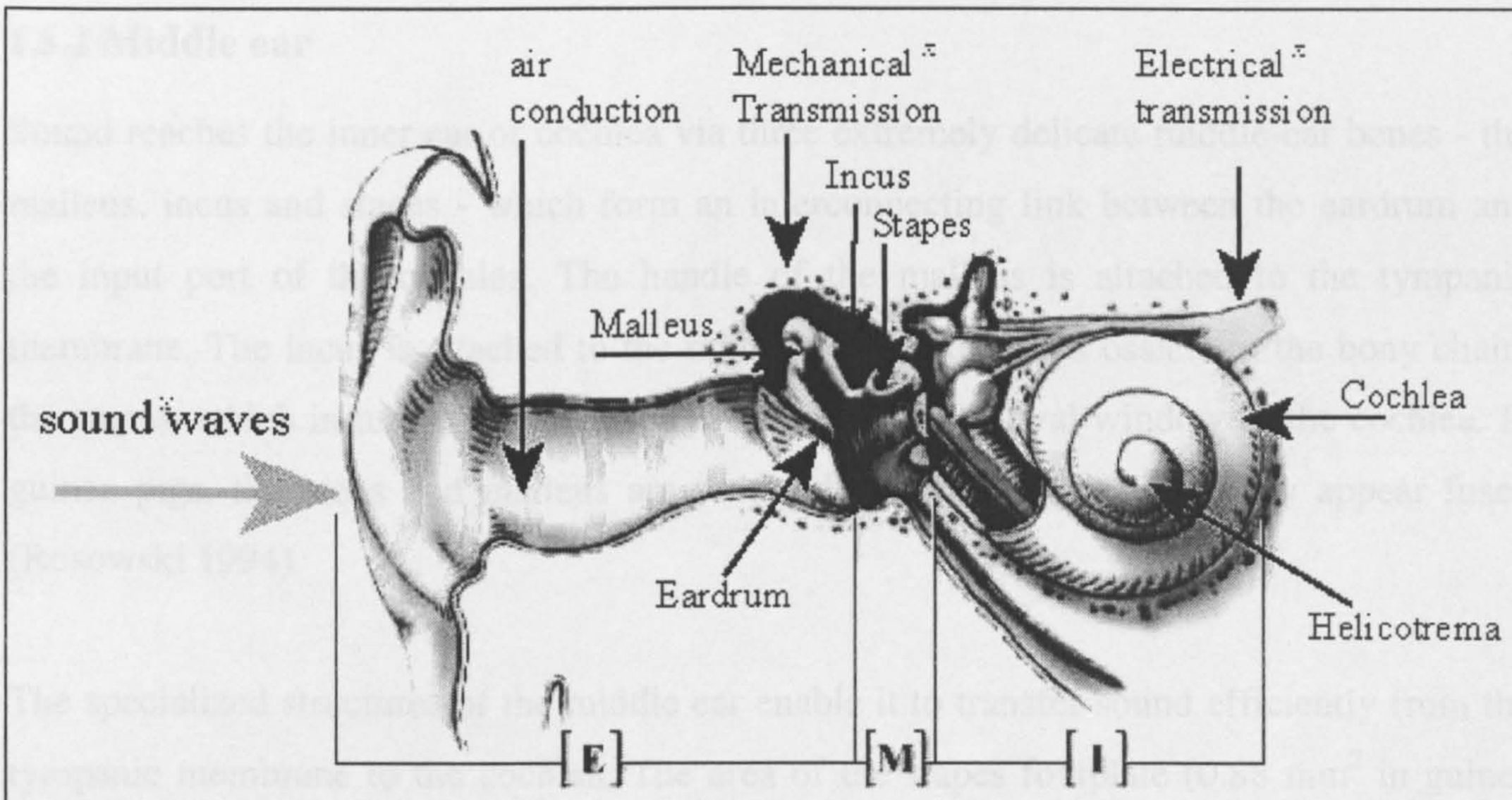

Figure 1-2 sound transmissions in the ear. The external ear (E) collects the sound and delivers it to the eardrum. The vibrations of the eardrum are transmitted to the cochlea of the inner ear (I) via the three delicate bony structures in the middle ear (M) (modified from http://ctl.angie.edu/perry/ar/speech/htm).

The peripheral auditory system may be divided into three parts: the external, middle and inner ears. Their structural relationships, highly schematized, are shown in Fig. 1-2. Sound waves, collected from the external environment by the pinnae, propagate along the ear

canal and impinge upon the eardrum, causing it to vibrate. The vibrations of the eardrum are conveyed to the fluid-filled cochlea by the three bones that span the air-filled middle ear cavity.

1.5.1 External ear

Sound is collected by the external ear, which consists of the pinna (which includes a resonant cavity called the concha) and the ear canal (the external auditory meatus), leading to the eardrum or tympanic membrane. The concha, meatus and tympanic membrane form a complex acoustic cavity, whose resonance increases the sound pressures acting at the eardrum across a limited range of frequencies. In human beings this frequency range extends from 2 to 7 kHz and in guinea pigs it extends from 2 to 9 kHz (see review Rosowski 1994). The external ear therefore increases the efficiency of sound transmission to the middle ear. The external ear also aids sound localization by altering the spectrum of the sound, depending on the direction of the source (see review Rosowski 1994).

1.5.2 Middle ear

Sound reaches the inner ear or cochlea via three extremely delicate middle-ear bones - the malleus, incus and stapes - which form an interconnecting link between the eardrum and the input port of the cochlea. The handle of the malleus is attached to the tympanic membrane. The incus is attached to the malleus and to the third ossicle in the bony chain, the stapes, which in turn is attached via its footplate to the oval window of the cochlea. In guinea pigs, the incus and malleus are so tightly bound together that they appear fused (Rosowski 1994)

The specialized structures of the middle ear enable it to transfer sound efficiently from the tympanic membrane to the cochlea. The area of the stapes footplate (0.88 mm^2 in guinea pigs) is smaller than that of the tympanic membrane (25 mm^2, (see Rosowski 1994)), and together with the mechanical advantage produced by a rotation of the longer malleus and shorter incus about a fixed axis, this results in a gain of sound pressure within the cochlear vestibule (Dallos 1973; Olson 1998).

The middle ear system is an impedance matching device. It transfers sound energy from low-impedance air to the higher impedance cochlear fluids and reduces the reflection of sound energy that would otherwise occur. Transmission through the middle ear is affected by the middle ear muscles, which reduce the transmission of low-frequency sounds. The muscles, the tensor tympani and stapedius muscles might serve to protect the ear to some extent from noise damage or from self-generated sounds. They also reduce the masking effects of low-frequency stimuli on higher-frequency stimuli, acting as an automatic gain control for low-frequency stimuli over a narrow range of intensities (see review Silman 1984).

1.6 Inner ear

The inner ear subserves two sensory functions: one part, the cochlea detects sound waves, while the other parts serve the sense of equilibrium (semicircular canals, utricle, and saccule). The cochlea within the inner ear contains sensory cells responsible for perception of sound and analysis of the sound in timing, frequency and intensity.

1.6.1 Structure of the cochlea

The cochlea is a fluid-filled spiral structure, which wraps around the auditory nerve (Fig. 1-3). The guinea pig cochlea has 4 turns while the human cochlea only has 2.5 turns. The interior of the bony labyrinth is divided into three chambers. The scala vestibuli (SV), scala tympani (ST) and scala media (SM) are separated from each other by the basilar membrane and Reissner's membrane respectively (see Fig.1-3). The scala vestibuli and scala tympani are filled with high-sodium perilymph and are actually continuous at the apical tip of the cochlea, connected by a narrow opening called the helicotrema. The scala media is filled with a potassium-rich endolymph. At the base of the cochlea, the scala tympani ends at free ending of the round window and the scala vestibuli ends at the oval window, where it is attached to the footplate of the stapes.

Inside the scala media, highly differentiated epithelial cells form the organ of Corti, which sits on the basilar membrane (BM, Fig. 1-4). The top of the hair cell consists of an epithelial surface, a number of stereocilia. The stereocilia are interconnected by small fibers called subapical bands. These bands extend down the length of the cilia and connect the cilia to each of its neighbors. Each stereocilia also connects to its next tallest neighbor by a

single tip link. It is thought that tension in these tip links caused by the bundle being deflected opens small channels in the cilia. As these channels open, ions from the surrounding fluid rush in due to an electrochemical gradient, causing the cell to fire. The single row of inner hair cells (IHCs) contains goblet-shaped cells with centrally placed nuclei. The stereocilia of the IHCs are arranged in a characteristic flattened "U" shape on the cell's apical surface and their imprints have not been observed attached to the tectorial membrane in guinea pigs (Lim 1980). The three rows of outer hair cells (OHCs) are long and cylindrical-shaped cells with basally placed nuclei and stereocilia arranged in a "W" shape. The OHCs sit on Deiter's cells. The longest row of OHC stereocilia is firmly

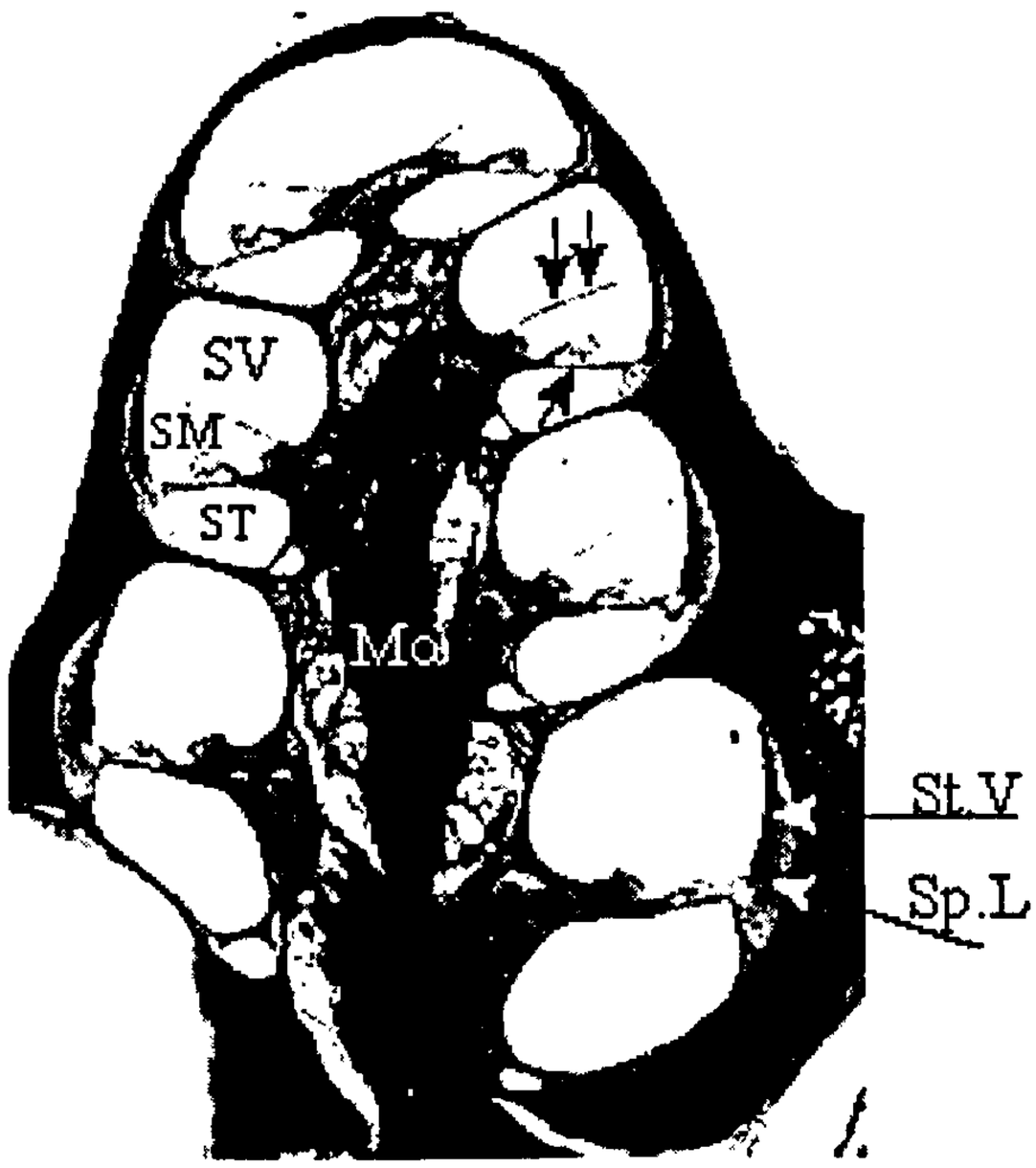

Figure 1-3 The cross section of guinea pig cochlea. The three fluid-filled spaces of scala vestibuli (SV), scala tympani (ST) and scala media (SM) are separated from each other by basilar membrane (single arrow) and Reissner's membrane (double arrow). The organ of Corti can be seen sitting on the basilar membrane. The stria vascularies (St.V) and the spiral ligament (Sp.L) lie close to the bone along the lateral wall of the cochlea. Auditory nerve fibers run in the modiolus (Mo). (modified from http://oto.wustl.edu/cochlea)

attached to the tectorial membrane (TM, (Spoendlin 1971)). In guinea pig, nearly 90-95% of the fibers in the auditory nerve contact only IHCs, and others connect OHCs (Slepecky 1996). The IHCs are separated from the OHCs by the inner and outer pillar cells, which form a triangular support within the organ of Corti. Hensen's cells are directly adjacent to the third row of Deiters cells and contain glistening lipid droplets in the apical turn of the cochlea (Henson et al. 1983; Spicer and Schulte 1994).

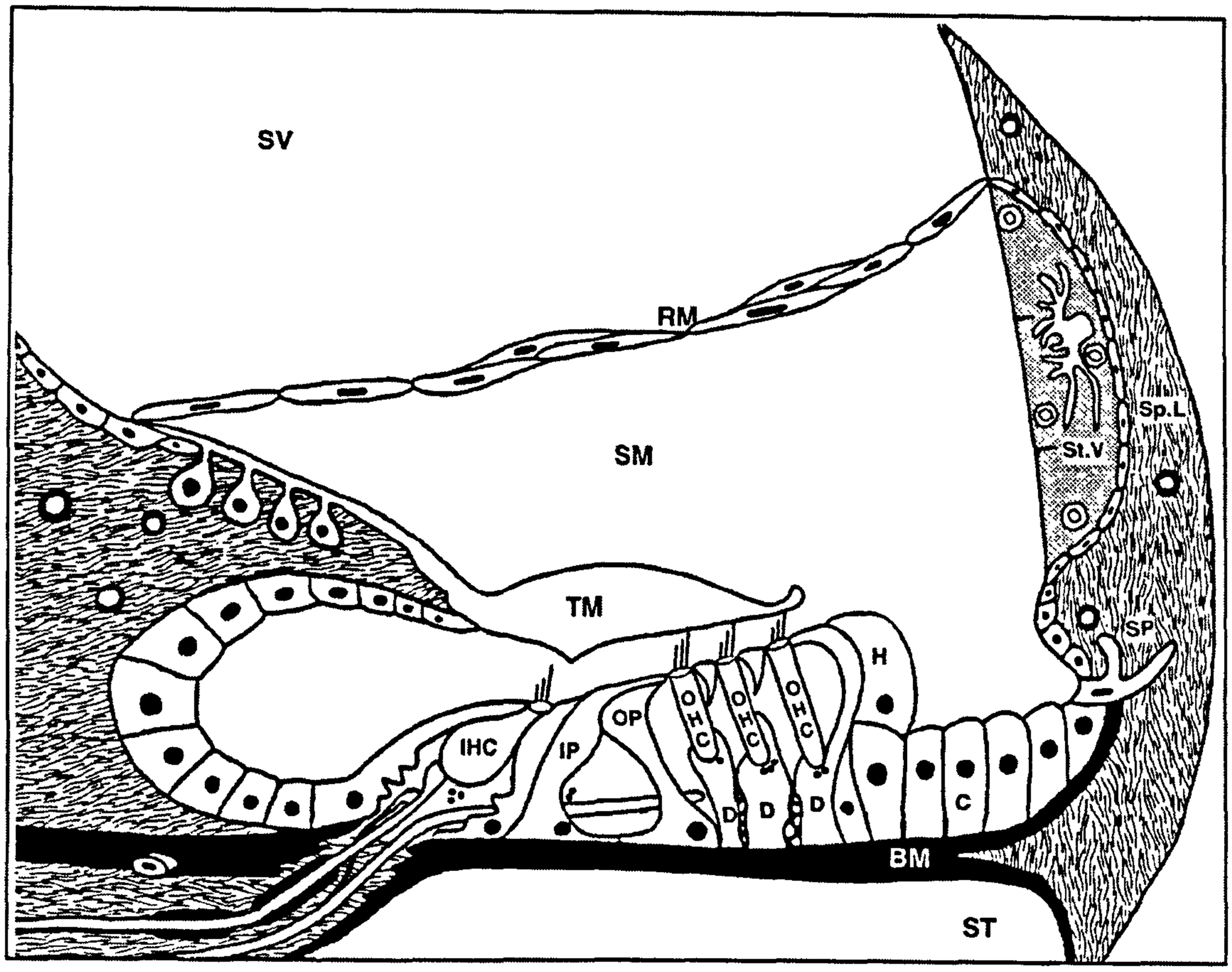

Figure 1-4 The Organ of Corti contains sensory and supporting cells. The inner (IHC) and three rows of outer (OHC) sensory cells, along with the inner pillar (IP), outer pillar (OP), Deiter's (D), Hensen's (HC) and Claudius (C) cells rest on the basilar membrane (BM). The tectorial membrane (TM) covers the apical surface of the sensory and supporting cells. The scala vestibuli (SV), scala tympani (ST) and scala media (SM) are three fluid-filled compartments. The scala media, containing endolymph, has as its boundaries the reticular lamina of the organ of Corti, Reissner's membrane (RM), and the lateral wall made up of the stria vascularies (St.V), the spiral ligament (Sp.L), and the spiral prominence (SP) (reprinted of Fig. 2-2 from Slepecky 1996)

Supporting cells provide support to the sensory cells both in physiological and mechanical terms. The inner pillar cells, outer pillar cells and Deiter's cells are specialized to withstand mechanical stress, to maintain the integrity of the reticular lamina, to submit stimulus-induced motion of the BM to the reticular lamina, and to transmit stimulus-induced motion of the hair cells between the reticular lamina and the BM (Holley and Ashmore 1988). The microvilli on the apical surface of Hensen's cells probably increase their surface area to facilitate ion exchange to their attachment with the TM (Henson et al. 1983; Spicer and Schulte 1994). Claudius' cells, as a group, fill the distance between the Deiter's cells and the lateral wall of the cochlea (Kimura 1975; Slepecky 1996). In the base of the cochlea,

Boettcher Cells (Kimura 1975; Henson et al. 1982; Slepecky 1996) fill in some of the radial distance from the base of the Deiters cell to the basilar crest of the spiral ligament. However, toward the apex of the cochlea, they decrease in number and eventually disappear. External Sulcus cells (root cells) are located at the junction of the BM with the cells of the lateral wall (Slepecky 1996).

There are tight juctions, adherens junctions, desmosomes, and gap junctions linking the sensory and supporting cells. Tight and adherens junctions are present at the apical surface of cells, usually where they face a lumen. Desmosomes and gap junctions are found along the basolateral surface when and if they are present (Slepecky 1996). These linkages integrate the organ of Corti to permit movement of the sensory epithelium in response to mechanical stimuli and to separate endolymph from perilymph.

Throughout the organ of Corti, cochlear hair cells and surrounding supporting cells are joined at their apices by tight junctions, forming a reticular lamina. The tight junction within this lamina, together with those found within the lateral wall and roof of the cochlear duct, provide a fluid barrier, which effectively seals the endolymph-filled scala media from the surrounding perilymph-filled scalae.

The tectorial membrane is a gel-like structure that overlies the reticular lamina of the organ of Corti. It is anchored at the spiral limbus, extends outwards to beyond the third row of outer hair cells and forms rather fragile connections with the surface of the organ of Corti. It is thought to play a crucial role in sensory transduction, because the longest of the three row of OHC stereocilia is firmly attached to the TM.

The diameter of the bony labyrinth decreases from the base to apex of the cochlea (Smith 1968; Cabezudo 1978; Strelioff and Flock 1984; Wright 1984; Bohne and Carr 1985; Lim 1986). However, most of the structures within organ of Corti increase in size along the length of the basilar membrane, from base to apex. For the organ of Corti, the cells in the apex are larger than those in the base, the stereocilia on the hair cells are longer and less stiff (Wright 1984; Bohne and Carr 1985; Lim 1986; Roth and Bruns 1992), the BM is wider (such that its stiffness decreases while the mass increases), and the tectorial membrane has a greater mass (Lim 1980).

The overall effect of this grading in geometry and morphology is to make the cochlear partition slightly larger, more massive, and less stiff in the apex than it is in the base. Although mass is estimated to increase very little in moving from base to apex, the stiffness of the BM is estimated to decrease by about 100:1 over the same range (Lim 1980; Bruns et al. 1988; Echteleler 1994). The friction or damping associated with vibration of each of the components is very difficult to estimate, either theoretically or by direct measurement, but some estimates suggest that it may decrease in moving toward the apex, based on the fact that the distance between the TM and the reticular lamina is larger in the apex because of the lengthening of the hair cell stereocilia (Wright 1984; Bohne and Carr 1985; Lim 1986; Roth and Bruns 1992).

1.6.2 Mechanism of the cochlea

The cochlea is the place to analyze sound in terms of its intensity, timing and frequency content. It can detect the fluctuations in the atmospheric pressure (sound) as low as 1/2000000000 of normal atmospheric pressure (20 μPa), and it can withstand sounds of up to 120 dB SPL without permanent damage. Based on numerous observations of basilar membrane's motion at basal sites within the cochlea (see reviews Ulfendahl 1997; Robles and Ruggero 2001), an active, nonlinear and positive feedback model has been suggested to illustrate the mechanisms of the basal turn (Yates et al. 1992). On the other hand, an active, nonlinear and negative feedback loop was suggested to model the apical turn of the cochlea by a few researchers (Khanna and Hao 2000; Zinn et al. 2000).

1.6.2.1 Active, nonlinear and positive feedback loop of the basal turn of the cochlea

Fig. 1-5 shows the general idea about the active, nonlinear, positive feedback model of the basal turn of the cochlea (Yates et al. 1992). Pressure waves reaching the eardrum are transmitted via vibrations of the middle ear ossicles to the oval window at the base of the cochlea, where they create pressure differences between scala tympani and scala vestibuli, therefore displacing the BM (step 1 of Fig. 1-5). The basilar membrane, on which the organ of Corti rests, is responsible for controlling the 'von Békésy-type' traveling wave and delivers the mechanical stimuli to the organ of Corti (von Bekesy 1960). For a pure tone stimulus, the wave grows as it travels along the basilar membrane, reaching a maximum at the characteristic frequency position, and then collapses abruptly so that there

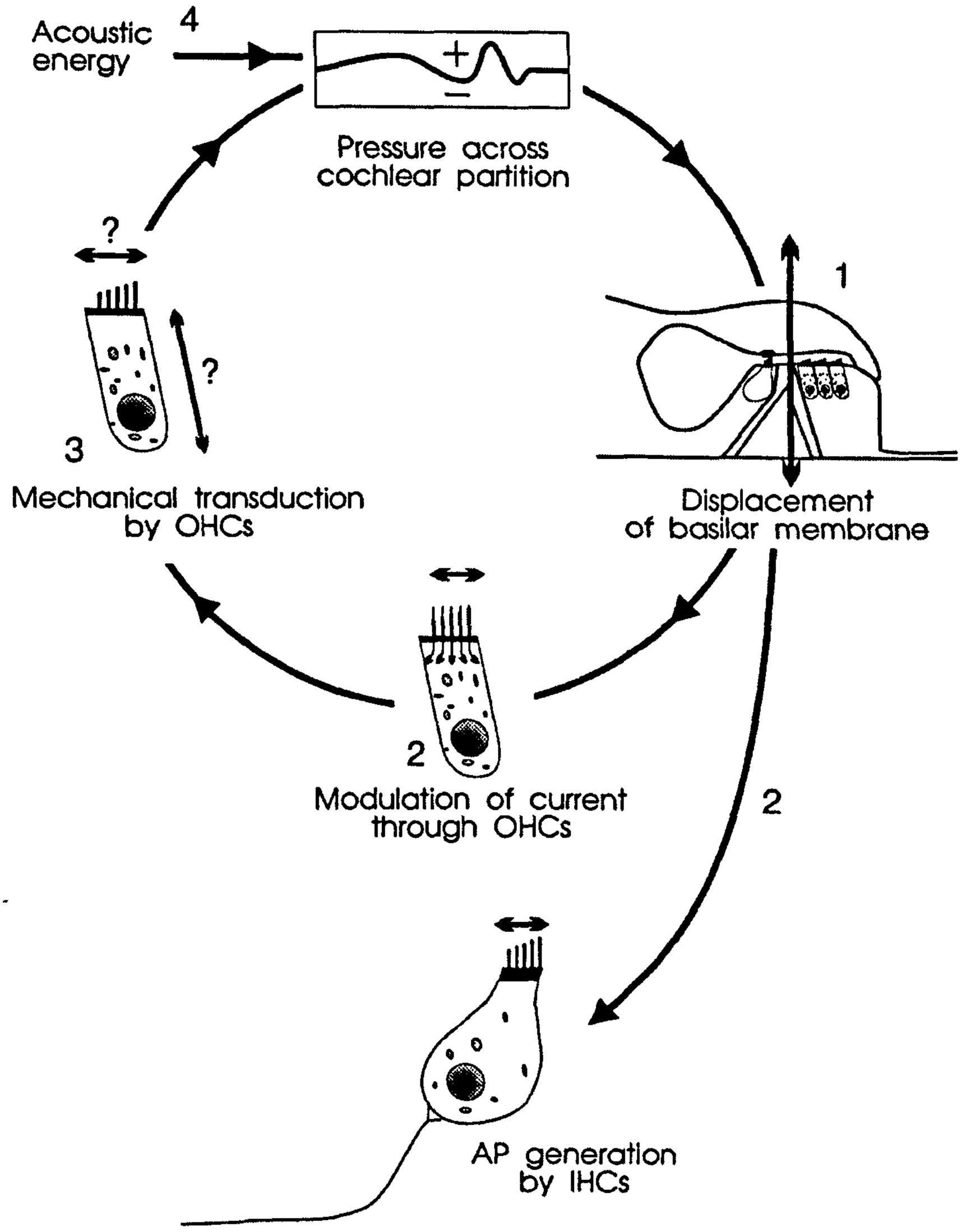

Figure 1-5 Active process loop of the cochlea. Step 1. Acoustic stimulation produces pressure differences between scala tympani and scala vestibuli, causing the BM to vibrate. Step 2. The resulting shearing between the tectorial membrane and the tops of the hair cells modulates the standing current, driven by a K+ electrochemical gradient, through the inner hair cell (IHCs) and outer hair cells (OHCs). Step 3. The resulting receptor potential within the outer hair cells triggers the active process, causing some form of mechanical activity in the outer hair cell. Step 4. This in turn feeds pressure fluctuation back into the cochlea to complete the loop. The receptor potential within the inner hair cell leads to transmitter release across the afferent synapse (reprinted from Yates et al. 1992).

is no vibration beyond the wave's cutoff region. The characteristic place and the cutoff region are positioned along the cochlear length: high frequencies towards the cochlear base, closer to the stapes, and low frequencies closer to the apex of the cochlea.

The basilar membrane's vibration provides the basis of frequency analysis and forms the first band-pass filter inside the cochlea. The sharp tuning curves of the BM at its characteristic frequency show the cochlear sensitivity and frequency selectivity of the basal turn of the cochlea. In the early 1970's, Rhode demonstrated that BM vibration in live squirrel monkeys exhibits compressive nonlinearity. This means that the magnitude of the BM responses grows by less than 1 dB/dB with the sound pressure level (Rhode 1971). More and more confirmations were published over the next 30 years consistent with the existence of nonlinear and active cochlear processing (Le Page and Johnstone 1980; Rhode 1980; Sellick et al. 1982; Robles et al. 1986; Cooper and Rhode 1992; Cooper and Rhode 1992; Nuttall and Dolan 1996; Nuttall et al. 1997; Ruggero et al. 1997).

The tectorial membrane is involved in converting the vertical movement of the basilar membrane into radial displacement of the upper surface of the hair cells (reticular lamina) relative to the TM (von Bekesy 1960), which results in a shearing force and stimulus to the stereocilia of the IHCs and OHCs. The deflection of the hair bundles modulates the electrical conductance at the apices of the cells by opening and closing mechanoelectrical transduction (MET) channels near the tip of each stereocilium. This produces a sound-induced change in the current flowing through each hair cell known as its receptor current, and a change in the voltage across its membrane known as its receptor potential (Kros 1996). The receptor potential within both types of hair cells, IHCs and OHCs, acts to release neurochemicals and to stimulate neurons, and so is known as the 'sensory process' within the organ of Corti. IHCs appear to play a primary sensory role in the cochlea, based on the fact that most of the afferent nerve fibers synapse with them. The receptor potential or current of OHCs also seems to control a molecular force generation mechanism within the organ of Corti (and probably within the OHCs themselves) known as the 'active process'. OHCs, although providing some direct sensory input to the central nervous system, more likely modify the mechanical properties of the organ of Corti and the BM, forming the cellular basis of the active process in the loop step 2 of Fig. 1-5 (de Boer 1996; Holley 1996; Patuzzi 1996).

For each input frequency, the OHCs are motile and can convert receptor potentials into a force (step 3 of Fig. 1-5, Dallos and Evans 1995; Frank et al. 1999), which pushes back on the basilar membrane, exerting force and injecting mechanical energy into the traveling wave (step 4 of Fig. 1-5) with just the right amplitude and phase. This can enhance both the BM's sensitivity and its frequency selectivity, amplifying the acoustic signals, especially for faint sounds (Rhode 1971; Rhode 1974; Robles et al. 1976; Rhode 1978; Khanna and Leonard 1982; Sellick et al. 1982; Robles et al. 1986; Robles et al. 1991; Cooper and Rhode 1992; Ruggero 1992; Ruggero et al. 1992; Ruggero et al. 1992; Cooper et al. 1993; Cooper 1996; de Boer 1996; Holley 1996; Nuttall and Dolan 1996; Patuzzi 1996; Robles et al. 1997; Ruggero et al. 1997; Russell and Nilsen 1997; Cooper 1998; Narayan et al. 1998; Recio et al. 1998).

The active process of the OHCs is responsible for the high sensitivity, sharp tuning and compressive growth of BM vibration in the basal turn of the cochlea in a healthy cochlea. It will disappear immediately *post mortem* or even with acute occlusion of cochlear blood flow, and hence make the basilar membrane movement proportional to the sound level in a damaged cochlea. The basal cochlear mechanics can be interpreted in such a simple positive feedback model and almost all the observations of the basal turn of the cochlea provide experimental support. However, some apical data do not fit with this model. A negative feedback model has hence been developed to interpret the apical cochlear mechanics.

1.6.2.2 Active, nonlinear and negative feedback loop of the apical turn of the cochlea

In the apical turn of the cochlea, the most representative responses were obtained from chinchillas *in vivo* (Cooper and Rhode 1996; Rhode 1996; Cooper and Rhode 1997). Compared with responses from the basal turn of the cochlea, broader and less compressive tuning were observed from gold-coated polystyrene beads introduced into the scala media via a small tear on the RM. The compressive growth rate of the response amplitudes with stimulus intensity was 0.5-0.8 dB/dB. However, in the cochlea of guinea pigs *in vivo*, several observations failed to observe such compressive nonlinearity in the apex (Hao and Khanna 1996; Khanna and Hao 1999). Moreover, a vulnerable expansive nonlinearity in an apical site of the guinea pig cochlea with CF ~300-400 Hz has been demonstrated (Khanna

and Hao 1999), and it disappeared postmortem. On the other hand, *in vitro* vibration recordings from the apex of the guinea pig cochlea show similar tuning characteristics compared with those of *in vivo* mechanical data (Khanna et al. 1989; Ulfendahl et al. 1995; Gummer et al. 1996; Ulfendahl et al. 1996; Hemmert et al. 2000).

Recently, a negative feedback model was suggested to interpret the mechanism of the apical turn of the cochlea based on two groups' observations (Khanna and Hao 2000; Zinn et al. 2000), which is different to the positive feedback in the base. In Zinn's experiment (Zinn et al. 2000), expansive nonlinearities (displacement changing with sound pressure level with a slope of greater than 1 dB/dB) were found below 80 dB SPL instead of physiologically vulnerable, compressive nonlinearities at low to medium sound pressure levels. The expansive nonlinearities were most pronounced above CF and disappeared *post mortem*. For all 4 animals that the authors believed to be in good condition, response amplitudes were larger *post mortem* than *in vivo*. Also, their phase data was physiologically vulnerable below 80 dB SPL *in vivo*. All these observations were thought to provide evidence for active attenuation of the vibration of the organ of Corti at low sound pressure levels. As a result, a negative feedback was suggested to interpret the mechanics of the apex of the cochlea.

Khanna's suggestion of the negative feedback model (Khanna and Hao 2000) was raised in response to two observations that have been made in the apical turn of the cochlea: firstly, the Hensen's cell vibration amplitude is much higher than that of basilar membrane, indicating that amplification exists in the apical turn of the cochlea. Secondly, the Hensen's cell vibration amplitude decreases and the BM vibration increases after the sacrifice of the animal being observed. The ratio of the vibration amplitude between the HC and BM decreased after sacrifice from 900 to about 5, clearly showing that the ratio changed dramatically with cochlear condition. The best explanation for these phenomena is that there is negative feedback between reticular lamina and the BM. The amplification from the negative feedback was turned off when the animal died, therefore, the ratio of the vibration amplitude between the HC and the BM dropped as well.

Both Zinn et al and Khanna & Hao's recordings were made from *in vivo* guinea pigs which were claimed to be in good cochlear condition. However, one of the major concerns is 'how

normal' the condition of the cochleae were during these apical turns observations. It is obvious that the audiogram (threshold of compound action potential of nerve fiber) above 2 kHz could not provide any information on the condition of the apex of the cochlea. Cochlear potentials could show the information of the cochlear condition in general, but could not show anything about the local mechanical damage, such as the damage to OHCs (Zinn et al. 2000). Q_{10} value (the frequency of the response peak divided by the band-width 10 dB below the peak) highly depends on the resealing of the opening of the cochlea in the apex of the cochlea (Cooper and Rhode 1996; Khanna and Hao 2000). Therefore, neither Zinn et al. nor Khanna & Hao provide sufficient information to show that the cochleae from which they made recording were in 'normal' condition.

Negative feedback fits the above observations from certain points of view, but only based on the limited cases provided in these two studies. We are still short of experimental evidence about the nature of the mechanical responses to sound stimulation of the apical turn of the cochlea under normal conditions. There might be another way to interpret the recordings of Zinn et al and Khanna & Hao as resulting from all of the artifacts involved in direct approaches to the apex of the cochlea.

1.7 Round Window potentials

It is well known that mechanical vibration of the organ of Corti in the mammalian cochlea can explain much of the sensitivity, frequency selectivity and nonlinearity of the responses of hair cells and neurons. In addition, the fall in mechanical and neural sensitivities are highly correlated under certain conditions: for example, neural sensitivity and the vibration of the organ of Corti can change slowly during the course of an experiment to produce an insensitive, broadly tuned and linear response after some hours, or more rapidly following cochlear trauma during surgery (Sellick et al. 1982; Robles et al. 1986) or loud sound (Sellick et al. 1982; Patuzzi and Sellick 1983; Patuzzi et al. 1989). Therefore, the physiological condition of the cochlea is an essential issue of the mechanical studies of the cochlea.

One way of monitoring the physiological condition of the cochleae is to monitor its electrical responses to sound. The most convenient way to do this is to use the round

window potentials. Round window potentials have been widely used as indicators of the condition of the whole cochlea (Tasaki 1954; Teas 1962).

The potential recorded on the niche near the round window when sound is delivered into the ear actually is a mixture of sound evoked potentials from three different sources. The first is the cochlear microphonic (CM), an a.c. response, which reflects the modulation of hair-cell receptor currents produced by BM and stereocilia displacement (Davis 1965; Dallos et al. 1972; Dallos and Durrant 1972; Dallos et al. 1974; Patuzzi et al. 1989). The CM is dominated by the electrical output of the outer hair cells (Dallos et al. 1972; Dallos 1973; Dallos et al. 1974; Russell and Sellick 1983) especially at low frequencies (Sellick and Russell 1980; Nuttall et al. 1981; Russell and Sellick 1983; Dallos 1986; Patuzzi and Yates 1987). Dallos et al. (Dallos et al. 1972) have also demonstrated that in animals in which the OHCs of the first turn were destroyed by chronic kanamycin intoxication the amplitude of the cochlear microphonic potential recorded in the first turn was greatly reduced. Patuzzi et al. (Patuzzi et al. 1989) demonstrated that apical component of the low-frequency CM may be as large as 20 to 40% of the resultant amplitude at low intensities of the stimuli (much below 100 dB SPL) even though most of the low frequency microphonic at the round window emanates from the OHCs of the first turn. At low intensities of the low frequency stimuli, none of the hair cells would be saturated, and the amplitude of the apical component may be significant. Therefore, the low-frequency CM at low stimuli intensities can be used to indicate the integrity of mechano-electrical transduction of the OHCs in the apical turn of the cochlea.

The second potential recorded from the round window is the summating potential (SP), a d.c. potential, which is mainly produced by hair cells and reflects the responses from hair cells at the base of the cochlea (Davis 1958; Dallos 1973; Russell and Sellick 1978). It can be positive or negative, depending on the recording electrodes' location and the stimulus intensity and frequency (Davis 1958; Dallos et al. 1972; van Deelen and Smoorenburg 1986). The summating potential recorded from the round window in animal and humans tends to be positive at low sound pressure levels but negative at high sound pressure levels (Margolis et al. 1992; Tilanus et al. 1992). Some previous studies (Davis 1958; Dallos and Wang 1974; Dallos and Cheatham 1976; McMullen and Mountain 1985; Harvey and Steel 1992; Cheatham and Dallos 1994) indicate that the summating potentials have multiple

sources, and the outer hair cells were suggested to be the major generator. However, recent studies indicates that the inner hair cells might be the major generator of the summating potentials recorded remotely, due to the fact that basal OHCs produce little dc receptor potential when stimulated with high frequency stimuli at low and moderate levels (Russell and Sellick 1978; Cody and Russell 1988; Russell and Kossl 1992). Zheng et al.(Zheng et al. 1997) provided evidence that the IHCs are the major generator of SP recorded from the round window, in particular at low to moderate stimulus levels. The SP recorded from the round window largely reflects the responses from hair cells at the base of the cochlea (van Emst et al. 1998).

The third potential recorded from the round window is the compound action potential (CAP), which represents a spatial summation of neural activity in the auditory nerve. The size and form of the action potentials reflects the number and the degree of synchrony of individual neural responses (Tasaki 1954). The CAP is the result of the nearly-simultaneous discharge of hundreds of neurons in the auditory nerve. When a large, extra-cochlear electrode is used, individual neural discharges (called spikes) cannot be seen, but the electrical sum of those discharges can be detected by presenting stimuli repeatedly and then obtaining an average of the electric responses seen by the recording electrode. The CAP can provide useful information about peripheral auditory function in normal and abnormal ears (Dallos and Cheatham 1976; Dallos et al. 1978; Harris and Dallos 1979; Johnsson et al. 1979; Abbas and Gorga 1981; Gorga and Abbas 1981; Harrison 1981; Harrison et al. 1981; Brown et al. 1983).

The sound-evoked round window potentials can therefore provide information about both nerve fibres (CAP) and hair cells information (CM and SP). Since it is known that there is a very good correlation between neural sensitivity and BM mechanical sensitivity at the CF (Sellick et al. 1982), the CAP visual detection threshold was used as an indicator of BM vibration at the CF and, therefore, the integrity of the electro-mechanical feedback loop. Therefore, both of these gross measurements of cochlear function, the CAP and low frequency CM, have the advantage of being stable and sensitive indicators of OHC transduction and BM vibration. These measurements also give us immediate information regarding the physiological condition of the cochlea.

Chapter 2 Tectorial membrane

The tectorial membrane (TM) is a transparent gel-like structure composed of an extracellular matrix of fibrils that overlies the inner and outer hair cells in the cochlea (Figure 2-1). It originates from the spiral limbus, extends outwards to beyond the third row of the outer hair cells (Edge et al. 1998), and attaches to the Hensen's cell band (Lim 1980; Steel 1983). Because of its strategic location in the organ of Corti, the TM is supposed to be involved in converting the vertical movement of the basilar membrane into a radial displacement between the upper surface of the hair cells (reticular lamina) and itself. This radial shear is expected to deflect the stereocilia of the OHCs directly, and to excite the OHC's by changing their transmembrane potentials (Kros et al. 1992; Preyer et al. 1994). The OHCs are then thought to contract and elongate their cell body axially following the

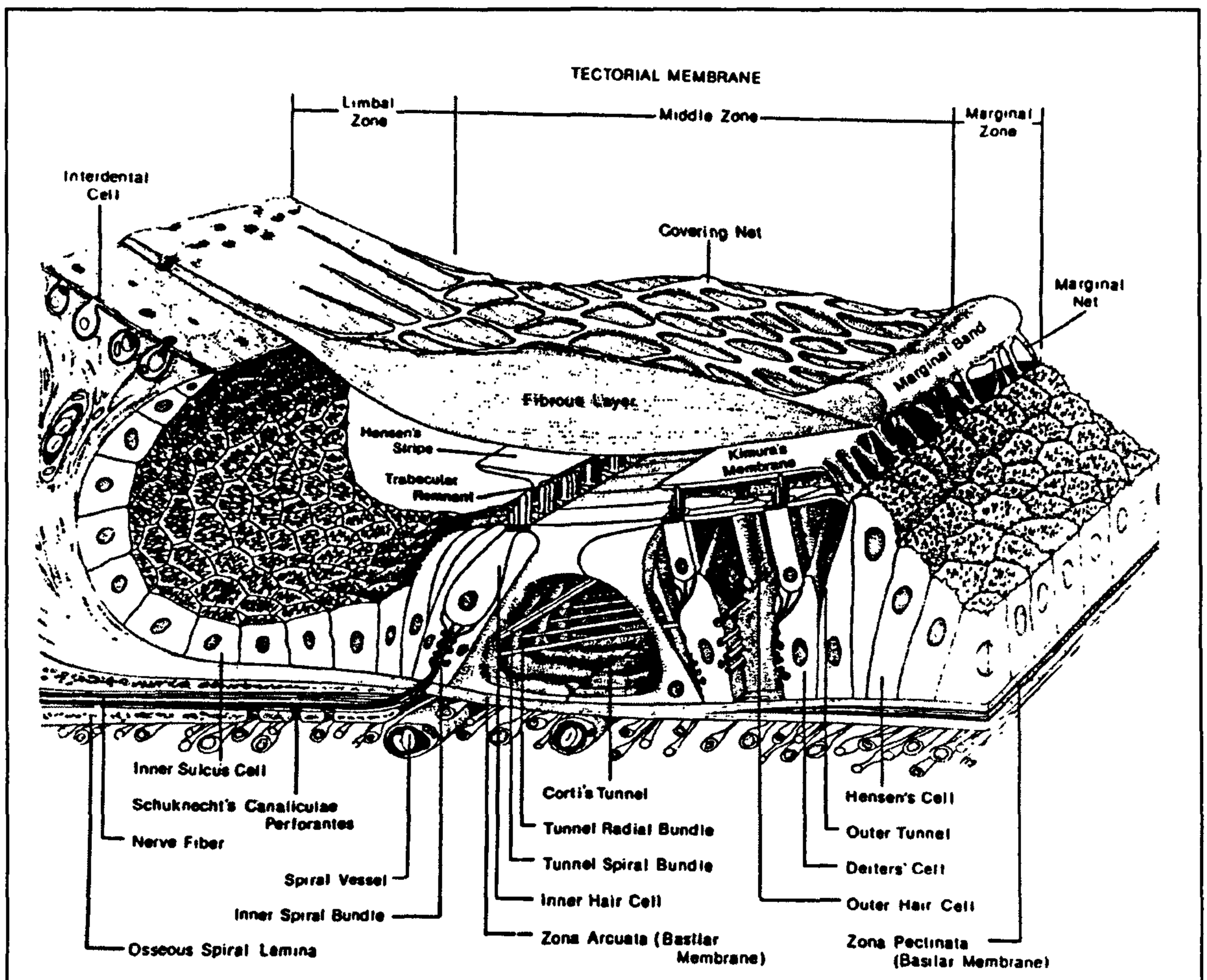

Figure 2-1 Schematic diagram of the Organ of Corti and the tectorial membrane (reprinted from Lim 1980)

changing of their membrane potentials (Dallos and Evans 1995) and to inject mechanical energy into the organ of Corti (Brownell et al. 1985; Zenner et al. 1985). The OHCs motion is supposed to contribute to the sharp tuning observed in the basilar membrane's motion. In addition, the stereocilia of the IHCs are also sheared either due to movement of the fluid around them or perhaps due to contact with the overlying TM at Hensen's stripe (Ross 1974). Therefore, the nature of the TM must be a critical factor in the sound delivery procedures inside the cochlea.

2.1 Structure

The TM is a fibrous structure, which is divided into limbal, middle and marginal zones as shown in Figure 2-1 (Lim 1972; Lim 1980). The limbal zone is attached to the limbus spiralis and the middle and marginal zones form the major body of the TM and overly the sensory cells of the organ of Corti. The main body of the TM is made up fibers embedded in an amorphous substance (Lim 1972). The main body is thought to be made up of type A fibrils and the amorphous substance is made up of type B fibrils (Kronester-Frei 1978; Hasko and Richardson 1988).

Type A fibrils are straight and un-branched, 10 nm in diameter, with obvious cross-striations. These fibrils run radially in parallel bundles in the basal layer and middle zone of the TM. Type A fibrils are composed of collagen (Hasko and Richardson 1988). Type B fibrils are branched and coiled, 1.5-2 nm in diameter, and lie among the type A fibers in two different states of hydration (Kronester-Frei 1978; Lim and Anniko 1985; Thalmann et al. 1987; Weaver and Schweitzer 1994). Weakly hydrated type B fibers form the marginal zone and net, Hensen's strip, and attachment layers of the limbal zone, while strongly hydrated type B fiberes are found throughout the remainder of the tectorial membrane. Type B fibrils consist of noncollageneous glycoproteins (Santi et al. 1990; Killick et al. 1995; Killick and Richardson 1997; Legan et al. 1997; Tsuprun and Santi 1997), which may count for up to 50% of the total protein in the TM (Richardson et al. 1987). The structural integrity of type B fibrils appears to be dependent on calcium (Hasko and Richardson 1988).

The major fibres in the main body of the TM radiate outwards from the inner zone in a distinctly slanted orientation while, the minor group runs more or less longitudinally (Lim

and Anniko 1985). The slant is most pronounced in the apex (about 30° towards the apex, Figure 2-2), followed by a slight turn in the middle turn, and the slant is not evident in the basal turn. This slanted fibrillar arrangement coincides well with the slanted arrangement of the 'W' formation of the OHC stereocilia (see review by Lim 1986).

There appears to be some difference between the mode of marginal attachment in the apex and in the base of TM (Lim 1980). In the apex the margin of the TM is irregular and forms the marginal net, a series of fingers or nets that are attached to the third row of Deiter's cell phalanges. In the base the TM margin is smooth, forming a marginal band that is attached to the third row of outer hair cell cilia. The margin may even form a seal *in vivo* (Kronester-Frei 1979; Orman and Flock 1983; Steel 1983).

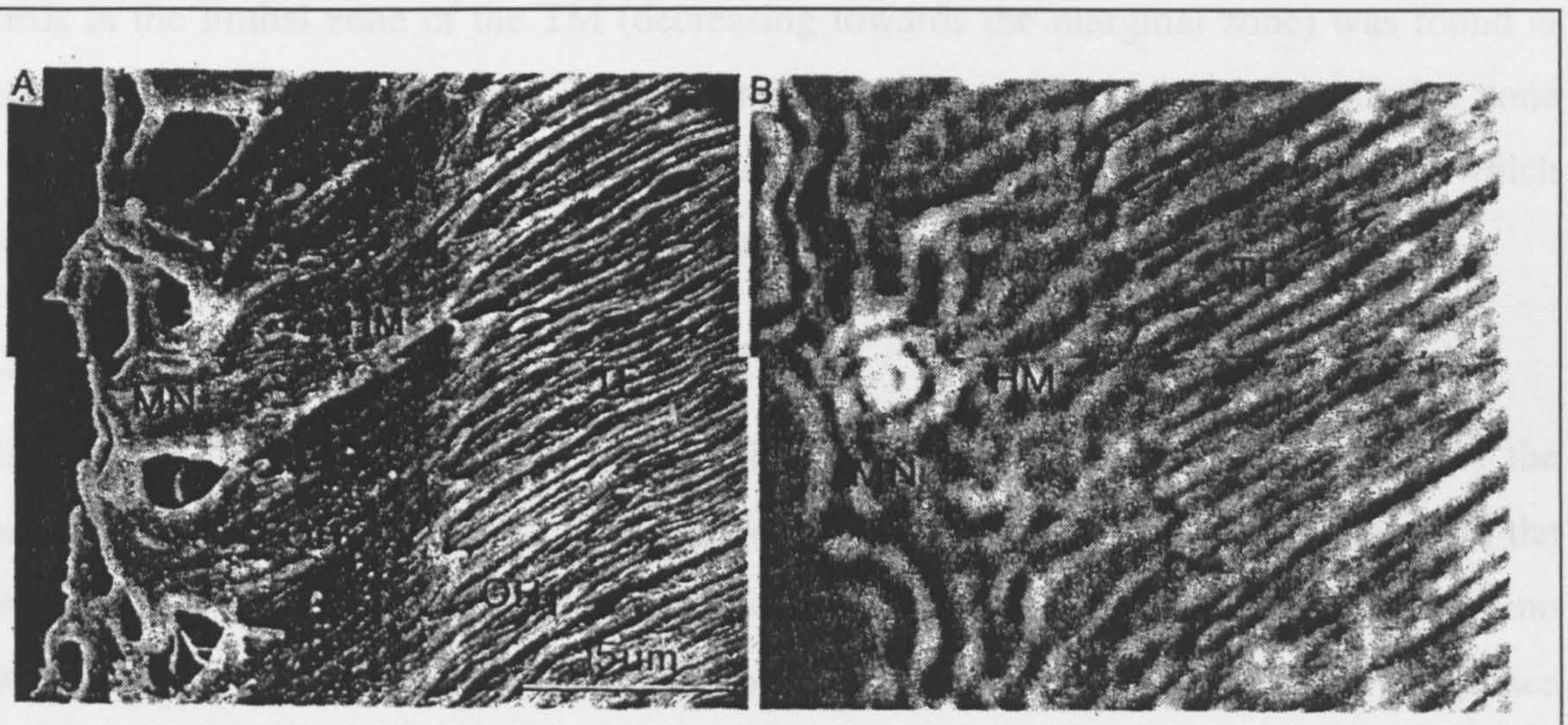

Figure 2-2 (A) Scanning electron microscopic view of undersurface of the TM at apical turn, showing homogenous layer or Kimura's membrane (KM), marginal net (MN), and the tectorial membrane fibres (TF). Clear imprints of first (OH1) and second (OH2) outer hair cell stereocilia are seen. The third row imprints are on the marginal net (MN). (Chinchilla) (B) Fresh tectorial membrane, showing tectorial membrane fibres (TF), Kimura's membrane (KM) and marginal net (MN). (chinchilla) (reprinted from Lim 1980).

The upper surface of the TM is the cover net (Figure 2-1), which is facing the endolymph and is made of densely packed type B fibres. It connects to the marginal band in the base and the marginal net in the apex. The middle layer is the major body of TM, which is composed of bundles of type A fibrils embedded in loosely packed type B fibrils. The

undersurface of the TM is composed of densely packed type B fibrils and forms Hensen's stripe above the IHCs and Hardesty's membrane over the OHCs region (Kimura 1966). In the gerbil hemicochlea preparation (Edge et al. 1998), the TM was found closely apposed to, and with its bottom surface parallel to the surface of the reticular lamina (Edge et al. 1998).

The width of the TM parallels that of basilar membrane from the base to the apex of the cochlea. The width and thickness of the TM increase from base to apex. The space between the RM and the upper surface of the TM is very small in the apical turn, and the cross-sectional area of the TM increases from base to apex (Steel 1986; Roth and Bruns 1992). There is no longitudinal gradient in any zone of gerbil TM fibril concentration. However, a radial gradient of fibril concentration marked by significantly higher concentrations of thick fibrils in the limbal zone of the TM (decreasing towards the marginal zone) was found at each cochlear level (Weaver and Schweitzer 1994). This might mean that the limbal zone of the TM is more inelastic and stiffer than the other zones. The marginal zone, which overlies the OHCs, may be the most compliant of the three radial zones.

2.2 Stereociliary attachment to the TM

The tallest OHC stereocilia are firmly attached to the TM along the entire length of the cochlea. Imprints of these stereocilia, arranged in 'W' patterns precisely coincide with the arrangement of the stereocilia directly below the TM (Kimura 1966; Lim 1972; Hoshino 1974; Hoshino 1976; Hoshino 1977; Hoshino 1981). In an in vitro preparation of the guinea pig cochlea, the OHC bundles are attached to the TM (Ulfendahl et al. 2001). Cochlear microphonics in proportion to the displacement of the basilar membrane provides physiological evidence that the stereocilia of OHCs are connected to the TM (Russell and Sellick 1983).

Conversely, there is little evidence that inner hair cell stereocilia are connected to the TM, especially in guinea pigs and chinchillas (Kimura 1966; Lim 1972; Hoshino 1974; Meyer zum Gottesberge and Tsujikawa 1993; Ulfendahl et al. 2001). Some investigators have observed that the IHC stereocilia are attached to the TM in certain species, while in others they are not. Even when they are attached, it must be a weak attachment, and the attachment is limited to only the basal turn, where the inner hair cell stereocilia are twice as

tall as the outer hair cell cilia (Lim 1980; Steel 1983; Lim 1986). Intracellularly-recorded IHC responses are observed in proportion to the basilar membrane's velocity at low frequencies of stimulation, which physiologically supports the suggestion that the IHC stereocilar are not attached to the TM (Russell and Sellick 1983). This is consistent with the concept that the IHC's stereocilia are stimulated by the viscous drag of fluid flowing above them. Russell and Sellick (Russell and Sellick 1983) also found that the IHC's seem to respond to basilar membrane displacement at higher frequencies of stimulation. This might be interpreted that IHC stereocilia are connected to the TM when the stimulus frequency exceed a certain value, although originally they are not attached to the TM. The stimulation mode of the IHC stereocilia changes from viscous drag of the fluid to the displacement of the basilar membrane at higher stimulus frequencies.

2.3 Molecular Composition of TM

The TM consists largely of protein. The nature of the protein will be important in determining the physical properties of the whole structure. For example, if the TM fibrils are composed of collagens, they may be expected to be rigid and strong and relatively inextensible. But if the fibrils consist of a protein like keratin, they may be fairly extensive and elastic instead. There are more than 20 protein sub-units of different molecular weights in the TM. The major components have relatively large molecular weights of 145,000, 155,000 and 165,000 (Steel 1980; Steel 1983). The TM also contains proteoglycans (PGs) (Richardson et al. 1987; Hasko and Richardson 1988; Santi et al. 1990; Thalmann 1993). In some regions of the TM, the collagen bound PGs formed crystalline-like arrays of linear aggregates, which run parallel to each other (Tsuprun and Santi 1996). About 40% of the protein in the guinea pig TM consists of collagen (Thalmann et al. 1987).

At least three types of collagen exist in TM (Thalmann et al. 1986; Richardson et al. 1987; Slepecky et al. 1992; Slepecky et al. 1992). Type II collagen is the major form of collagen in the cochlea, localized only in the thick type A fibers (Slepecky et al. 1992). Type IX collagen together with type II collagen was also found in the type A filaments (Richardson et al. 1987; Thalmann et al. 1987; Hasko and Richardson 1988; Slepecky et al. 1992; Thalmann 1993). Type V collagen is found in a reticular network of type B fibers (Steel 1980; Khalkhali-Ellis et al. 1987; Hasko and Richardson 1988; Prieto et al. 1990; Munyer and Schulte 1991; Slepecky et al. 1992; Sugiyama et al. 1992).

Water is the main component of the TM, and it probably forms an essential part of the fibrous network (95%, Naftalin 1976). The explanation for the loose-packed and dense-packed type B fibrils may be only because of the difference in their degree of hydration. The dry weight of TM consists of proteins and carbohydrates. Less than 3% of the total dry weight of the TM carbohydrates was found in the TM (Steel 1985). Approximately 20% of the dry weight of the TM is collagen and 15-20% is glycosaminoglycans. Both of these molecules contain ionizable charge groups (Thalmann et al. 1986; Richardson et al. 1987; Thalmann and Thalmann 1987; Thalmann 1993).

The molecular composition of the TM helps to determine the TM 's mechanical properties. Type II and IX collagen fibers in the TM are thought to contribute to its tensile strength and to resist stretch. There are fixed charges present on the matrix of TM, which may be associated with carbohydrate groups or the protein chains. These fixed charges will create a highly hydrated, loose gel matrix that resists compressive forces and controls the radial expansion and interaction of the collagens.

2.4 Permeability and electrical properties of TM

Based on the TM's molecular structure, a poly-electrolyte gel model (Weiss and Freeman 1997) was suggested to simplify our present knowledge of TM osmotic and electrical properties. Such gel consists of macromolecules with ionizable fixed charges, small solutes (including ions) and water. Many of the physicochemical properties of such a gel, including its volume, depend on the fixed charge concentration.

The TM is extremely sensitive to changes in its ionic environment (Kronester-Frei 1979; Freeman et al. 1994; Shah et al. 1995; Edge et al. 1998), which in turn lead to variation in its size, shape and structure. In an isolated TM preparation of the chick, replacing artificial endolymph by artificial perilymph caused a small and slow shrinkage (≈ 15%) of the thickness of the TM, which largely reversed on return to artificial endolymph, when the calcium concentration was held constant. The calcium concentration appears to be a major factor. The isolated TM of the mouse swells when the calcium concentration decreases below that normally found in the scala media (20 μM) and shrinks when the calcium concentration is increased. These results show that there is a possibility in the TM for the

selective binding of potassium, sodium, and calcium that can alter the fixed charge density of the tectorial membrane and cause shrinking and swelling.

The size and shape of the isolated mouse TM also change with different pH values of the surrounding artificial endolymph solution (Kronester-Frei 1979; Weiss and Freeman 1997). The TM swells in solutions with pH ≤ 6 or pH ≥ 9 (Weiss and Freeman 1997). Its thickness changes on the order of 1% for pH values of 7 to 9. There was little change in surface area. The thickness change decreased to a local minimum of -1% near pH 6, which is one isoelectric point (the pH level above which the substance would act as a base and below which it would act as an acid) of the TM, and reached a local maximum of 14% near pH 5.25. The radial dimension and area of the TM decreased rapidly in solution with low pH (<4), while the thickness of the TM increased transiently and then decreased. All these results suggested that the pH of the bath alters the state of ionization of charge groups in TM macromolecules.

Changing the ionic composition of the bath affected not only the thickness of the TM, but also it's other dimensions. Solution changes that increase TM thickness tend to cause radial shearing motions of the surface of the TM, which are accompanied by small decreases in width. The state of hydration of the TM depends on the composition of the bathing solution. Therefore, the mechanical properties may also depend on solution composition. Thus, solution induced changes in mechanical properties of the TM are likely to modulate the audio-frequency mechanical input to the hair bundles of hair cells (Shah et al. 1995).

The solution-induced changes in dimensions of the TM can have another effect on hair bundles – they can subject hair bundles to a static force, giving rise to a static displacement. The displacements of the TM that are effective in changing the responses of hair cells are radial displacement of the TM (von Bekesy 1960; Hudspeth and Corey 1977). The anisotropy of the TM tends to produce much smaller changes in dimensions in the radial than in the transverse (thickness) direction. Nevertheless, even relatively small radial displacement of the TM could have a large effect.

However, in a hemicochlea preparation of the Mongolian gerbil, ion substitution experiments suggested that no significant swelling or shrinking occurs when the

preparation is bathed in normal culture medium, keeping the calcium concentration at endolymph – like (20 μM) levels (Edge et al. 1998). The tectorial-reticular lamina relationship appears to remain well preserved. Hensen's stripe maintains a close relationship with the inner hair cell bundles.

2.5 Physical properties of TM

The volume of the TM is not known because there is no proper method to measure it without shrinkage or swelling with the changing of the bath solution. It presumably has a similar density *in vivo* to that of endolymph. Kraus (Kraus et al. 1973) suggested that the density of the fixed and sectioned TM decreases during development from 1.27 g/cm^3 in newborn guinea pigs to 1.11 g/cm^3 in old animals. But the density is not clear for unfixed TMs. The dry weight of guinea pig TM has been estimated to be 46 μg (Saito and Daly 1970), and that of the mouse TM is 2 μg (Steel 1980).

The physical characteristic of TM depends upon the fluid surrounding it. Zwislocki (Zwislocki 1988) claimed that for the Mongolian gerbil, there are no dramatic qualitative changes in TM mechanics within 45 min after death. The TM was about 35 μm thick at the experimental position he observed. The viscosity of the TM gradually increased in the postmortem preparations. Much bigger changes in the TM appearance and mechanical properties set in about one hour after death. In living Mongolian gerbils, the TM is highly compliant and resilient and has a relatively high tensile strength. Its viscosity is low. This result is consistent with the observations that Tonndorf et al (see review of Steel 1983) made on living guinea pigs that the TM shrunk and became more viscous when perilymph overflowed into the scala media in fresh preparation. The results are also consistent with the demonstration by I. Thalmann (Thalmann et al. 1986; Thalmann et al. 1987) that the TM consists to a large extent of collagen II fibers, which is the reason of its high tensile strength. The TM is highly compliant in all directions - radial, transversal, and longitudinal. Under natural conditions, the TM acts much more like a rubber band than a stiff board or a book cover.

The mechanical properties of the TM have been studied using mechanical probes, including hairs, needles, compliant glass pipette and magnetic beads. Pressing the tip of a small hair onto the surface of the TM was shown to generate a depression in the tissue that was long

and narrow, running radially across the TM (von Bekesy 1960). The shape of the depression suggests that the TM is mechanically more rigid in the radial direction than in the longitudinal direction. The elasticity of the TM was calculated to be 0.01 cm/dyne. Similar experiments with a needle vibrating at 200 Hz suggested that the TM was stiff at that frequency, but lacked resistive force for slow static displacement (von Bekesy 1960).

Zwislocki (Zwislocki and Cefaratti 1989) measured the transversal and radial stiffness of the TM *in vivo* in the second cochlear turn in Mongolian gerbils using a fine glass pipette. The pipette was inserted into the cochlea so that the TM could be deflected in the radial and transverse directions. The stiffness of the TM was found to be approximately 0.125 N/m and 0.116 N/m in the transversal and radial direction, respectively. Both are smaller by almost an order of magnitude than the corresponding aggregate stiffness of the OHC stereocilia (Strelioff and Flock 1984). As a consequence, the TM can't act as a stiff anchor for the stereocilia but only as a mass load, except at relatively low sound frequencies where mass effects are negligible.

Measurements have also been made of the isolated TMs of mice by applying oscillatory shear forces to the TM with magnetic beads whose dimensions were similar to those of hair cells. Forces with equal amplitude and phase were applied radially and longitudinally. The longitudinal displacement in response to longitudinal forces is 1-10 times as large as radial displacements in response to radial forces. This suggests that the TM is stiffer in the radial direction than in the longitudinal direction. The point stiffness of TM is 0.18 N/m. The magnitude of the displacements decreased when the stimulus frequency increased. Displacement of the adjacent tissue decreased as the distance from the magnetic bead increased. All these results suggest that both the viscous and elastic characteristics of the TM are important. The hair bundles could interact mechanically with adjacent hair bundles via the TM. The mechanical impedance is greater in the radial direction than it is in the longitudinal direction, which correlates with the radially oriented fibrillar structure of the TM (Abnet and Freeman 2000).

2.6 Development of TM

The tectorial membrane is formed of two distinct parts: the major (medial) and the minor (distal) parts (Lim and Anniko 1985). The major portion is produced by the cells of the

greater epithelial ridge prior to the formation of the minor part, which is produced largely by the primordial supporting cells of the lesser epithelial ridge. The radial fibers (found mainly in the major part) extend towards the lesser epithelial ridge and eventually cover the stereocilia bundles of the OHCs. The minor part of TM is composed of slanted fibers, which fuse with the extending radial fibers of the major TM and become the cover net. The marginal zone of the developing tectorial membrane is completely sealed during development by the third row of Deiters' cells. With the development going on, the TM loses its tight connection with all the underlying cells, its lower layer shrinks progressively, giving rise to Hensen's stripe (Lim 1980), while the marginal pillars appear to anchor the outer edge of the TM (Kraus and Aulbach-Kraus 1981).

2.7 Function of TM

The function of TM is poorly understood although the strategic position and its composition suggest that it play a key role in delivering sound stimuli to the hair cells. The

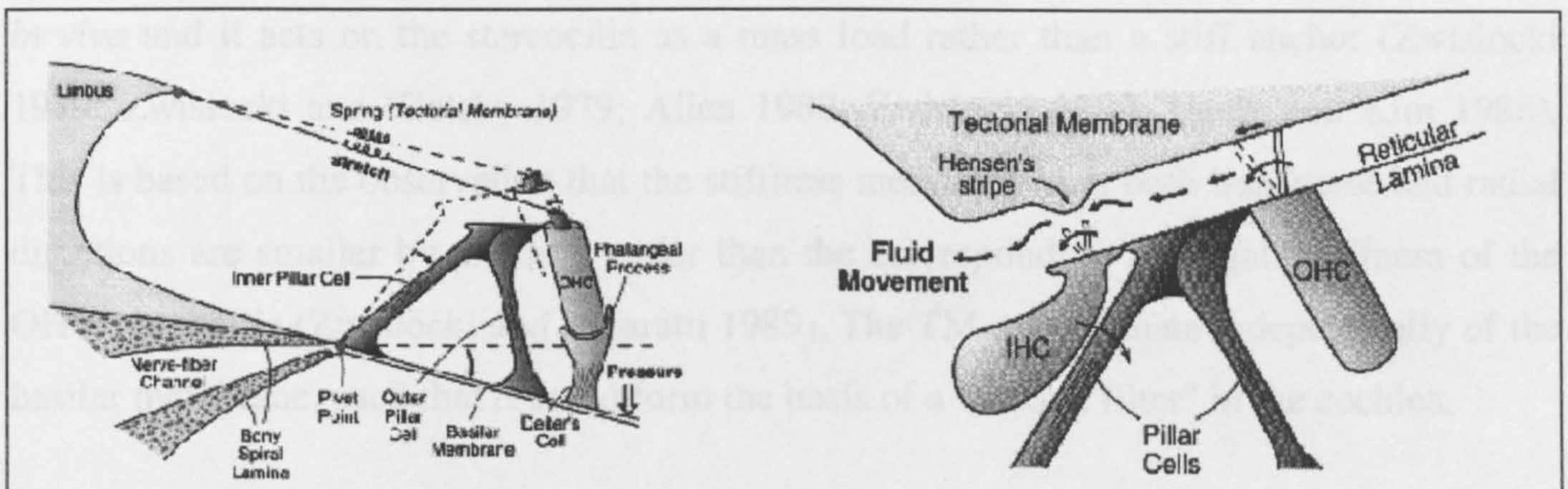

Figure 2-3 Schematic representation of TM mechanical function. The BM and TM rotate about different pivot points, leading to a shearing motion between the TM and the reticular lamina, as a result, deflecting the hair cells stereocilia (reprinted from Fig.6.7 and Fig. 6.8 of Geisler 1998).

TM is expected to be functional not only in providing the input to the mechanoelectrical transducer in hair-cell stereocilia, but also in providing an output load for the electromechanical transducers of the OHC membrane. Besides its mechanical role, Steel (Steel 1983) suggested that a major function of the TM is to control the chemical microenvironment of the stereocilia by sequestering ions from the endolymph. This function could be important for the transduction channels.

There are several conceptions of cochlear micromechanics. The classical model, suggested by ter Kuile (cited by von Bekesy 1960; Rhode and Geisler 1967), suggested that the TM is involved in converting the vertical movement of the basilar membrane into a radial shear displacement between the upper surface of the hair cells (reticular lamina) and the TM, which results in a shearing force and deflection of stereocilia (von Bekesy 1960). The BASILAR MEMBRANE and the TM are presumed to rotate about different pivot points (Figure 2-3): the BASILAR MEMBRANE pivots around the shelf of bone at its inner edge, and the tectorial membrane moves in cross-section like a stiff beam, rotating around the lip of the spiral limbus. This produces a shearing motion against the reticular lamina and, as a result, a radial deflection of the hair-cell stereocilia. The shearing motion between the TM and the reticular lamina occurs in proportion to the amplitude of the basilar membrane motion, and forms an essential step in the transduction process (see chapter 1). This view is widely accepted today and forms the basis of several models.

In contrast, more modern theories suggest that the tectorial membrane is a gel-like structure *in vivo* and it acts on the stereocilia as a mass load rather than a stiff anchor (Zwislocki 1979; Zwislocki and Kletsky 1979; Allen 1980; Zwislocki 1980; Neely and Kim 1986). This is based on the observation that the stiffness measured from both transverse and radial directions are smaller by almost a order than the corresponding aggregate stiffness of the OHC stereocilia (Zwislocki and Cefaratti 1989). The TM can resonate independently of the basilar membrane, such that it could form the basis of a "second filter" in the cochlea.

The TM is very difficult to observe, however: it is very thin, almost transparent, and highly susceptible to experimental manipulations. Very few experimental observations have been made showing how the TM responds to sound.

The first direct measurements comparing the sound induced vibration pattern of the TM with that of the reticular lamina were presented by Ulfendahl et al (Figure 2-4, Ulfendahl et al. 1995) using the guinea pig temporal bone preparation. The vibrations of beads attached firmly on the TM were compared with the vibrations of the reticular lamina. In most cases, the mechanical responses of the TM and the reticular lamina had the same characteristic frequency. The relatively wide optical access to the cochlear partition in the temporal bone

preparation allows mechanical measurement from different viewing angles. From these measurements, the two-dimension motion of the TM and reticular lamina were reconstructed. The magnitudes of the transversal and radial motion were very different. The TM moves essentially in an up-and-down fashion while the reticular lamina exhibits motion components in both transversal and radial directions. The combined motion of these two structures would result in a shearing motion. The shearing was produced predominantly by the radial motion of the reticular lamina, possibly controlled by the motor of the outer hair cells

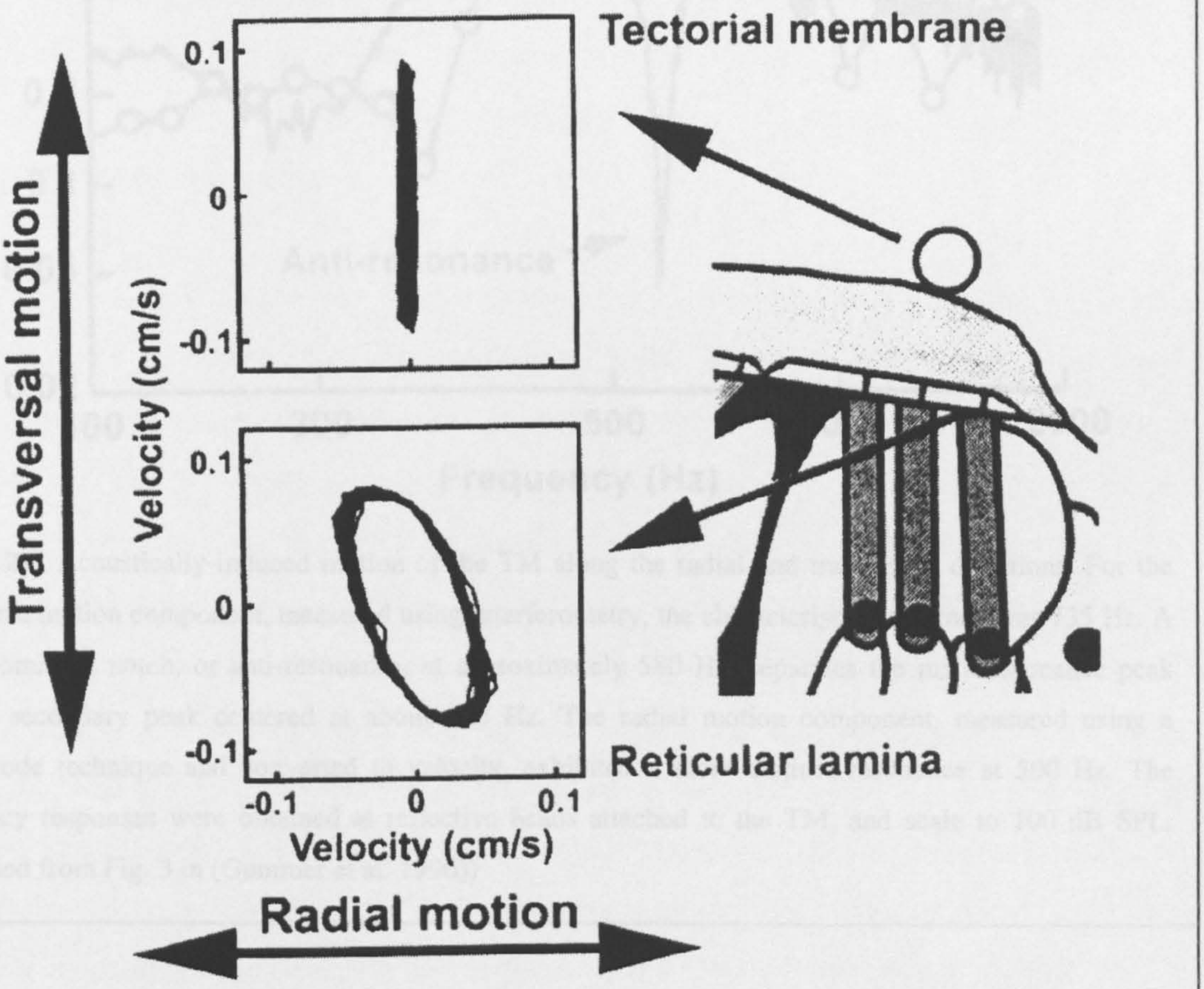

Figure 2-4 Two dimensional velocity components at the characteristic frequency for the TM and an outer hair cell at the reticular lamina directly below. The motion components were calculated from laser interferometric measurements made at three different viewing angles. (Reprinted from Fig. 24 Ulfendahl 1997).

In their experimental results, the tectorial membrane moves less than the hair bundles, which suggests these measurements do not support the notion that the tectorial membrane is a resonant structure.

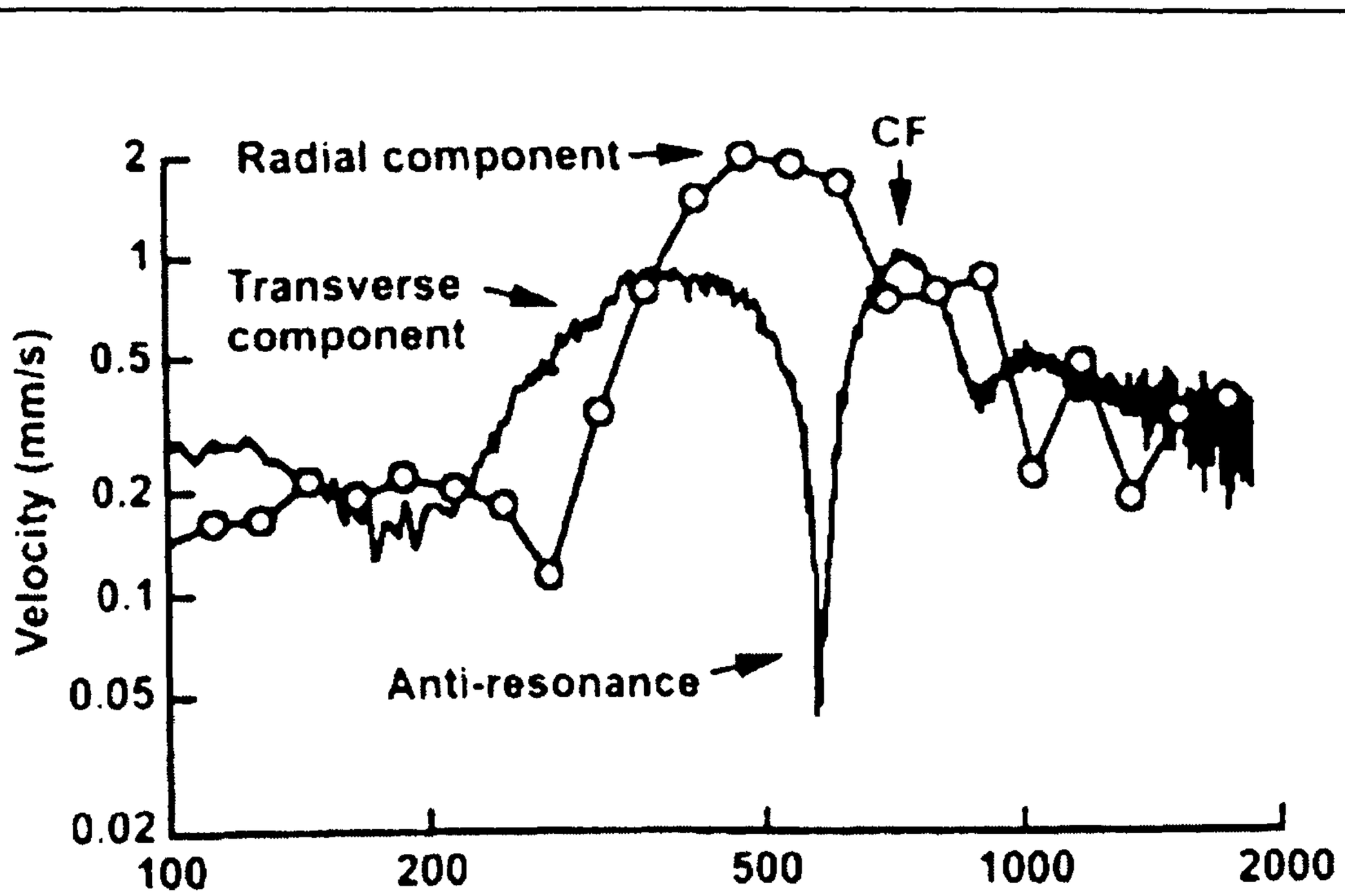

Figure 2-5 Acoustically-induced motion of the TM along the radial and transversal directions. For the transverse motion component, measured using interferometry, the characteristic frequency was 735 Hz. A very prominent notch, or anti-resonance, at approximately 580 Hz, separates the main resonance peak from a secondary peak centered at about 400 Hz. The radial motion component, measured using a photodiode technique and converted to velocity, exhibited a more distinct resonance at 500 Hz. The frequency responses were obtained at reflective beads attached to the TM, and scale to 100 dB SPL. (Modified from Fig. 3 in (Gummer et al. 1996))

Contrasting observations have been made by Gummer's group (Figure 2-5, Gummer et al. 1996) using a similar *in vitro* preparation. The vibrations of the TM were measured in two orthogonal directions by using a combination of laser interferometry (transversal, up-and-down direction) and a photodiode technique (radial motion). The results suggested that the TM resonates at a frequency of 0.5 octave below the characteristic frequency of the basilar membrane. The resonant motion of the TM is due to a parallel resonance between the mass

of the TM and the compliance of the stereocilia of the outer hair cells. Moreover, in combination with the contractile force of outer hair cells, it is proposed that inertial motion of the TM provides the necessary conditions to allow positive feedback of mechanical energy into the cochlear partition, thereby amplifying and tuning the cochlear response.

Further studies have been made by the same group by coupling the light of a laser Doppler vibrometer into the side arm of an epifluorescence microscope (Hemmert et al. 2000). This set-up allows the measurement from three mutually orthogonal directions. Displacements were measured in the orthogonal plane to the transversal direction from the fourth turn of a temporal bone preparation of the guinea pig cochlea. A second vibration mode was again detected in the motion of the TM. This vibration mode was directly parallel to the reticular lamina and became apparent for frequency above ~0.5oct below the characteristic frequency. The radial vibration mode presumably controls the shearing action of the hair bundles of the outer hair cells.

The mass and stiffness of the TM will determine its resonance properties. If the TM acts as second resonator and vibrates at a frequency that is half an octave below the characteristic frequency of the basilar membrane, at frequencies above its resonance, the mechanical impedance of the TM will be dominated by its mass. The TM's influence on the characteristic frequency of the basilar membrane will be dominated by the strength of the coupling between the TM and the organ of Corti. If the rotational stiffness of the hair bundles is about an order of magnitude less than that the radial stiffness of the TM (Strelioff and Flock 1984; Hemmert et al. 2000), the mechanical coupling between the radial motion of the TM and the basilar membrane is likely to be weak, therefore the TM should act as an inertial mass against which the hair bundles of the OHCs react (Gummer et al. 1996). In this case, the TM should not contribute toward the characteristic frequency of the basilar membrane. However, if the stiffness of the OHCs hair bundles and the TM are similar, the TM is expected to influence the characteristic frequency of the basilar membrane.

Recently, a targeted deletion in the mouse α-tectorin gene has been generated. The deletion results in mice with no functional TM (Legan et al. 1997; Legan et al. 2000). The outer hair cells still respond to sound in this animal model. Comparing with the wild animal, in

Tecta$^{\pm/\pm}$ mice, the basilar membrane vibration still shows some tuning, presumably reflecting the passive mechanical resonance of the basilar membrane. The characteristic frequency is the same as expected, so that the passive tuning seems not to depend on the mass and stiffness of the TM. However, the amplification and the very sharp tuning at low sound levels disappeared. The movement with increasing sound level is nearly linear and it changes little after sacrificing the animal. In this case, without the TM, the stereocilia of outer hair cells are obviously moved by the fluid drag, which does not provide sufficient coupling. Therefore, deflection of the stereocilia of OHCs by the TM is a critical step in the amplification in the cochlea. The TM acts as an inertial mass and is a structure against which the OHC hair bundles can react. It ensures the forces from OHC feedback are delivered with optimal gain and at the appropriate time in each cycle of BASILAR MEMBRANE displacement. It may also be required for the compression observed in the responses of the cochlea and hence the broad dynamic range of the system.

Because of the technical difficulties in making a direct approach to measuring the mechanical responses of the TM and the difficulties in maintaining the cochlea and TM in 'normal' conditions, different animal models and techniques have been used to investigate the function of the TM so far. However, experimental evidence on the function of TM is still sparse and inconclusive, especially *in vivo*.

The aim of this thesis is to investigate the role of the tectorial membrane in cochlear mechanics *in vivo* – whether the TM resonates to a second filter inside the cochlea or not. Very sensitive, linear and reliable heterodyne laser interferometry will be used to detect the sound-evoked vibration of the tectorial membrane. A three-dimensional reconstruction technique will be developed using the interferometer system combined with a two-axis goniometer, which detects vibration in three orthogonal directions. During the direct approach to the TM, a complete audiogram will be used to monitor the cochlear condition. Moreover, a mechanical sealing of the opening of the cochlea will be performed in order to reduce the artifacts. The responses of the TM will be compared with those of Hensen's cell before and after rupturing Reissner's membrane so that a whole picture of the cochlear mechanics can also be achieved in the study.

Chapter 3 Methods

3.1 Stimulus generation and control

The experimental stimuli used in this study included short series of tone pips and clicks. These were generated by a 16-bit digital-to-analog converter and attenuated by programmable attenuators as shown in Fig. 3-1. The attenuated signals were delivered to a reverse driven condenser microphone cartridge (Bruel & Kjaer model 4134).

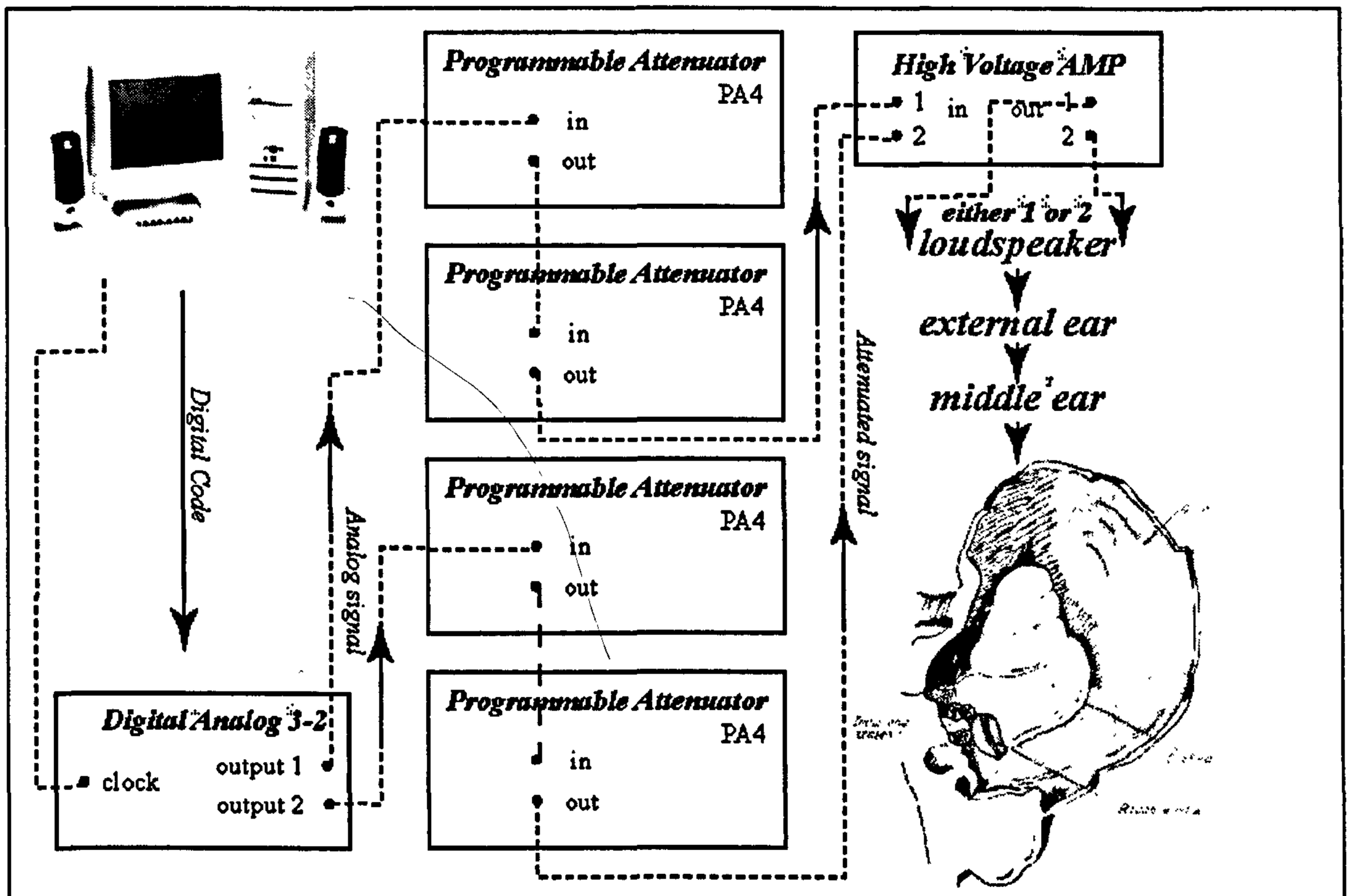

Figure 3-1 Schematic representation of the sound generation system. The digital codes from the computer are converted into voltage signals by the digital to analog converter before being attenuated in programmable attenuators. The attenuated signals are amplified before going into the ear. (Picture of guinea pig cochlea was reprinted from von Bekesy 1960).

In the experiment, the dissected ear canal was firmly sealed to the closed-field acoustic system, so that the sound stimuli could be transferred to the eardrum. The stimuli were pre-compensated to negate the transducer's square-law non-linearity. The stimuli were

calibrated within 3 mm of the eardrum using a condenser microphone with a 1 mm diameter probe tube. All experiments were performed on a vibration-isolated workstation (Newport) in a soundproof room (IAC).

The sound calibrations were performed by presenting short tones at increasing frequencies, sampling the output of a microphone, which senses the pressure near the eardrum of the subject, and averaging the responses at each frequency. After all the frequencies had been presented, the acoustic transfer function was calculated (the microphone and probe tube had been calibrated previously so that the number of dB SPL per Volt at the input to the analog and digital converter was known). The calibrations were performed from 50 to 20,000 Hz in 0.125 octave steps. The resulting amplitude plots correspond to the sound pressure levels (dB relates to 20 μPa) for signals at 0 dB attenuation. The calibration curves were stored in the computer for use in the data collection process (so that the amplitudes of the stimuli could be corrected for the phone characteristic).

The acoustic stimuli for the cochlear mechanical parts of the experiments were pure tone pips and clicks (rarefaction and condensation), generated by the equipment described above. The sinusoidal stimuli ranged from 50 to 3000 Hz in steps of 0.125 octaves. The responses to the tone pips were recorded in bursts of 6000 samples at 8 or 10 μs intervals and averaged 100 times. The intensity and frequency of the stimuli were varied when necessary. Normally, the duration of the pure tone pips were 50 ms with rise/fall periods at the onsets and offsets of 5 ms. Clicks (rarefaction and condensation) were used for their wide-band characteristic and precise time tracing of the system's responses. The responses to the clicks were recorded using 2048 or 4096 samples at 8 μs intervals, and averaged across 250 stimulus presentations. The duration of each click was (normally) 0.1 ms.

3.2 Data Analysis

Off-line data analysis was performed in MATLAB version 6.1.

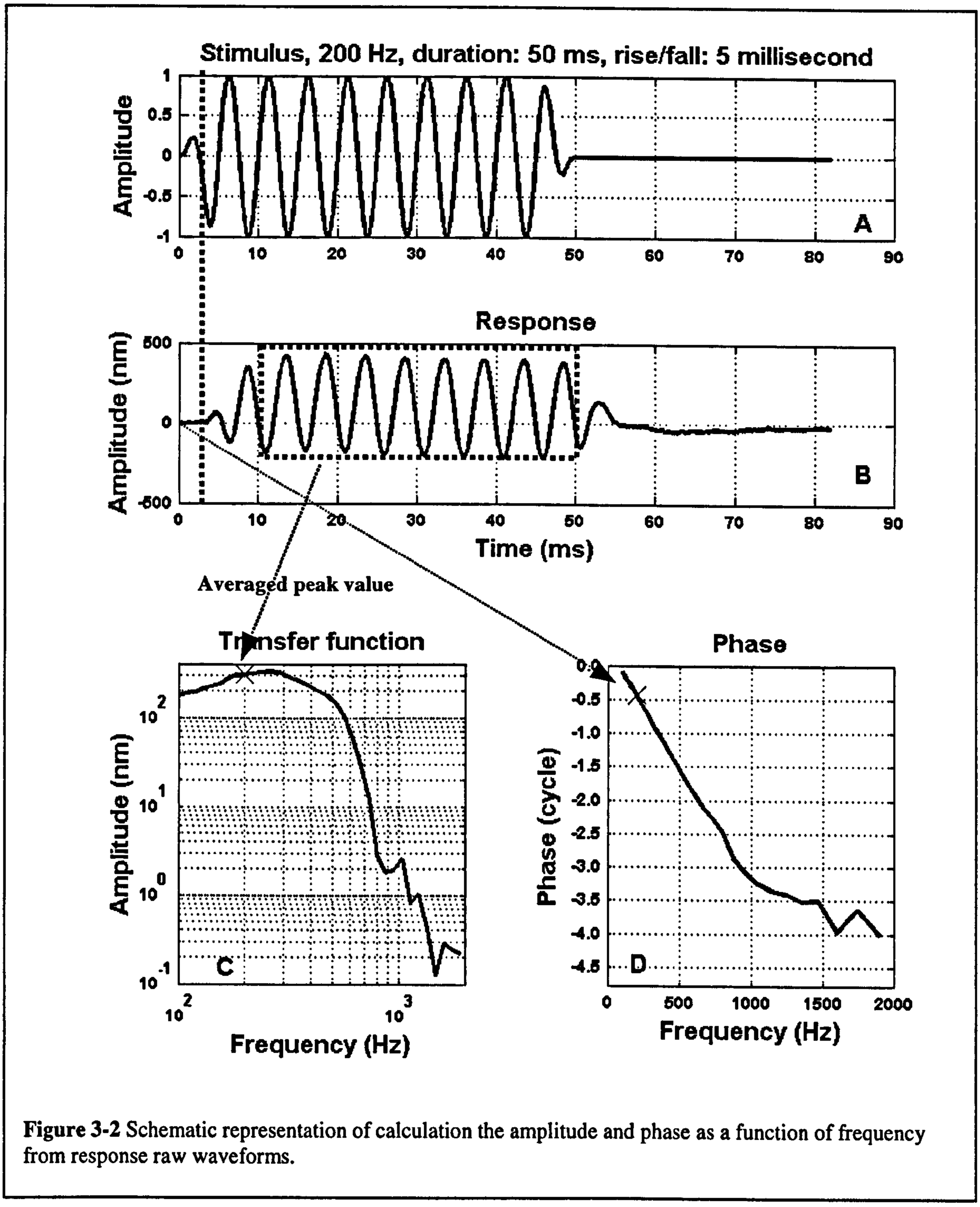

Figure 3-2 Schematic representation of calculation the amplitude and phase as a function of frequency from response raw waveforms.

3.2.1 Analysis of tone-evoked responses

3.2.1.1 Transfer functions

Transfer functions provide a way to illustrate frequency selectivity in hearing research. They provide information on the amplitude and phase of a response at particular stimulus frequencies and sound pressure level. Fig. 3-2 illustrates the general idea used in an experiment to calculate the vibration amplitude and phase from the raw response waveform. As an example, Fig. 3-2A shows the waveform of a 200 Hz stimulus used in the experiment. The stimulus is a tone pip with a duration of 50 ms and a rise/fall time of 5 milliseconds. The tone pips were delivered to the cochlea through the ear canal and the middle ear at a certain sound pressure level. The response waveform of the cochlear partition was recorded in bursts of 6000 or 8192 samples at 10 or 8 μs intervals and averaged 100 times (Fig. 3-2B). After that, the waveform of the response was compared with a fixed frequency sinusoid whose amplitude and phase could be varied (the frequency was always fixed at the stimulus frequency). The averaged peak-to-peak value of the best-fitting sinusoid was evaluated between 0 and 50 ms and appears in the transfer function curve as shown by the cross in Fig. 3-2C. The phase of the best-fitting sinusoid was plotted in the phase curve as the cross shows in Fig. 3-2D. Repeating this procedure frequency by frequency, the amplitude and phase of transfer functions were calculated as a function of stimulus frequency.

3.2.1.2 Input-output functions

If the responses were collected at different sound pressure levels, but at a fixed frequency, then a curve, which plots the response amplitude as a function of input sound pressure level was calculated. This curve is known as an input-output function.

3.2.2 Analysis of click-evoked responses

3.2.2.1 Splitting fast and slow waves of click responses in time domain

Responses to rarefaction and condensation clicks contain two parts in the time domain as shown in Fig. 3-3A (Cooper and Rhode 1996). The first part was initiated almost instantaneously and possibly caused by reflection from the cochlear opening in scala vestibuli of the 'fast' fluid pressure wave which travels at the speed of sound. The second

part shares the feature of a traveling wave, which was named the 'slow' wave. The `slow' and `fast' waves can interfere destructively to produce deep notches in the total vibration response. Cooper and Rhode (Cooper 1996; Cooper and Rhode 1996) concluded that the vibration response in the apical turn of the guinea-pig cochlea is contaminated by the fast response.

Based on further experimental observation of this phenomenon from the vibration reponses of the apical turn of the cochlea. The 'slow' travelling-wave component was separated from the 'fast' response component in the time domain by multiplying the responses by a window function (Fig. 3-3B). The window function is a typical cosine-rise function, similar to that used by Hemmert (Hemmert et al. 2000). This window is better than rectangular window because it reduces truncation artifacts.

In our approach, the window function to isolate the 'slow' component is

$$y = \begin{cases} 0 & t < t_0 - 0.5\ ms \\ \cos^2(x), & 0 \le x \le \pi/2,\quad t_0 - 0.5\,ms \le t \le t_0 + 0.5\,ms \\ 1 & t > t_0 + 0.5\,ms \end{cases}$$

$$t_0 = 1.8\,ms \qquad (1)$$

where t_0 is the dividing time between 'fast' and 'slow' components. The value of t_0 may vary with different cochlear sealing conditions and it did not make significant change to the results between 1.0 to 2.5ms. In the example of Fig. 3-3, t_0 is 1.8 ms. the 'fast' component equals the raw response minus the 'slow' component. Reconstructed 'slow' and 'fast' components are plotted in Fig. 3-3C and D.

3.2.2.2Fourier Transformation

Fast Fourier transform (FFT) were used to analyze the responses in the frequency domain. To normalize a cochlear response by a middle ear impulse response, the FFT amplitude of a cochlear response is divided by the FFT amplitude of the middle ear of the same preparation. The normalized phase is the FFT phase difference between the cochlear partition and the middle ear responses.

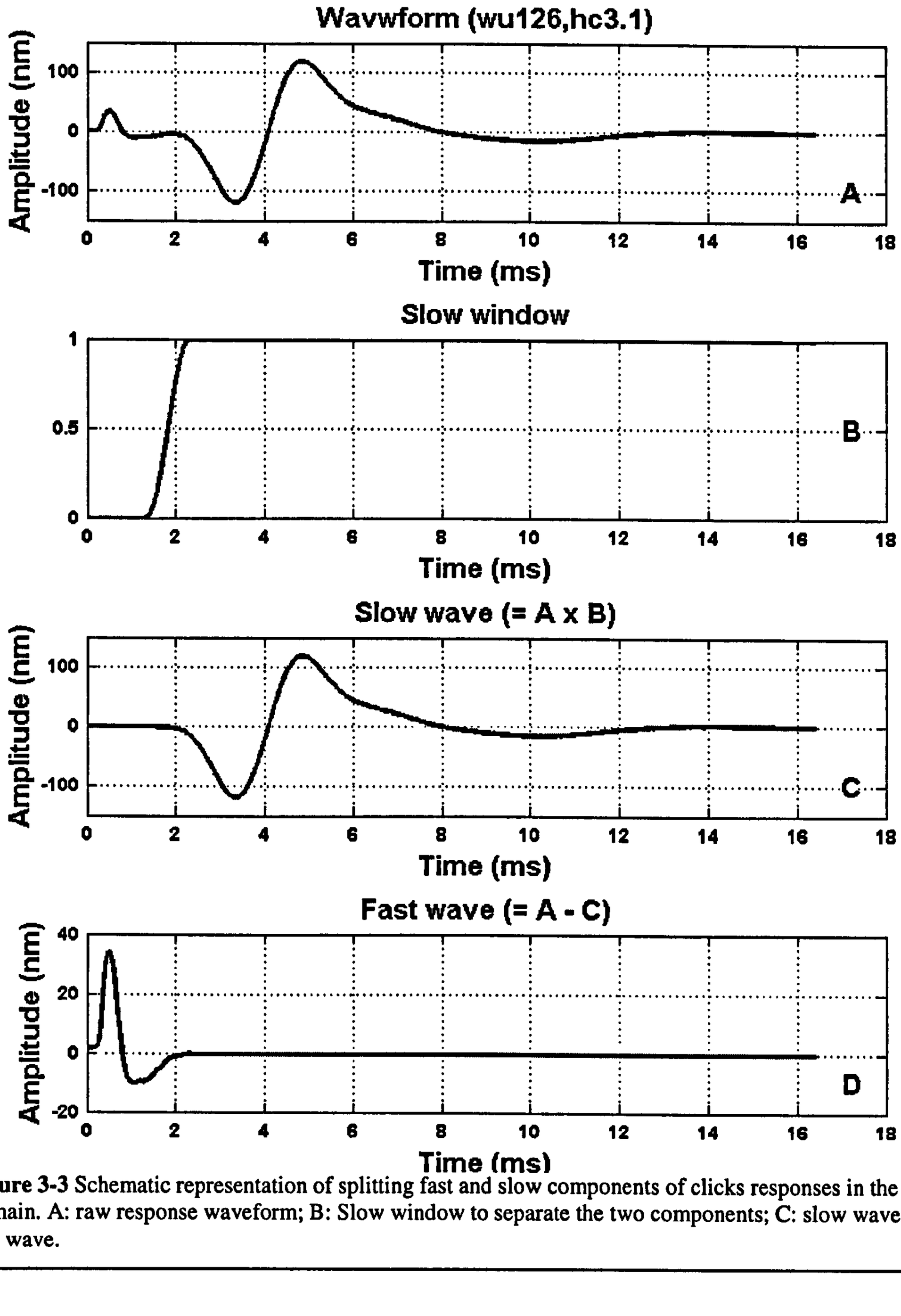

Figure 3-3 Schematic representation of splitting fast and slow components of clicks responses in the time domain. A: raw response waveform; B: Slow window to separate the two components; C: slow wave; D: fast wave.

3.3 Animal model

3.3.1 Preparation of the animal

128 guinea pigs of 320 to 800 g were used in this study. Nearly 90 animals were used in *post mortem* studies directly. General anesthesia was induced by a combination of sodium pentobarbitone (Sigma) and Hypnorm (Janssen). Initially, sodium pentobarbitone was injected intraperitoneally (30 mg/kg of body weight). It was freshly prepared in 1 ml physiological saline from powder to avoid the toxic effects of the preservatives employed in many veterinary preparations of this drug. Atropine (C-Vet, 0.01mg/kg body weight) was then administered subcutaneously, to minimize the volume of bronchial and salivary secretions. This is necessary because the relatively narrow airways of guinea pigs are prone to obstruction. Hypnorm (fluanisone 10 mg/ml and fentanyl 0·315 mg/ml) was then injected intramuscularly, at a dose of 0·6 ml kg^{-1}, to produce additional sedation and analgesia.

Further doses of sodium pentobarbitone (1/3 of the original dose) were given every 2-3 hours and additional doses of Hypnorm were given as needed (usually around once every hour) to maintain deep anaesthesia. The pedal withdrawal reflex was used to assess the depth of anaesthesia. Lethal overdoses of sodium pentobarbitone were given on completion of the *in vivo* measurements.

The core temperature of the animal was monitored using a rectal probe thermometer and was maintained at 37-38 °C using a thermostatic heating blanket.

The trachea was exposed, divided, and cannulated with a 6-7 mm long plastic T-tube. Following cannulation, the guinea pig was artificially ventilated. End-tidal CO_2 concentration was monitored and maintained at 4.5% by adjusting the stroke-volume of the ventilator.

The care and use of the animals reported in this study were approved by the Animal Care and Use Committee of the University of Bristol.

3.3.2 Preparation of the ear

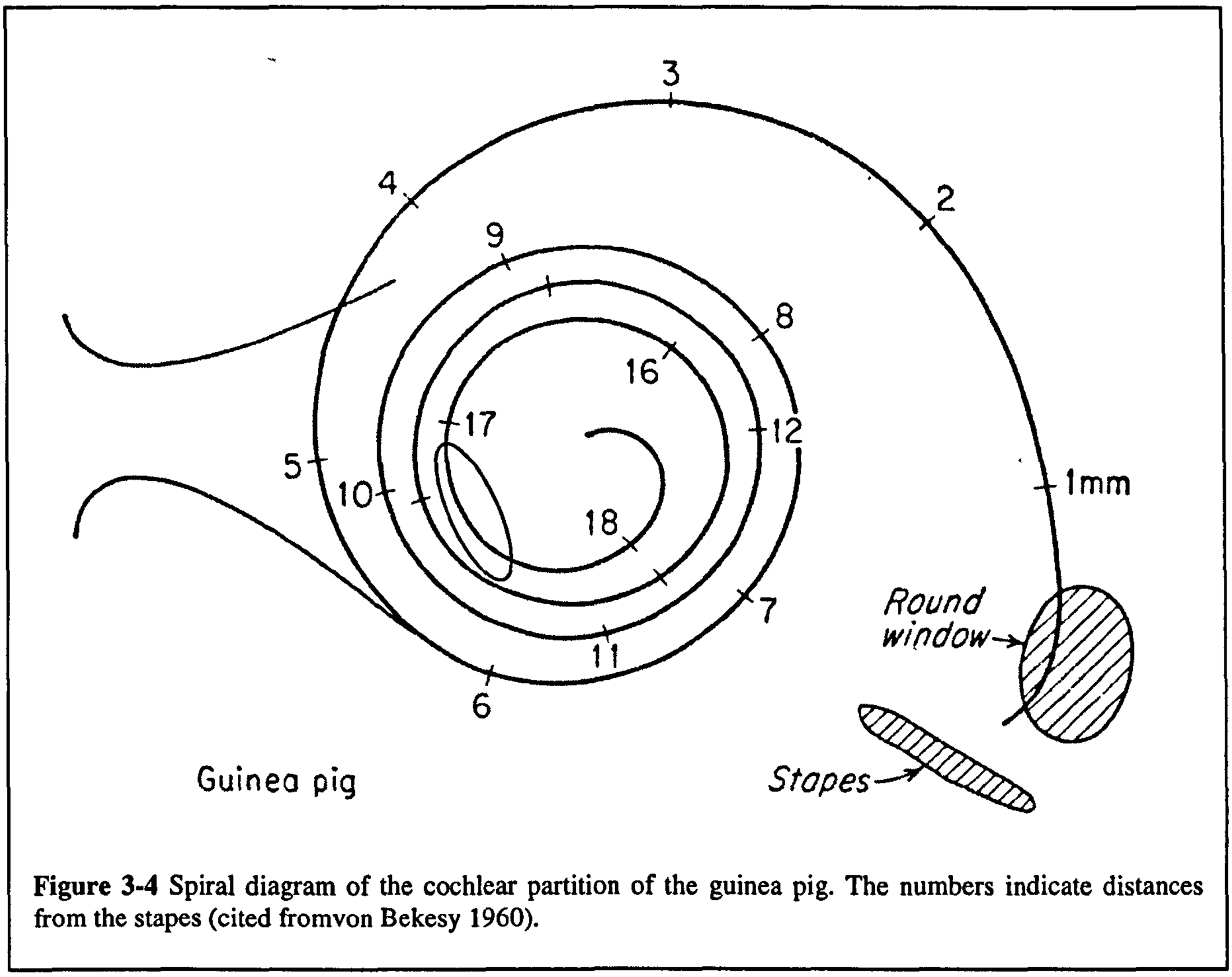

Figure 3-4 Spiral diagram of the cochlear partition of the guinea pig. The numbers indicate distances from the stapes (cited fromvon Bekesy 1960).

The right pinna was removed, taking care not to damage the auricular arteries underneath it. Only a short (~2 mm) length of the external auditory meatus was left. Any detritus covering the tympanic membrane was removed under microscopic observation. The closed-field sound-delivery system described in section 3.1 was inserted into the meatal opening and sealed using sticky wax.

In order to expose the bulla from the ventral side, the masseter and digastric muscle were removed together with one-third of the jaw. The mandibular labial branch of the facial artery, branches of salivary glands and lymph nodes, caudal auricular, lingual, facial and occipital arteries were ligated to prevent excessive blood-loss.

The skull was fixed into a combined head-holder and ear-piece using two small bone-screws and ample hard-setting dental cement (Redifast, powder and liquid, Wright). The

ventral aspect of the bulla was opened widely to permit different views of the cochlea and ossicles. A small metallic chamber was built around the apical cochlea to allow the cochlea to be resealed (after the initial opening). A small hole (~ 600 x 800 µm) was made to access the scala vestibuli in the apical turn of the cochlea. The hole was made with care to avoid breaking the helicotrema and the Reissner's membrane at the site of 17.5 mm away from the stapes as the ellipse shown in Fig. 3-4.

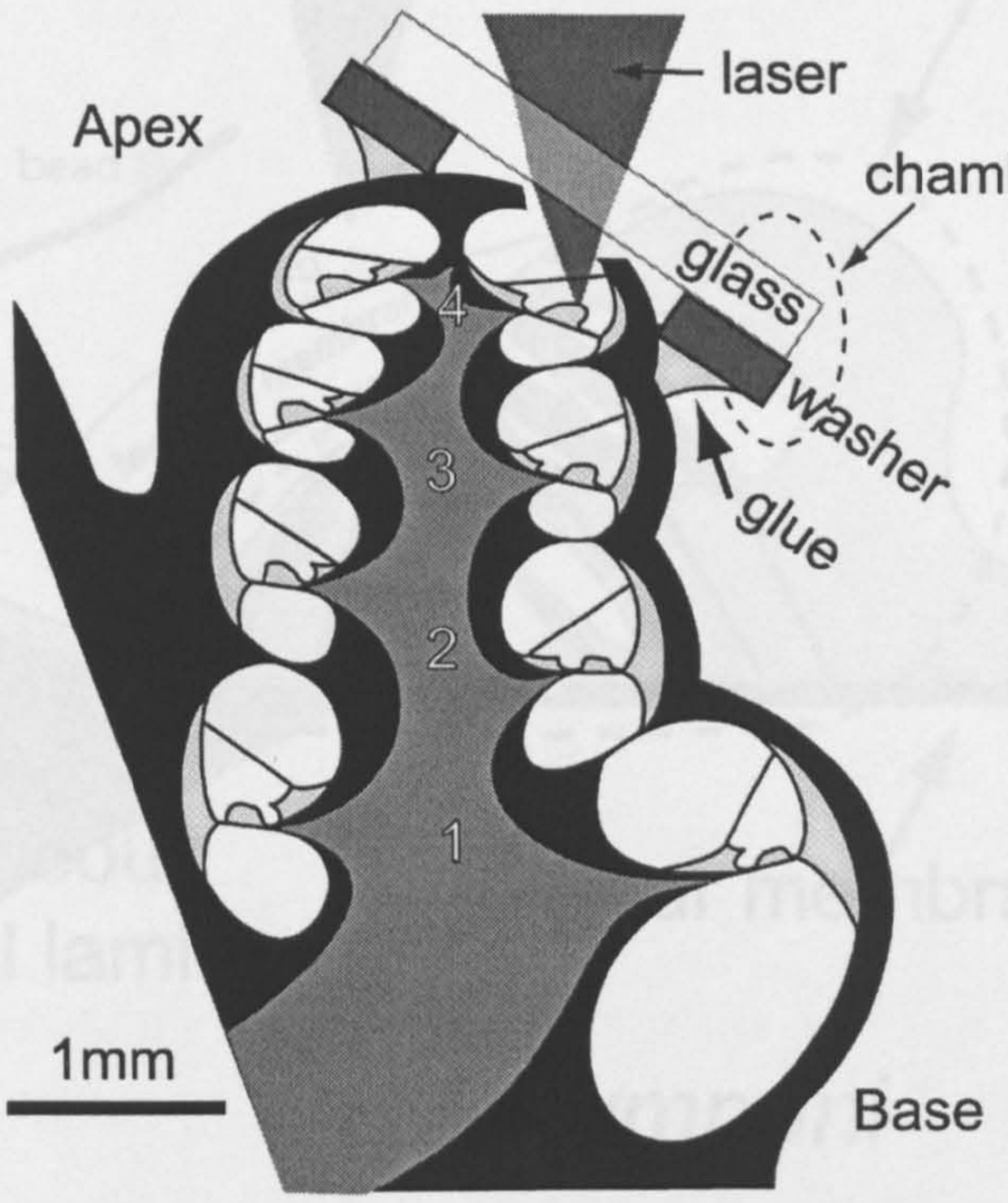

Figure 3-5 Schematic representation of the preparation of the cochlea. 1, 2, 3 and 4 show the four turns of the guinea pig cochlea. The initial opening of the cochlea was resealed using a glass coverslip and high-vacuum grease. Measurements were made from sealed and unsealed cochleae (diagram prepared by N. Cooper).

The initial opening of the cochlea was resealed using a glass coverslip and high-vacuum grease (DOW CORNING GMBH, see Fig. 3-5). Measurements were made from sealed and unsealed cochleae. In the sealed condition, the glass coverslip was firmly attached to the support chamber by high-vacuum grease. Care was taken to prevent air bubbles from being trapped inside the sealed cochlea. In contrast, when the cochlea was unsealed, there was no tight connection between the coverslip and the grease with the result that fluid escaped from the apical cochlea.

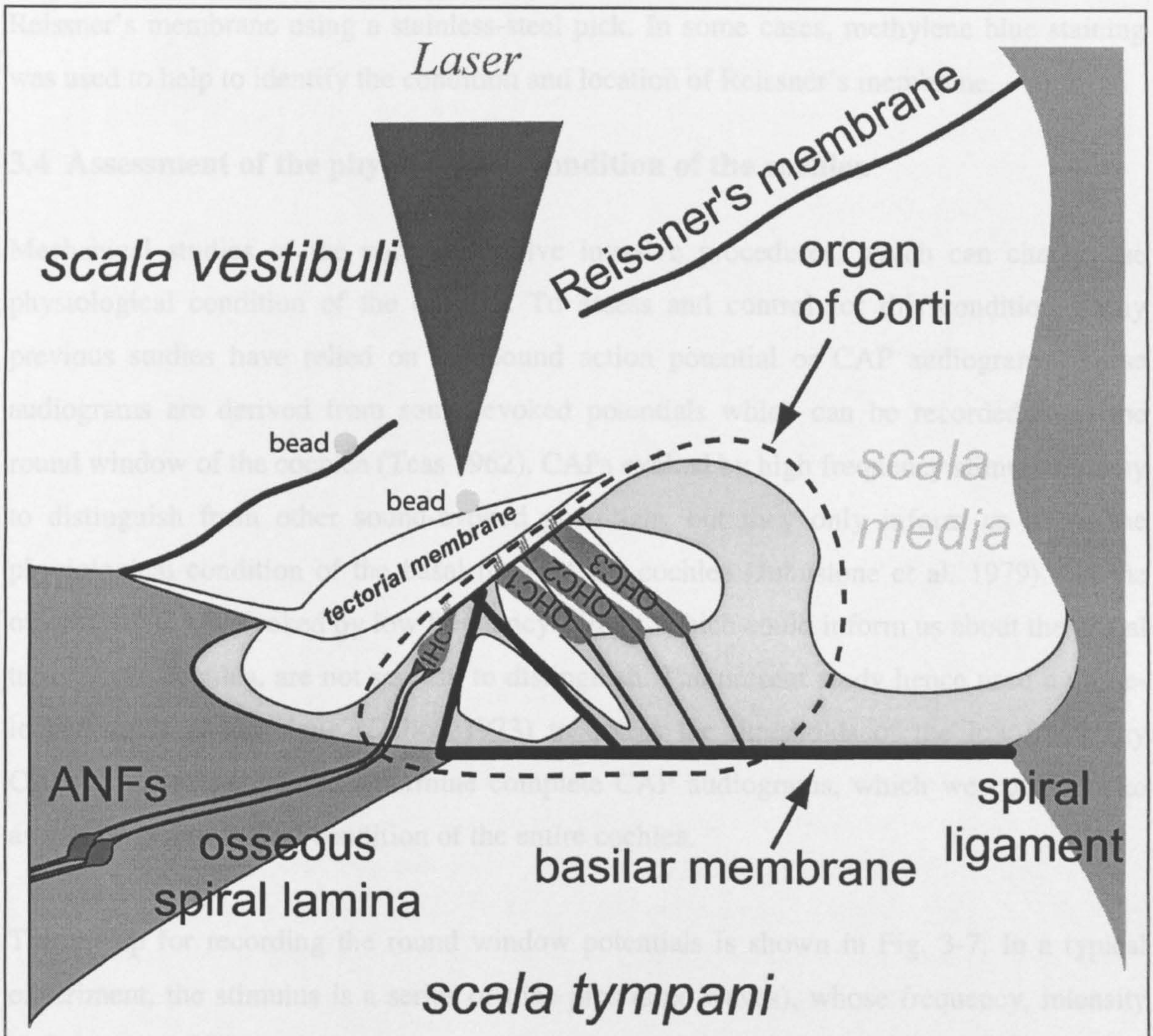

Figure 3-6 Schematic representation of preparation of organ of Corti. Sound evoked responses were collected either from the lipid droplet of a single shining Hensen's Cell or from single gold-coated polystyrene microbeads which had settled on the cochlea partition (on RM when the RM was intact and on the TM when the RM was torn). (Modified from original diagram prepared by N.P. Cooper.)

Sound evoked responses were recorded either from the lipid droplets in a single Hensen's Cell or from single gold-coated polystyrene microbeads which had settled on the cochlear partition with or without tearing the Reissner's membrane (Fig. 3-6). The microbeads had similar density to water (25 μm diameter, 1.05 g/cm^3; Polysciences Inc.). Because most of the cochlear partitions under study are transparent, reflective gold-coated beads are used to provide the high reflectivity demanded by our displacement measurement technique. The

reflective gold-coated beads were introduced into the scala media through a small tear in Reissner's membrane using a stainless-steel pick. In some cases, methylene blue staining was used to help to identify the condition and location of Reissner's membrane.

3.4 Assessment of the physiological condition of the cochlea

Mechanical studies of the cochlea involve invasive procedures, which can change the physiological condition of the cochlea. To assess and control for this condition, many previous studies have relied on compound action potential or CAP audiograms. These audiograms are derived from sound-evoked potentials which can be recorded from the round window of the cochlea (Teas 1962). CAPs evoked by high frequency stimuli are easy to distinguish from other sound-evoked potentials, but they only inform us about the physiological condition of the basal turns of the cochlea (Johnstone et al. 1979). On the other hand, CAPs evoked by low frequency stimuli, which could inform us about the apical turns of the cochlea, are not so easy to distinguish. The present study hence used a phase-locked analysis technique (Dallos 1973) to assess the thresholds of the low-frequency CAPs. This allowed us to determine complete CAP audiograms, which we could use to assess the physiological condition of the entire cochlea.

The set up for recording the round window potentials is shown in Fig. 3-7. In a typical experiment, the stimulus is a series of tone pips (sine waves), whose frequency, intensity and phase could be varied. A silver-wire electrode was placed on the bony niche near the round window of the cochlea to pick up the evoked response, while the reference and ground electrodes were attached to the neck muscle. The sound evoked responses passed through a CAP amplifier headstage, with a gain of 10 times, and were further amplified by an AC pre-amplifier (gain = 100), which acts as a buffer. The electrical noise level was reduced by filtering the signal between 100 and 10000 Hz. The responses were viewed on an oscilloscope as well as being sampled via the A/D (analog to digital) converter, fed back to the computer, and displayed on the screen. Signal averaging (100 times) was usually necessary to further reduce the effects of background electronic noise.

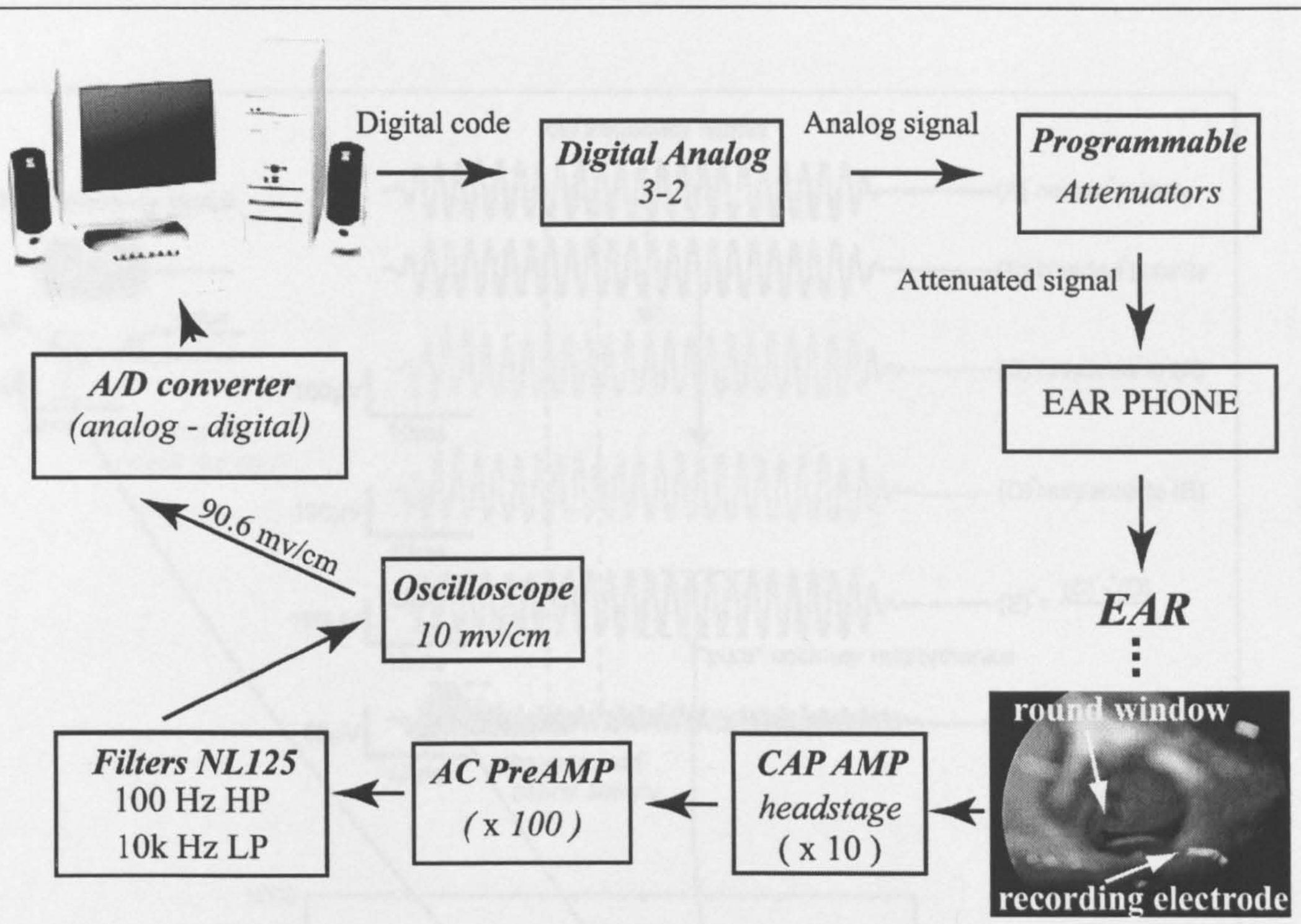

Figure 3-7 Schematic representation of experimental setup for recording round window potentials. The digital signals from the computer are converted into voltage signals by a digital to analog converter before being attenuated in programmable attenuators. The attenuated signals are amplified before going into the ear. A silver-wire electrode was placed on the bony niche near the round window of the cochlea to pick up the sound evoked response, while the reference and ground electrodes were attached to the neck muscle. The sound evoked responses passed through a CAP amplifier headstage, with a gain of 10 times, and were further amplified by an AC pre-amplifier (gain = 100), which acts as a buffer. The noise was reduced by filtering the signal between 100 and 10000 Hz. The responses were viewed on an oscilloscope as well as being sampled via the A/D (analog to digital) converter, fed back to the computer, and displayed on the screen.

CAP audiograms were measured at four key points during the experiments: (a) following minimal surgery, (b) after more extensive surgery, as needed to expose the apical aspects of the cochlea, (c) after shaving a hole into the apical turn of cochlea, and (d) after tearing Reissner's membrane and placing several reflective microbeads on the apical cochlear partition.

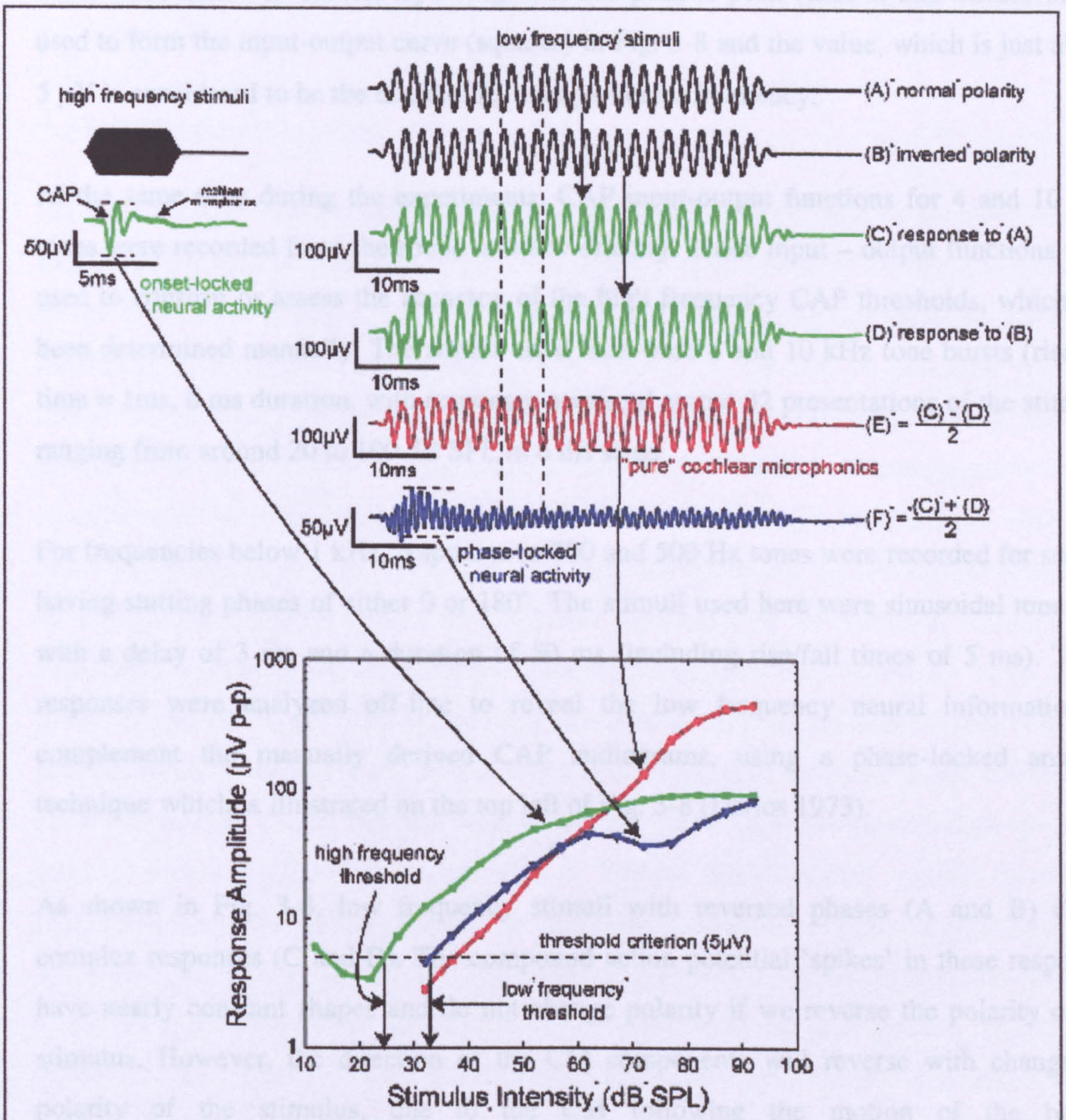

Figure 3-8 Schematic representation of CAP recording. Top left: high frequency (10 kHz) stimulus and response waveform. Top right: 500 Hz stimuli with normal and 'reverse' polarity (A and B), and responses to these two stimuli (C and D). Derived pure microphonics from the raw responses (E) and phase-locked neural activity waveform (F). Bottom: squares indicate peak-to-peak values of high frequency CAP responses plotted as a function of sound pressure level; Circles show the I/O curve of the pure cochlear microphonic; triangle stands for biggest peak values derived from phase-locked of neural activities as a function of sound pressure level. Dotted line is the arbitrarily set threshold criterion of 5 μV.

For frequencies between 2 k and 20 kHz, the CAP audiogram was determined manually, by determining the SPL of the tones necessary to evoke a just noticeable CAP waveform on the computer screen. In this procedure, the intensities were varied in 1 dB steps under all

the physiological conditions concerned in the experiment. The form of the CAP waveforms observed is shown on the left top of Fig. 3-8. The peak-to-peak value of this waveform was used to form the input-output curve (squares) in Fig. 3-8 and the value, which is just above 5 μV is considered to be the threshold at that particular frequency.

At the same time during the experiments, CAP input-output functions for 4 and 10 kHz tones were recorded from the round window directly. These input – output functions were used to confirm or assess the accuracy of the high frequency CAP thresholds, which had been determined manually. The stimuli used here were 4 and 10 kHz tone bursts (rise/fall time = 1ms, 6 ms duration, with responses averaged across 32 presentations of the stimuli), ranging from around 20 to 100 dB SPL in 6 dB steps.

For frequencies below 1 kHz, responses to 300 and 500 Hz tones were recorded for stimuli having starting phases of either 0 or 180°. The stimuli used here were sinusoidal tone pips with a delay of 3 ms and a duration of 50 ms (including rise/fall times of 5 ms). These responses were analyzed off-line to reveal the low frequency neural information to complement the manually derived CAP audiograms, using a phase-locked analysis technique which is illustrated on the top left of Fig. 3-8 (Dallos 1973).

As shown in Fig. 3-8, low frequency stimuli with reversed phases (A and B) evoke complex responses (C and D). The compound action potential 'spikes' in these responses have nearly constant shapes and do not change polarity if we reverse the polarity of the stimulus. However, the direction of the CM components will reverse with changes in polarity of the stimulus, due to the CM following the motion of the basilar membrane(Dallos et al. 1974). Therefore, by subtraction of the "negative" response from the "positive" response, the action potentials are attenuated but the CM is left (Fig. 3-8 E). Calculating the average peak-to-peak value at each sound pressure level, the input-output function for the cochlear microphonic was derived and is plotted as the circles in the bottom panel of Fig. 3-8. By summing the reversed polarity round window potentials, the neural activities could be derived from the round window potentials (Fig. 3-8 F). The biggest peak value of these derived potentials was calculated and is plotted as a function of sound pressure level (triangles in the bottom of Fig. 3-8). The arbitrarily set threshold

criterion of 5 μV is plotted as a dotted line in the figure. The SPL value with its I/O curve just above 5 μV was considered as the CAP threshold at this frequency (see the arrows in Fig. 3-8).

3.5 Interferometer system

All the techniques used to investigate cochlear mechanics must first be sensitive, that is, their response must be sufficient so that mechanical displacements of the organ of Corti can be resolved above the noise, which is inherent in every measuring technique. Secondly, the measuring device must be physically very small, or capable of precisely localized measurement. This is because the cochlea is difficult to approach anatomically, and it is accessible at only a very limited number of places. Thirdly, measurements must be insensitive to the inescapable variations in animal-to-measuring-device distance which are caused by the animal's own physiology and by room vibrations. So far, several techniques have been successfully applied to study the mechanics of the cochlea, including the Mössbauer technique, capacitive probes and interferometers (see review by Yates 1979). Since the late 1960s, the most widely used technique in cochlear mechanical studies is laser interferometry (Dragsten et al. 1976; Khanna et al. 1989). The technique is not essentially a laser technique at all, but benefits greatly from the advantages that the coherent, spectrally pure, low-noise light source brings with it. Various interferometry systems have been designed to study the auditory mechanism and many of them are still in use today (Ruggero and Rich 1991; Cooper and Rhode 1992; Kossl and Russell 1995; Mammano and Ashmore 1995; O'Neill and Bearden 1995). The most sensitive, linear and reliable technique is heterodyne laser interferometry, which was first described by Willemin et al. (Willemin et al. 1988).

A displacement sensitive heterodyne laser interferometer system is used in our laboratory. The layout of this interferometer is shown in Fig. 3-9 (Cooper 1999). The technique is essentially a phase modulation technique whereby path length between the light source and a detector is varied by the vibrations of the object under study. An interference-induced modulation of the light beam entering the detector is obtained by combining two target beams. The reference beam travels a fixed optical path. The objective beam passes through the working path, phase modulated by the object displacement under study. The phase

difference between the two components of light is used to estimate the instantaneous displacement of the object with respect to an arbitrary reference point.

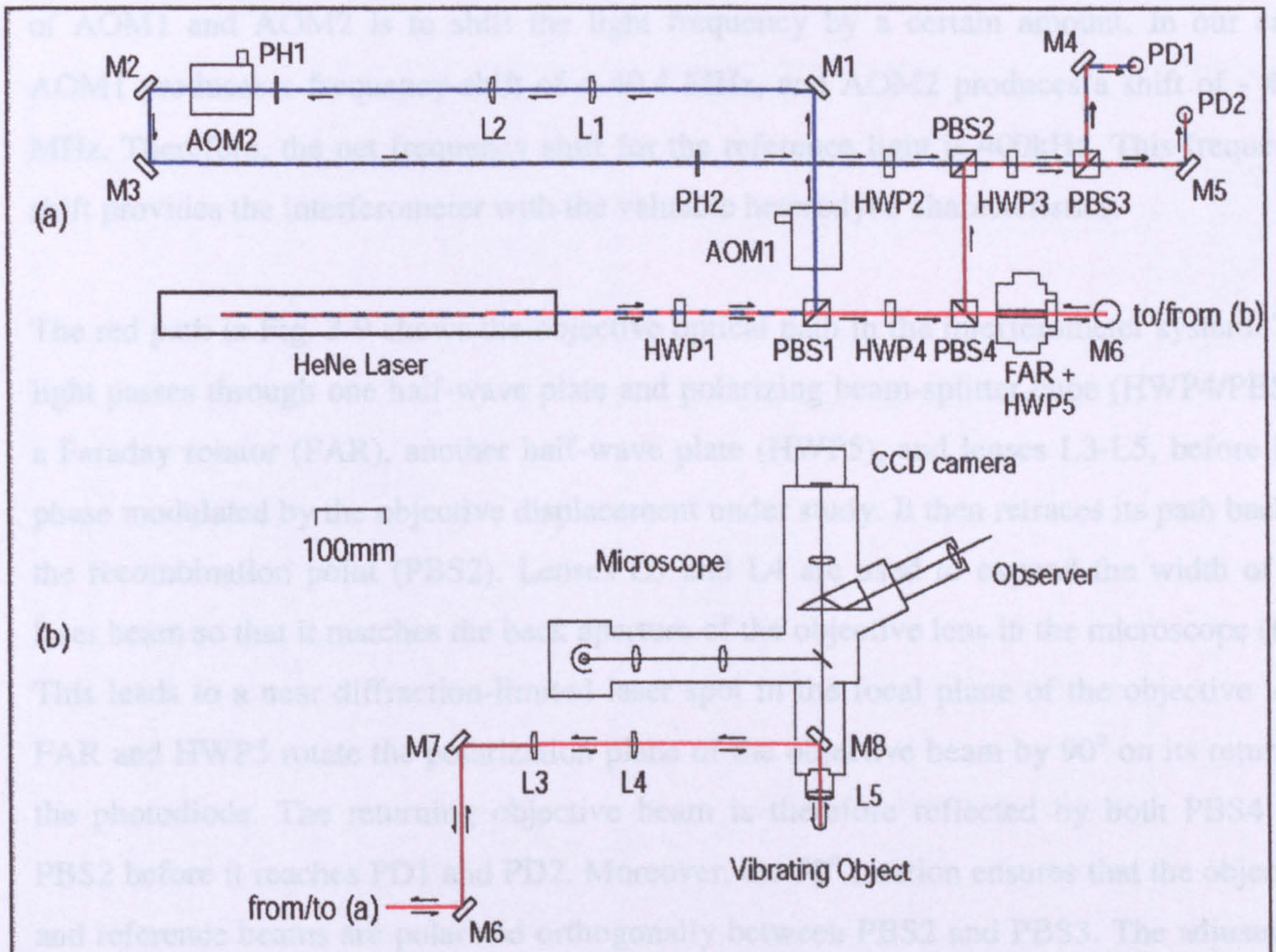

Figure 3-9 Schematic representation of the interferometer system. Red and blue paths represent objective and reference beams respectively. Arrows indicate laser beam propagation direction. Top panel (a) and bottom panel (b) show the interferometer system in horizontal and vertical plane, respectively. AOM: acousto-optic modulator (Bragg cell); FAR: Faraday rotator; L: lens; M: mirror; PD: photodetector; PH: pinhole; PBS: polarizing beam-splitter; HWP: half-wave plate (modified from Cooper 1999).

The laser, an intense monochromatic light, originates from an unstabilized Helium-Neon laser tube (Uniphase model 1200P). The theoretical output power (P_o) is 5 mW, with a 633 nm wavelength in air and 475 nm in the fluids of the cochlea. The light first passes through a quartz half-wave plate (HWP1), which adjusts the polarization plane of the beam. Then the laser beam is reflected and transmitted equally by a polarizing beam-splitter cube (PBS1) to form the reference and objective beams (blue and red paths in Fig. 3-9). Subsequently, the reference and objective beams follow different paths and recombine to interfere on the surface of the interferometer's two photodiode detectors (PD1 and PD2).

The reference optical path (blue line path in Fig. 3-9) consists of two acoustic-optic modulators (AOM1 and AOM2), two lenses (L1 and L2) and two half-wave plates and polarizing beam-splitter cubes (HWP2/PSB2 and HWP3/PSB3, respectively). The function of AOM1 and AOM2 is to shift the light frequency by a certain amount. In our case, AOM1 produces a frequency shift of + 40.4 MHz, and AOM2 produces a shift of - 40.0 MHz. Therefore, the net frequency shift for the reference light is 400kHz. This frequency shift provides the interferometer with the valuable heterodyne characteristics.

The red path in Fig. 3-9 shows the objective optical path in the interferometer system. The light passes through one half-wave plate and polarizing beam-splitter cube (HWP4/PBS4), a Faraday rotator (FAR), another half-wave plate (HWP5), and lenses L3-L5, before it is phase modulated by the objective displacement under study. It then retraces its path back to the recombination point (PBS2). Lenses L3 and L4 are used to expand the width of the laser beam so that it matches the back aperture of the objective lens in the microscope (L5). This leads to a near diffraction-limited laser spot in the focal plane of the objective lens. FAR and HWP5 rotate the polarization plane of the objective beam by 90° on its return to the photodiode. The returning objective beam is therefore reflected by both PBS4 and PBS2 before it reaches PD1 and PD2. Moreover, the 90° rotation ensures that the objective and reference beams are polarized orthogonally between PBS2 and PBS3. The adjustment of HWP3 causes PBS3 to split both the reference and the objective beam equally between PD1 and PD2.

The displacement of an object (d) can be expressed as $d = (\phi_{ref} - \phi_{obj}) \bullet \lambda/4\pi - k/2$, where $(\phi_{ref} - \phi_{obj})$ is the phase difference between the reference and objective beams, which is accomplished by a simple electronic circuit; λ is the wavelength of the objective beam (475 nm in air and ~ 475 nm in cochlear fluid); k is an arbitrary constant relating to the optical path-length difference when the axial displacement of the object under study is zero.

The optical path lengths of the interferometer's reference and objective beams are matched to within ± 25 mm with the help of properly localized mirrors (M1 - M8). This is shorter than the coherence length of the laser, which is ~100 mm. This range allows the

microscope to be focussed on different objective planes between -12.5 mm and +12.5 mm without moving the experimental preparation. The reflectance of the mirrors at the laser wavelength is over 99%. The CCD camera enhances the imaging system greatly, although it is not absolutely essential.

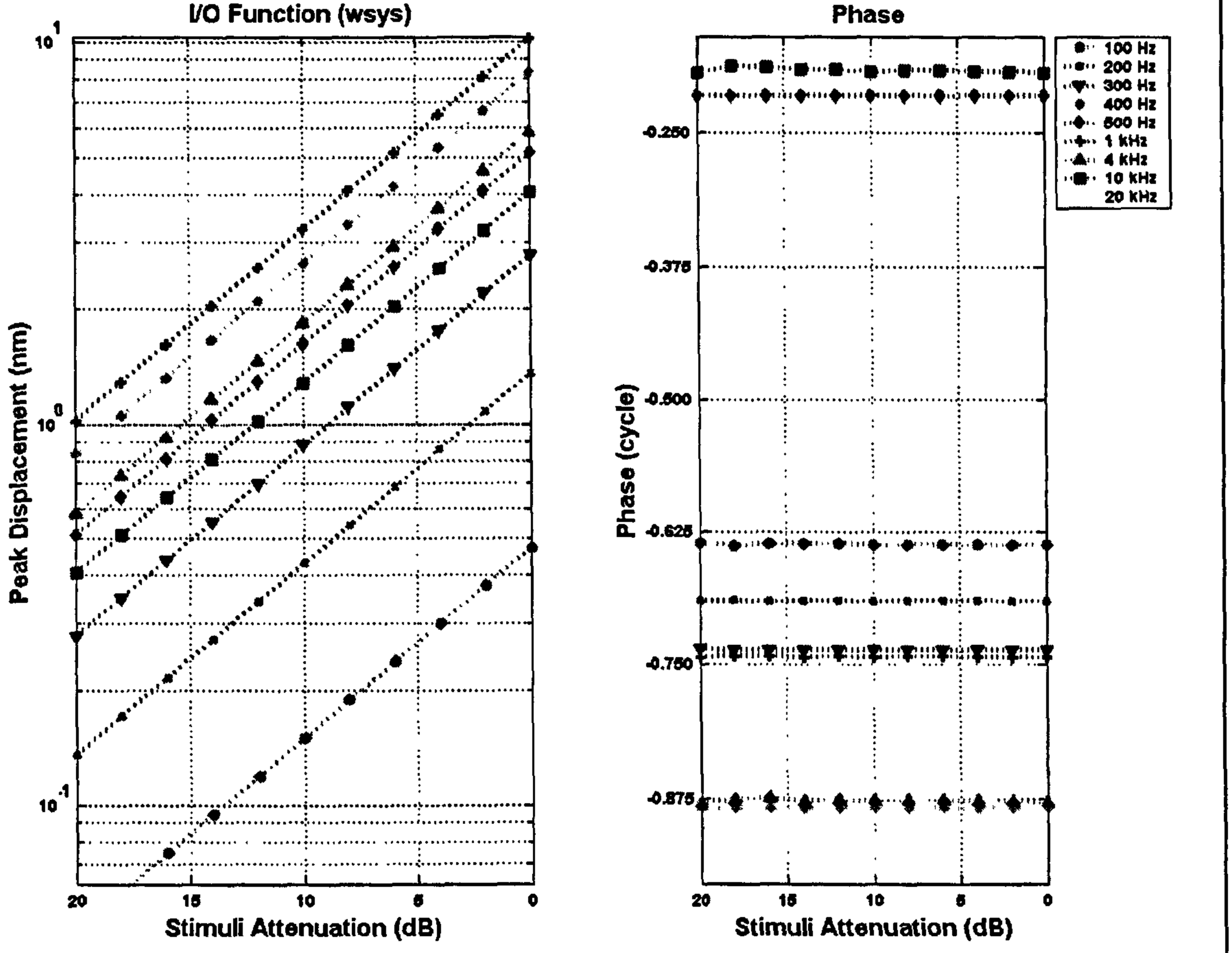

Figure 3-10 Input-output functions of a loudspeaker diagram, as measured using the interferometer system.

The linearity of the interferometer was tested using the cone of a 7.2-cm-diameter moving loudspeaker. The output of the interferometry is plotted in the left panel of Fig. 3-10 as a function of stimulus attenuation in a 2 dB steps. The right of the figure shows the phase variation with stimuli attenuation. The responses were averaged 64 times. The I/O plots grow linearly with a slope of 1 dB/dB for all the tested frequencies (0.1 – 20 kHz) as the dotted lines shows. This figure confirms that our recoding system is a linear system. The

interferometer system described here has a low noise floor (<1 pm $Hz^{-0.5}$), wide bandwidth (from d.c. to 63 kHz) and linear dynamic range (>300 μm). It is sensitive enough to detect motion from the organ of Corti in living animals (Cooper 1999).

3.6 Goniometer system

The displacement sensitive heterodyne laser interferometer system used in this study is combined with a two-axis goniometer system (Fig. 3-11). The two axes are perpendicular horizontal axes, in the coronal and sagittal planes respectively. The rotation ranges from -

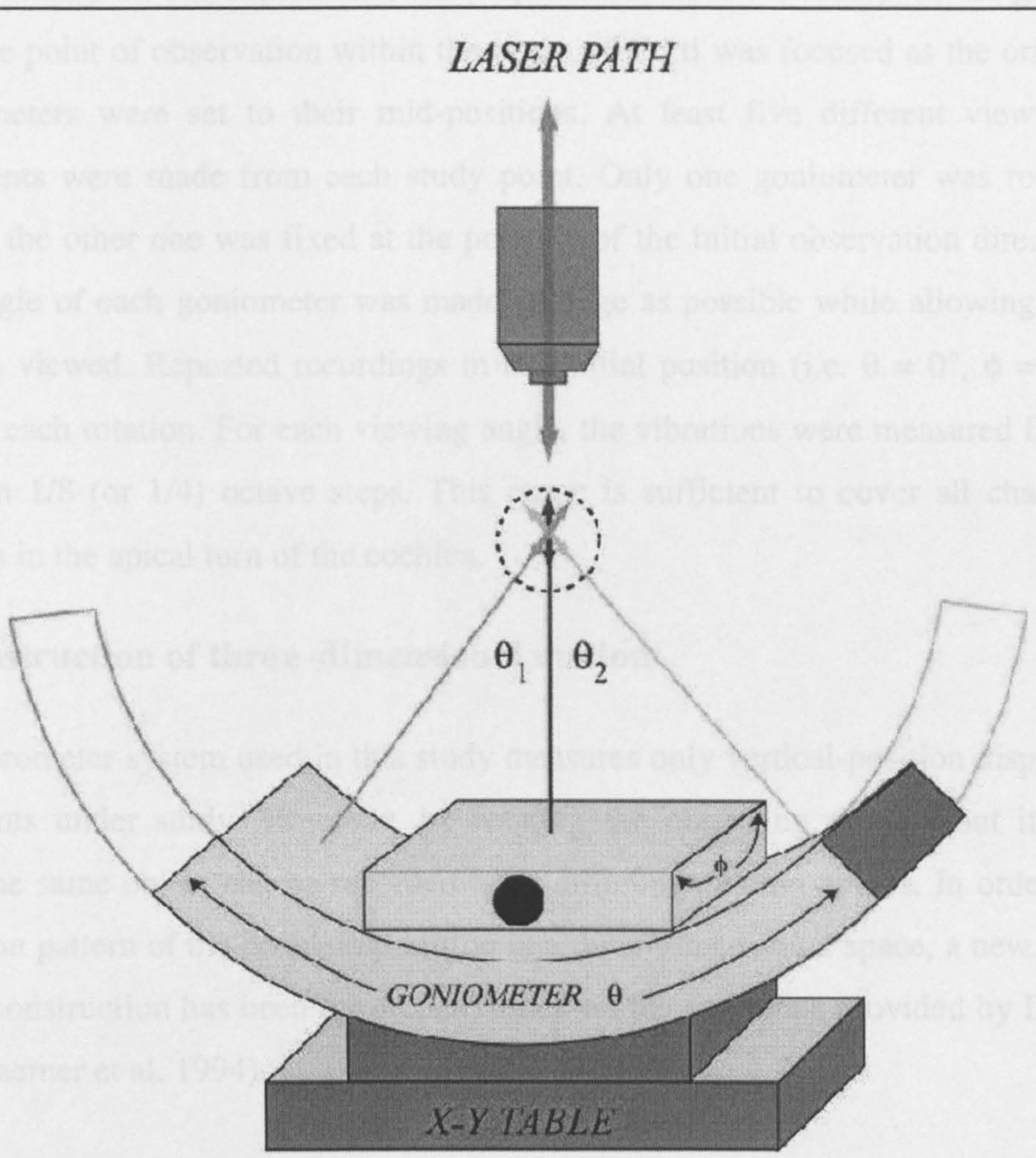

Figure 3-11 Schematic representation of goniometer system. Goniometers θ and φ can rotate from -45° to +45° with an accuracy of $1/100^{th}$ of a degree. The X-Y table can move the preparation in the x-y plane by up to 25 mm with an accuracy of less than 100 nm.

45° to +45° with respect to a vertical line in both coronal and sagittal planes. The accuracy of the goniometer system is 1/100th of a degree. The design for the goniometer system allows us to observe the vibration under study from different viewing angles without moving the actual position of the object in space. The observation direction, which is always vertical, is only perpendicular to the horizontal plane when the goniometer system is set in its mid position (i.e. $\theta = 0°$, $\phi = 0°$). The X-Y table underneath the goniometer can move the preparation in the x-y plane by up to 25 mm with an accuracy of less than 100 nm.

For the recordings in our experiment, the preparation was fixed firmly on the goniometer system. The point of observation within the organ of Corti was focused as the origin when the goniometers were set to their mid-positions. At least five different viewing angle measurements were made from each study point. Only one goniometer was rotated at a time while the other one was fixed at the position of the initial observation direction. The rotation angle of each goniometer was made as large as possible while allowing the same point to be viewed. Repeated recordings in the initial position (i.e. $\theta = 0°$, $\phi = 0°$) were made after each rotation. For each viewing angle, the vibrations were measured from 50 to 1000 Hz in 1/8 (or 1/4) octave steps. This range is sufficient to cover all characteristic frequencies in the apical turn of the cochlea.

3.7 Reconstruction of three-dimensional motion

The interferometer system used in this study measures only vertical-position displacements of the points under study. However, by rotating the observing point about its original position, the same object can be recorded from different viewing angles. In order to show the vibration pattern of the cochlear partition in a three-dimensional space, a new algorithm for 3-D reconstruction has been developed, based on the equations provided by Decraemer et al.(Decraemer et al. 1994).

A single point in space can be addressed with different locations in different right-handed Cartesian coordinates. Generally, in right handed Cartesian coordinates (or rectangular coordinates), the 'address' of a point P is given by three real numbers (x, y, z) indicating the positions of the perpendicular projections from the point to three fixed, perpendicular

axes. The transformation of a point with an address of (x, y, z) in the base coordinates into a point with an address of (x', y', z') in a different coordinate system can be describes by a rotation R and a translation T.

$$\begin{vmatrix} x' \\ y' \\ z' \end{vmatrix} = R \bullet \left(\begin{vmatrix} x \\ y \\ z \end{vmatrix} + T \right), \text{ with } T = \begin{vmatrix} Tx \\ Ty \\ Tz \end{vmatrix}$$

Here T denotes a 3-D translation vector and R denotes a 3-D rotation matrix. The matrix R represents three partial transformations R_x, R_y and R_z with

$$R = R_x \bullet R_y \bullet R_z$$

The matrix R_x describes a rotation about the x-axis by a certain angle α (tilt angle). It holds that

$$R_x(\alpha) = \begin{bmatrix} 1 & 0 & 0 \\ 0 & \cos(\alpha) & \sin(\alpha) \\ 0 & -\sin(\alpha) & \cos(\alpha) \end{bmatrix}$$

The matrix R_y describes a rotation about the y-axis by a certain angle β (roll angle). It holds that

$$R_y(\beta) = \begin{bmatrix} \cos(\beta) & 0 & -\sin(\beta) \\ 0 & 1 & 0 \\ \sin(\beta) & 0 & \cos(\beta) \end{bmatrix}$$

The matrix R_z describes a rotation about the z-axis by a certain angle γ (pan angle). It holds that

$$R_z(\gamma) = \begin{bmatrix} \cos(\gamma) & \sin(\gamma) & 0 \\ -\sin(\gamma) & \cos(\gamma) & 0 \\ 0 & 0 & 1 \end{bmatrix}$$

With the help of the transformation matrix, it is possible to locate a point in any set of right-handed Cartesian coordinates. If the point P moves along a trajectory in the base coordinates, the path in the derived coordinates also can be derived by the same

transformation matrix, but including a time parameter, e.g. as in $[x(t) \quad y(t) \quad z(t)]$ $\rightarrow [x'(t) \quad y'(t) \quad z'(t)]$.

Since the interferometer system we are using only can provide the vertical in-line information, it is technically impossible to measure the 3 orthogonal components of an observation point directly. However, transformations among different coordinates allow the reconstruction of the whole motion in 3-D space for the observation point when measurements are made with different viewing angles.

In our experiment, responses to different frequency stimuli are measured from single reflective beads on the preparation from a wide range of viewing angles, by rotating the goniometer system about its two axes. The stimuli are pure tones. The observed responses are assumed to be sinusoidal regardless of the observed direction or the location of the observed point (confirmation of this assumption is provided in chapter 6 and 7).

A right-handed Cartesian coordinate system is used in describing the motion of the recording point. The origin is at the focus point of the objective lens. The z-axis coincides with the observation direction of the interferometer (i.e. it is vertical and points downwards). The x-axis is horizontal rightward and the y-axis is horizontal forwards (i.e. towards the viewer). The outer goniometer rotates about the y-axis (θ) and the inner goniometer (ϕ) rotates about x-axis when $\theta = 0$. Both goniometers are set to 0° at their mid position and the appropriate signs (positive or negative) are given by the anti-clockwise rule.

For the i-th viewing angles (ϕ_i and θ_i), at every measuring frequency ω, the displacement of the recording point along the z direction d'_{zi} is:

$$d'_{zi} = Ai \bullet \sin(\omega t + \xi_i) \qquad \textbf{Equation 3-1}$$

where i = 1, 2, ... n, A_i and ξ_i are the amplitude and phase of the vibration

The x, y, z components of the recording point motion are described as harmonic functions of time, i.e.

$$d_x = A_x \bullet \sin(\omega t + \zeta_x)$$
$$d_y = A_y \bullet \sin(\omega t + \zeta_y)$$
$$d_z = A_z \bullet \sin(\omega t + \zeta_z) \qquad \textbf{Equation 3-2}$$

with appropriate amplitudes and phases. At each instant of time, d_x, d_y, d_z may be considered as the components of the instantaneous displacement vector **d.**

Practically, the rotation of the recording point can be described as a first rotation about the y-axis over an angle θ, followed by a second rotation about the newly rotated position of the x-axis over an angle ϕ. The three orthogonal components of a displacement vector **d** can be described as $[d_x' \quad d_y' \quad d_z']$ after rotation of angles θ and ϕ, instead of $[d_x \quad d_y \quad d_z]$ in the original position.

$$\begin{vmatrix} d_x' \\ d_y' \\ d_z' \end{vmatrix} = \begin{vmatrix} \cos(\theta) & 0 & -\sin(\theta) \\ \sin(\theta)\sin(\phi) & \cos(\phi) & \cos(\theta)\sin(\phi) \\ \sin(\theta)\cos(\phi) & -\sin(\phi) & \cos(\theta)\cos(\phi) \end{vmatrix} \bullet \begin{vmatrix} d_x \\ d_y \\ d_z \end{vmatrix} \qquad \textbf{Equation 3-3}$$

The component along the z-direction, which is the only one that can be measured at any given time, is

$$d_z' = \sin(\theta)\cos(\phi) \bullet d_x - \sin(\phi) \bullet d_y + \cos(\theta)\cos(\phi) \bullet d_z \qquad \textbf{Equation 3-4}$$

At least 3 measurements of d_z' (specified by their θ_i and ϕ_i values) are necessary to determine the unknowns d_x, d_y, d_z from equation (4). In fact we make at least 5 measurements from different viewing angles for each recording point in order to reduce sensitivity to measurement errors. Therefore, the three d_x, d_y, d_z can be solved by the following overdetermined linear system.

$$\begin{vmatrix} d_{z1}' \\ d_{z2}' \\ d_{z3}' \\ d_{z4}' \\ d_{z5}' \end{vmatrix} = \begin{vmatrix} \sin(\theta 1)\cos(\phi 1) & -\sin(\phi 1) & \cos(\theta 1)\cos(\phi 1) \\ \sin(\theta 2)\cos(\phi 2) & -\sin(\phi 2) & \cos(\theta 2)\cos(\phi 2) \\ \sin(\theta 3)\cos(\phi 3) & -\sin(\phi 3) & \cos(\theta 3)\cos(\phi 3) \\ \sin(\theta 4)\cos(\phi 4) & -\sin(\phi 4) & \cos(\theta 4)\cos(\phi 4) \\ \sin(\theta 5)\cos(\phi 5) & -\sin(\phi 5) & \cos(\theta 5)\cos(\phi 5) \end{vmatrix} \bullet \begin{vmatrix} d_x \\ d_y \\ d_z \end{vmatrix}$$ **Equation 3-5**

Expressed in matrix notation, this becomes

$$\mathbf{d_z}' = \mathbf{G} \cdot \mathbf{d}$$ **Equation 3-5'**

Substituting equation (3-1) and (3-2) to equation (3-5), expanding the sine functions with the sum formula ($A \bullet \sin(c+d) = A \bullet \sin(c)\cos(d) + A \bullet \cos(c)\sin(d)$) and equating the $\sin(\omega t)$ and $\cos(\omega t)$ terms results in the following two sets of equations.

$$\begin{vmatrix} A_{z1}' \bullet \cos(\xi_1) \\ A_{z2}' \bullet \cos(\xi_2) \\ A_{z3}' \bullet \cos(\xi_3) \\ A_{z4}' \bullet \cos(\xi_4) \\ A_{z5}' \bullet \cos(\xi_5) \end{vmatrix} = G \bullet \begin{vmatrix} A_x \bullet \cos(\zeta_x) \\ A_y \bullet \cos(\zeta_y) \\ A_z \bullet \cos(\zeta_z) \end{vmatrix}$$ **Equation 3-6**

$$\begin{vmatrix} A_{z1}' \bullet \sin(\xi_1) \\ A_{z2}' \bullet \sin(\xi_2) \\ A_{z3}' \bullet \sin(\xi_3) \\ A_{z4}' \bullet \sin(\xi_4) \\ A_{z5}' \bullet \sin(\xi_5) \end{vmatrix} = G \bullet \begin{vmatrix} A_x \bullet \sin(\zeta_x) \\ A_y \bullet \sin(\zeta_y) \\ A_z \bullet \sin(\zeta_z) \end{vmatrix}$$ **Equation 3-7**

or in matrix notation,

$$\mathbf{d_{zc}} = \mathbf{G} \cdot \mathbf{d_c}$$ **Equation 3-6'**

$$\mathbf{d_{zs}} = \mathbf{G} \cdot \mathbf{d_s}$$ **Equation 3-7'**

Equations (3-6) and (3-7) can provide the solution of $\mathbf{d_c}$ (the transpose of $[A_x \bullet \cos(\zeta_x) \quad A_y \bullet \cos(\zeta_y) \quad A_z \bullet \cos(\zeta_z)]$) and $\mathbf{d_s}$ (the transpose of

$[A_x \bullet \sin(\zeta_x) \quad A_y \bullet \sin(\zeta_y) \quad A_z \bullet \sin(\zeta_z)])$, which in turn, may yield the solution of **d** with its three orthogonal component amplitudes (A_x, A_y, A_z) and corresponding phases $\zeta_x, \zeta_y, \zeta_z$. Using the singular matrix decomposition to compute the generalized inverse of the design matrix G can solve these equations. The solution is then given by

$$\mathbf{d_c} = (\mathbf{G^T \cdot G})^{-1} \cdot (\mathbf{G^T \cdot d_{zc}})$$

$$\mathbf{d_s} = (\mathbf{G^T \cdot G})^{-1} \cdot (\mathbf{G^T \cdot d_{zs}}) \qquad \textbf{Equation 3-8}$$

where G^T represents the transpose of G (i.e. $G \bullet G^T = I$).

3.8 Method Testing

Two methods were used to test the stability and accuracy of the three-dimensional reconstruction technique. These involved (1) the use of mathematical signals and (2) measurements of a tiny dot on the surface of a loudspeaker, respectively. The loudspeaker was assumed to move in a straight line, since it was of the moving-coil type. The 3-dimensional reconstruction results were compared either with the original paths (in the case of the mathematical model data), or the expected direction of the motion (for the loudspeaker). The effects of adding noise to the mathematical signal data used for the 3-D reconstructions were also investigated. This was done because unavoidable noise is bound to exist in the recording system, such as noise from the background mechanical vibrations at low frequencies and light reflected from surrounding structures, but the level of this noise cannot be predicted. In the testing experiments, 0-100% random noises (relative to the amplitude of the signals) were added to the displacement vectors calculated for different viewing angles for the 3-D reconstruction.

3.8.1 Mathematical signals

A path of a point moving in three-dimensional space could be described by equation 3-9, which contains three orthogonal harmonic time functions x, y and z, with the same frequency (ω), and with amplitudes (A_x, A_y and A_z) and phases (θ_x, θ_y and θ_z), respectively. The path could be a straight line, an ellipse or a circle, depending on the values of the six parameters. If the three orthogonal components move in phase or in anti-phase in three-dimensional space, the path will be a straight line; if there are any differences among the phases, most probably the paths will be elliptical; if one phase

differs from the other two by exactly 90°, the path might be a circle, but this will depend on the amplitude values as well.

$$x = Ax \bullet \sin(\omega t + \theta x)$$
$$y = Ay \bullet \sin(\omega t + \theta y)$$
$$z = Az \bullet \sin(\omega t + \theta z) \qquad \textbf{Equation 3-9}$$

A_x	A_y	A_z	θ_x	θ_y	θ_z	Path in 3-D Space
1	1	1	π/3	π/3	π/3	straight line at 45° to x, y and z axes
1	1	1	π/4	π/3	π/3	ellipse in plane at 45° x and z axes
1	1	1.41	π/4	π/4	π/4	Circle in plane at 45° x and z axes

Table 3-1 Parameters for different paths in 3-D space. A: amplitude; θ: phase.

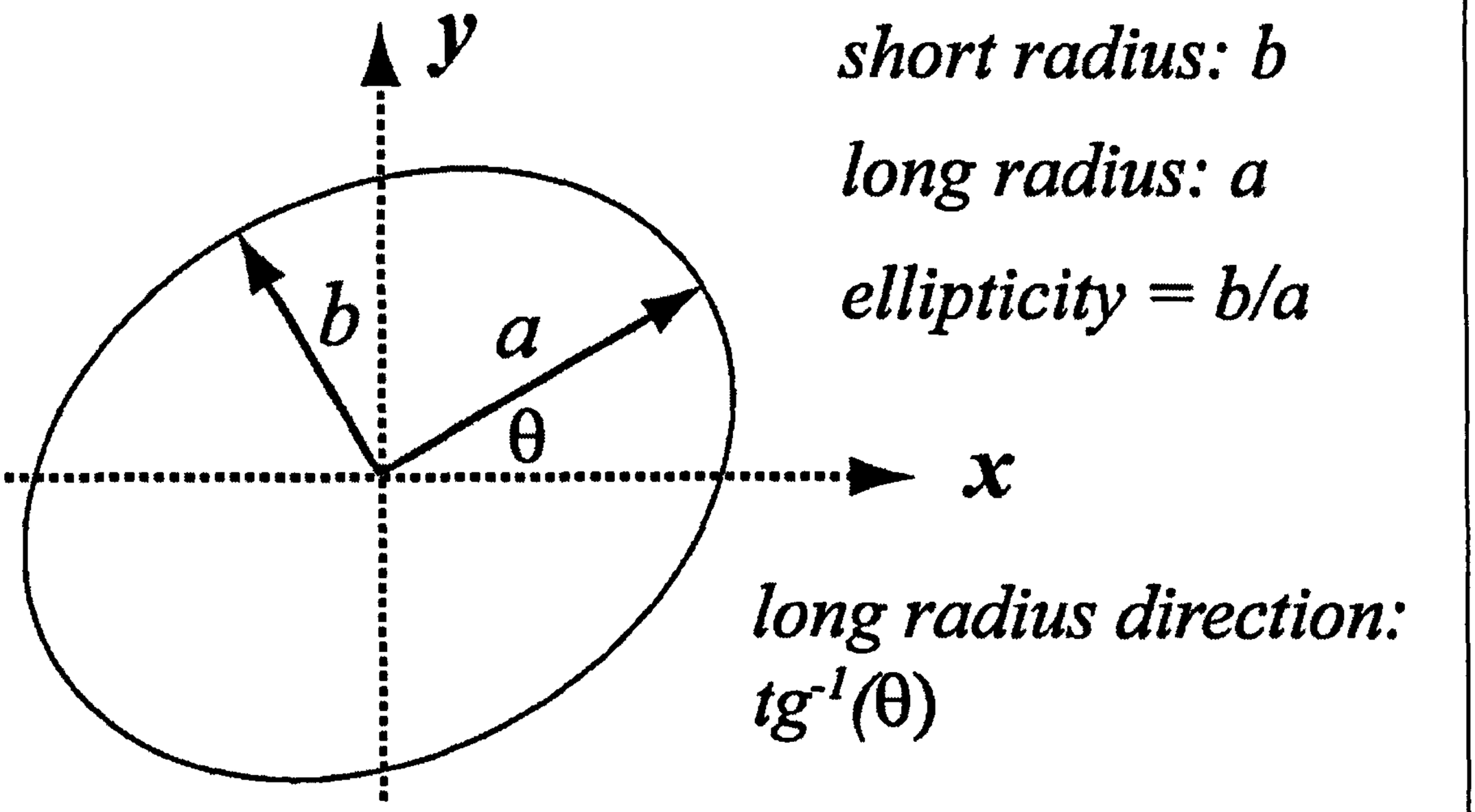

Figure 3-12 Schematic representation of the characteristics of an ellipse. Ellipticity is defined as the ratio of short radius and long radius of an ellipse. The direction of the ellipse in 3-D space or any two-dimensional plane is shown by the long radius direction.

To describe a path in 3-D space or any two-dimensional planes, ellipticity and the direction of the long radius are normally used (Fig. 3-12). The ellipticity is a key characteristic to

describe the shape of an ellipse. It is defined as the ratio of the short radius and the long radius of an ellipse. If the ellipticity equals 0, the path will be a line instead of an ellipse. When the ellipticity equals 1, the path must be circular. The ellipticity of all ellipses must lie between 0 and 1. The direction of the ellipse in 3-D space or any two-dimensional planes is given by the direction of the long radius.

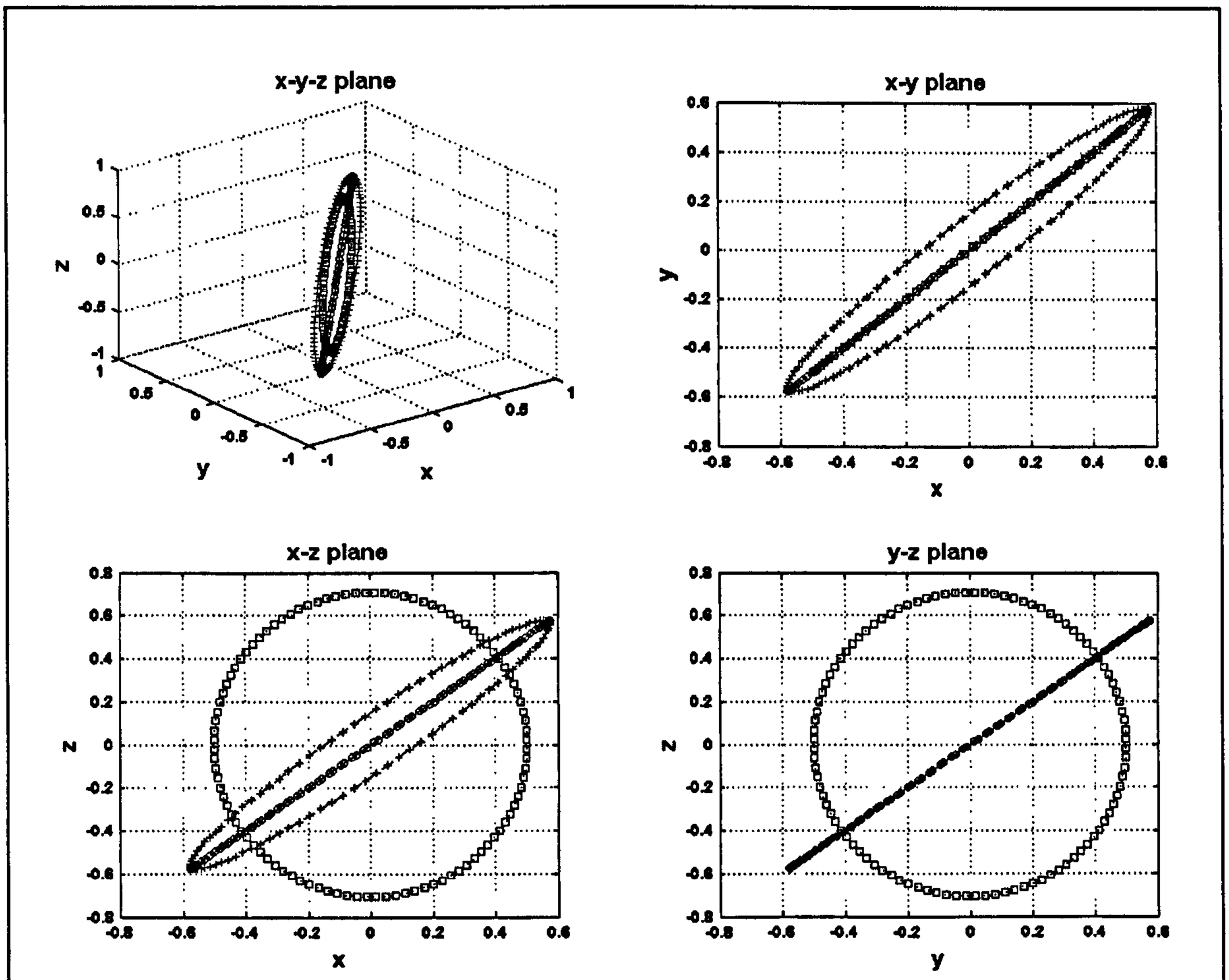

Figure 3-13 Tested paths of a point in three-dimensional space and three orthogonal planes. Circles, pluses and squares represent the paths of line, ellipse or circle, respectively.

To test the 3-D reconstruction technique across a wide range of models, the amplitude (A_x , A_y and A_z) and phase (θ_x,θ_y and θ_z) combinations defined as in Table 3-1 were used as model inputs. With these parameter values, the imaginary point under observation will appear to move along a straight line or an ellipse or a circle in the three-dimensional space as shown in Fig. 3-13. The projections of these trajectories in three orthogonal planes (x-y,

x-z, y-z) are also shown in the figure. Circles, pluses and squares represent the paths of the line, ellipse or circle, respectively.

5 displacement vectors along the z-direction were calculated by "viewing" the model paths from 5 different observation angles {(30° 0°), (-30° 0°), (0° 0°), (0° 30°), (0° –30°)}. From these 5 displacement vectors, the 3-D reconstruction technique described above was used to 'reconstruct' the 3-D path. The results followed exactly the same paths as the original models as expected. Six other straight line models were tested as well, including slant lines with different angles in three-dimensional space, a line along the x direction only, a line along the y direction only and a line along the z direction only. All of the reconstruction results duplicated the original paths, which basically confirms that the technique works well when the measurements are ideal.

The effects of noise were studied in these same 9 models. A random noise ranging from 0 to 100% relative to the amplitude of the signal was added simultaneously to the studied displacement vector. The effects of noise on the characteristics of the original path were averaged across 50 trials.

As an example, the effects of adding noise to the 3-D reconstruction data for a 45°-slant-line are shown in Fig. 3-14. The random noise was added to the 5 displacement vectors as described above. The effects of the noise are obvious, and highly dependent on the amount of noise added. The first column of Fig. 3-14 shows the average effect of the noise on the length of the long radius (half-length of the line) in 3-D space and three orthogonal planes. The long radius of the line grows with the amount of noise added in 3-D space, x-y, x-z and y-z planes. However, below around 40% of added noise, calculation length of the long radius of the line changed little.

The second column of Fig. 3-14 shows ellipticity variation with noise in 3-D space, x-y, x-z and y-z planes. Without any noise added, the original path in 3-D space, x-y, x-z and y-z planes is a straight line with the ellipticity equals to 0. Adding noise changed the straight line into an elliptical path, with an ellipticity of up to 0.2 when the amplitude of the noise

exceeds 80%. The ellipticity increases with increases in the percentage of the noise added, but it changed less than 0.1 when less than 40% noise was added.

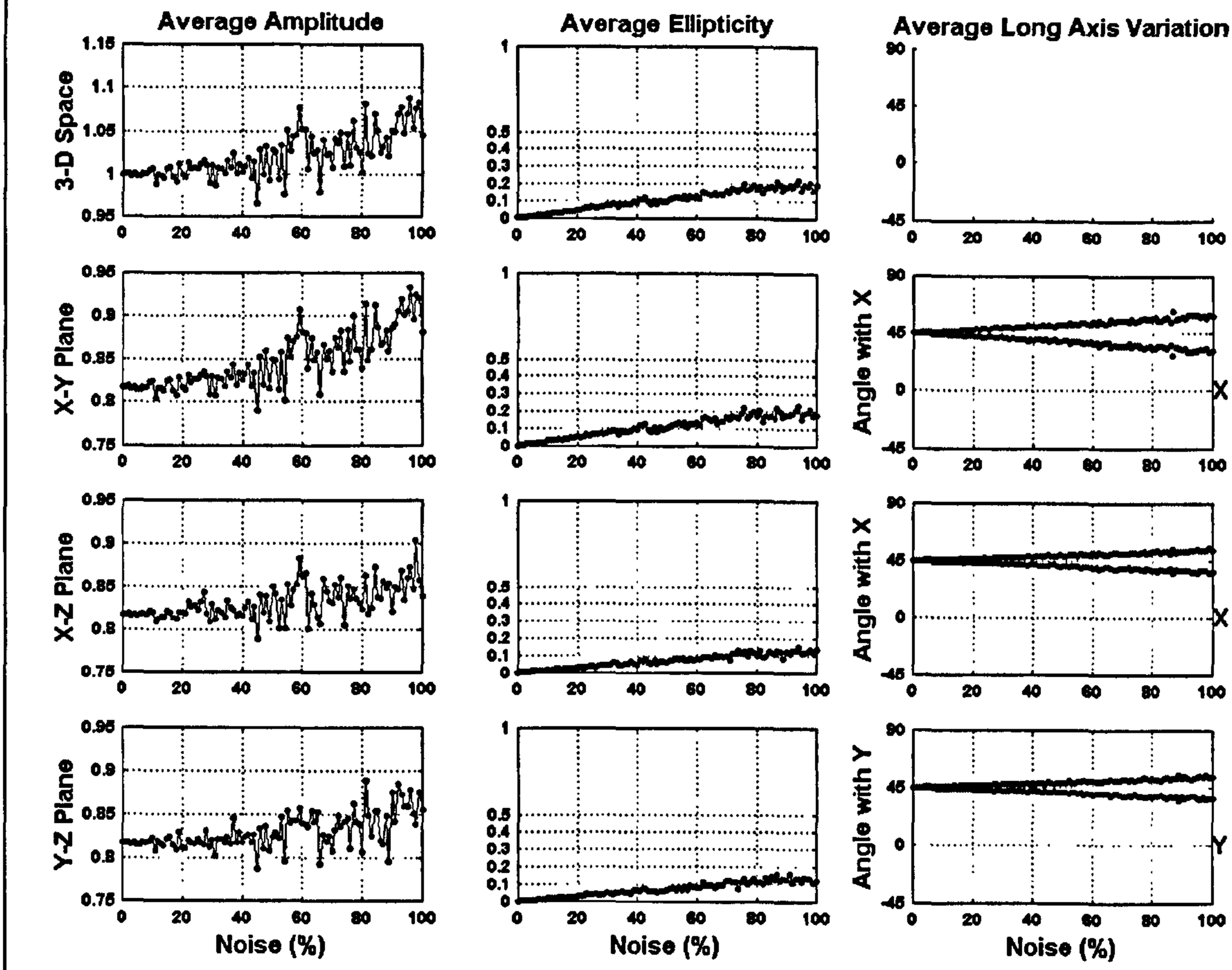

Figure 3-14 Effect of adding noise to straight-line three-dimensional reconstruction results. Column 1 shows effect of noise to the long radius of the ellipse (line) in 3-D space, x-y, x-z and y-z planes. Column 2 shows effect of noise to the ellipticity in 3-D space, x-y, x-z and y-z planes. Column 3 shows effect of noise to the long radius direction with x (x-y plane), x (x-z plane) and y (y-z plane).

Column 3 shows the effect of noise on the long radius' direction with x-axis, x-axis and y-axis in x-y, x-z and y-z plane, respectively. Adding noise could cause the long radius to deviate from its original direction in either positive or negative directions. The deviation of the long axis from its original direction increased with the increasing amounts of added noise. Deviations of up to 20° occurred when the 100% noise was added. The variation of the long radius direction is within 10° when the amount of noise added is less than 40%.

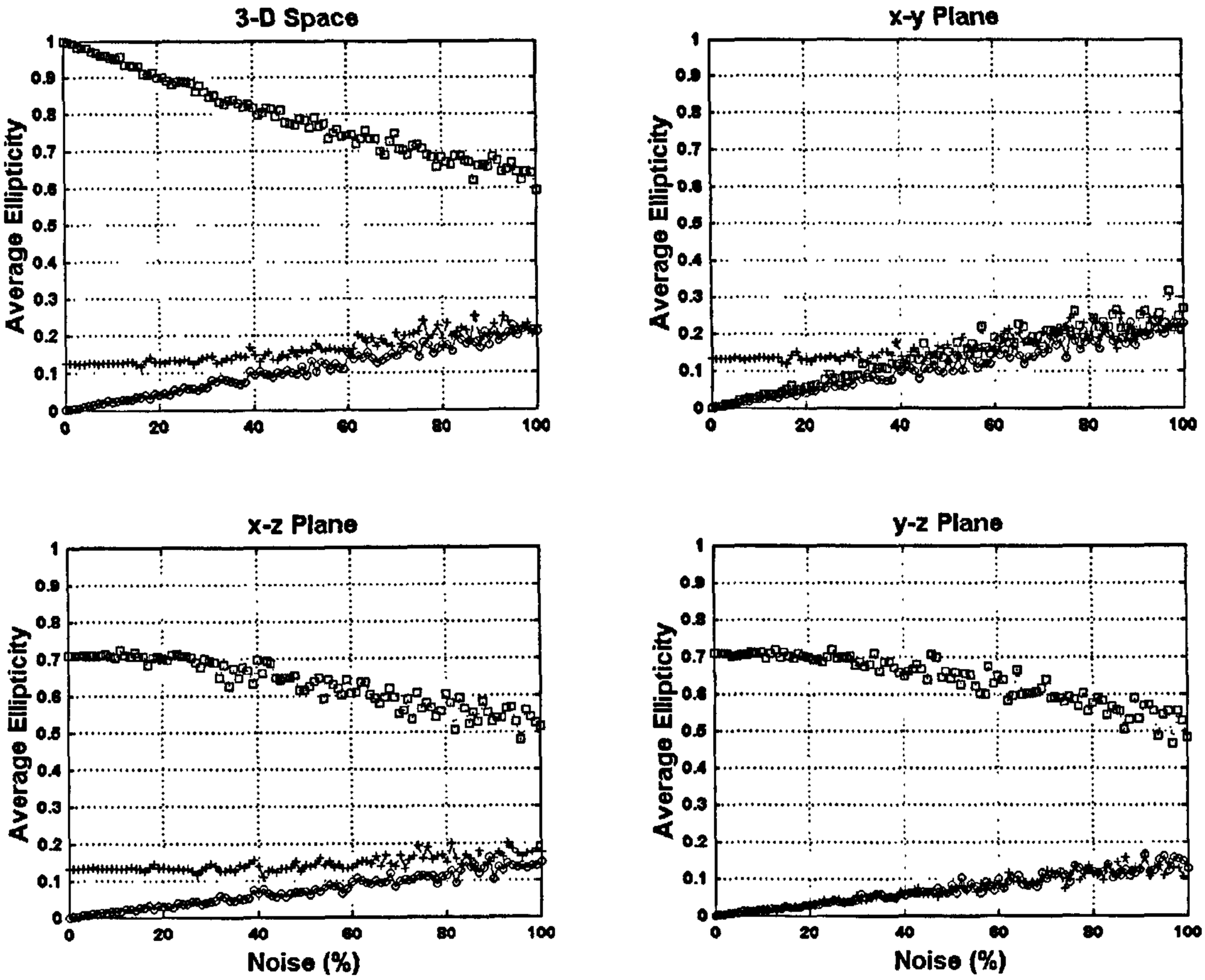

Figure 3-15 Effect of noise to ellipticity of line, ellipse and circle 3-D reconstruction results in 3-D space, x-y, x-z and y-z planes. Circles, pluses and squares represent results of line, ellipse and circle, respectively.

To illustrate the effect of noise on the characteristics of 3-D reconstructed lines, ellipses and circles, Fig. 3-15 shows the effects on the ellipticity of one line (circles), one ellipse (plusses) and one circle (squares) in 3-D space, x-y, x-z and y-z planes. Adding noises to the displacement vectors will change a straight line into an ellipse. The ellipticity increases with the amount of noise. Adding noise also increases the ellipticity of the elliptical path as the plusses show in the figure. However, if the original path is a circle, adding noise will change it into ellipse instead, and the ellipticity will decrease from 1 to an amount, which depends on the amount of noise. Adding noise to the displacement vectors can change the line and circle into ellipses, and also change the shape of the ellipse. However, the variation of the ellipticity is less than 0.2 in all cases when the amount of noise added is less than 40%.

The effects of noise were also studied for the other mathematical signals mentioned above. In summary, adding noise to displacement vectors can change the characteristics of the 3-D reconstruction paths. However, the overall effects of noise on 9 different mathematical paths shows that the 3-D reconstruction is fairly stable when measurements are contaminated by less than 40% noise. Therefore, in practice, the changes caused by less than 40% variation in displacement vectors could be ignored in 3-D reconstruction results. This correspond 8 dB-variation in the real experiments, when the "noise" is estimated by making repeated measurements from a single observation angle. This is also means that the 3-D reconstruction results could be considered as a straight line if the ellipticity was less than 0.2.

3.8.2 Loudspeaker

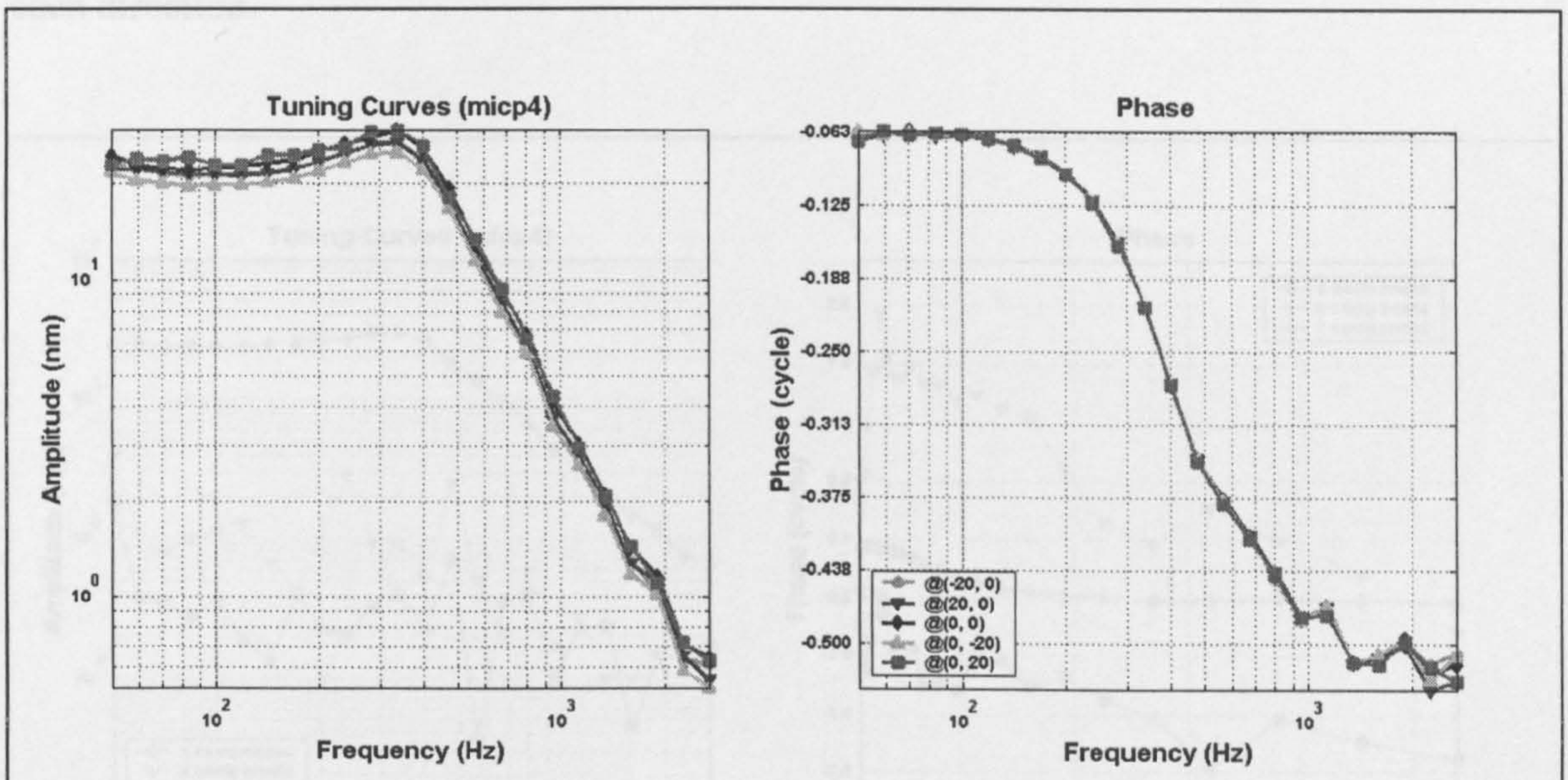

Figure 3-16 Transfer functions of a point on the surface of the loudspeaker.

The vibrations of a loudspeaker were also studied to show the results of the 3-D reconstruction method. The loudspeaker's surface was set almost perpendicular to the z-axis (along the interferometer observation direction). In this testing system, the origin is in the center of the vibrating surface with the goniometers reset to their zero positions (θ=0, ϕ=0).

A fixed point on the surface of the loudspeaker was measured from different viewing angles. First the horizontal goniometer position θ was changed from -30° to 30° with a step of 10°, while the vertical goniometer was set in its original position. After that, goniometer θ was rotated back and fixed in its original position, and the vertical goniometer ϕ was changed from -30° to 30° in steps of 10°. Transfer functions from five different viewing angles are shown in Fig. 3-16 with frequency from 50 to 3000 Hz. These angles were chosen on purpose to approximate the angles used in the real experiments. All transfer function curves showed that the loudspeaker behaves like a low pass filter with a cutoff frequency of around 400 Hz.

Repeatability recordings from same point and same viewing angles were also made in between the measurements. Variations in frequency responses at different observation angles are significant in spite of the fact that the viewing angles only changed by 40° in each direction.

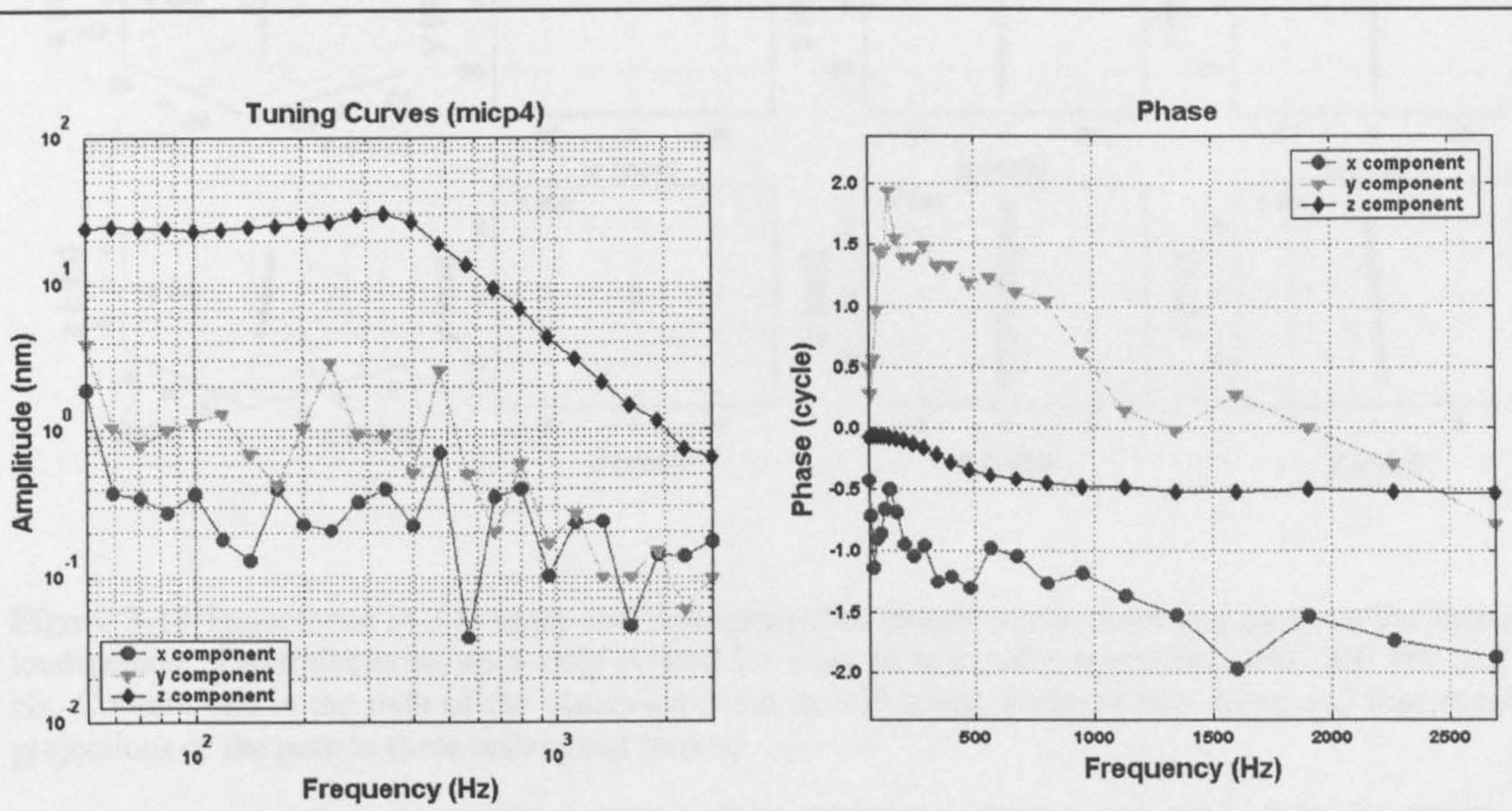

Figure 3-17 Reconstruction amplitudes and phases of the three orthogonal components along x, y, and z directions.

Fig. 3-17 shows the 3-D reconstruction amplitudes and phases for the three orthogonal components along x, y and z directions. Circles, triangles and diamonds represent x, y and z direction components. It is obvious that motion along z direction is dominating the

motion of the surface of the loudspeaker and it is more than 10 times bigger than either x or y component. There is a clear pattern in the phase data in the z direction, but not in x or y directions.

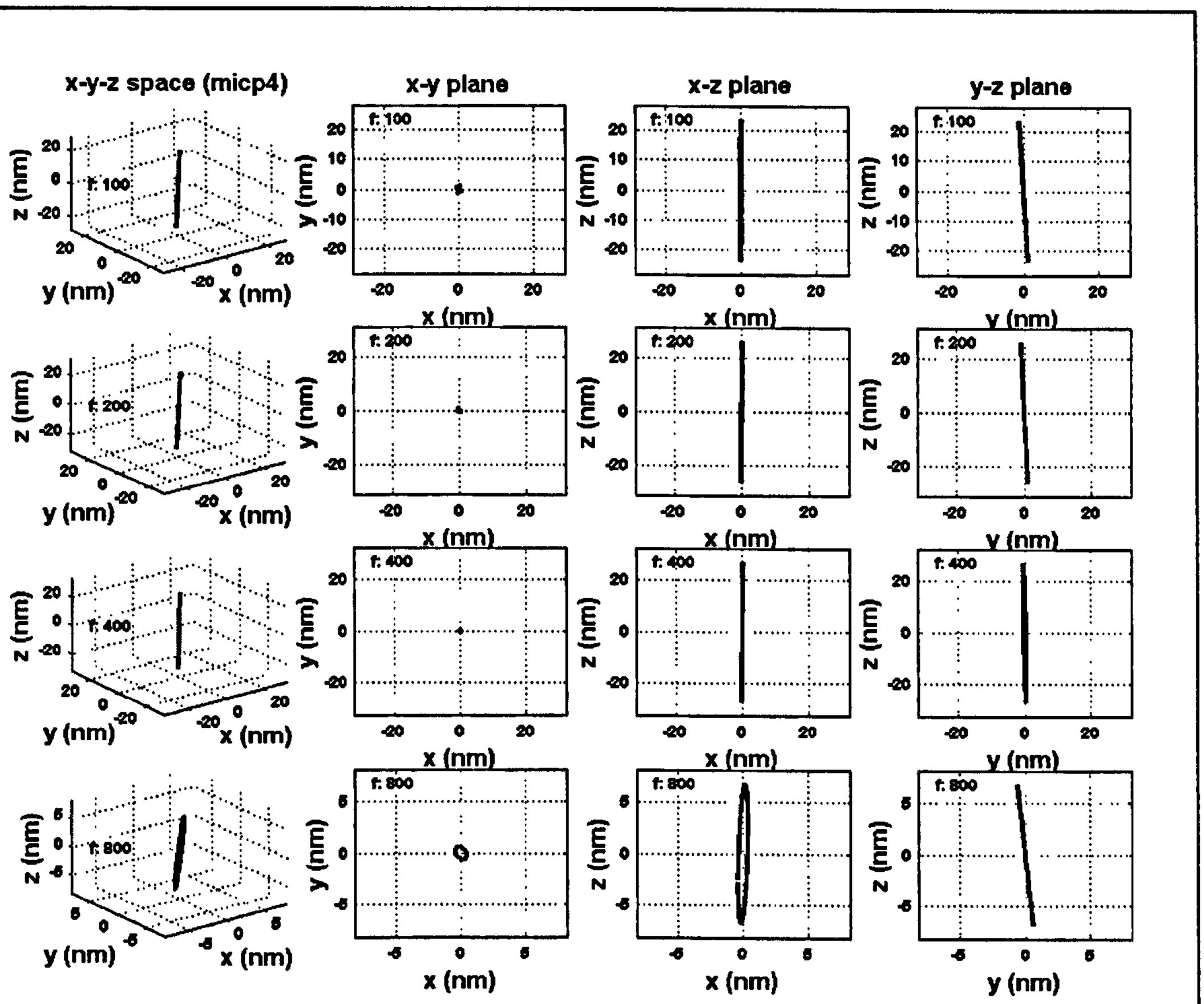

Figure 3-18 Trajectories in 3-D space and three projection planes of the observing point on the surface of loudspeaker. The trajectories were only plotted for a set of selected frequencies, 100, 200 400 and 800 Hz. Column one is the path of the observing point in 3-D space. Column two, three and four show the projections of the path in three orthogonal planes.

Fig. 3-18 shows the reconstructed 3-D motion in 3-D space and three orthogonal planes for the surface of loudspeaker. Only 100, 200, 400 and 800 Hz 3-D reconstruction results are shown in the figure, which were selected from frequencies ranging from 50 and 3000 Hz. The loudspeaker is seen to move in an up-and-down motion along z direction, no matter it vibrates at which frequency. The projections of its vibration path in x-z and y-z planes are

very close to straight lines along the z direction, but in the x-y plane, the path appears as a small dot in the center.

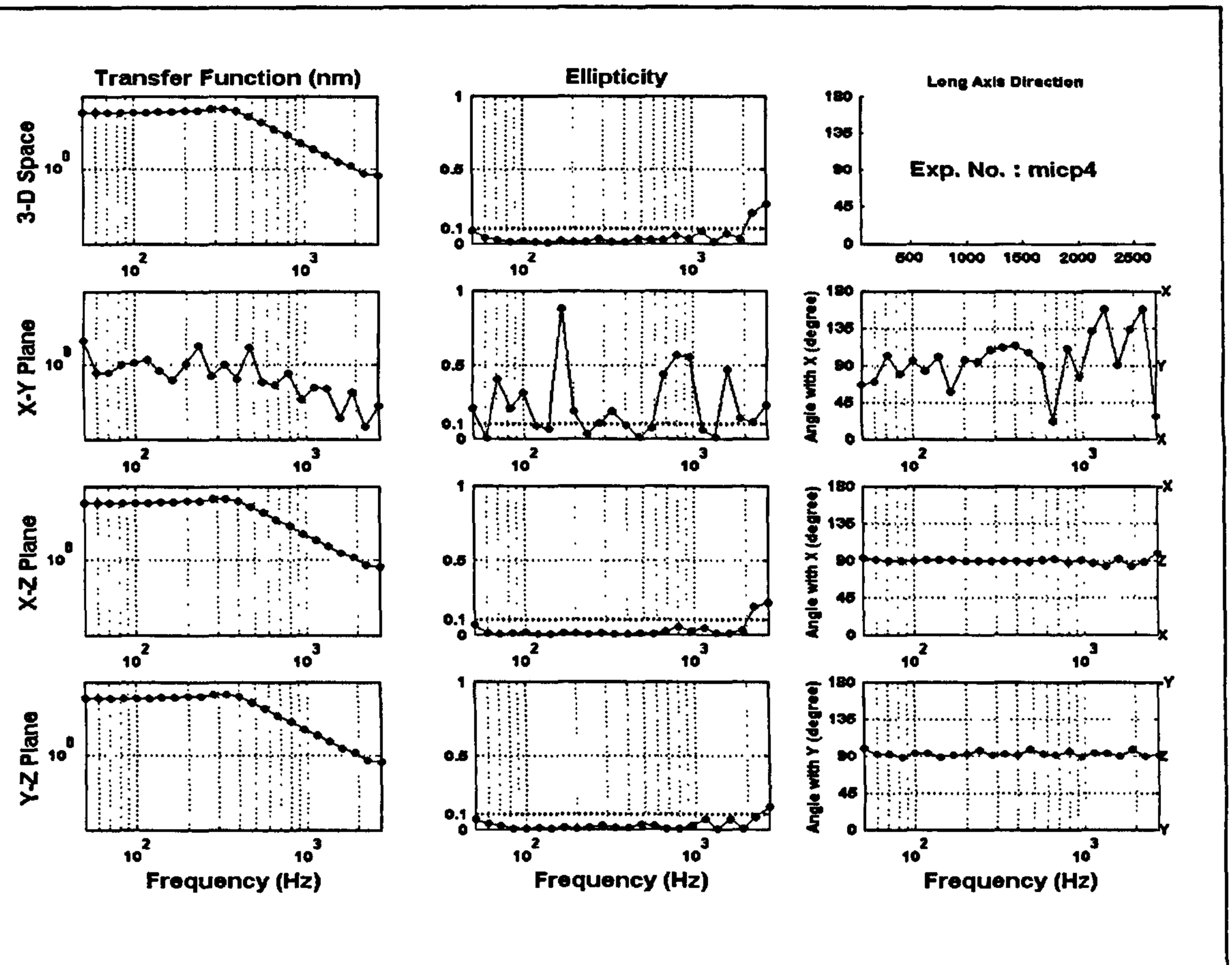

Figure 3-19 3-D reconstruction results of the observing point on the surface of the loudspeaker. Column 1: tuning of the observing point in 3-D space and three orthogonal planes. Column 2: ellipticity of the reconstruction path in 3-D space and three orthogonal planes. Column 3: long radius direction of the path in x-y, x-z and y-z planes.

Fig. 3-19 shows an analysis of the 3-D reconstruction results for the surface of the loudspeaker at all the frequencies tested. The first column plots the tuning of the loudspeaker in 3-D space and three orthogonal planes. Tuning in 3-D space, x-z and y-z planes appears like that of a low-pass filter with a cutoff frequency of around 400 Hz. However, in x-y plane, the amplitudes of the vibrations are lower than those in the other two planes and tuning appears noisy or irregular. The second column shows the ellipticity of the reconstructed paths in 3-D space and in three orthogonal planes. For frequencies between 80 and 1000 Hz, the ellipticity in 3-D space, x-z and y-z planes are very close to 0,

which means the loudspeaker moves along a straight line in 3-D space and in the x-z and y-z planes. For very low frequencies and frequencies above 1000 Hz, the ellipticity rises from 0, which might means that for these frequencies, the vibration pattern of the loudspeaker becomes elliptical, or background noise has to be taken into account due to the vibration amplitude in these frequencies are very low. In the x-y plane, the loudspeaker moves either along a line or an ellipse, which is highly affected by the background noise. The third column shows the long radius direction of the path in x-y, x-z and y-z planes. There is no regular direction for the vibration of the observing point in x-y plane, however, in the x-z and the y-z planes, the paths are oriented along the z direction at all frequencies.

In summary, the 3-D reconstruction technique appears to work properly for both mathematical signals and the loudspeaker model. These results show that the 3-D reconstruction technique used in this study can reveal the 3-D nature of the motion of an observation point from one-dimensional information. The technique yields stable results even with added noise up to 40% of the measurement value.

One thing that is not taken into account in the 3-D reconstruction technique is the fact that, due to refraction at the air/glass/fluid interfaces that are used in real experiments, the angles set and measured by the goniometers might differ slightly from the actual incidence angles of the laser light on the tectorial membrane. There is no way of correcting for this without knowing the exact angles of the interfaces (which were not measured during this study), but the effects are likely to be very small. For interface angles of around 30 degrees, which is probably around the mean of those used in this study, and goniometer angle variations of around +/- 20 degrees, the maximum angular errors would be less than 7 degrees, and reconstruction magnitudes (for straight line motion along the z-axis) would be affected by less than 1%.

Chapter 4 Assessment of cochlear condition using round window potentials

4.1 Introduction

Mechanical studies of the apex of the cochlea involve invasive procedures, which can change the physiological condition of the cochlea. Therefore, the physiological condition of the cochlea is an essential issue of the mechanical studies of the apical turn of the cochlea. The effects of direct access to the apical turn of the cochlea on the physiological condition of the cochlea are unknown, but may be dramatic. Under some circumstances, a drop in neural sensitivity is due almost solely to a drop in mechanical sensitivity.

To assess and control for this condition, many previous studies have relied on compound action potential or CAP audiograms. These audiograms reflect the minimum sound pressure level needed to excite a minimum amount of neural fibers. The CAP threshold correlates well with the behavioural thresholds in humans and animals, and single-fibre thresholds in animals and can be derived from sound-evoked round window potentials of the cochlea. CAPs evoked by high frequency stimuli are easy to distinguish from other sound-evoked round window potentials, but they only inform us about the physiological condition of the basal turns of the cochlea. On the other hand, CAPs evoked by low frequency stimuli recorded at the round window niche, which could inform us about the apical turns of the cochlea, are not so easy to distinguish.

The present study aimed to investigate the CAP threshold and CM variation by tracing them at each surgical stage, providing basic data of the cochlear physiological condition in the process of approaching the apical turn of the cochlea. A phase-locked analysis technique was used to assess the thresholds of the low-frequency CAPs from the round window potentials. This allows us to determine complete CAP audiograms, which we can use to assess the physiological condition of the entire cochlea.

4.2 High frequency round window potentials

In order to access the physiological conditions of the cochlea, CAPs were recorded from the round window from 2k to 20 kHz under different physiological conditions: (1) before

extensive surgery – only the posterolateral bulla was open. (2) after more extensive surgery – as necessary as expose the ventral side of the bulla. (3) after opening the ventral bulla. (4) after opening the cochlea – but with RM intact. (5) after tearing the RM.

The results presented here are representative of those from 20 animals in which similar experiments were performed. Figure 4-1 shows typical CAP waveforms recorded from the round window directly after the electrodes were set up. Stimuli are 10 and 4 kHz tone bursts (rise/fall time = 1ms, 6 ms duration with responses were averaged across 32 presentations of the stimuli), which are shown on the top of Figure 4-1. The response waveforms are presented directly below the stimuli at different sound pressure levels (steps of 6 dB, values indicated at the right of each line). The whole nerve action potential appears as one or two negative peaks in the recordings and is labeled $N_1$and N_2. As the intensity was raised from low levels, N_1 was the first to appear, followed at higher intensities by N_2. At higher intensities the response became more complex, with the appearance of other components of different latency. The amplitudes of N_1 and N_2 increased with the sound pressure level.

All the CAP waveforms under different physiological conditions show similar patterns as Figure 4-1, but they usually differ in amplitude. To illustrate this, the peak-to-peak values of N_1 were calculated and plotted as a function of stimuli intensity under different cochlear conditions.

Figure 4-2 shows two examples of such input-output functions of CAPs (10 kHz at the top and 4 kHz at the bottom) under different physiological conditions of the same preparation. For both 10 and 4 kHz stimuli, circles were recordings measured before the extensive surgery; downright-triangles were collected after more extensive surgery; squares represent recordings after opening the ventral bulla; upright-triangles were recorded after opening the cochlea with the RM intact and diamonds were recorded 2 hours after tearing the RM

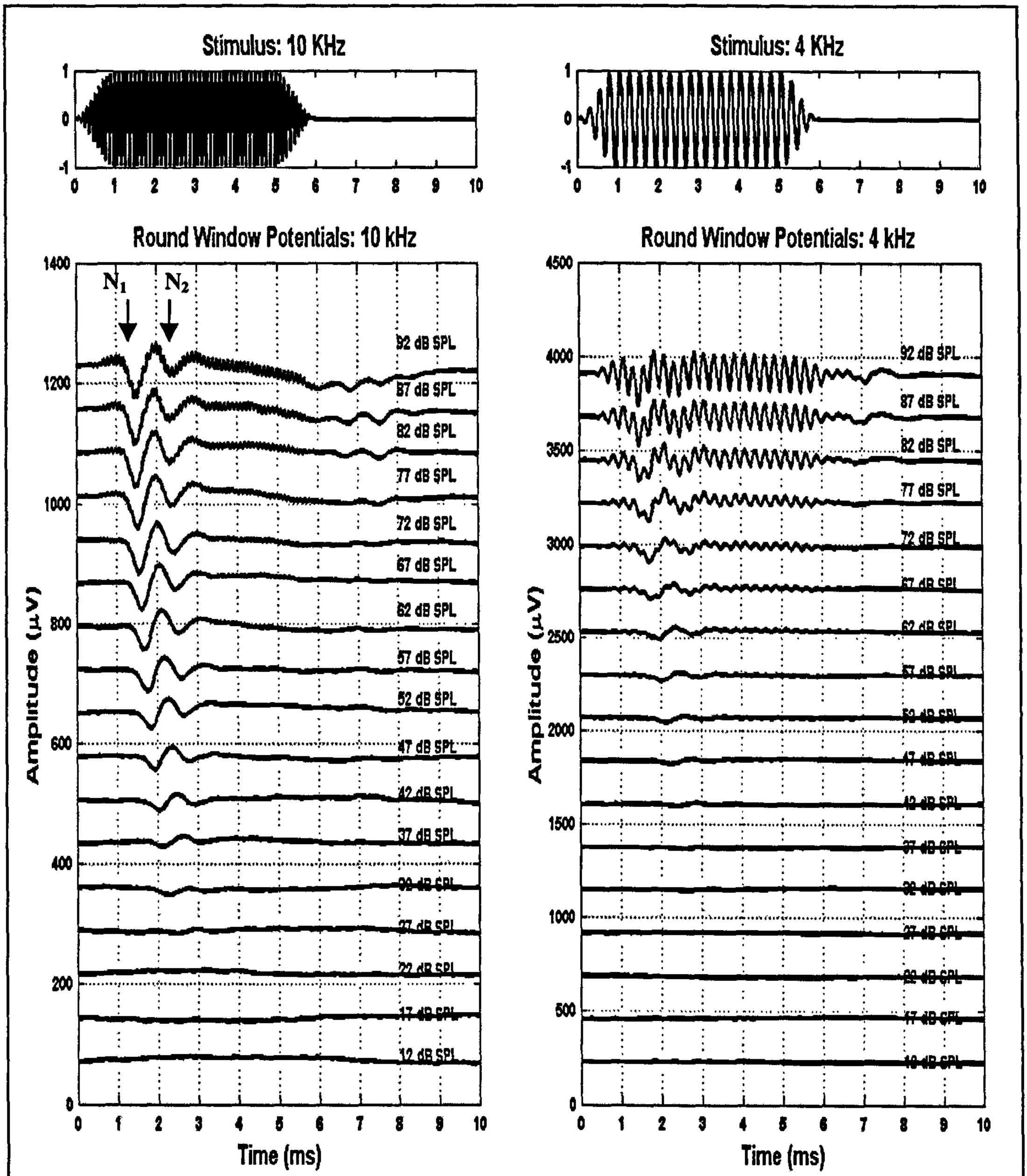

Figure 4-1 CAP waveforms to 10 and 4 kHz tone bursts at different sound pressure levels. Sound pressure levels are labeled on the right of every waveform in steps of 6 dB. The whole nerve action potential appears as one or two negative peaks in the recordings and is labeled N_1 and N_2.

The peak-to-peak values of CAP N_1 increase with the intensity under all the cochlear conditions of 10 and 4 kHz (Figure 4-2). This is because while single auditory nerve fibres responds only to limited range of tone frequencies at low SPLs (Kiang 1965; Kiang and Moxon 1974), at relatively high stimulus levels, almost every tone whose frequency lies below the characteristic frequency of the fibres will activate it (Kiang and Moxon 1974). This means that a continuous tone or tone bursts at high stimulus levels will excite a relatively large part of the cochlear partition. At low-intensity levels only a few nerve fibres will respond. With the increase of the sound pressure level, more and more of the cochlear partition is excited and the amplitude of CAP increases almost linearly. At the highest sound pressure levels being tested (92 dB SPL in this case), there is some evidence of saturation.

The CAP thresholds were determined from the I/O functions by defining a suitable criteron for threshold. If the criteria of the CAP threshold is 10 μV, as the lines shown in the figure, the values where the I/O curves cross the criteria line were considered to be the CAP threshold at that frequency and under that physiological condition. It is obvious that with the proceeding of the experiment, the CAP input-output functions shifted downwards and rightwards, indicating that the CAP threshold increased at that frequency and hearing was damaged to some extent. The criteria may vary in different animals. In the experiment, the high frequency CAP threshold (2-20 kHz) was determined visually, with a criterion that might be slightly different from the values calculated from the I/O functions.

The latency of CAP was defined as the time when the amplitude of CAP N_1 equalled 20% of the N_1 peak value. The latency provides the information on both neural and non-neural delays. The neural delay is comprised of (1) synaptic delay in the release and action of a chemical mediator between the hair cell and the afferent nerve endings; and (2) post-synaptic delay due to the conduction velocity of the action potentials in the cochlear nerve. The non-neural delay is comprised of (1) traveling wave delay; (2) a delay before a trigger point in the amplitude and phase of the displacement of the basilar membrane or the cochlear microphonic is reached to initiate the neural excitation; and (3) possibly some other unknown factors.

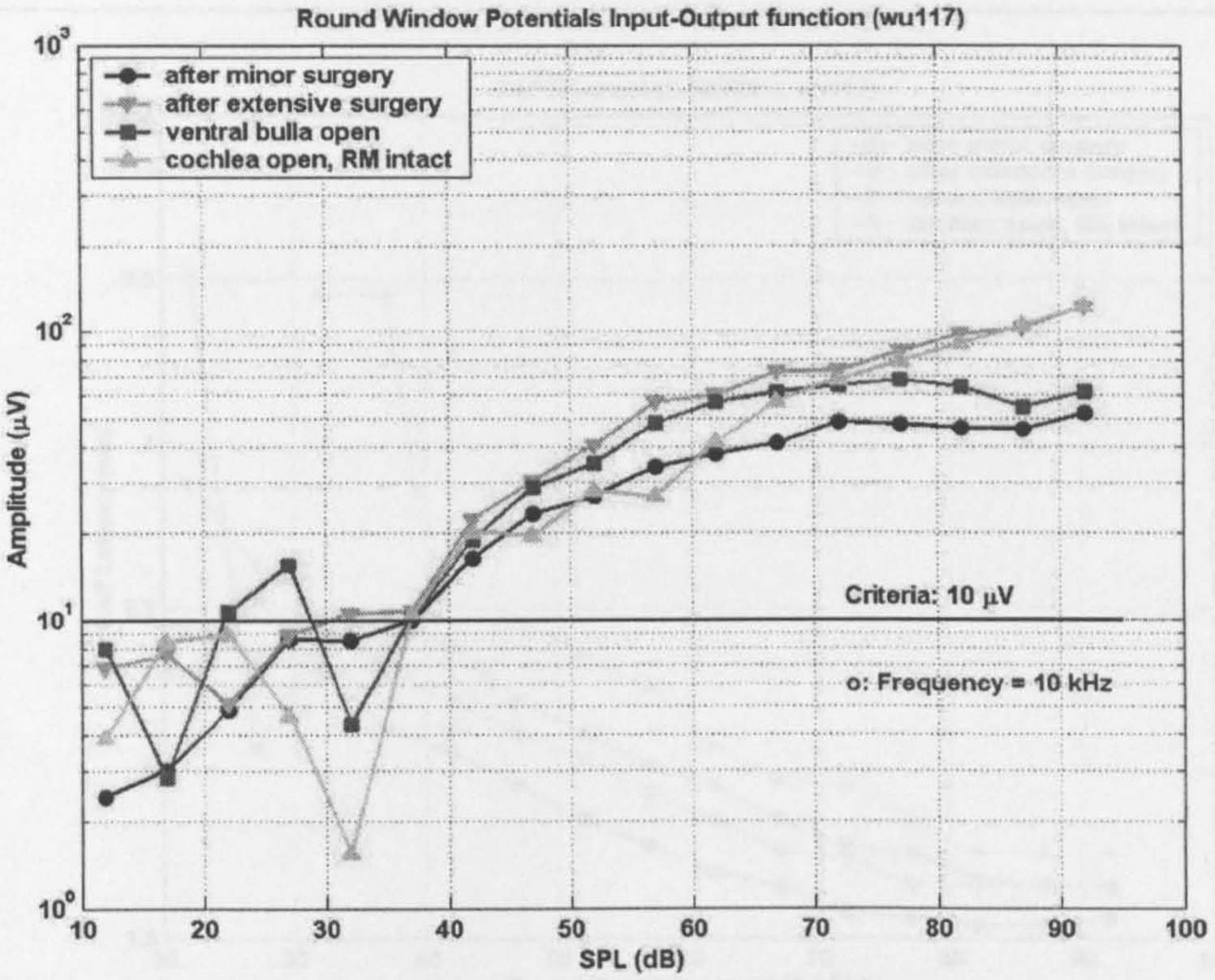

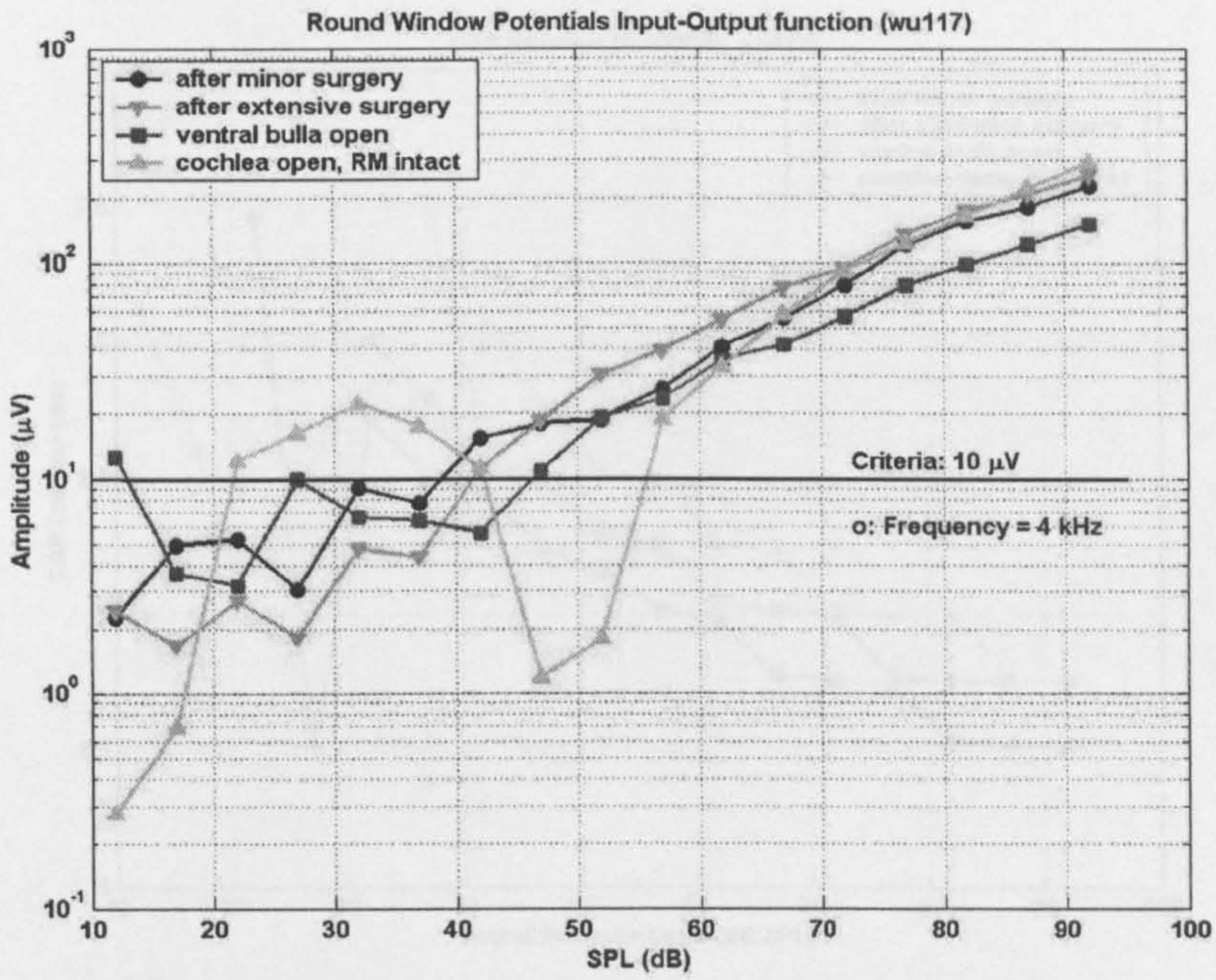

Figure 4-2 Input-output functions of round window potentials at 10k (top) and 4 kHz (bottom) under different cochlear conditions.

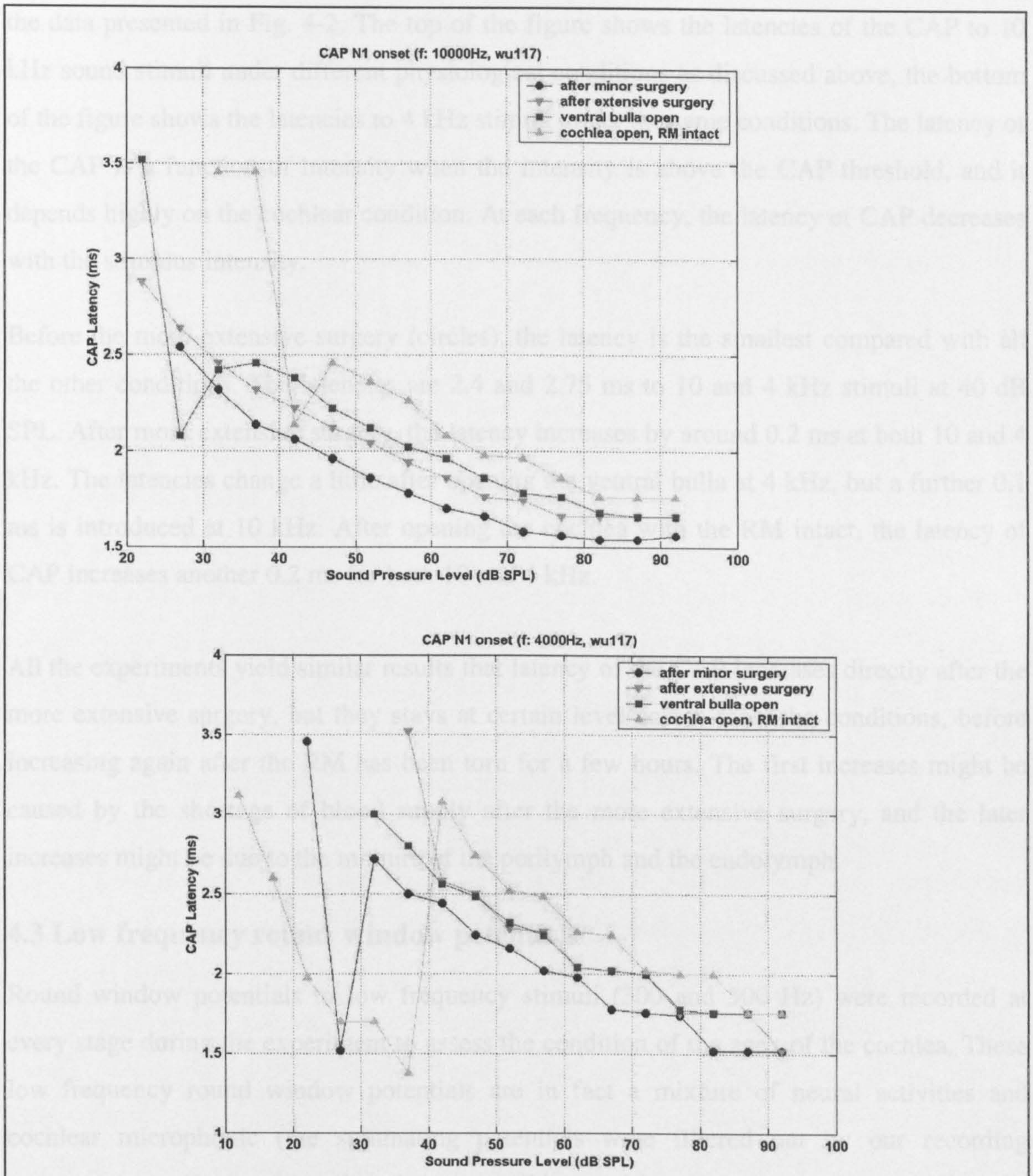

Figure 4-3 Delays of CAP N_1 onset (peak time) as a function of sound pressure level to 10 and 4 kHz stimuli at different conditions.

Figure 4-3 shows the latency of CAP N_1 calculated as a function of sound pressure level for the data presented in Fig. 4-2. The top of the figure shows the latencies of the CAP to 10 kHz sound stimuli under different physiological conditions as discussed above, the bottom of the figure shows the latencies to 4 kHz stimuli under the same conditions. The latency of the CAP is a function of intensity when the intensity is above the CAP threshold, and it depends highly on the cochlear condition. At each frequency, the latency of CAP decreases with the stimulus intensity.

Before the more extensive surgery (circles), the latency is the smallest compared with all the other conditions. The latencies are 2.4 and 2.75 ms to 10 and 4 kHz stimuli at 40 dB SPL. After more extensive surgery, the latency increases by around 0.2 ms at both 10 and 4 kHz. The latencies change a little after opening the ventral bulla at 4 kHz, but a further 0.1 ms is introduced at 10 kHz. After opening the cochlea with the RM intact, the latency of CAP increases another 0.2 ms for both 10 and 4 kHz.

All the experiments yield similar results that latency of the CAP increases directly after the more extensive surgery, but they stays at certain level across most the conditions, before increasing again after the RM has been torn for a few hours. The first increases might be caused by the shortage of blood supply after the more extensive surgery, and the later increases might be due to the mixture of the perilymph and the endolymph.

4.3 Low frequency round window potentials

Round window potentials to low frequency stimuli (300 and 500 Hz) were recorded at every stage during the experiment to assess the condition of the apex of the cochlea. These low frequency round window potentials are in fact a mixture of neural activities and cochlear microphonic (the summating potentials were filtered out by our recording equipment, see chapter 3), and so, it was possible to achieve the neural information by off-line data analysis.

In the experiments, low-frequency (300 and 500 Hz) stimuli were used with starting phases of 0° and 180°, respectively. The top panel of Figure 4-4 shows an example of the 500 Hz stimuli with the solid line representing the stimulus with 0° starting phase and the dotted line the stimulus with 180 ° starting phase. Just below this panel are the response

waveforms of round window potential to the two stimuli at 70 dB SPL. These raw waveforms consist both neural activities and the cochlear microphonic potentials. Pure cochlear microphonic waveforms can be obtained by subtracting the negative-phase responses from the positive-phase responses (third panel). As described in the methods section (chapter 3), the neural activities become attenuated, but the CM is left by this phase-locked technique. The neural component of the round window potentials was obtained by summing the raw potentials evoked by the reversed polarity stimuli (bottom panel).

The low frequency round window potentials evoked by reversed phase 300 and 500 Hz tone pips was studied as a function of sound pressure level (varied in a step of 5 dB) under all experimental conditions. With the increasing of the sound pressure level, the amplitude of the responses increases, and the shape of the waveforms changes. This is because each waveform represents a different mixture of neural and CM – derived activities. As shown in Figure 1, for high frequency stimuli, the neural responses of the cochlea have nearly constant shapes and so not change polarity if we reverse the polarity of the stimulus. However, the polarities of the CM potentials do change with changes in polarity of the stimulus, due to the CM "following" the motion of the basilar membrane.

Pure CM potentials were separated from the neural activities by the phase-locked technique. The average peak value of the derived CM potentials for 300 and 500 Hz stimuli were calculated and plotted as a function of sound pressure level shown in the left of Fig. 4-5. The maximum peak value of the derived neural activities of 300 and 500 Hz was calculated and plotted as a function of sound pressure level shown in the right of Fig.4-5. Data were collected under different conditions as the legend labeled in the figure. Both the CM potentials and neural activities increase with the sound pressure level, no matter what the condition of the cochlea. This is because when the sound pressure level is raised, more and more neural fibres were excited. Also, at higher sound pressure levels, the CM summed more potentials produced by the OHCs located at different points along the basilar membrane. For the CM potentials (left), little change occurred before and after the more extensive surgery and opening of the ventral bulla at low intensities. This indicates that the OHC function was little affected by the surgical approach to the apex of the cochlea.

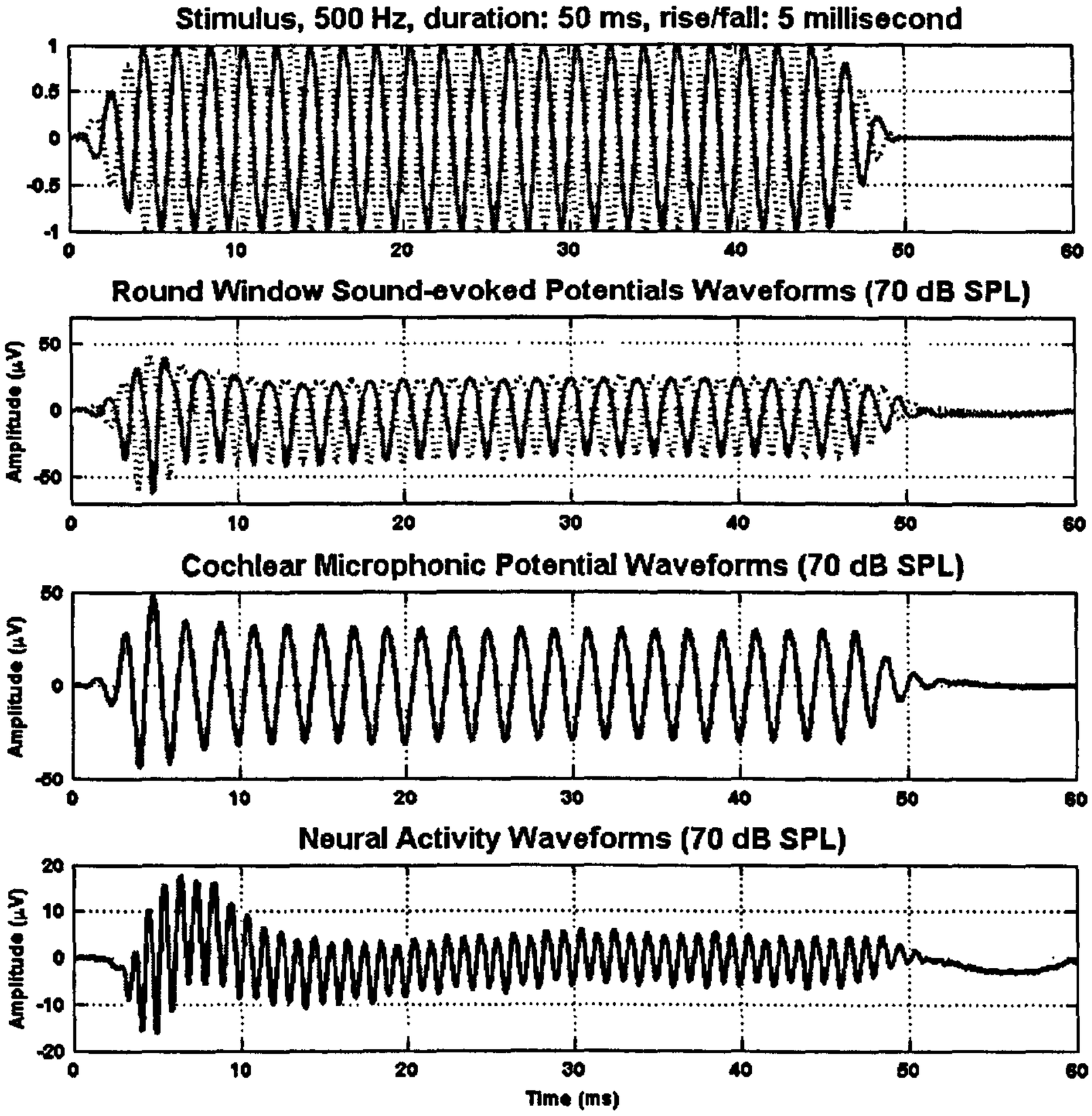

Figure 4-4 Illustration of driving pure CM potential and neural activity from round window potential. Top panel: 500 Hz stimuli with starting 0° (line) and 180° phases; Second panel: round window response waveform to the above two reversed phases stimuli (line - 0° phase and dotted line -180° phase); Third panel: derived pure CM potential waveform using phase-locked technique; Bottom panel: derived neural activity using phase-locked technique.

However, opening the cochlea decreased the amplitudes of the 300 Hz responses, but did not change much to the 500 Hz CM responses. This might indicate that opening the cochlea caused local damage to the low frequency part of the cochlea.

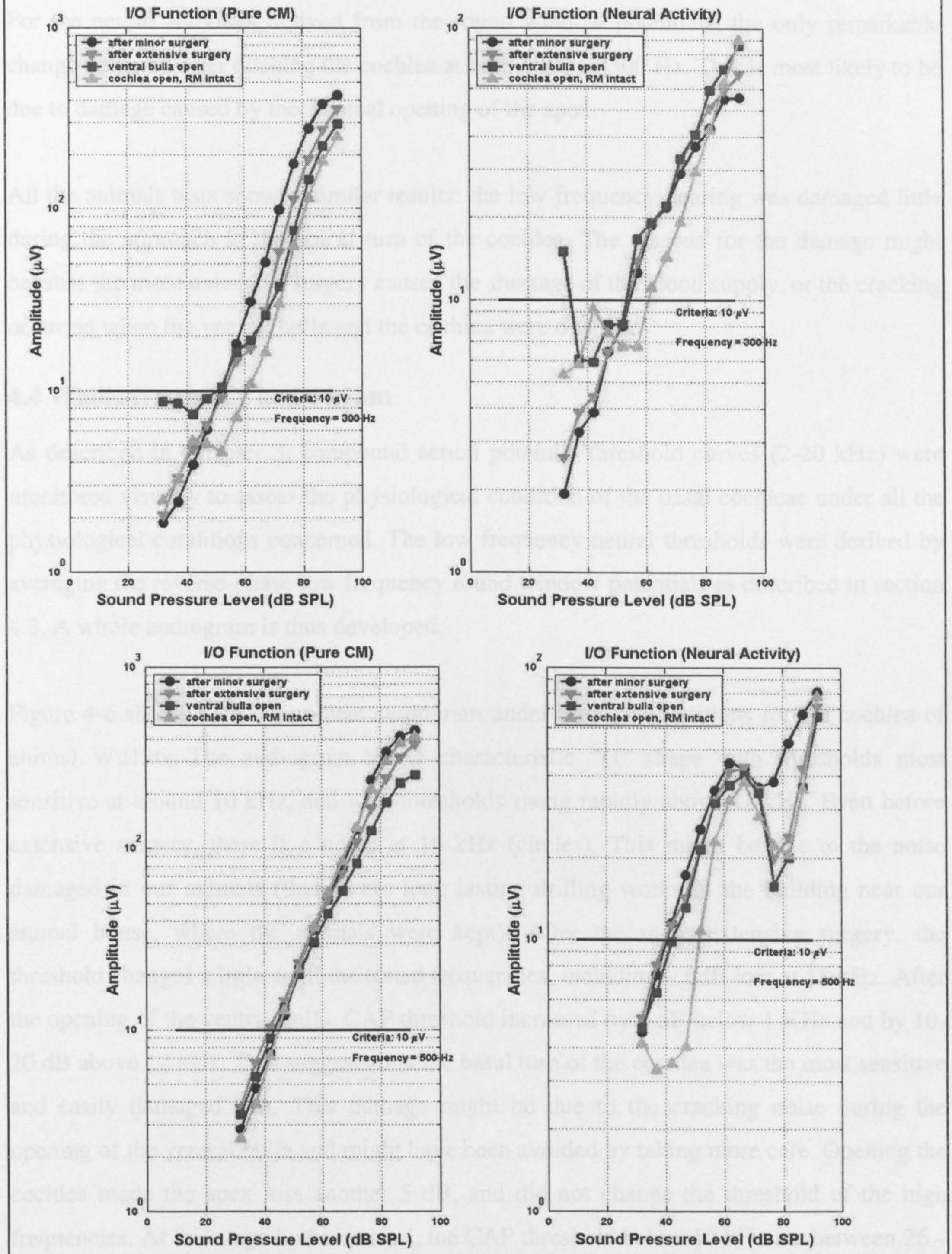

Figure 4-5 Input-output function of pure CM potential and neural activities derived from round window potentials.

For the neural activities derived from the round window potentials, the only remarkable change occurred after opening the cochlea at both 300 and 500 Hz. This is most likely to be due to damage caused by mechanical opening of the apex.

All the animals tests showed similar results: the low-frequency hearing was damaged little during the approach to the apical turn of the cochlea. The reasons for the damage might because the more extensive surgery caused the shortage of the blood supply, or the cracking occurred when the ventral bulla and the cochlea were opened.

4.4 Whole frequency audio gram

As described in Chapter 3, compound action potential threshold curves (2-20 kHz) were monitored visually to assess the physiological condition of the basal cochleae under all the physiological conditions concerned. The low frequency neural thresholds were derived by averaging the reverse-phase low frequency round window potentials as described in section 4.3. A whole audiogram is thus developed.

Figure 4-6 shows such a complete audiogram under 6 major conditions for the cochlea of animal Wu126: The audiogram has a characteristic "U" shape with thresholds most sensitive at around 10 kHz, and with thresholds rising rapidly above 12 kHz. Even before extensive surgery, there is a notch at 16 kHz (circles). This might be due to the noise damaged in our animals (there were long lasting drilling works in the building near our animal house, where the animals were kept). After the more extensive surgery, the threshold changes a little at all the tested frequencies, including ~ 6dB loss at 18 kHz. After the opening of the ventral bulla, CAP threshold increased by 5 dB below 1 KHz and by 10-20 dB above 12 kHz. This suggests that the basal turn of the cochlea was the most sensitive and easily damaged part. This damage might be due to the cracking noise during the opening of the ventral bulla and might have been avoided by taking more care. Opening the cochlea made the apex loss another 5 dB, and did not change the threshold of the high frequencies. At this stage in this animal, the CAP threshold below 10 kHz are between 26 – 40 dB SPL, which suggests that the cochlea is still working well, especially in low-frequency range. Because of the time consuming nature of making some mechanical measurements before opening the RM and trying to introduce reflective beads into the scala

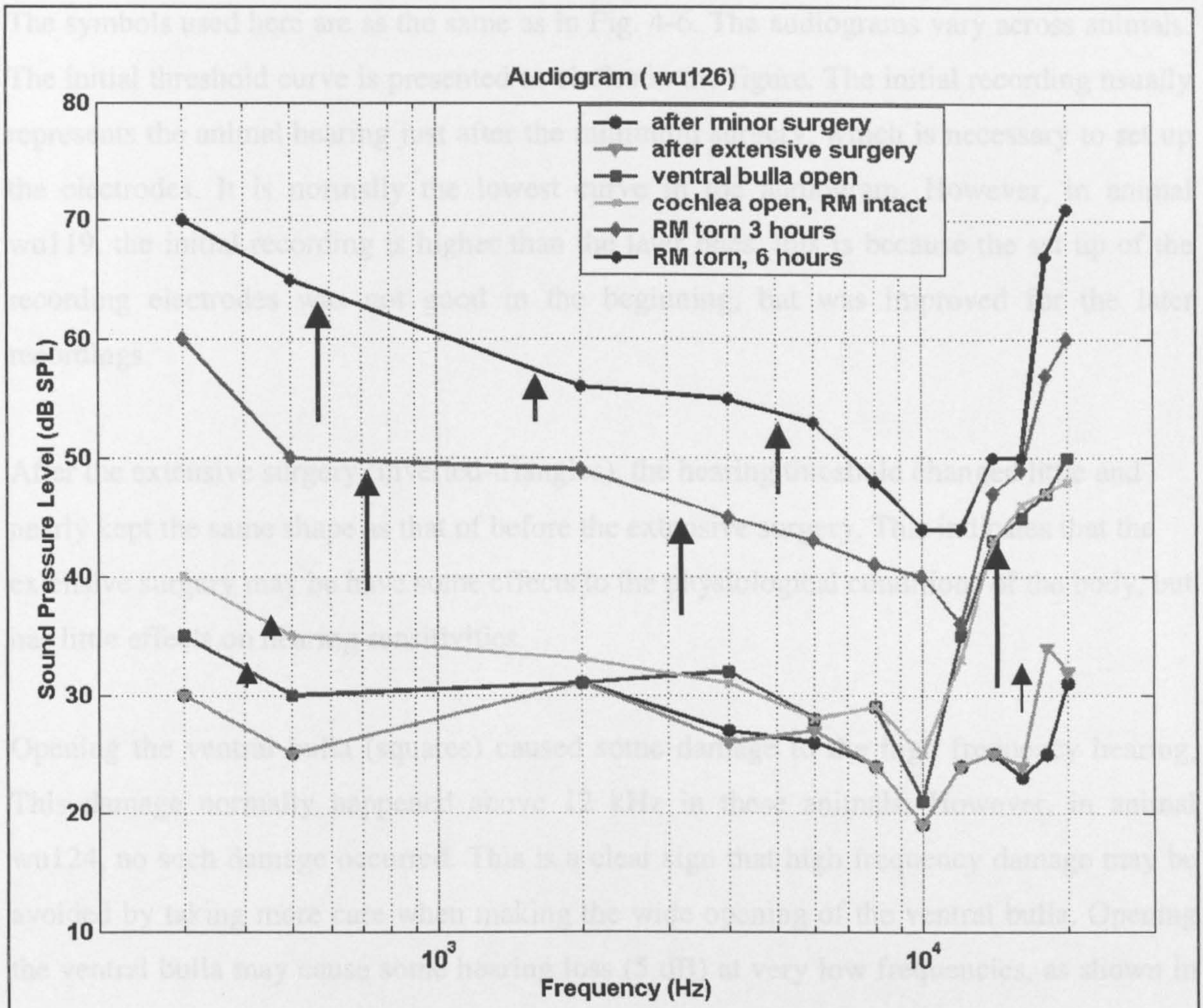

Figure 4-6 audiogram of animal wu126 under different cochlear conditions.

media, the next time the round window potentials were measured was 3 hours later after rupturing the RM. At this stage, there was a dramatic sensitivity loss of nearly 20 dB below 12 kHz and 5-10 dB above 12 kHz. The high frequency loss here was most likely just a continuation of the damage done earlier, the sensitivity continuing to get worse with time. The sensitivity loss below 10 kHz, might be caused by the mixing of the perilymph and the endolymph, which caused the cochlear condition to get worse with time. Another 3 hours later, further sensitivity loss of 10 dB occurred across almost all the frequencies. The CAP thresholds at 4 and 10 kHz were further confirmed by the input-output functions of these frequencies.

Figure 4-7 shows 6 more examples of audiograms under different physiological conditions. The symbols used here are as the same as in Fig. 4-6. The audiograms vary across animals. The initial threshold curve is presented as circles in the figure. The initial recording usually represents the animal hearing just after the minimum surgery, which is necessary to set up the electrodes. It is normally the lowest curve in the audiogram. However, in animal wu119, the initial recording is higher than the later ones, this is because the set up of the recording electrodes was not good in the beginning, but was improved for the later recordings.

After the extensive surgery (inverted-triangles), the hearing threshold changed little and nearly kept the same shape as that of before the extensive surgery. This indicates that the extensive surgery may be have some effects to the physiological conditions of the body, but has little effects on hearing sensitivities.

Opening the ventral bulla (squares) caused some damage to the high frequency hearing. This damage normally happened above 12 kHz in these animals. However, in animal wu124, no such damage occurred. This is a clear sign that high frequency damage may be avoided by taking more care when making the wide opening of the ventral bulla. Opening the ventral bulla may cause some hearing loss (5 dB) at very low frequencies, as shown in wu124. For other 5 animals, there is little hearing loss being observed.

Opening the cochlea (upright-triangles) caused some damage to hearing sensitivities, but the extent of this was usually within 10 dB, especially in the low-frequency range. This might be because the opening of the apex affects the low frequency hearing directly, or it might be due to some other reasons. There is one exception which shows that the hearing sensitivity could be maintained when opening the apex of the cochlea (wu117). Some high frequency hearing loss was observed at this stage, which most likely just a continuation of the damage done earlier, the sensitivity of hearing getting worse with time.

The thresholds were normally recorded between 1 and 3 hours after rupturing the RM (diamonds) and all the necessary mechanical recordings were collected. The hearing sensitivity got worse at almost all frequencies in animals wu128, wu125 and wu119. The

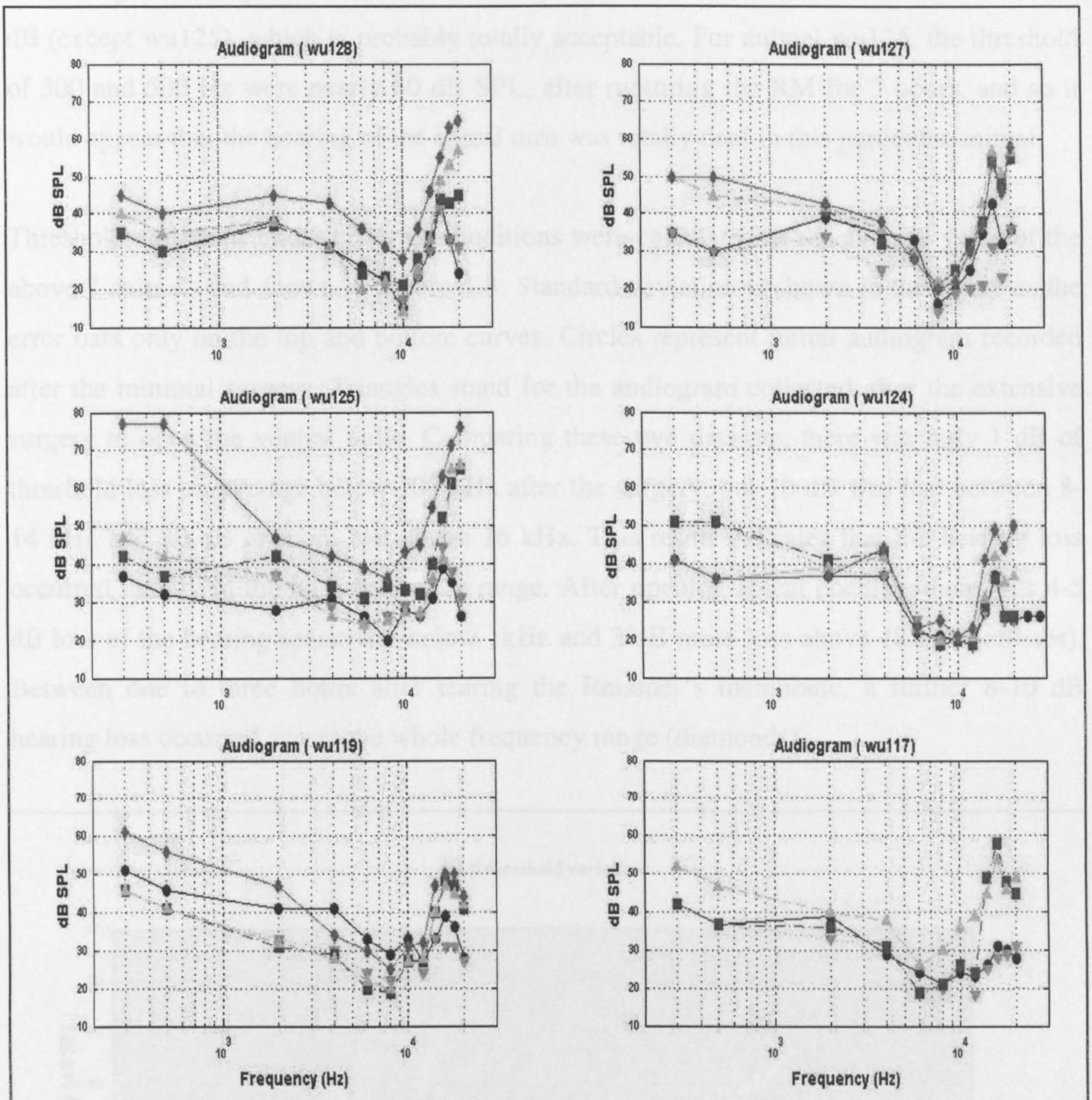

Figure 4-7 CAP audiograms of animals under different cochlear conditions. Circles: before surgery; Downright-triangles: after more extensive surgery. Squares: after opening the ventral bulla; Upright-triangles: after opening the cochlea with the RM and the helicotrema intact; diamonds: after rupturing the RM for 3 hours; Triangles: after rupturing the RM for 6 hours

possibility for this hearing damage could due to the mixing of the perilymph and the endolymph, which changed the ionic environment of the organ of Corti. However, for animals wu127 and wu125, the hearing sensitivities are nearly as the same as the previous recordings. This leaves some ground for us to believe that it is possible to keep the hearing sensitivities in good condition during a direct approach to the apex of the cochlea. Even for

the damaged hearing sensitivities, the threshold of 300 and 500 Hz are between 35 and 60 dB (except wu125), which is probably totally acceptable. For animal wu125, the threshold of 300 and 500 Hz were nearly 80 dB SPL, after rupturing the RM for 3 hours, and so it would appear that the hearing of the apical turn was totally deaf in this particular animal.

Threshold variations under different conditions were calculated as the average value of the above 7 animals and shown in Figure 4-8. Standard deviation is shown in the figure as the error bars only on the top and bottom curves. Circles represent initial audiogram recorded after the minimal surgery. Triangles stand for the audiogram collected after the extensive surgery to open the ventral bulla. Comparing these two datasets, there was only 1 dB of threshold loss on average below 1000 Hz after the surgery, but 10 dB was lost between 8-14 kHz and 20 dB or more lost above 16 kHz. This result indicates that the hearing loss occurred mainly in the high frequency range. After opening apical cochlea, there was 4-5 dB loss of the hearing sensitivity below 1kHz and 3 dB more loss above 18 kHz (crosses). Between one to three hours after tearing the Reissner's membrane, a further 8-10 dB hearing loss occurred across the whole frequency range (diamonds).

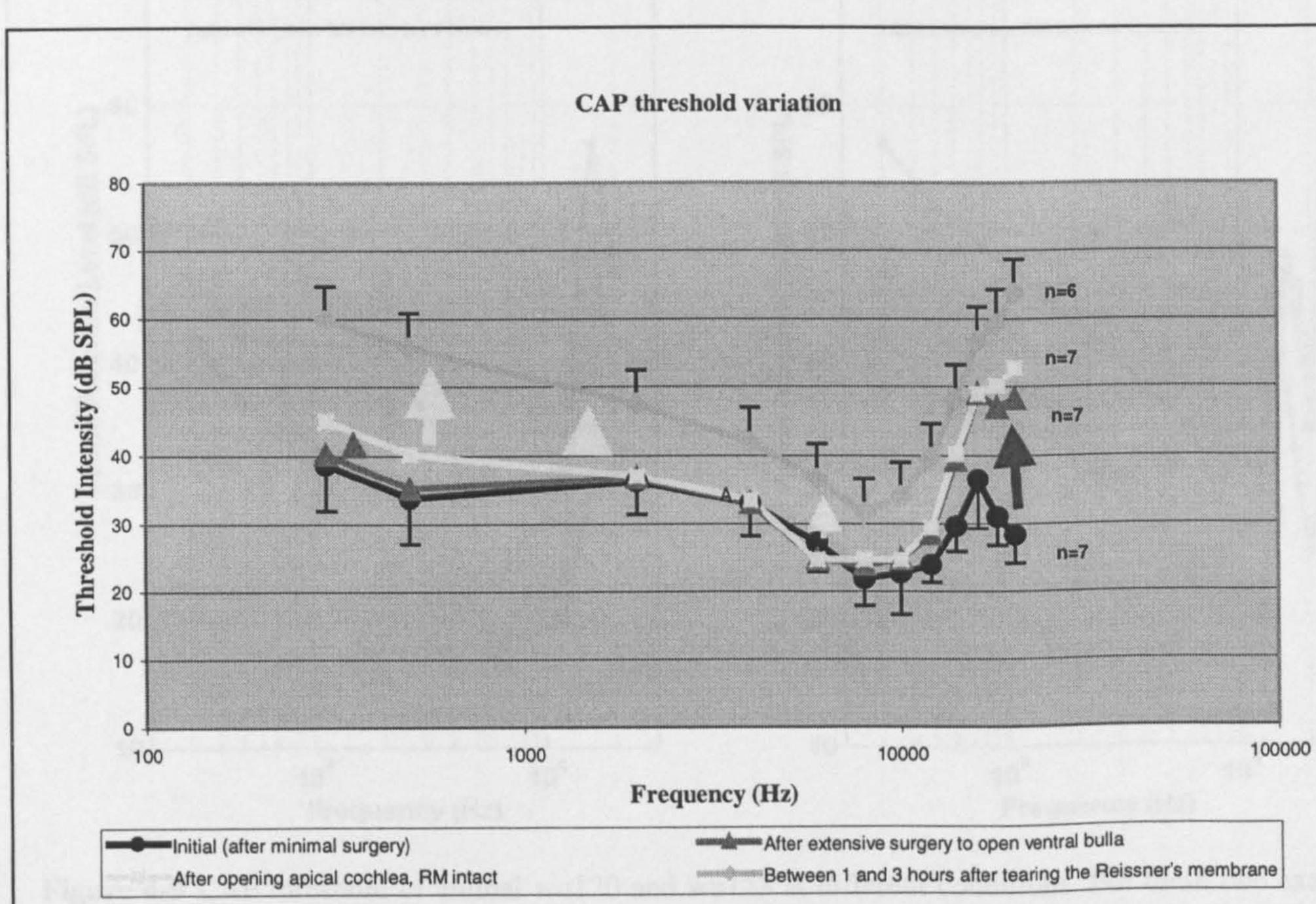

Figure 4-8 CAP threshold variation under different physiological conditions. The CAP threshold was averaged across 7 animals at four major stages during the approaching to the apical turn of the cochlea.

The time course of this loss was explored in greater detail in two animals, as illustrated in Figure 4-9. In these animals, the RM was torn immediately after opening the cochlea. In the figure, downright triangles represent the audiograms after the extensive surgery, squares stand for the audiogram after the ventral bulla was widely open, diamonds shows the hearing sensitivity after the opening of the apex of the cochlea, when the RM was torn simultaneously, and triangles represent the audiogram 3 hours after tearing the RM. Opening the apical turn of the cochlea and tearing Reissner's membrane caused little or no immediate hearing loss (compare squares and diamonds in audiograms in Figure 4-9). Most of the high frequency loss was incurred on opening the ventral bulla, as opposed to during the surgical exposure of the bulla. Both the surgery and the opening of the bulla could

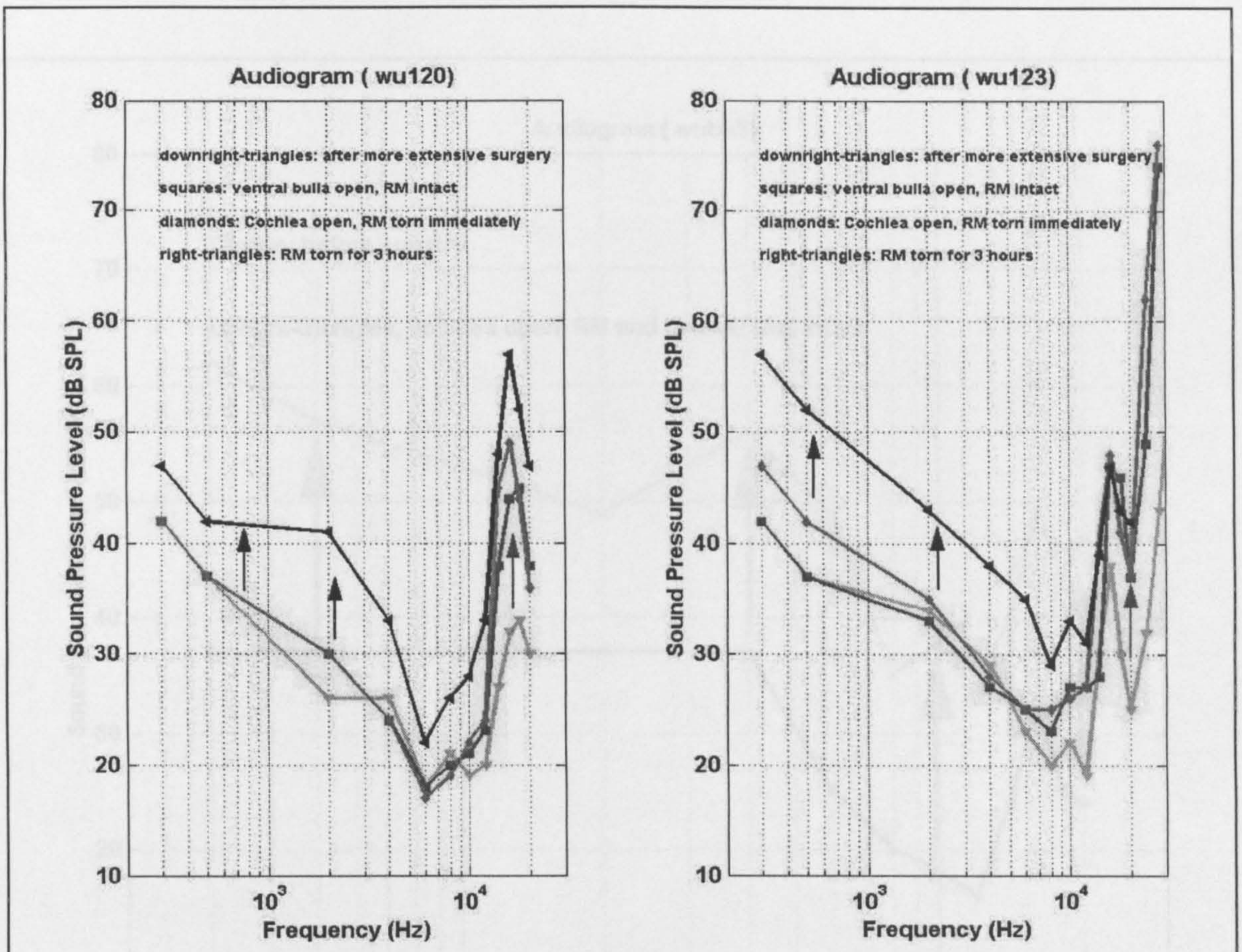

Figure 4-9 CAP threshold of animal wu120 and wu123 at different conditions. For these two examples, the RM was torn directly after opening the cochlea. This didn't cause immediately hearing loss. However, under the same condition, three hours later, the hearing became worse for the whole testing frequency range and CAP threshold kept worse after another three more hours between 2 to 6 kHz.

cause around 5 dB of low-frequency hearing loss. Three hours after tearing the RM, however, the audiogram showed 2-10 dB loss across the whole range of frequencies tested.

4.5 General findings

Most cochleae were both sensitive and very vulnerable. By comparison with the initial audiogram, which was collected before the more extensive surgery, in 10 cases out of 17, the thresholds to a wide range of frequencies increased more than 10 dB after the opening of the cochleae. One extreme example is shown in Figure 4-10, in which the hearing sensitivity decreases roughly 20-dB after the cochlea was opened. The reason for this hearing loss is still uncertain. These losses could be due to acoustic trauma (damage to the hair cells), they could be due to mechanical/physiological damage (e.g. accidental tearing of the RM or surgical shock to blood supply), or they could be due to the

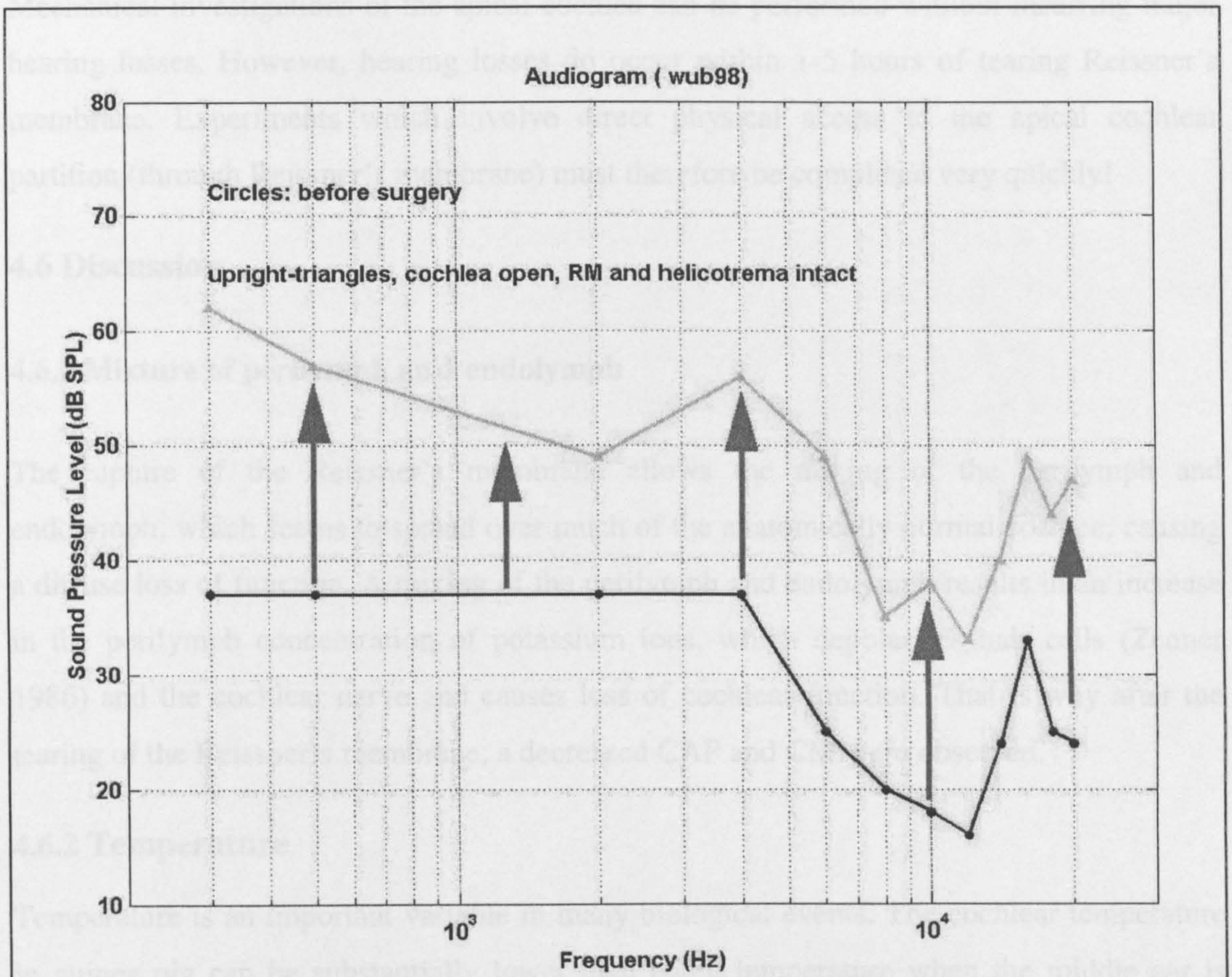

Figure 4-10 Audiogram of wub98. Circles are the audiogram before the more extensive surgery. Diamonds are the audiogram after the opening of the apex of the cochlea.

hydrodynamic/mechanical effects of opening the scala vestibuli.

In summary, based on the recording of round window potentials of high and low frequencies, a complete audiogram provides the assessment of physiological condition of the entire cochlea. During mechanical investigations of the apical cochlea, the surgery and/or the opening of the bulla caused significant hearing loss at high frequencies, but could have negligible effects on low frequency thresholds. Opening the apical turn of the cochlea caused an average threshold elevation of 5 dB at low frequencies, but had little effect on the high frequency thresholds. Further threshold losses of between 8 and 16 dB occurred within 1 to 5 hours of tearing Reissner's membrane in the apical turn of the cochlea. These losses were not restricted to low frequencies, and were probably caused by long term changes in the ionic compositions of the cochlea's endolymphatic and perilymphatic fluids.

Mechanical investigations of the apical cochlea can be performed without incurring major hearing losses. However, hearing losses do occur within 1-5 hours of tearing Reissner's membrane. Experiments which involve direct physical access to the apical cochlear partition (through Reissner's membrane) must therefore be completed very quickly!

4.6 Discussion

4.6.1 Mixture of perilymph and endolymph

The rupture of the Reissner's membrane allows the mixing of the perilymph and endolymph, which seems to spread over much of the anatomically normal cochlea, causing a diffuse loss of function. A mixing of the perilymph and endolymph results in an increase in the perilymph concentration of potassium ions, which depolarizes hair cells (Zenner 1986) and the cochlear nerve and causes loss of cochlear function. That is why after the tearing of the Reissner's membrane, a decreased CAP and CM were observed.

4.6.2 Temperature

Temperature is an important variable in many biological events. The cochlear temperature in guinea pig can be substantially lower than rectal temperature when the middle ear is surgically exposed. This lower temperature is the result of heat transfer by evaporation,

convection and radiation from the exposed area to cooler air and surrounding. Previous studies have shown that decreased cochlear temperature causes a reversible reduction in cochlear microphonic amplitude (Butler 1960) with little or no change in CM latency (Eggermont 1974). Small losses in CM sensitivity were observed and these were also progressively less for lower frequencies. Summating potential changes also occur with hypothermia. Experiments have also shown that hypothermia affects the CAP to a greater extent than CM. The CAP threshold elevations are usually greatest at in high frequencies with decreased temperature in the guinea pig and the CAP latency is increased (Brown et al. 1983; Brown et al. 1983). However, it should also be mentioned that the CAP threshold shifts restricted to high frequencies can occur when cracking noises are made during removal of segments of bone from the auditory bulla in guinea pigs. Thus surgical trauma may also be an additional factor in some acute preparations (Brown et al. 1983).

4.6.3 Different guinea pig audiograms

Some published guinea-pig audiograms are shown in Figure 4-11 and compared with our audiogram averaged of 17 animals under normal condition (before more extensive surgery). Our data presented here (crosses) are consistent with those of Johnstone (Johnstone et al. 1979) and Liberman (Liberman and Gao 1995), but not with Nuttall (Nuttall et al. 1997) and Murugasu (Murugasu and Russell 1996) for most of the frequencies. However, there was a distinct notch in our data at 16 kHz. The only explanation for this notch was that our animals were subjected to lasting noise-exposures caused by building work during these studies. This noise could explain the notch because 16 kHz is usually one of the most sensitive frequencies in the guinea pig, which is also easily damaged by noise. Other possibilities are that the notch was peculiar to the particular strains of guinea pigs that we used.

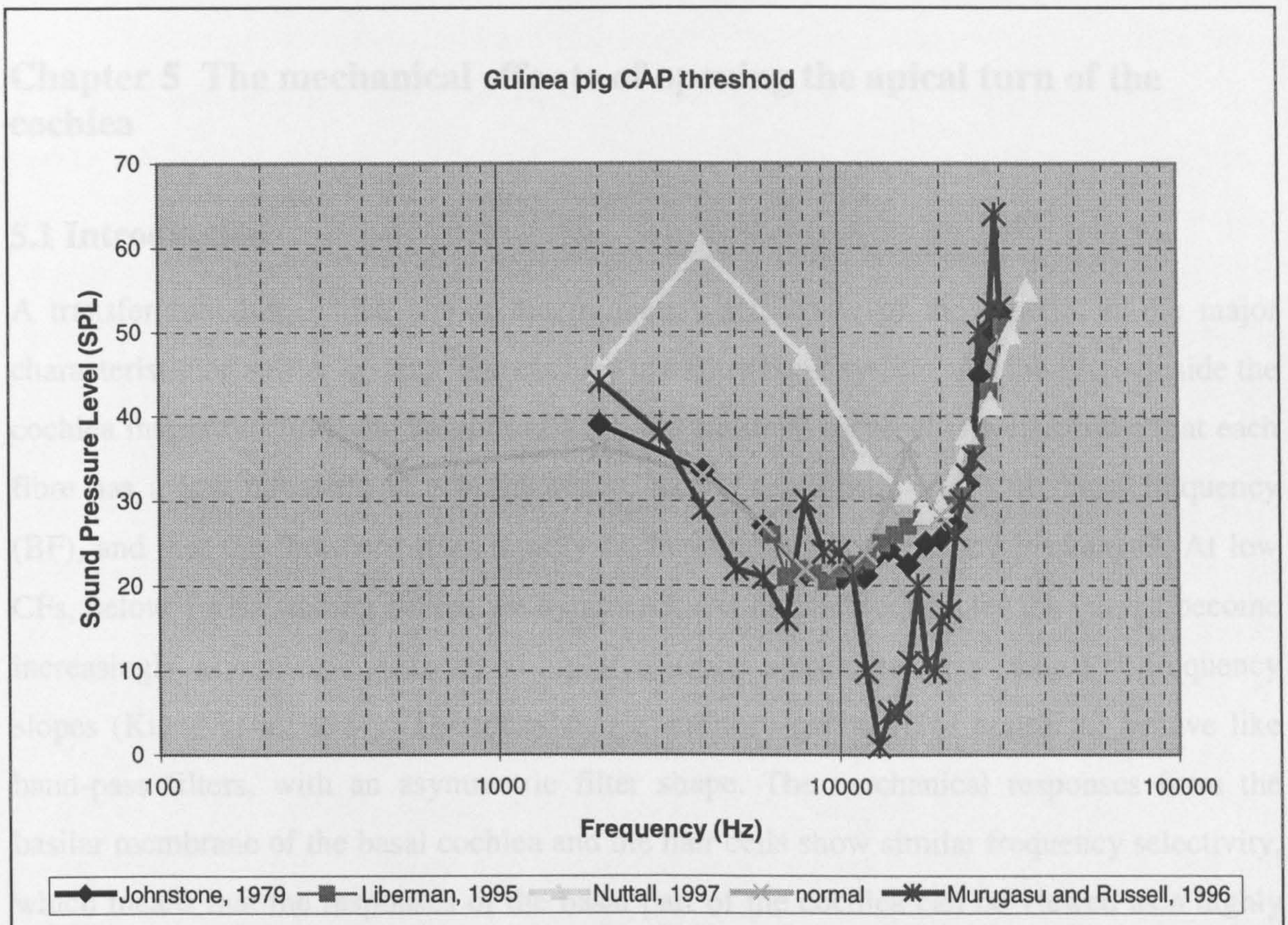

Figure 4-11 Comparison Guinea-pig audiogram with published data. Diamonds stand for the data published by Johnstone in 1979. Squares represent the audiogram described by Liberman in 1995. Triangles are the audiogram published by Nuttall in 1997. Starts are the audiogram measured by Murugasu and Russell in 1996 and the crosses are our averaged audiogram over 17 animals.

Chapter 5 The mechanical effects of opening the apical turn of the cochlea

5.1 Introduction

A transfer function, which shows the frequency selectivity of the system, is the major characteristic of a filter system. The cochlea is a filter bank system. All the filters inside the cochlea interact to fulfil the hearing task. In the auditory nerve, it is well known that each fibre has a low threshold at one frequency, the 'characteristic' (CF) or 'best' frequency (BF), and that the threshold rises rapidly as the stimulating frequency is changed. At low CFs, below 1 kHz, tuning curves are symmetric. At higher frequencies the curves become increasingly asymmetric, with steep high-frequency slopes and less steep low-frequency slopes (Kiang et al. 1967). Therefore, single auditory nerve fibres appear to behave like band-pass filters, with an asymmetric filter shape. The mechanical responses from the basilar membrane of the basal cochlea and the hair cells show similar frequency selectivity, which means that the responses of the basal part of the cochlea can be viewed as a highly tuned filter too.

However, the shapes of the mechanical transfer functions observed in the apical turn *in vivo* show distinct notches (Cooper and Rhode 1995; Cooper 1996; Cooper and Rhode 1996; Gummer et al. 1996; Cooper and Rhode 1997; Hemmert et al. 2000; Zinn et al. 2000), which are not present either in the basal turn of the cochlea (Rhode 1974; Khanna and Leonard 1982; Sellick et al. 1982; Johnstone et al. 1986; Robles et al. 1986; Cooper and Rhode 1992; Cooper and Rhode 1992; Ruggero 1992; Ruggero et al. 1997; Narayan et al. 1998), or in nerve-fibre recordings (Evans 1972; Rose and Weiss 1988). Gummer (Gummer et al. 1996) suggested that the notches observed from the tectorial membrane are evidence of a second filter in the cochlea. On the other hand, Cooper and Rhode (Cooper and Rhode 1996) suggested that the notches were artifacts produced by opening the cochlea.

The ideal approach to study the function of the apical turn of the cochlea is to measure the mechanical vibration *in vivo*. This requires direct access to the inside of the cochlea. The effects of opening the fluid-filled cochlea might be dramatic, but they are not well understood. This chapter presents an investigation of the factors responsible for the notches

in the mechanical recordings from the apical turn of the cochlea *in vivo*. Experiments were performed under two different cochlear conditions: sealed and unsealed cochleae. The sealed condition was achieved by sealing a glass coverslip onto the support chamber using high-vacuum grease after the initial opening of the cochlea. For unsealed cochleae, the tight connection between the coverslip and the grease was broken, allowing fluid to escape from the apical cochlea. Responses were collected both from Hensen's cells (HC) and from the tectorial membrane. The Hensen's cells (the only natural structure in the apex of the cochlea which provided enough reflection for the laser interferometer system) recordings were compared with recordings from single reflective beads settled on the tectorial membrane in the same preparation. The recordings from HC were collected from the cochlea both before and after the Reissner's membrane (RM) was torn. However, recordings from the tectorial membrane could only made after the RM was torn and the perilymph and endolymph mixed together. Pure tone pips and clicks were used to study the responses of the cochlear partition both in the time and the frequency domains. The experimental evidence supports the suggestion that the notches in the transfer function curves are due to the interaction of 'fast' and 'slow' waves, and that the 'fast' wave is very sensitive to the hydraulic state of the cochlea.

Due to the difficulties of re-sealing cochleae after the initial openings, only 8 out of 38 cochleae provided convincing data on the mechanical effects of opening the apical turn of the guinea-pig cochlea. Data from two of the best experiments (wub92 and wu126) are highlighted in this chapter. Responses from these cochleae were selected for presentation because: (1) the responses were stable (remaining invariant over several hours of the recording); (2) responses were available for comparison under two different conditions; and (3) responses were especially sensitive and vulnerable to the cochlear condition. In one case (wub92), the cochlea was judged to be in good physiological condition during the measurements, because clear shifts in the baseline position of its partition were evoked by sound before rupturing the RM.

5.2 Effects on responses to pure tone stimuli – in the frequency domain

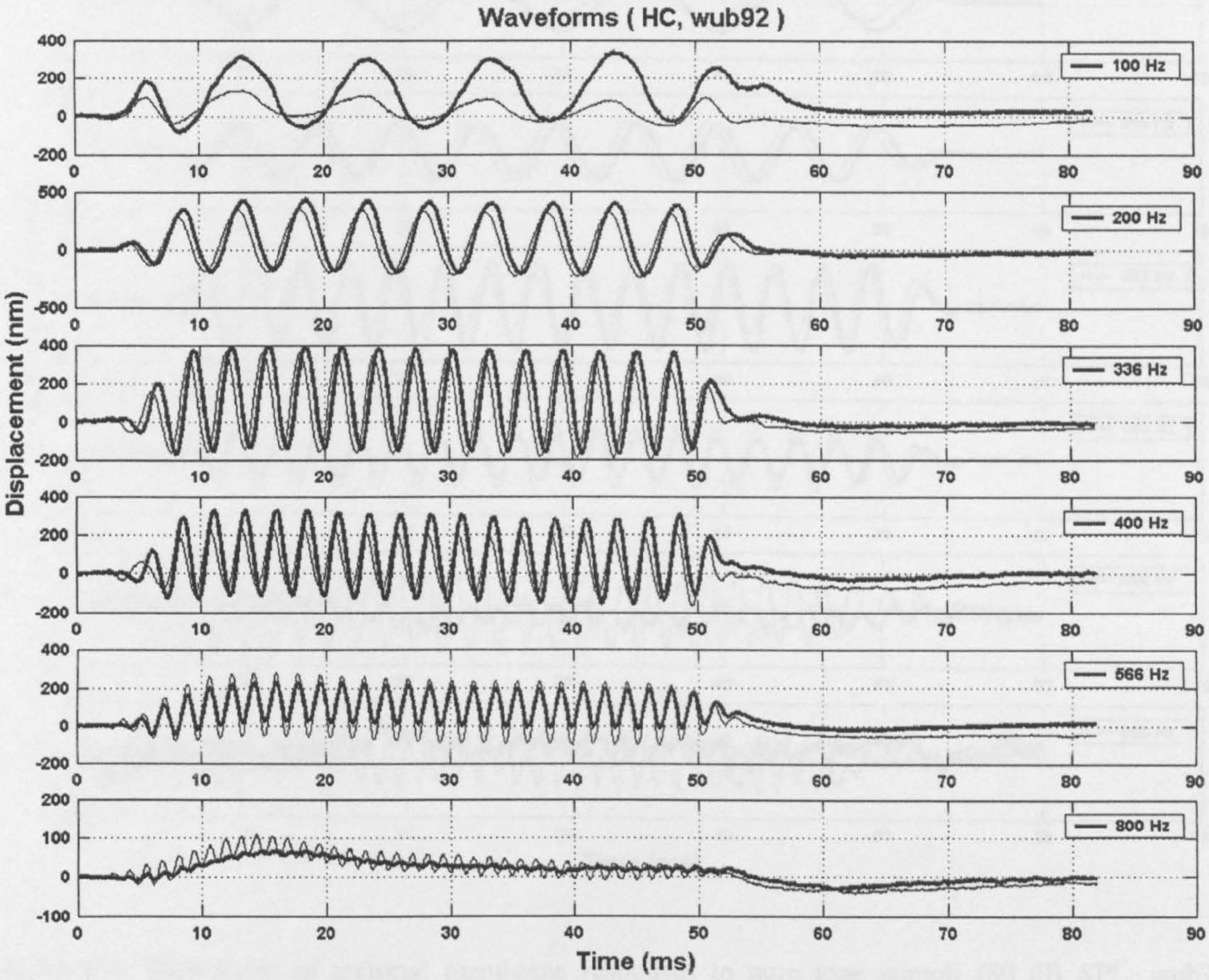

Figure 5-1 Waveforms of Hensen's cell responses to pure tone stimuli (80 dB SPL, wub92). Responses were collected from the cochlea when the Reissner's membrane was intact. Thick lines represent recordings from a single Hensen's cell when the cochlea was sealed. Thin lines indicated responses from a different single Hensen's cell when the seal was broken. Stimulus frequencies are labeled on the right of the figure.

In vivo responses to pure tone pips are presented for one animal (wub92) in Figures 5-1 and 5-2. These waveforms to pure tone stimuli were collected from a single Hensen's cell (Fig. 5-1) and a reflective bead settled on the tectorial membrane (Fig. 5-2), respectively. Thick lines show responses under sealed conditions, while the thin lines show responses from the same locations but under unsealed conditions. The stimulus frequencies were 100, 200, 336, 400, 566 and 800 Hz as labeled on the figures. The stimulus intensity was 80 dB SPL. All responses include a clear sinusoidal component both under sealed and unsealed conditions. There is also an upward baseline position shift in the recordings from the Hensen's cells,

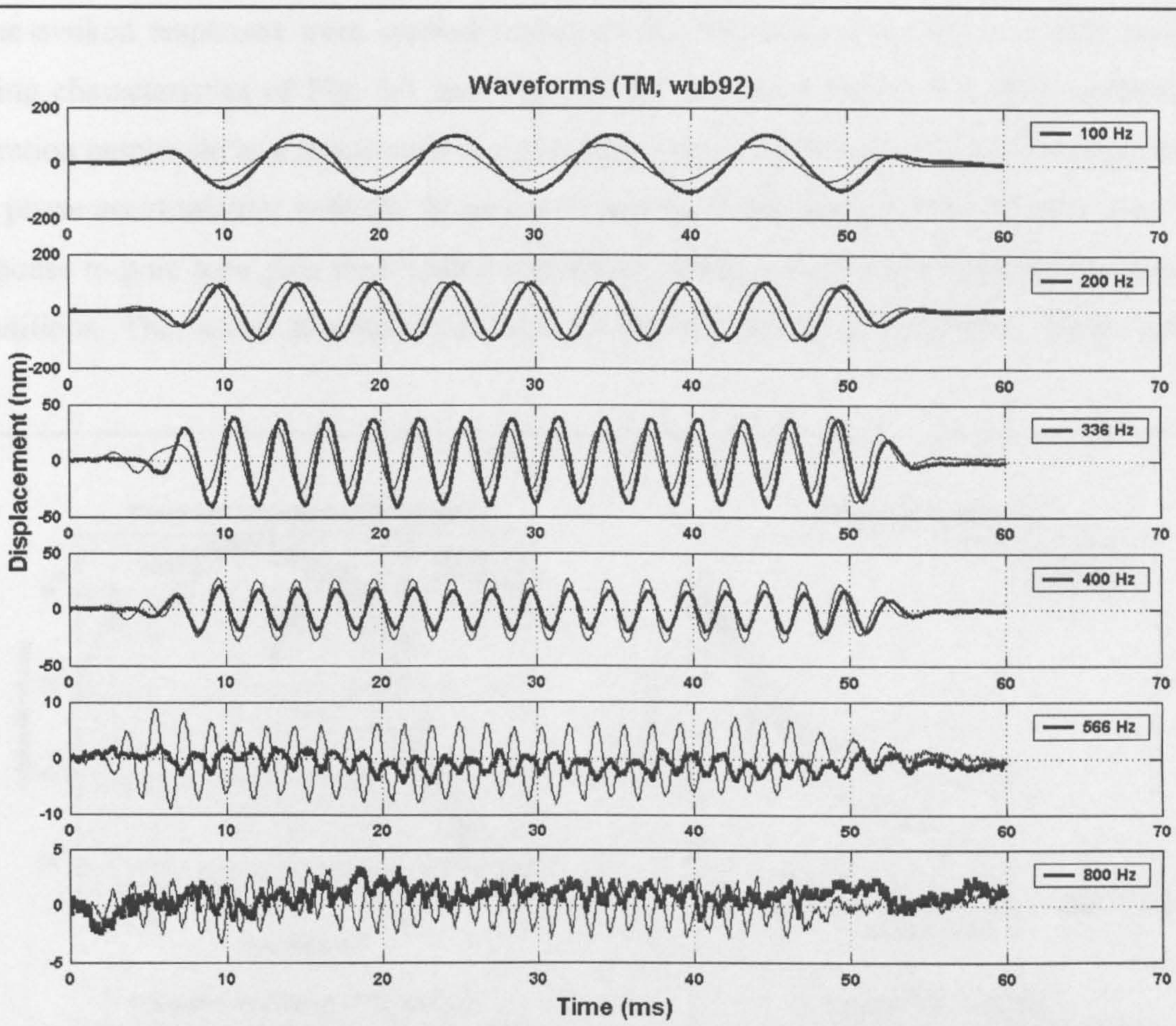

Figure 5-2 Waveforms of tectorial membrane responses to pure tone stimuli (80 dB SPL, wub92). Responses were collected from the cochlea when the Reissner's membrane was torn. Thick lines represent recordings from single reflective bead on the tectorial membrane when the cochlea was sealed. Thin lines indicate responses from the same bead when the seal was broken. Stimulus frequencies are labeled on the right of the figure.

but this will be discussed in later chapters. At low frequencies (less than the BF of around 300 Hz), the responses from the sealed cochleae are bigger than those from the unsealed cochleae. For example, the amplitude of Hensen's cells vibrations fall by 9 dB (Fig. 5-1) and those of the tectorial membrane fall by 4 dB at 100 Hz (Fig. 5-2) respectively, after breaking the seal of the cochlea. Above the best frequency, the amplitudes of the responses from sealed cochleae are less than those from unsealed ones. For example, there were 4 dB losses at 566 Hz for the Hensen's cell (Fig. 5-1) and at 400 Hz for the tectorial membrane (Fig. 5-2) under sealed conditions. Moreover, it is worth to noting that responses under unsealed condition occurred earlier than those from sealed conditions.

Tone-evoked responses were studied frequency by frequency from 50 to 2 kHz and the tuning characteristics of Fig. 5-1 and Fig. 5-2 are shown in Figure 5-3. The variation in vibration amplitude as a function of stimulus frequency is depicted in the left column, while the phase accumulation with the frequency is shown in the right column. Circles show the response to pure tone pips from sealed conditions, while crosses show those from unsealed conditions. The sound stimulus level was 80 dB SPL for these examples. Under sealed

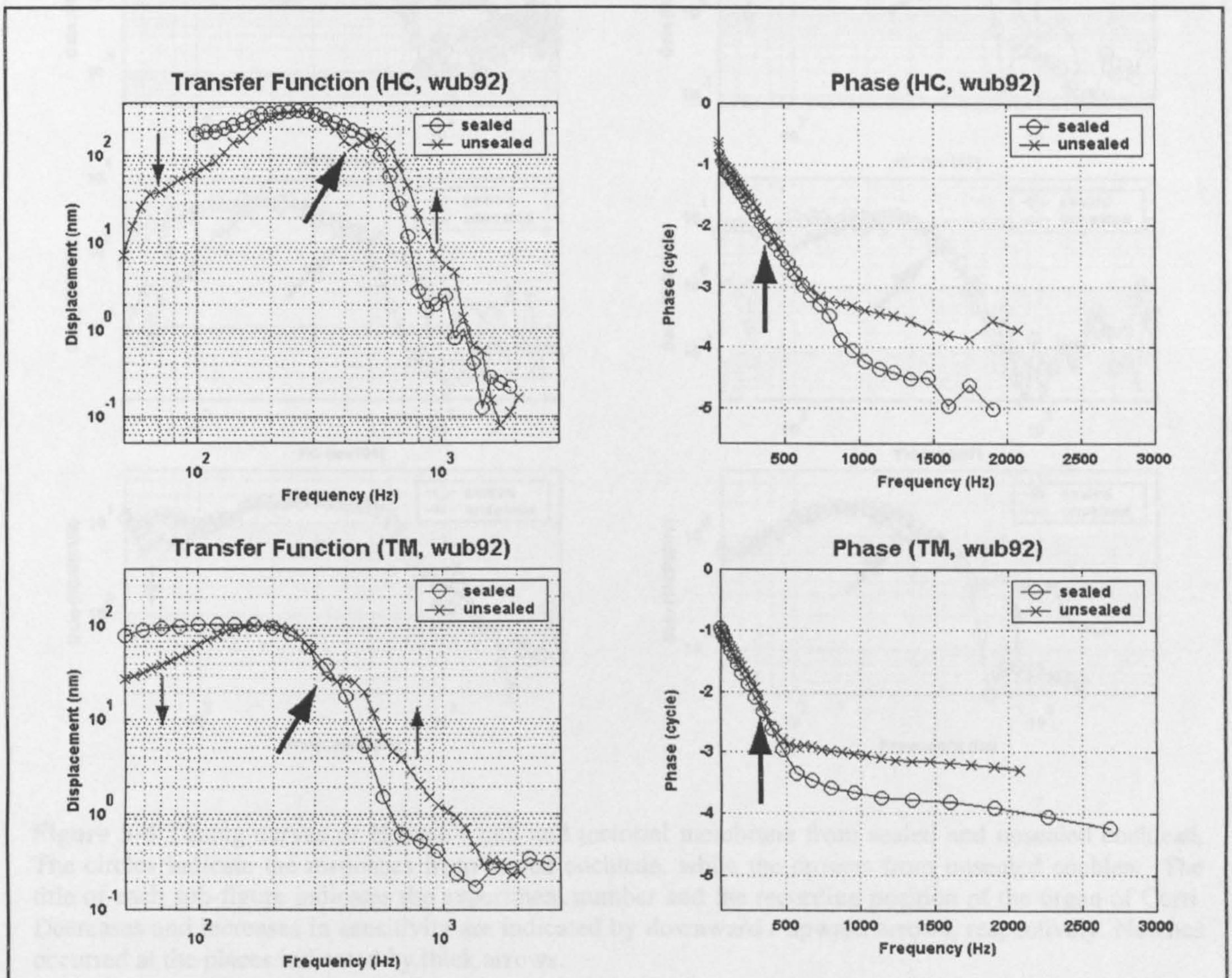

Figure 5-3 Tuning curves derived from tone-evoked responses of Hensen's cell (top, left) and tectorial Membrane (bottom, left) from the same recording location as in Fig. 5-1 and Fig. 5-2. Sound pressure level is 80 dB SPL. Circles show the transfer functions from sealed cochlea. Crosses indicate responses from unsealed cochlea. Right column shows the phase accumulation as a function of frequency.

conditions, the tuning curves were relatively flat below the preparation's BF. The low frequency cut-off slopes for the 4 data sets in Fig. 5-3 are 3.7, 10.4, 0.2 and 7.8 dB/oct. between 100 and 200 Hz (HC sealed and unsealed, TM sealed and unsealed, respectively).

Above the BF of around 200 – 300 Hz, the tuning curves fall progressively and after the cut off frequencies of around 400 – 600 Hz, they decrease quickly with slopes of –30.4, -37.5, -9, and –20.05 dB/oct at 800 Hz, respectively. For the unsealed conditions, the tuning curves

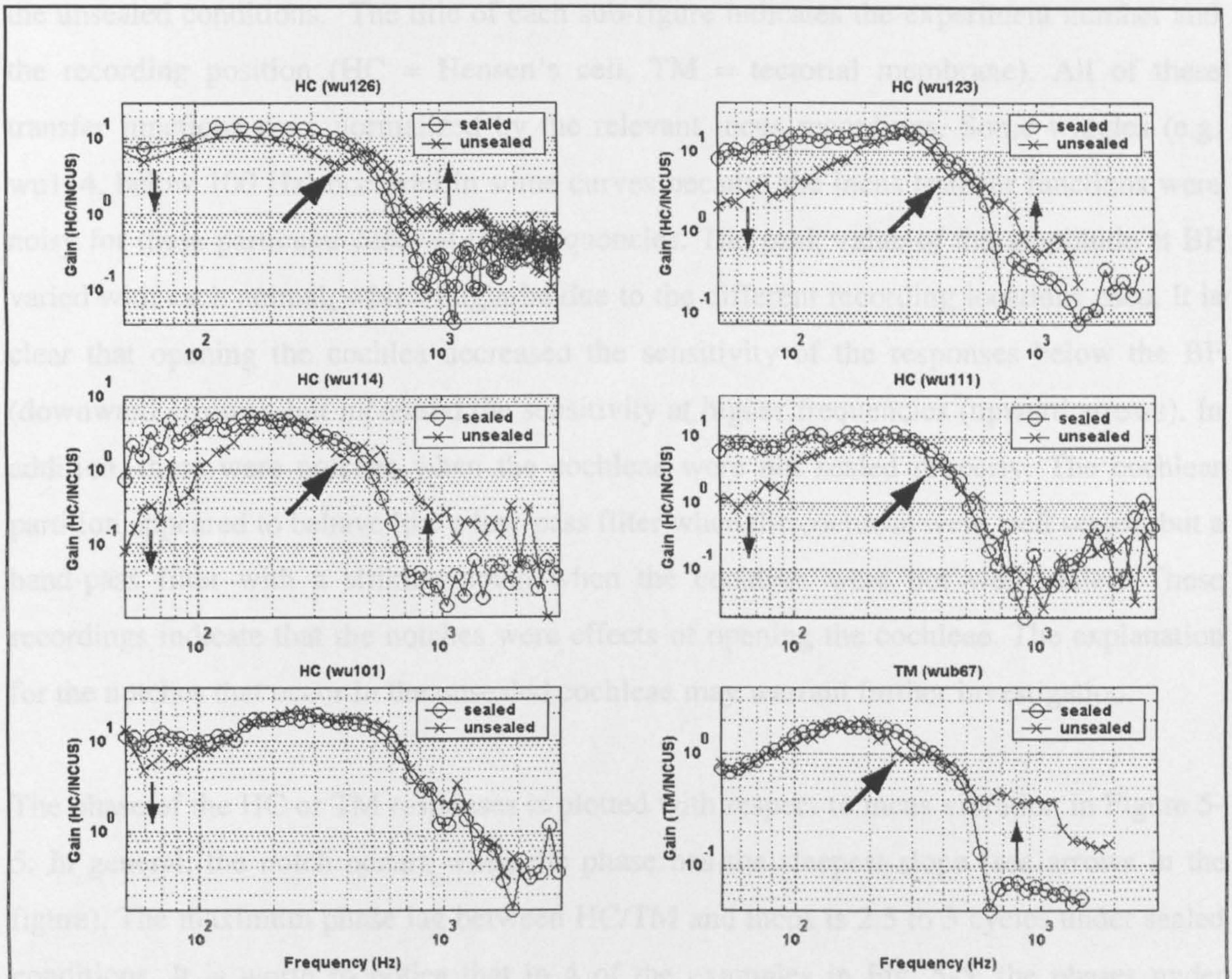

Figure 5-4 Tuning curves of Hensen's cell and tectorial membrane from sealed and unsealed cochleae. The circles indicate the responses from sealed cochleae, while the crosses from unsealed cochlea. The title of each sub-figure indicates the experiment number and the recording position of the organ of Corti. Decreases and increases in sensitivity are indicated by downward / upward arrows, respectively. Notches occurred at the places indicated by thick arrows.

look like bell-shaped band-pass filters with significant notches at 436 Hz and 367 Hz (see large arrows in Fig. 5-3). The BFs were the same as those of the sealed cochleae. Below the BF, the tuning curves decreased faster than those from sealed cochleae, while above the BF, there were notches before the tuning curves decreased with steep slopes. The phase accumulation from the unsealed cochleae was less than that from the sealed cochleae over much of the frequency range.

Tuning curves derived from 6 other cochleae under sealed and unsealed conditions are shown in Figure 5-4. The variation in amplitude is plotted as a function of frequency. The circles indicate the responses from the sealed conditions, while the crosses show those from the unsealed conditions. The title of each sub-figure indicates the experiment number and the recording position (HC = Hensen's cell, TM = tectorial membrane). All of these transfer functions were normalized by the relevant incus recordings. Some wiggles (e.g. wu114, below 100 Hz) occurred in some curves because the incus transfer functions were noisy for these particular cases at low frequencies. The peak value of the amplitude at BF varied with each animal, which might be due to the different recording locations used. It is clear that opening the cochlea decreased the sensitivity of the responses below the BF (downward arrows), but increased the sensitivity at higher frequencies (upward arrows). In addition, there were notches when the cochleae were not sealed properly. The cochlear partition appeared to behave like a low-pass filter when the cochleae were well sealed, but a band-pass filter with a striking notch when the cochleae were not well sealed. These recordings indicate that the notches were effects of opening the cochleae. The explanation for the notches that occur in the unsealed cochleae may warrant further investigation.

The phase of the HC or TM responses is plotted with respect to incus vibration in Figure 5-5. In general, the notch occurs when the phase has the steepest slope (see arrows in the figure). The maximum phase lag between HC/TM and incus is 2.5 to 3 cycles under sealed conditions. It is worth to notice that in 4 of the examples in Fig. 5-5, the phases under unsealed conditions are a cycle ahead of the phases under sealed conditions.

In summary, unsealing the cochlea decreased the sensitivity at low frequency (below CF), but increased the sensitivity at high frequency (above CF). The partition's low-pass tuning characteristics were hence transformed into a more band-pass form. Also, a notch occurred just above the CF in the unsealed cochleae, but not in the sealed ones. The amount of phase accumulation is generally higher under sealed conditions.

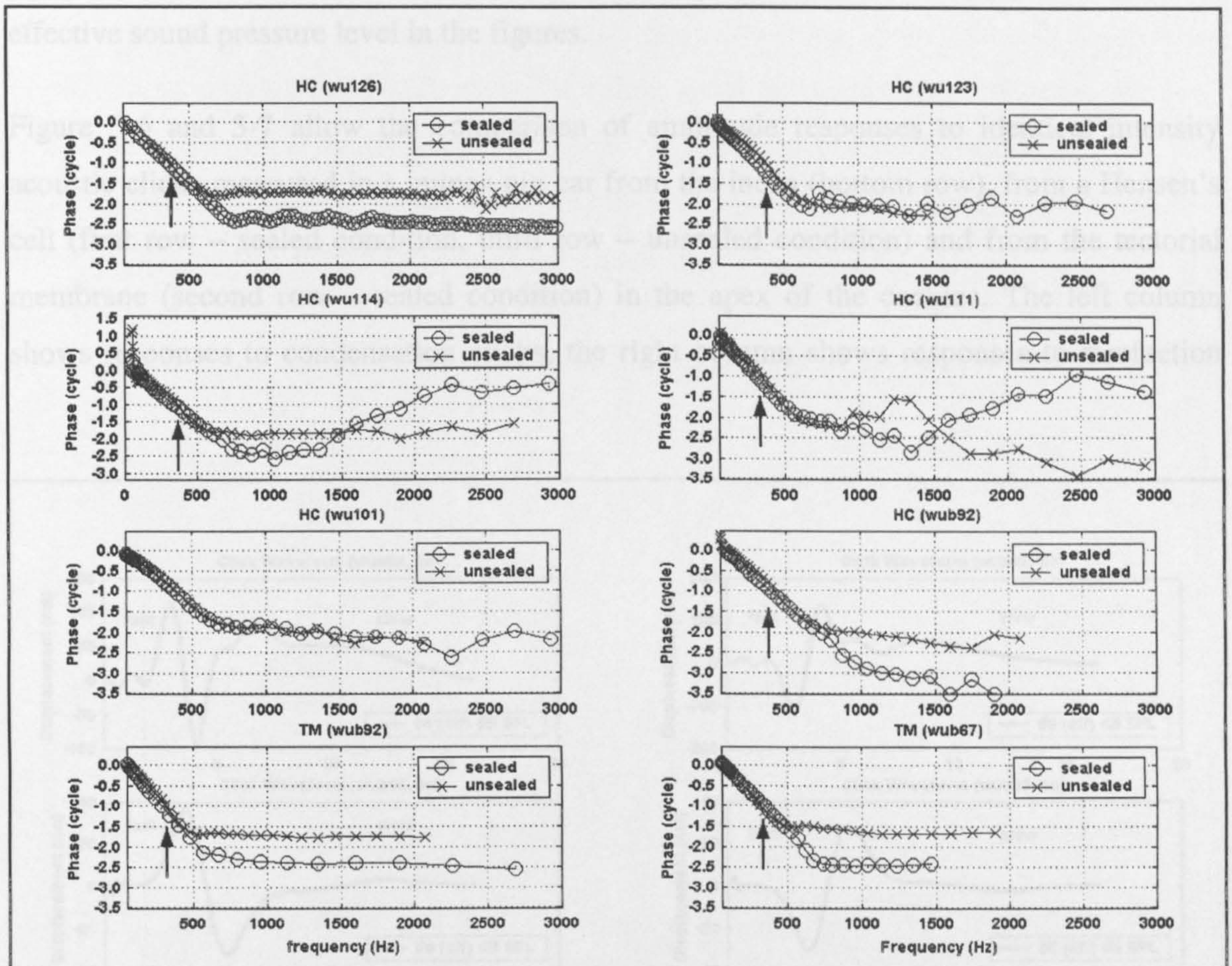

Figure 5-5 Phase relationship between Hensen's Cell or tectorial membrane responses and incus responses in sealed and unsealed cochleae. The circle lines indicate the responses were from sealed cochleae, while the cross lines were from unsealed cochlea. The title of each sub-figure indicates the experiment number and the recording position of the organ of Corti.

5.3 Effects to click stimuli responses – in the time domain

To explore the origin of the notches in the transfer function curves, condensation and rarefaction clicks were used to provide broad frequency stimuli in phase. Responses to clicks permit the precise timing of a system's response to be traced. In the case of a linear system, the Fourier transform of the unit impulse response is identical to the system's transfer function. Condensation and rarefaction click responses of a HC and a bead on the TM are shown in Figure 5-6 (wub92) and Figure 5-7 (wu126). The sound pressure levels of the click responses were obtained by comparing FFT results for the click responses with

tone-derived iso-intensity curves at the same recording point. The click levels are named effective sound pressure level in the figures.

Figure 5-6 and 5-7 allow the comparison of amplitude responses to identical intensity acoustic clicks measured in a guinea pig ear from the incus (bottom row), from a Hensen's cell (first row – sealed condition, third row – unsealed condition) and from the tectorial membrane (second row – sealed condition) in the apex of the cochlea. The left column shows responses to condensation clicks, the right column shows responses to rarefaction

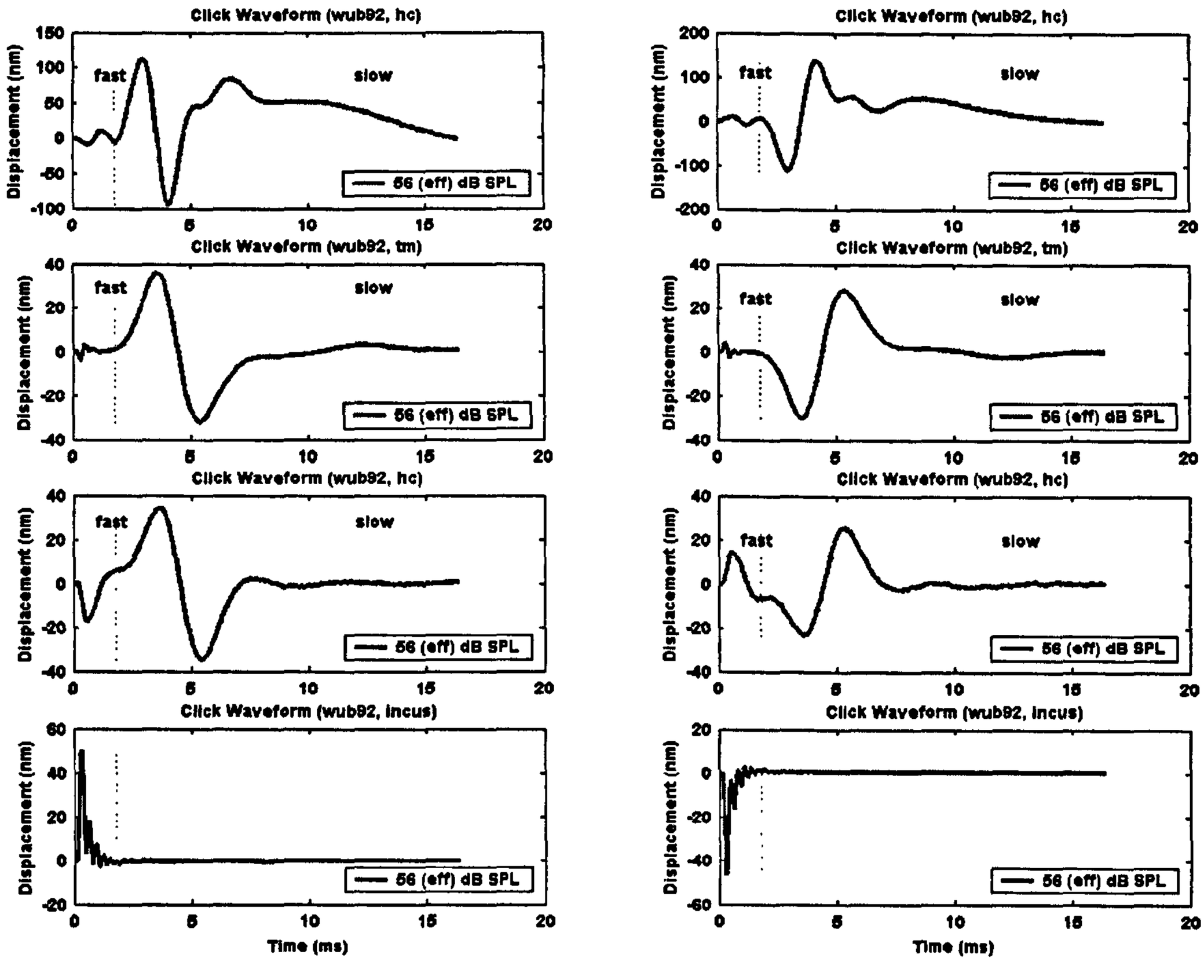

Figure 5-6 Clicks responses of wub92. Left column shows the condensation click responses, while the right column shows the rarefaction responses. Sub-titles give the information about the experimental animal and recording locations. The first two rows show recordings from HC and TM under sealed conditions. The third row shows recordings from HC under unsealed conditions. The bottom row shows incus responses. Click responses were separated into 'fast' and 'slow' components as the dotted line shows in the time domain. Effective sound pressure level is 56 dB SPL.

clicks. The incus responses to condensation and rarefaction clicks were recorded from the incus-stapes junction as measured through the ventral opening of the bulla. The responses of the incus consisted of a short, almost uni-directional pulse, consistent with the untuned, wide-band nature of middle-ear vibrations, which mostly finish within 2 ms. The condensation click caused the incus to push the oval window inwards, while the rarefaction click pulled the oval window outwards with respect to the cochlea.

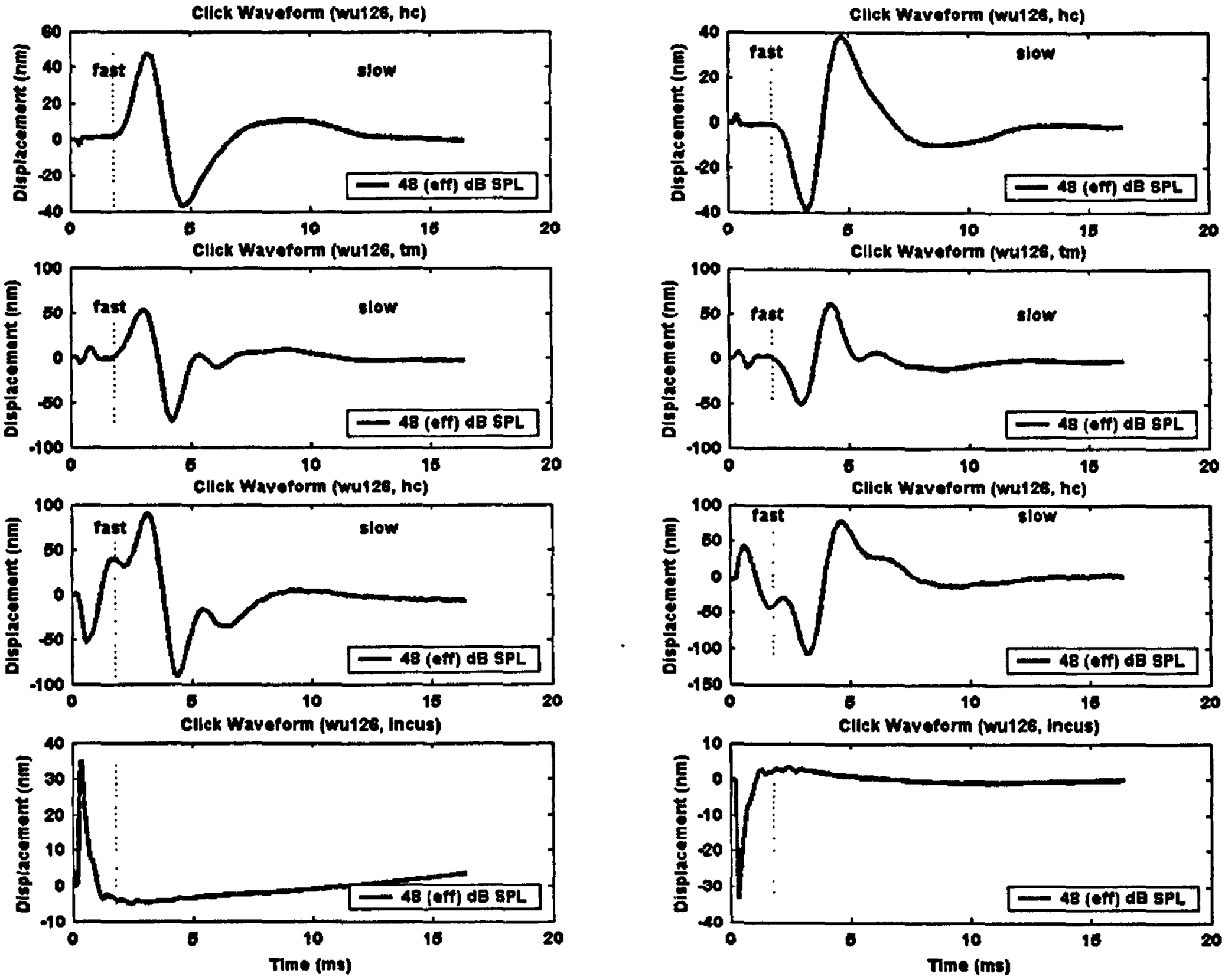

Figure 5-7 Clicks responses of wu126. Left column shows the condensation click responses, while the right column shows the rarefaction responses. Sub-titles give the information about the experimental animal and recording locations. The first two rows show recordings from HC and TM under sealed conditions. The third row shows recordings from HC under unsealed conditions. The bottom row shows incus responses. Click responses were separated into 'fast' and 'slow' components as the dotted line shows in the time domain. Effective sound pressure level is 48 dB SPL.

The typical responses to condensation and rarefaction clicks of HC and TM consist of two parts in the time domain: The first part is small in amplitude and occurred almost

simultaneously as the incus vibrates. This part was suggested to be the 'fast' component in the travelling wave of the cochlear partition (Cooper and Rhode 1996) and might be responsible for making all the points along the length of the cochlea begin to move almost simultaneously. The major part of the response formed a 'slow' wave, which is much larger in amplitude and longer in duration than the responses of the incus. This part is known as a displacement wave that propagates on the basilar membrane (BM) from base to apex (von Bekesy 1960), which is famous for its frequency-dependent location map. The Organ of Corti is set in motion by the BM travelling wave, which leads to cochlear micromechanics.

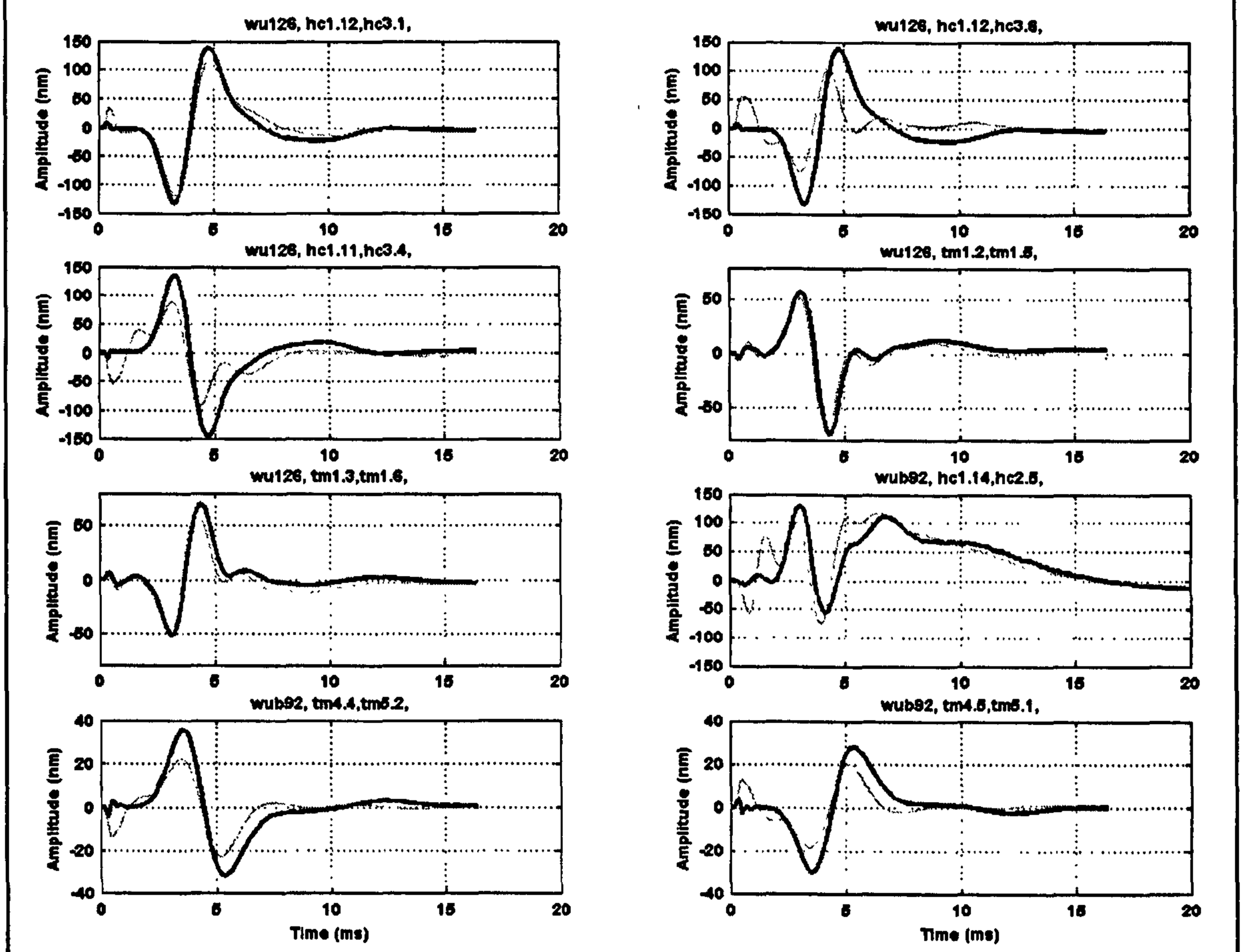

Figure 5-8 Comparison of click responses from sealed (thick lines) and unsealed (thin lines) cochleae. Wub126 and wub92 are experiment numbers. HC indicates recordings from a single HC and tm shows recordings from the tectorial membrane.

For these two examples (Fig. 5-6 and 5-7), the intensities of the stimuli to incus, Hensen's cell and tectorial membrane are identical (the effective sound pressure level are 56 dB SPL for wub92 and 48 dB SPL for wu126). When the cochleae were well sealed (row 1 and row 2), the 'fast' and 'slow' components could be easily separated in the time domain. The waves that occurred before 1.8 ms may be considered as the 'fast' component while the later waves may be considered as the 'slow' waves, which typically last for another 6 ms. When the cochleae were not well sealed (row 3), the 'fast' and 'slow' components merged together and were not easily separated in the time domain.

The polarities of the initial peaks are also different between 'fast' and 'slow' waves (Figure 5-6 and 5-7). In response to condensation click stimuli, the stapes pushed the oval window in, causing the organ of Corti to move towards first scala vestibuli and second, the scala tympani. In response to rarefaction clicks, the cochlear partition responses were first a 'fast' small peak in the direction of scala tympani, and second a 'slow' large peak in the direction of scala vestibuli.

The amplitude of the click responses is affected by the sealing condition of the cochleae. Figure 5-8 compares click responses from sealed (thick lines) and unsealed (thin lines) cochleae. The opening of the cochleae increased the amplitudes of the 'fast' component, but decreased those of the 'slow' waves. The time course of the 'fast' response components was extended dramatically by breaking the seal of the cochleae, so that in some cases, the ending of the 'fast' component combined with the beginning of the 'slow' wave. As a result, the two components could not be separated in the time domain. The amplitudes of the fast waves were rather small compared with those of the slow waves when the cochleae were well sealed. The minimum peak-to-peak value of the 'fast' wave could be as low as only 4.4% of that of the 'slow' wave. The peak-to-peak ratio is defined as the peak-to-peak value of the fast wave divided by peak-to-peak value of the slow wave. Peak-to-peak ratios were calculated for all the click responses of these two animals (wub92 and wu126) and are shown in Figure 5-9. The peak-to-peak ratios are very sensitive to the sealing condition of the cochleae. At the beginning of these experiments, the cochleae were well sealed, the peak-to-peak ratio was around 0.1 (open circle for wub92, open diamond for wu126). This means that the amplitude of the fast component was only about 10% of that slow component or even less (minimal is 4.4%). When the seal was broken (filled circles and

diamonds), the peak-to-peak ratios increased immediately and appears to settle down to around 40-45% (although in one example, the maximum peak-to-peak ratio is 0.66). The peak-to-peak ratio returned to around 0.1 after re-sealing the cochlea (open symbols). Therefore, normally for the sealed cochleae, the peak-to-peak ratio is around or less than 0.1 (open symbols), which indicates that the 'fast' wave only carries a limited energy during normal sound delivery and might be ignored. The peak-to-peak ration generally is bigger than 0.2 and can reach 0.4-0.66 for the unsealed conditions. This indicates that the fast wave carries nearly half of the energy during the sound delivery procedure and the characteristic of the cochlear partition response to sound should be determined by both the fast and the slow waves.

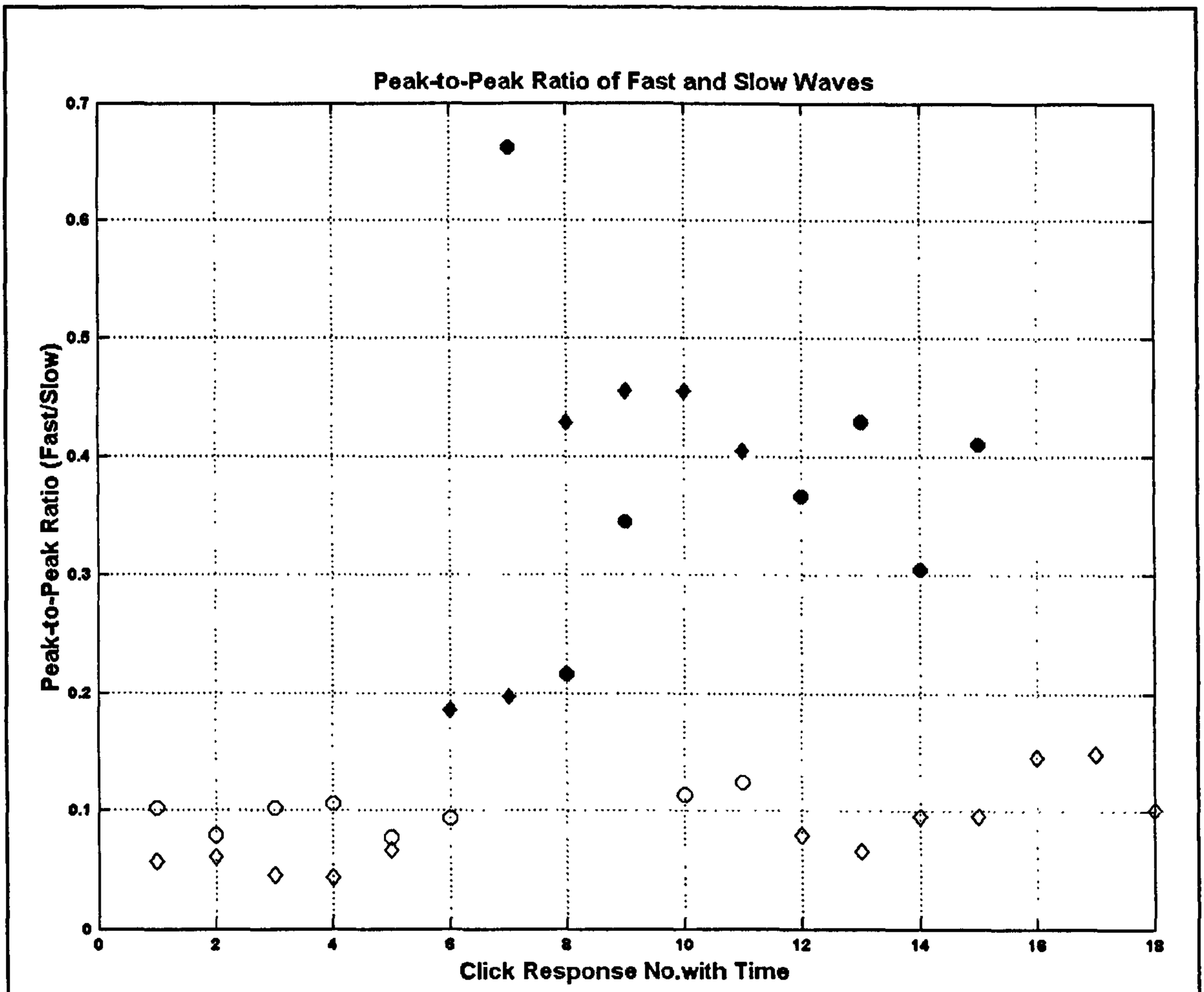

Figure 5-9 Peak-to-peak ratio of the fast and the slow component. Filled circles show peak-to-peak ratio under unsealed conditions, while, open circles represents peak-to-peak value under sealed conditions.

Therefore, click responses from Hensen's cells and the tectorial membrane provide evidence for both 'fast' and 'slow' waves in the cochlea. The 'fast' responses occur nearly simultaneously as the incus vibrates, the 'slow' responses occurs later in the time course. Both the time course and the vibration amplitude of the 'fast' wave are dramatically affected by the sealing conditions. The amplitude of 'fast' waves could be as small as 1/16th of those of the 'slow' waves in a well-sealed cochlea, but could also be as big as 2/3 of those of the 'slow' waves in an unsealed cochlea. The 'fast' wave could be easily separated from the 'slow' wave in the time domain under sealed condition; however, it extends and merges with the 'slow' under unsealed cochlea. The 'slow' waves are little affected by the sealing conditions. No changes were evident in control measurements made from the incus in the middle earin sealed and unsealed cochleae.

5.4 Interaction between fast and slow components

To explore the interaction of 'fast' and 'slow' waves in the cochlea, responses to rarefaction and condensation clicks were studied using Fourier analysis (FFT). Figure 5-10 shows such an analysis for some rarefaction click responses. Column one shows the control measurements made from the incus. The rest of this data set was collected from HC (wu126) *in vivo* under sealed and unsealed cochlear conditions. During the measurement, the Reissner's membrane was intact.

The experiment of Fig. 5-10 involved going through the procedure of sealing and then breaking the seal of the cochlea in succession. Fig. 5-10B to 5-10E are the raw waveforms recorded from HC under different cochlear sealing conditions. The waveform of Fig. 5-10B was considered to be collected from a well-sealed cochlea, that of Fig. 5-10C was recorded from the same HC, just after trying to break the seal condition of the cochlea, but having failed. In this instance, the grease around the chamber clearly held on to the glass cover and re-sealed the cochlea. The waveform of Fig. 5-10D recorded when the sealing was broken, but there was some connection left between the cover glass and the grease. The waveform of Fig. 5-10E is the typical rarefaction click response from a completely unsealed cochlea.

In row two (Fig. 5-10F – 10I), the raw waveforms are divided into two non-overlapping parts ('fast'- thin lines and 'slow' - thick lines) in the time domain using a cosine raised window function. In Figs. 5-10F and 5-10G, the 'fast' and 'slow' component are very easy to separate in the time domain. However, in Figs. 5-10H and 5-10I, separating of the 'fast' and the 'slow' was not so easy because the 'fast' and 'slow' merged together, especially when the cochlea was completely unsealed (Fig. 5-10I). The amplitudes of the 'fast' and 'slow' components are also affected by the seal condition. The amplitude of the 'fast' component appears to increase when the seal of the cochlea was broken, while the amplitude of the 'slow' component decreases. The peak-to-peak ratios of the 'fast' and 'slow' waves are 0.04, 0.07, 0.19 and 0.43 in Figs 5-10 F-I, respectively, which means that the 'fast' component becomes larger in a relative sense when the cochlea is unsealed.

Row three of Fig. 5-10 shows the magnitude gain (compared with the incus movement – 10J) of the Fast Fourier transforms (FFT, computed using 2048 points, 16.384 ms windows) of the waveforms of raw data, fast and slow waves. The contribution of 'fast' and 'slow' waves is presented in the frequency domain. Circles, thick and thin lines show the FFT results of the raw waveform, the 'slow' wave and the 'fast' wave, respectively. The shape and the amplitude of the 'slow' wave spectra are nearly identical under all the conditions (thick lines in Fig. 5-10K – 10N) with the plateau responses (above ~ 1 kHz) around 40 dB below the peak (100-300 Hz). The slow component transfer function was quite stable in all the cases and relatively flat before 366 Hz, and then dropped down very quickly till 671 Hz. The slow components appear as a low-pass filter rather than band pass. This indicates that the condition of the cochlear seal has little effect on the slow wave. However, the amplitude and shape of the 'fast' wave spectra change with the condition of the seal of the cochlea (thin lines in Fig. 5-10K – 10N). Under sealed conditions, the 'fast' wave at low frequency is nearly 40 dB down from the 'slow' wave, but it becomes similar in amplitude to the 'slow' wave above 800 Hz (Fig. 5-10K and 10L). This suggests that the 'fast' wave is too small to affect the tuning curve and the 'slow' wave dominates the tuning of the cochlea below 800 Hz. Above that frequency, it is the 'fast' component that takes control of the tuning. After breaking the seal, the amplitude of the 'fast' wave grows and the effect of the 'fast' component could not be ignored any more (Fig. 5-10M -10 N). In this case, the overall tuning is a result of interaction of both the 'fast' and the 'slow' waves.

The bottom row of Fig. 5-10 plots the phase of click responses as a function of frequency, which provides the necessary information about the timing of the 'fast' and 'slow' components. This was obtained by Fast Fourier transformation of the waveforms in row 1 and row 2. Fig. 5-10O shows the phase of the incus vibration. Fig. 5-10P – 10S are the HC phase data with respect to the incus (cycles) for the raw, 'slow' and 'fast' waves (circle, thick and thin lines), respectively. The phase of the 'fast' and the 'slow' waves is not identical, which means that these two waves propagate in the cochlea with different time courses with respect to the incus vibration. The phase of the 'fast' wave is pretty flat and changed little across the frequency range, which suggests that the 'fast' wave vibrates nearly at the same time as the incus (as described earlier). The 'slow' wave's phase increased with a relatively steep slope at frequencies less than the cut-off frequency and became flat thereafter. The maximum amount of phase accumulation was around 5 cycles for some slow waves. The phase of the raw data is the sum of phase of the 'fast' and the 'slow' waves.

Returning to the tuning curves of the raw data in Fig. 5-10K - 10N, the magnitude gain of raw waveforms changed little at low frequencies, but increased by 10 dB in the plateau when the seal of the cochlea was broken. The shapes of the raw data FFT results are similar in the first three panels (Fig. 5-10K – 10M), but a notch appears around 430 Hz when the seal is completely broken (arrow in Fig. 5-10N). Looking into the 'fast' (thin line) and 'slow' (thick line) components in this case, neither of them presents a notch in the frequency domain. Therefore, the only possibility for the notch is because the 'fast' and the 'slow' interact and produce a notch at that frequency. Fig. 5-10S provides further support for this hypothesis by showing that the phase difference between the 'fast' and the 'slow' components at around 430 Hz is 0.5 cycles (see first pair of arrows in Fig. 5-10S). This means that at this particular frequency, these two waves in the cochlea working in anti-phase and canceling each other, leading to a notch in the tuning curve. It is true that whenever the phases of the two components are in anti-phase, the two waves in the cochlea will cancel each other and yield a notch in the tuning (for example see second pair of arrows in Fig. 5-10S).

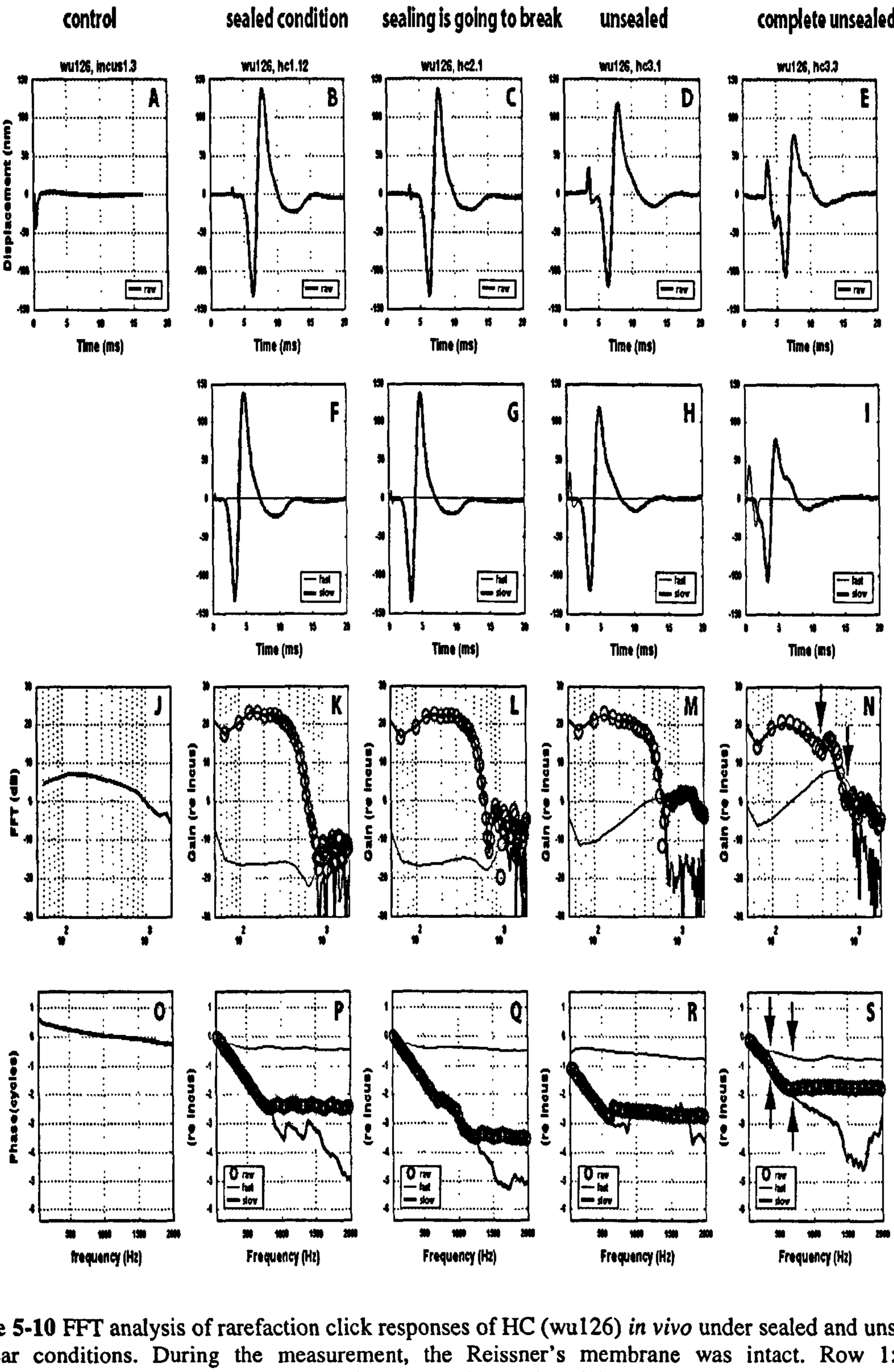

Figure 5-10 FFT analysis of rarefaction click responses of HC (wu126) *in vivo* under sealed and unsealed cochlear conditions. During the measurement, the Reissner's membrane was intact. Row 1: raw waveform; row 2: separation of 'fast' (thin line) and 'slow' (thick line) by a consine rised window function of raw data; row 3: FFT results in the frequency domain respect to incus vibratio; row 4: phase data of raw, fast and slow waves. Column 1: control measurement of incus; column 2:responses collected from sealed condition; column 3: response from sealed condition; column 4: seal of the cochlea was broken; column 5: seal of the cochlear was completely broken.

5.5 Middle ear responses to pure tone pips

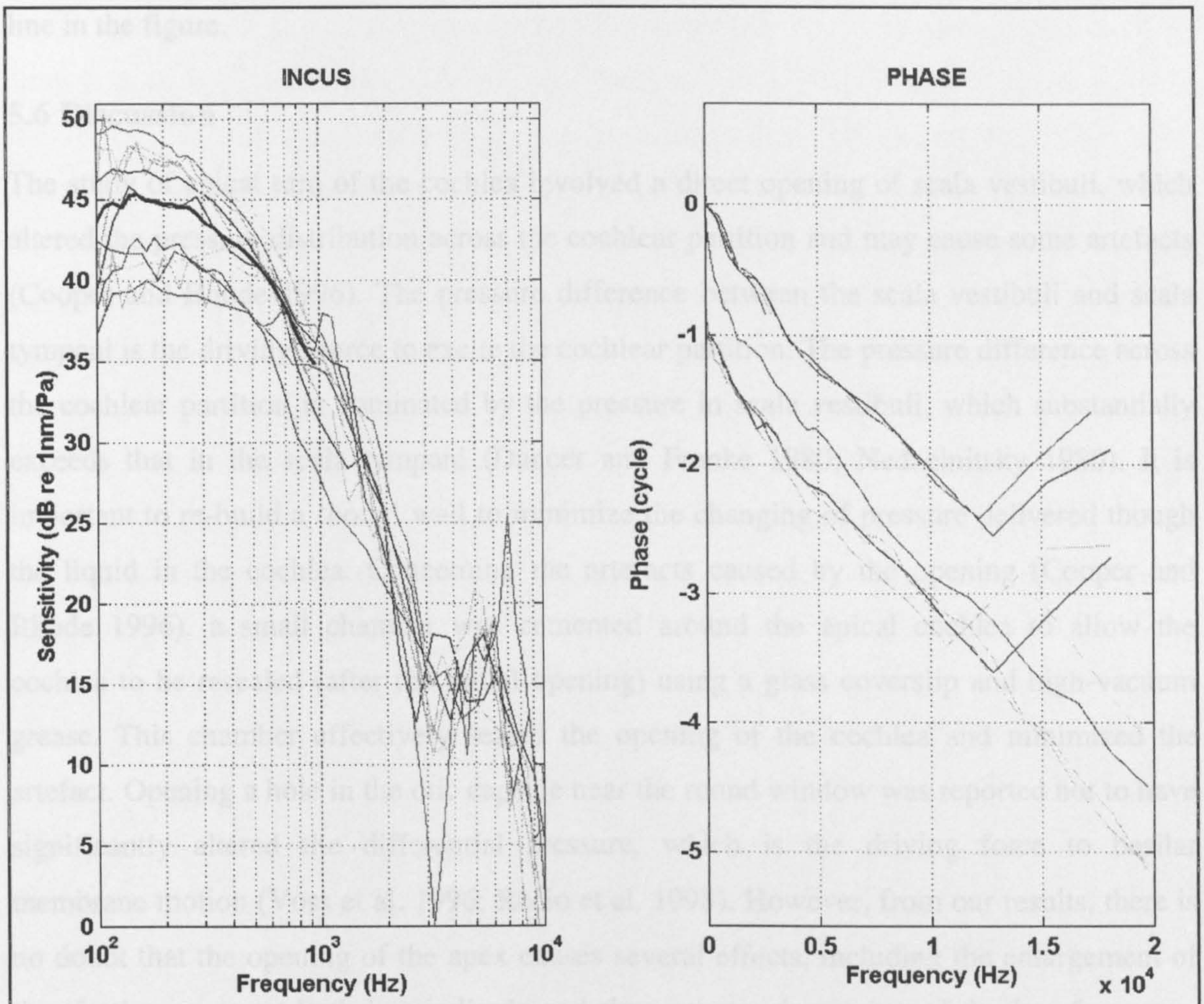

Figure 5-11 Middle ear tuning curves of 11 animals and phase responses. Left: sensitivity variation with frequency; Right: phase variation with frequency.

All the measurements of the cochlear partition responses to tone bursts and clicks were made with the anterior and ventral aspects of the bulla widely opened, which increases the incus response at low frequencies (Wilson and Johnstone 1975; Ruggero et al. 1990). Therefore, the input to the cochlea, middle-ear responses to tone burst play an important role in the responses. Fig. 5-11 shows 11 examples of the middle-ear responses to tone bursts as a function of frequency. These responses were recorded from ventral aspects of the bulla *in vivo*. All the tuning sensitivities are similar and consistent with those recorded from different angles in other open-bulla studies (Manley and Johnstone 1974; Rhode 1978; Cooper and Rhode 1992; Cooper and Rhode 1995). For our animals, the transfer

function of the middle-ear is not perfectly flat at low frequencies (below 1000 Hz), but drops slightly with frequency. The averaged tuning below 1000 Hz was plotted by the thick line in the figure.

5.6 Discussion

The study of apical turn of the cochlea involved a direct opening of scala vestibuli, which altered the pressure distribution across the cochlear partition and may cause some artefacts (Cooper and Rhode 1996). The pressure difference between the scala vestibuli and scala tympani is the driving source to excite the cochlear partition. The pressure difference across the cochlear partition is dominated by the pressure in scala vestibuli, which substantially exceeds that in the scala tympani (Dancer and Franke 1980; Nedzelnitsky 1980). It is important to re-build a 'bony' wall to minimize the changing of pressure delivered though the liquid in the cochlea. Concerning the artefacts caused by the opening (Cooper and Rhode 1996), a small chamber was cemented around the apical cochlea to allow the cochlea to be resealed (after the initial opening) using a glass coverslip and high-vacuum grease. This chamber effectively sealed the opening of the cochlea and minimized the artefact. Opening a hole in the otic capsule near the round window was reported not to have significantly altered the differential pressure, which is the driving force to basilar membrane motion (Voss et al. 1996; Recio et al. 1998). However, from our results, there is no doubt that the opening of the apex causes several effects, including the enlargement of the 'fast' component both in amplitude and time course, decreasing of the low-frequency sensitivity and increasing of the high frequency sensitivity. The interaction between the fast and slow components is clearly displayed in time course and analyzed in frequency domain. The frequency dependent interaction between the fast and slow components of a response is responsible for the sharp sensitive notches and the fast component was very sensitive to the hydraulic state of the cochlea. As suggested by Cooper and Rhode (1996), the fast component might even be expected to vanish in a truly intact cochlea.

The present study was consistent with the main findings of the work of Cooper and Rhode (Cooper and Rhode 1996) at similar sites in chinchillas and guinea pig cochleae. At this site, cochlear partition's responses to clicks consisted of two parts. The initial part was a short duration, with lower amplitude and could be abolished by restoring the hydraulic seal of the cochlea. The later part lasted longer and corresponded to the site's characteristic frequency.

The 'fast' and 'slow' traveling waves were distinguished by their traveling speeds. The 'fast' traveling waves propagate at the speed of sound in water (~ 500 m/s). The 'slow' waves were known as a displacement waves that propagate on the basilar membrane (BM) from base to apex at around ~ 10 m/s (von Bekesy 1960). The Organ of Corti was set in motion by the BM traveling wave, which lead to cochlear micromechanics. The 'fast' waves are affected dramatically by the sealing condition of the cochlea. The 'fast' wave was at least 30 dB lower in amplitude than the 'slow' wave in a well-sealed cochlea. The 'slow' wave behaves like a low-pass filter rather than band-pass filter in a sealed cochlea. This is completely inconsistent with the low frequency nerve fiber characteristics. The notches observed in some transfer functions are likely to be due to interactions between the 'fast' and 'slow' waves in improperly sealed cochleae because they could be diminished in well sealed cochlea. This indicates that the notches observed in the tuning curves are artifacts of the opening of the cochlea and nothing related to the mechanism of function of the cochlea in the apical turn.

Chapter 6 The effects of tearing Reissner's membrane on the mechanics of the apical turn of the cochlea

6.1 Introduction

The interferometer system provides the possibility to measure the cochlear partition vibration without any reflective enhancement. However, the TM is too transparent to measure in this way! Hence we have to use beads, and have to tear the RM. To control for this, we use HC. The highly reflective lipid droplets of individual Hensen's cells in the organ of Corti are the only structure that could be seen from the apex.

This chapter aims to compare the mechanics in the apical turn of the cochlea before and after rupturing the Reissner's membrane. Recordings are from Hensen's cells and single reflective beads introduced on the tectorial membrane before and after tearing the RM. A total of 8 cochleae provide convincing results that rupturing Reissner's membrane causes a loss of nonlinearity in mechanics in the apical turn.

6.2 Tone – evoked responses

6.2.1 Baseline position shifts

Pure tone pips were used to study the responses from Hensen's cells (HC) and single reflective beads on the tectorial membrane (TM) before and after tearing the RM. Averaged waveforms (sweep = 8 or 16) of responses to 60 – 80 dB SPL sound stimuli are displayed in Fig. 6-1 and 6-2 for a selected series of frequencies (100, 200, 336.3, 400, 565.7 and 800 Hz) from the wide band of frequencies that were actually tested (50 Hz to 2k Hz). Thick lines show the raw response waveforms and thin lines show sound-evoked shifts in the baseline position. These shifts were uncovered using Butterworth low-pass filters to filter the original waveforms. The stimulus frequencies and sound pressure level are labeled on the right of each figure.

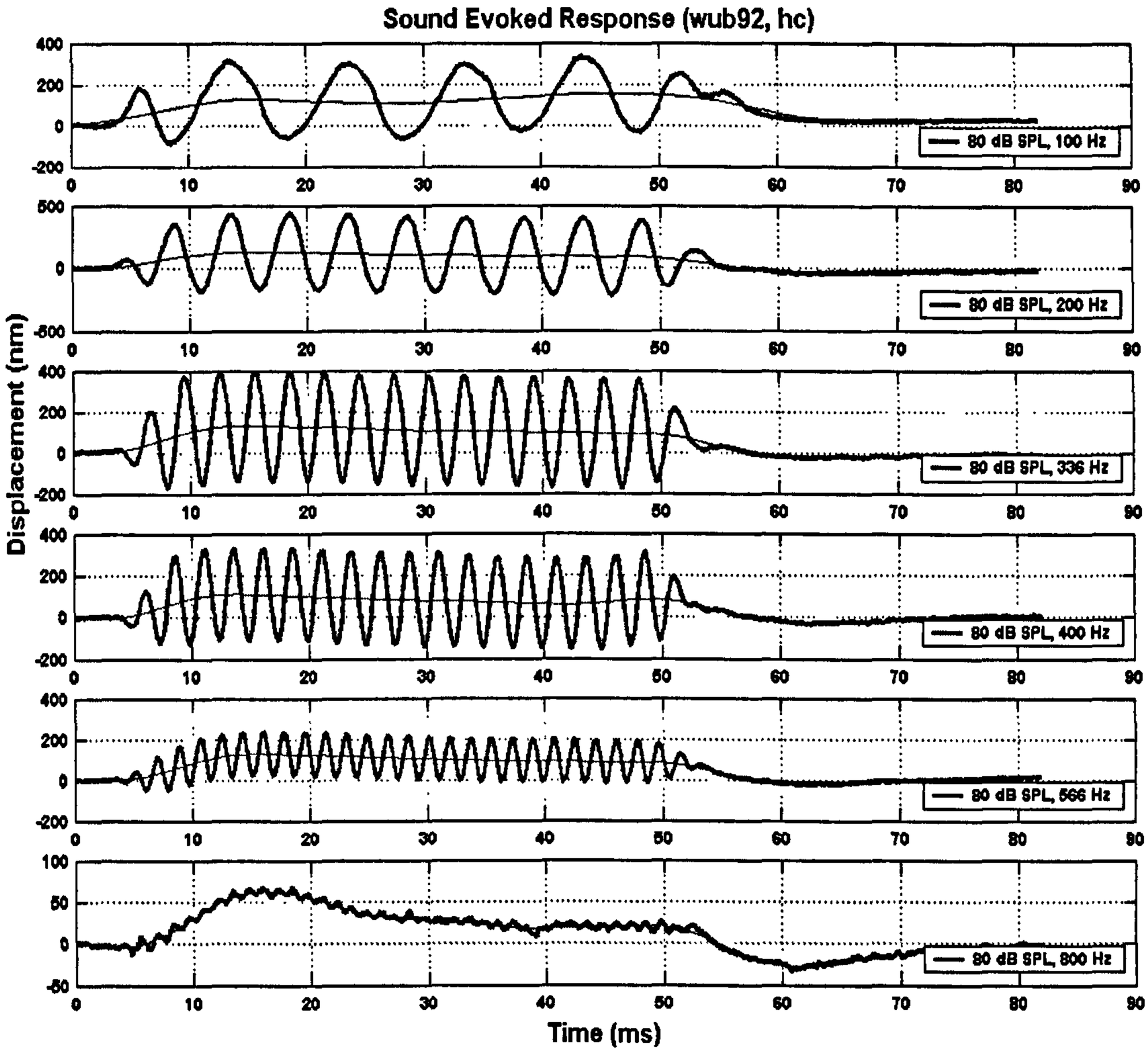

Figure 6-1 Tone evoked responses from a single HC in wub92 before tearing Reissner's membrane. Stimulus intensity was 80 dB SPL. Stimulus frequencies are 100, 200, 336, 400, 566 and 800 Hz. Thick lines show the single HC's oscillatory responses and thin lines show baseline position shifts.

Before tearing the Reissner's membrane, besides the sinusoidal components to the pure tone pips, strong sound-evoked baseline position shifts were observed in 8 cochleae and one example is shown in Fig. 6-1. Almost all shifts were directed towards the scala vestibuli. The shifts were evoked across a wide range of frequencies (from 25 to 1000Hz). The shifts developed progressively over the first few milliseconds of the responses; they adapted to a steady-state after 30-40 ms; and they decayed progressively after reversing their polarity within a few milliseconds of stimulus termination. The largest shifts occasionally approached the size of the partitions oscillatory (i.e. ac) responses.

After tearing the Reissner's membrane, responses to the same stimulus frequencies at 60 dB SPL of a single HC are shown in Fig. 6-2. These responses are all sinusoidal, but do not have systematic positive baseline position shifts.

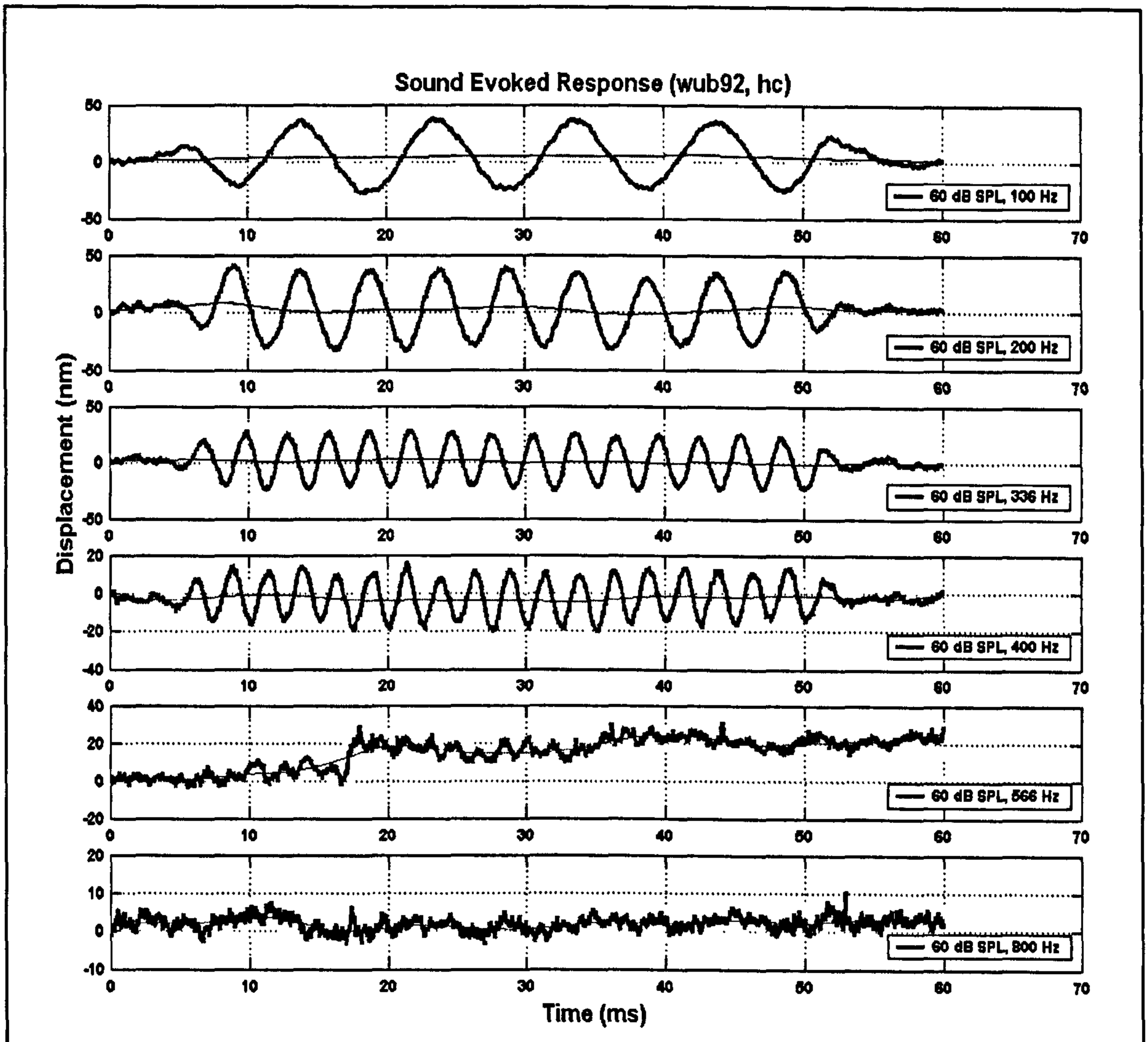

Figure 6-2 Tone evoked responses from a single HC of wub92 after tearing the Reissner's membrane. Stimulus intensity was 60 dB SPL. Stimulus frequencies are 100, 200, 336, 400, 566 and 800 Hz. Thick lines show the single HC's oscillatory responses and thin lines show baseline position shifts.

Similar results were observed in 8 preparations. These results provide evidence that sound evokes shifts in the baseline position of the cochlear partition in the apical turn of the guinea-pig cochlea when the Reissner's membrane is intact. They also show that these shifts are physiologically vulnerable, because they disappear after tearing the RM.

6.2.2 Tuning curves

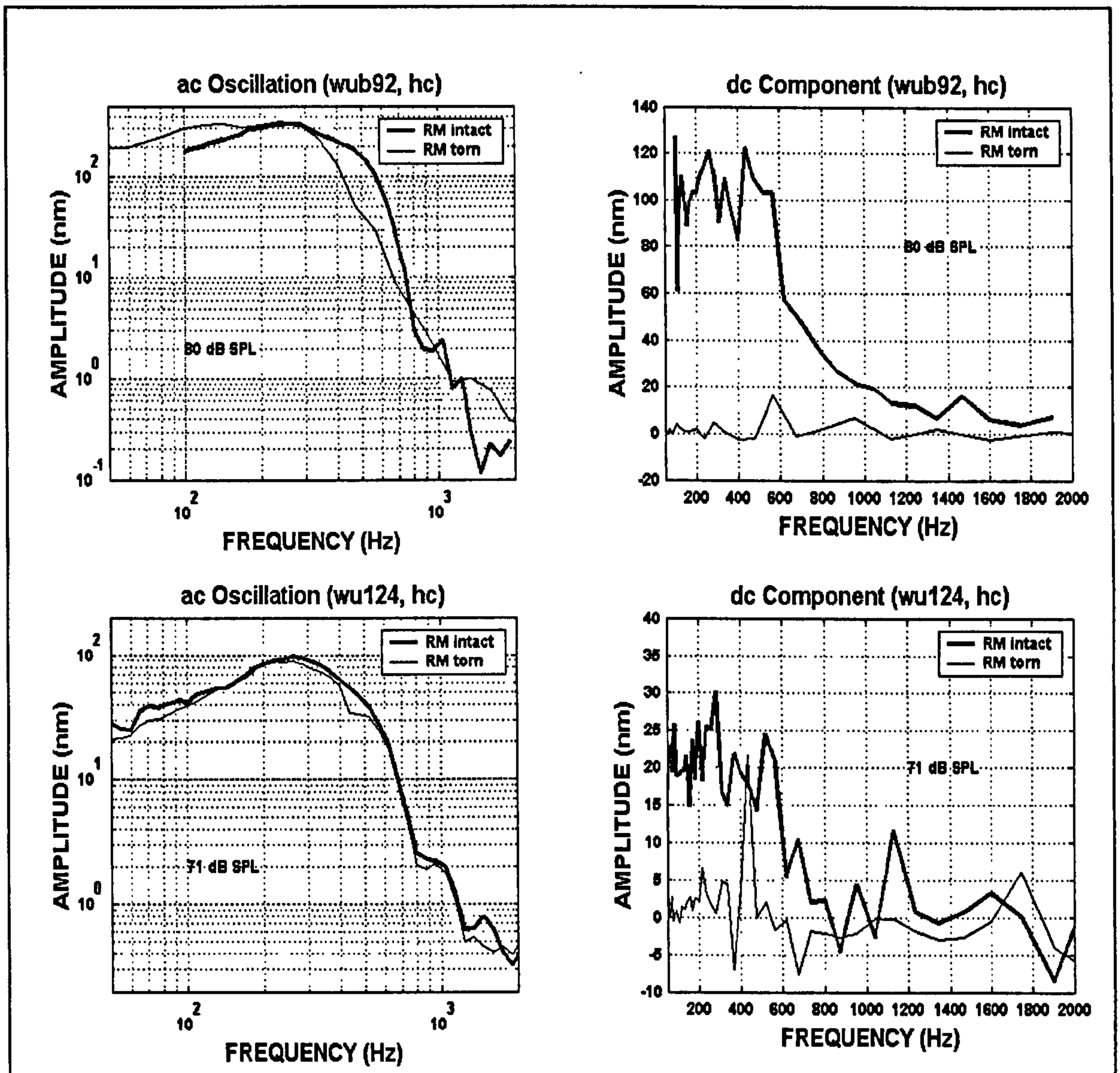

Figure 6-3 Comparison of tuning curves of ac and dc components before and after tearing the Reissner's membrane. Thick lines show ac oscillation (right) and dc baseline position shifts (left) before tearing the RM and thin lines represent responses after tearing the RM. Responses were collected from a single HC at 80 (wub92) and 71 dB SPL (wu124) respectively.

Sound evoked responses of a single HC were studied frequency by frequency from 50 to 2000 Hz. The variation of Hensen's cells vibration amplitude as a function of stimulus frequency at a certain intensity is depicted in Fig. 6-3. This figure allows comparison of

isointensity characteristics from two preparations (wub92 and wu124) out of 8 cochleae before and after rupturing the Reissner's membrane. Both the partitions oscillatory (i.e. ac) responses (left column) and sound-evoked (dc) baseline position shifts (right column) were plotted as a function of stimuli frequency. Responses were collected from a single HC before (thick line) and after tearing the RM (thin line). The sound pressure levels for these two animals were 80 (wub92) and 71 dB SPL (wu124), respectively.

Significant changes happened to the sound-evoked baseline position shifts before (thick line) and after (thin line) tearing the Reissner's membrane (left column in Fig. 6-3). Before tearing the RM, sound-evoked baseline position shifts were observed in responses to a wide range of frequencies. There is a clear pattern to the sound-evoked baseline position shifts with the stimulus frequency. For animal wub92, sound-evoked baseline position shifts are all positive at all tested frequencies and above 100 nm below 600 Hz at 80 dB SPL. For animal wu124, the baseline position shifts are greater than 0 below 800 Hz and lie between 20 – 30 nm below 600 Hz at 71 dB SPL. It appears that the baseline position shifts are nearly equal at all the frequencies below 600 Hz and suddenly drop down above that frequency. The baseline position shifts are smaller in wu124 than that in wub92. This may be because the responses of wu124 were evoked by lower sound pressure level, or perhaps because the cochlear condition differed between these two animals. After tearing the Reissner's membrane, the baseline position shifts in each animal could be negative or positive and wiggle around 0. There is no obvious pattern that could be observed across the tested frequency range.

For the cochlear partition oscillation (i.e. ac) responses (left column of Fig. 6-3), little change occurred before and after rupturing the Reissner's membrane for each animal. The ac oscillation responses were broadly tuned below 400 Hz, but fell quickly above this frequency. This is quite different from the sharp tuning curves in the basal turn of the cochlea. The apical tuning curves behave more like a low-pass filter, for the example of wub92, or an asymmetric bell-shaped filter, for animal wu124. There is also a small notch on the tuning curve shoulder after tearing the RM for animal wu124. This kind of difference was due to the different sealing condition of the cochleae, which was discussed in chapter 5.

Fig. 6-4 shows the other 6 sensitivity transfer functions from these cochleae before and after tearing the RM. Circles represent tuning curves recorded before tearing the RM, and crosses represent tuning curves collected after the RM was torn. There is little change in the tuning curves before and after tearing the RM. This suggests that the tearing of the RM has little effect on the ac components.

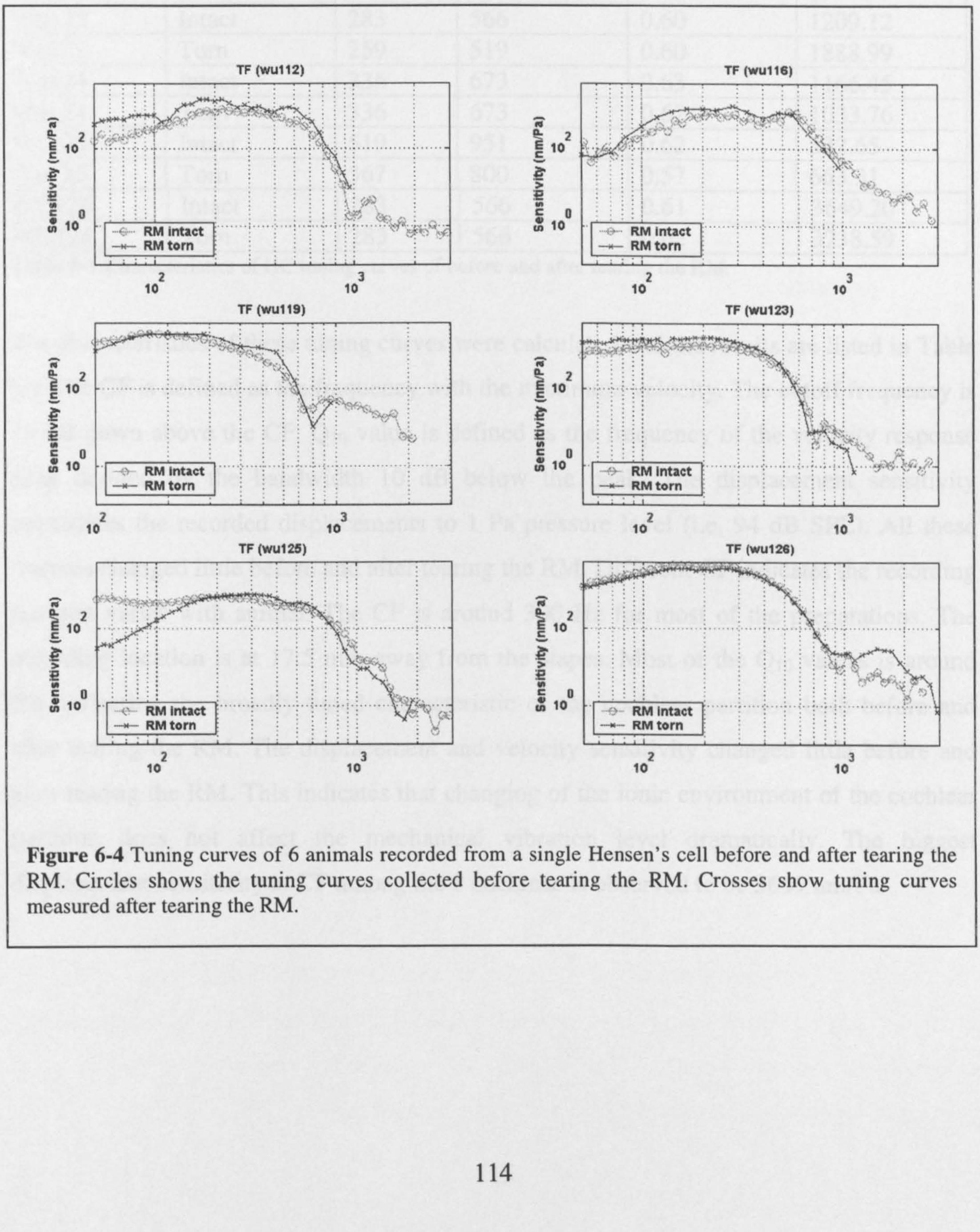

Figure 6-4 Tuning curves of 6 animals recorded from a single Hensen's cell before and after tearing the RM. Circles shows the tuning curves collected before tearing the RM. Crosses show tuning curves measured after tearing the RM.

Exp. No.	Reissner's Condition	CF (Hz)	Cutoff Frequency (Hz)	Q_{10} Value	Displacement Sensitivity at CF (nm/Pa)
Wub92	Intact	308	673	0.57	1485.86
Wub92	Torn	283	476	0.59	1610.69
Wu112	Intact	436	733	0.74	673.70
Wu112	Torn	476	733	0.79	1173.20
Wu116	Intact	587	761	1.03	832.08
Wu116	Torn	538	761	0.86	819.72
Wu119	Intact	259	617	0.50	2106.36
Wu119	Torn	283	673	0.52	2577.90
Wu123	Intact	283	566	0.60	1209.12
Wu123	Torn	259	519	0.60	1888.99
Wu124	Intact	336	673	0.63	1166.45
Wu124	Torn	336	673	0.62	1033.76
Wu125	Intact	519	951	0.62	332.65
Wu125	Torn	367	800	0.57	663.31
WU126	Intact	283	566	0.61	3649.20
WU126	Torn	283	566	0.62	3238.59

Table 6-1 Characteristics of HC tuning curves of before and after tearing the RM.

The characteristics of these tuning curves were calculated and the results are listed in Table 6-1.The CF is defined as the frequency with the maximum velocity. The cutoff frequency is 10 dB down above the CF. Q_{10} value is defined as the frequency of the velocity response peak divided by the bandwidth 10 dB below the peak. The displacement sensitivity normalizes the recorded displacements to 1 Pa pressure level (i.e. 94 dB SPL). All these features changed little before and after tearing the RM. Different CF indicates the recording position varies with animal. The CF is around 300 Hz for most of the preparations. The recording location is at 17.5 mm away from the stapes. Most of the Q_{10} values is around 0.6, reflecting the broadly tuned characteristic of the cochlear partition both before and after tearing the RM. The displacement and velocity sensitivity changed little before and after tearing the RM. This indicates that changing of the ionic environment of the cochlear partition does not affect the mechanical vibration level dramatically. The biggest displacement sensitivity at CF among the 8 cochleae is observed to be 3649 nm/Pa.

6.2.3 Distortion analyses

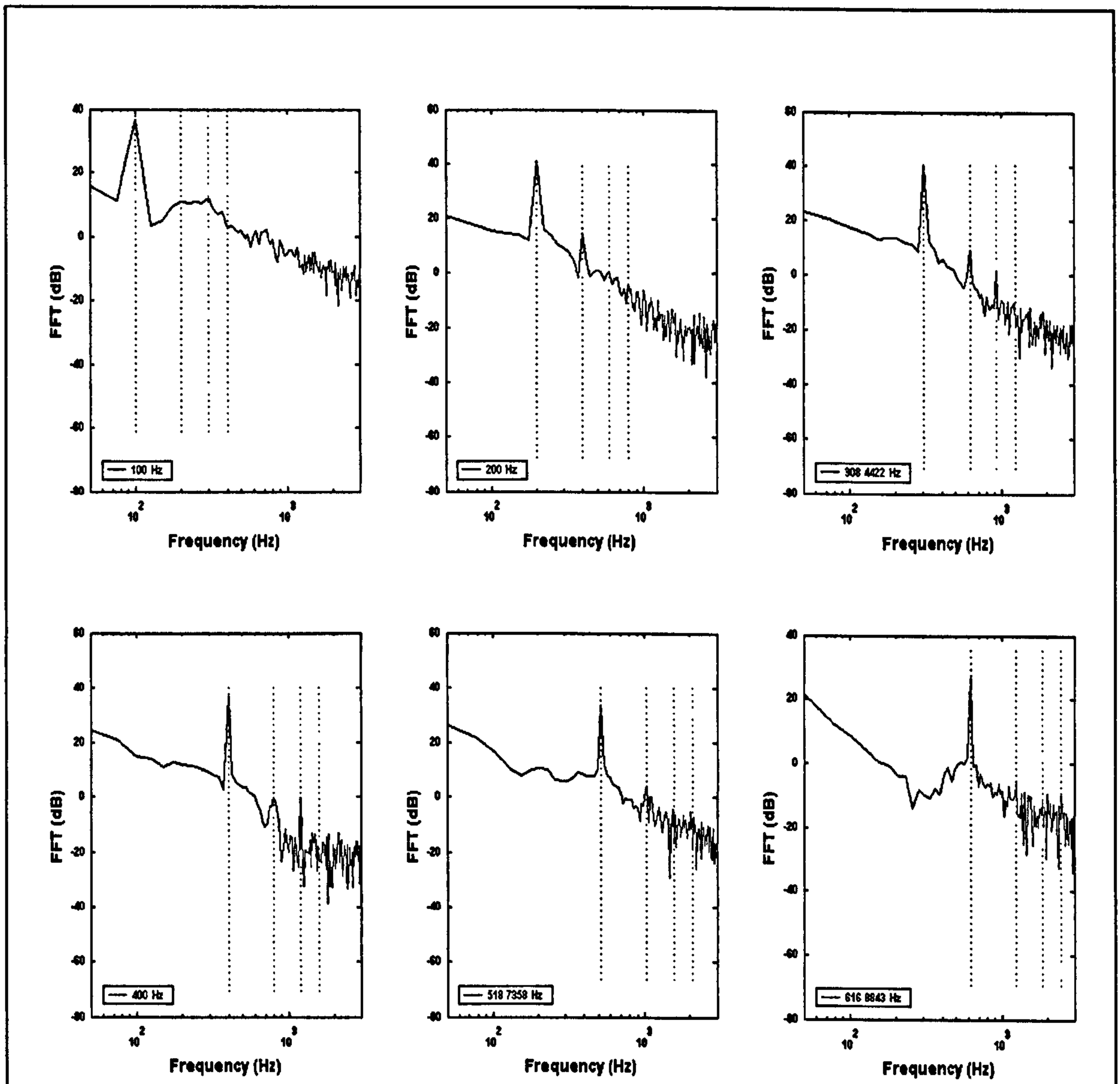

Figure 6-5 FFT of HC responses before tearing the RM at 70 dB SPL. Stimulus frequency is labeled on the bottom left corner. Dotted lines show harmonic #1-4.

The Fast Fourier Transform of each raw waveform was analyzed frequency by frequency. All the responses yield similar FFT results and one example is shown in Fig. 6-5 for a series of selected stimulus frequencies. The first, second and third harmonic components are observed in the FFT results. It is obvious that the first harmonic provides the major

energy in the responses. The second and the third order distortions are nearly 30 - 40 dB down compare with the first harmonic.

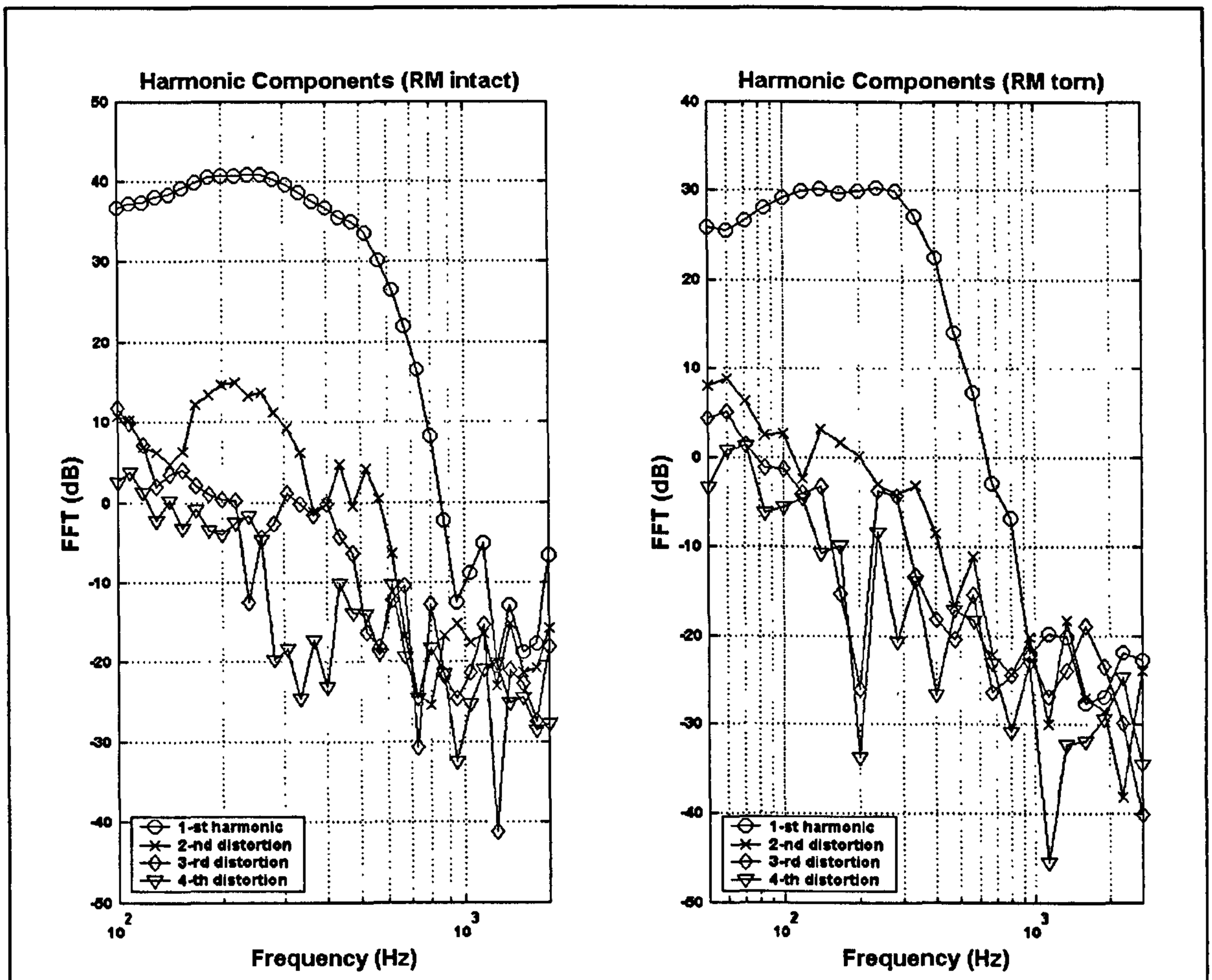

Figure 6-6 Distortion analysis for the oscillatory responses of HC before and after tearing the RM.

Distortion was studied frequency by frequency for the HC responses before and after tearing the RM and one example is shown in Fig. 6-6. This figure shows the distortion products of the data presented in the top panel of Fig. 6-3. There is little difference between the harmonic distortion products between the HC responses before and after tearing the RM. Under both conditions, the first harmonic component dominates below 900 Hz across the whole frequency range. The first harmonic is more than 30 dB higher than the second, third and fourth harmonic distortion. The second, third and fourth harmonic distortions are nearly in the same level. Therefore, the major response before and after tearing the RM is

the first harmonic, and hence, the response to pure tone pips can be considered to be sinusoidal.

6.2.4 Intensity dependence of ac and dc components

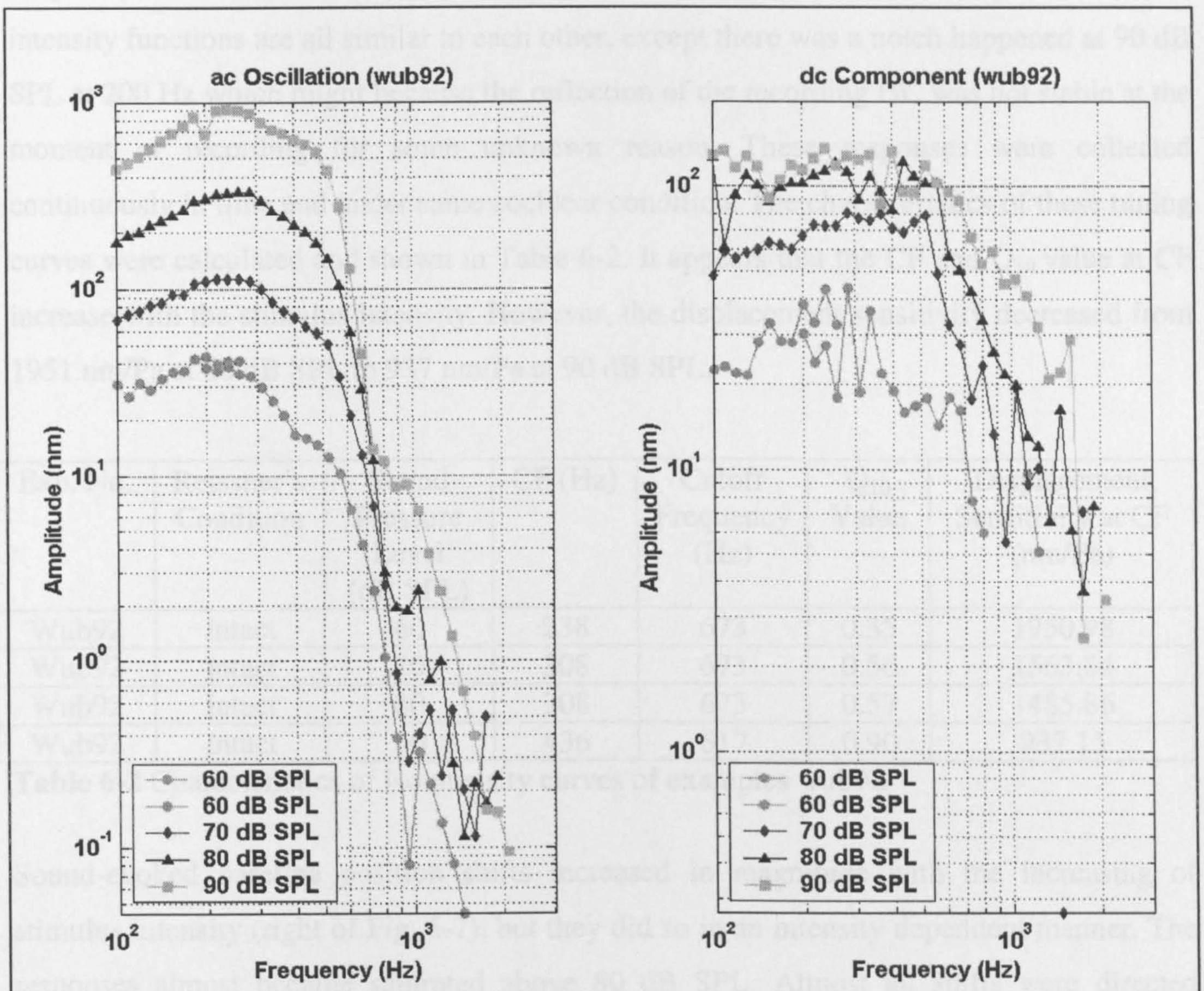

Figure 6-7: HC isointensity functions taken directly after the cochlea was open, with Reissner's membrane and helicotrema was intact (wub92). Circles, diamonds, triangles and squares indicate sound pressure level of 60, 70, 80 and 90 dB SPL. Left: HC isointensity functions of ac components. Right: HC isointensity functions of dc components.

Figure 6-7 plots a family of isointensity functions for HC responses to pure tone pips. These were recorded from a single Hensen's Cell at sound pressure levels of between 60 and 90 dB SPL (circles, diamonds, triangles and squares represent 60, 70, 80 and 90 dB SPL, respectively). Measurements were made directly after the opening of the cochlea, when the Reissner's membrane and helicotrema were intact and the cochlear opening was well sealed by a glass slip and high vacuum grease (wub92). The cochlear partition's

oscillatory responses are plotted on the left and its sound-evoked baseline position shifts are plotted on the right. The amplitude of the ac component of responses increased with the sound pressure levels, with a peak value at around 240 Hz, which is the best frequency of this recording location. Below the BF, the ac amplitude increased with the stimulus frequency and above that, it decreased with stimulus frequency. The shapes of the iso-intensity functions are all similar to each other, except there was a notch happened at 90 dB SPL at 200 Hz which might because the reflection of the recording HC was not stable at the moment of recording for some unknown reason. These responses were collected continuously in time and under same cochlear condition. The characteristics of these tuning curves were calculated and shown in Table 6-2. It appears that the CF and Q_{10} value at CF increase with the stimulus intensity. However, the displacement sensitivity decreased from 1951 nm/Pa at 60 dB SPL to 937 nm/Pa at 90 dB SPL.

Exp. No.	Reissner's Condition	Sound Pressure Level (dB SPL)	CF (Hz)	Cutoff Frequency (Hz)	Q_{10} Value	Displacement Sensitivity at CF (nm/Pa)
Wub92	Intact	60	238	673	0.35	1950.98
Wub92	Intact	70	308	673	0.56	1563.84
Wub92	Intact	80	308	673	0.57	1485.86
Wub92	Intact	90	436	617	0.90	937.15

Table 6-2 Characteristics of isointensity curves of examples wub92

Sound-evoked baseline position shifts increased in magnitude with the increasing of stimulus intensity (right of Fig. 6-7), but they did so in an intensity dependent manner. The responses almost became saturated above 80 dB SPL. Almost all shifts were directed towards the scala vestibuli at the tested frequencies and sound pressure levels.The dc components are nearly identical at certain sound pressure level below 500 Hz and begin to drop quickly above that frequency.

6.2.5 Sensitivity curves

Sensitivity curves show the displacement per unit of sound pressure level as a function of frequency. If the responses grew linearly, the sensitivity curves measured at different sound pressure level should be identical. Sensitivity curves were calculated from the data of Fig. 6-7 and are shown in Fig. 6-8. Different symbols present different sound pressure levels, which are labeled same as Fig. 6-7. For the ac component (left), the biggest sensitivity

occurred at 60 dB SPL with the maximum value around 2000 nm/Pa at CF. The sensitivity curves could be divided into 4 parts as the dotted lines shows in the left of the figure. In the first and the third frequency ranges, the sensitivity curve grew bigger when the sound pressure decreased. This indicates that the compressive nonlinearity existed at these frequencies. For part 2, the sensitivity curves are almost identical, which might mean that for these frequencies the system behaves in a linear manner. There was no regularity to the data in part 4. This is probably because the displacements at these high frequencies were too small to record accurately in the apex of the cochlea. Therefore, in part 1 and 3, clear compressive nonlinearity exists although it is weak. It appears that the level of the compressive nonlinearity is frequency dependent, lower frequency presents higher degree

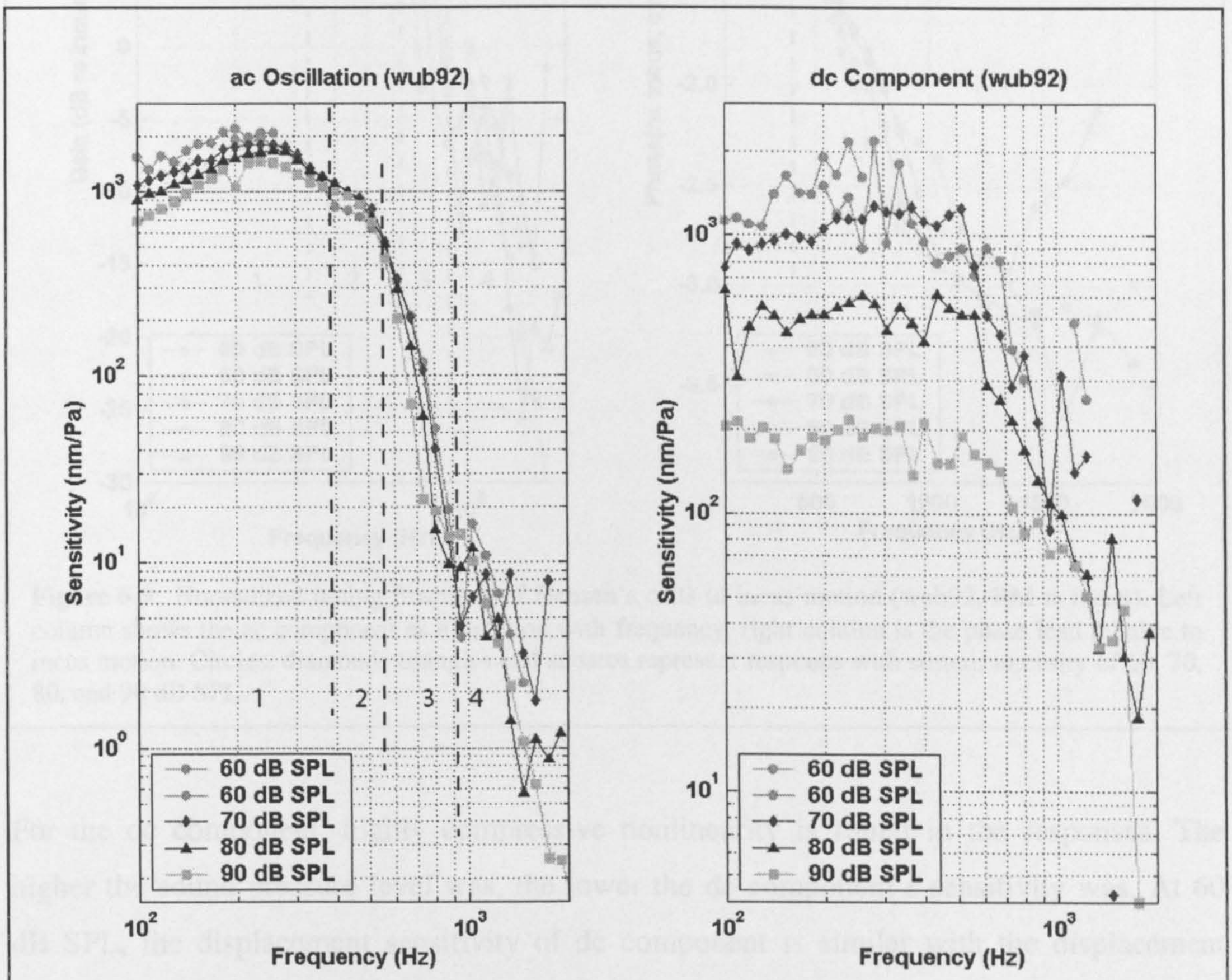

Figure 6-8 Sensitivity curves of Hensen's cells (wub92) when the RM is intact. Left: sensitivity curves of ac component at different sound pressure levels. Right: sensitivity curve of dc component at different sound pressure levels. Circles, diamonds, triangles and squares represent response with stimuli intensity of 60, 70, 80, and 90 dB SPL

of compressive nonlinearity. In part 2, the responses appear to be linear, for the sensitivities at different stimulus intensities are nearly identical.

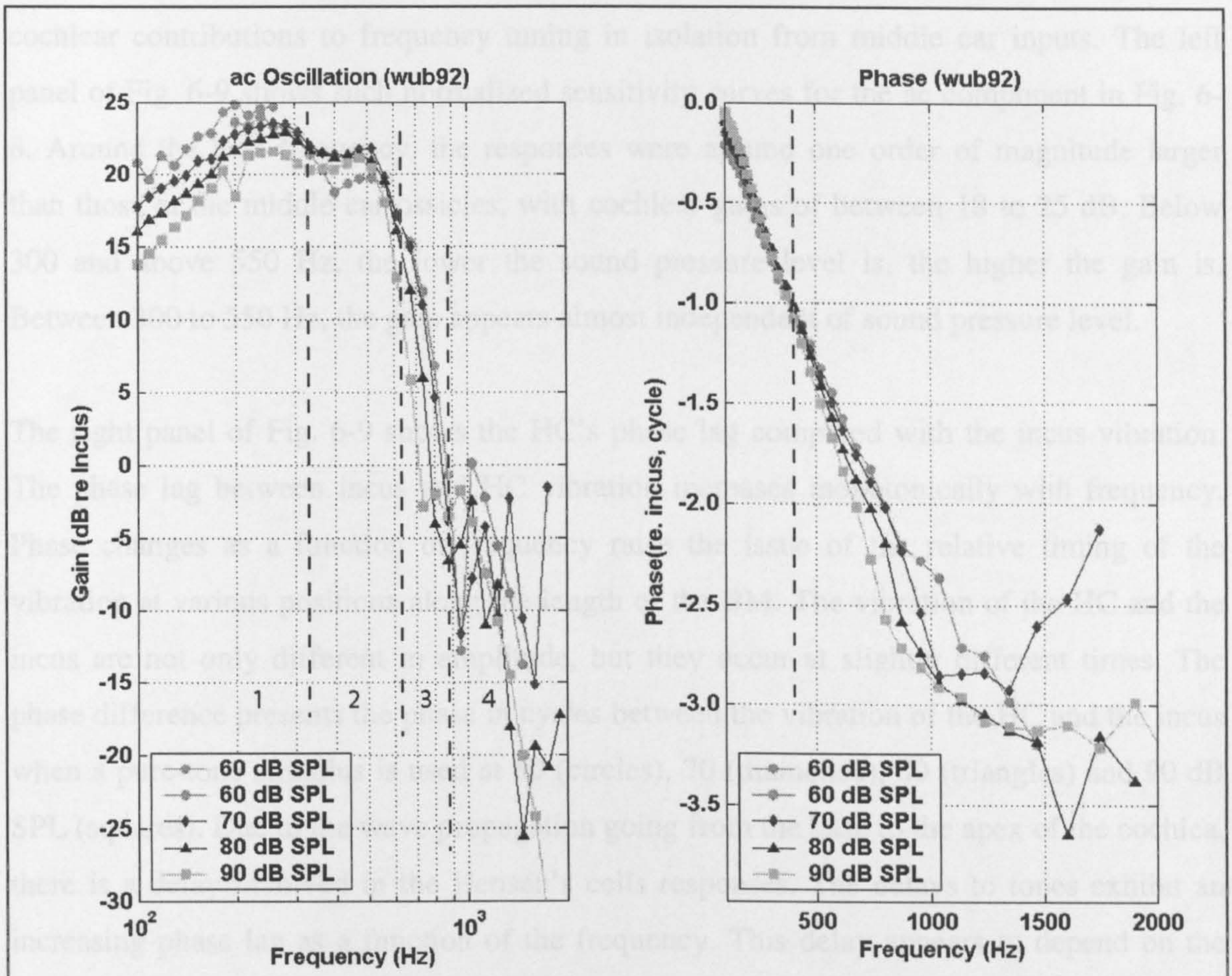

Figure 6-9: Normalized tuning functions of Hensen's cells to incus motion (wub92, RM is intact). Left column shows the ac component as a function with frequency, right column is the phase lead relative to incus motion. Circles, diamonds triangles and squares represent response with stimuli intensity of 60, 70, 80, and 90 dB SPL.

For the dc component, highly compressive nonlinearity is found in the responses. The higher the sound pressure level was, the lower the dc component's sensitivity was. At 60 dB SPL, the displacement sensitivity of dc component is similar with the displacement sensitivity of the ac component, with the maximum above 2000 nm/Pa. However, at 90 dB SPL, the displacement sensitivity of the dc component is far less than that of the ac component (200 nm/Pa).

6.2.6 Gain curves

When Hensen's cell sensitivity functions are normalized by incus motion, they can yield estimates of cochlear gain as a function of stimulus frequency, permitting an assessment of cochlear contributions to frequency tuning in isolation from middle ear inputs. The left panel of Fig. 6-9 shows such normalized sensitivity curves for the ac component in Fig. 6-8. Around the best frequency, the responses were around one order of magnitude larger than those at the middle ear ossicles, with cochlear gains of between 18 to 25 dB. Below 300 and above 550 Hz, the lower the sound pressure level is, the higher the gain is. Between 300 to 550 Hz, the gain appears almost independent of sound pressure level.

The right panel of Fig. 6-9 shows the HC's phase lag compared with the incus vibration. The phase lag between incus and HC vibration increases monotonically with frequency. Phase changes as a function of frequency raise the issue of the relative timing of the vibration at various positions along the length of the BM. The vibration of the HC and the incus are not only different in amplitude, but they occur at slightly different times. The phase difference presents the phase in cycles between the vibration of the HC and the incus when a pure-tone stimulus is used at 60 (circles), 70 (diamonds), 80 (triangles) and 90 dB SPL (squares). Due to the wave propagation going from the base to the apex of the cochlea, there is a delay involved in the Hensen's cells responses. The delays to tones exhibit an increasing phase lag as a function of the frequency. This delay appears to depend on the intensity of stimulation. Below 366.8 Hz (dotted line in the figure), higher intensity data exhibit lower phase lags, but above 366.8 Hz, they exhibit higher phase lags. This intensity dependence is the opposite of that observed in the basal turn of the cochlea (see discussion). The maximum phase lag to incus motion is nearly 3 cycles.

6.2.7 Input-output functions

The nonlinear features of the system can be described using input-output functions, where the Hensen's cell or tectorial membrane vibration amplitude is plotted as a function of input sound pressure level. I/O curves should follow a straight line with 1 dB/dB slope if the system is linear. The system is expansively nonlinear if the slope of the I/O curve is greater than 1 dB/dB, or is compressively nonlinear if the slope of the I/O curve is less than 1 dB/dB. Another feature that can be shown from the I/O curve is the contribution of the

"cochlear amplifier" (CA, Davis 1983) to the sensitivity of the cochlea. The CA contribution is defined as the horizontal distance between the linear portion at low stimulus levels and the linear portion at high stimulus levels.

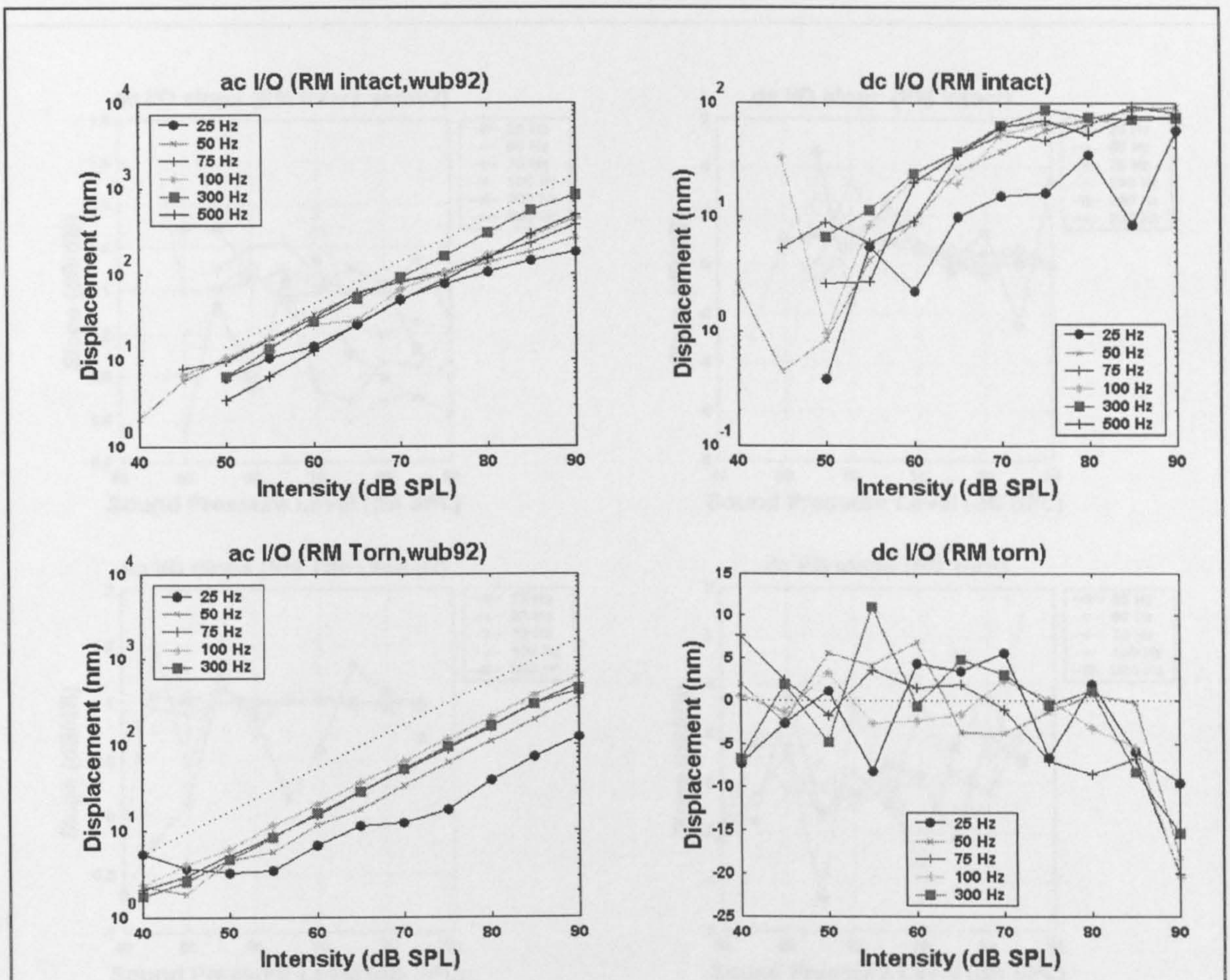

Figure 6-10 input-output functions of the cochlear partition's oscillatory (i.e. ac) and baseline position shifts (i.e. dc) responses of experiment wub92 before and after tearing the RM. Top row represents responses recorded from a single Hensen's Cell's directly after the opening of the cochlea, with the Reissner's membrane and helicotrema intact. Bottom row shows responses from a reflective bead on the TM when the RM was torn. Left column shows the I/O curve of ac component, right shows the I/O curve of dc component.

Fig. 6-10 shows such input-output functions for cochlear partition responses at different frequencies before and after tearing the RM in experiment wub92. The oscillatory responses (i.e. ac) are shown in the left panel, while the baseline position shifts (i.e. dc) are shown in the right panel. Different symbols represent different frequencies, which are labeled in each panel. A straight line with 1 dB/dB slope is plotted as the dotted lines in these figures as the criteria of a linear system. Responses were collected from a single HC

before tearing the RM. After the RM was torn, responses were collected from a single reflective bead on the TM. Slopes of each curve were calculated and are shown in Fig. 6-11.

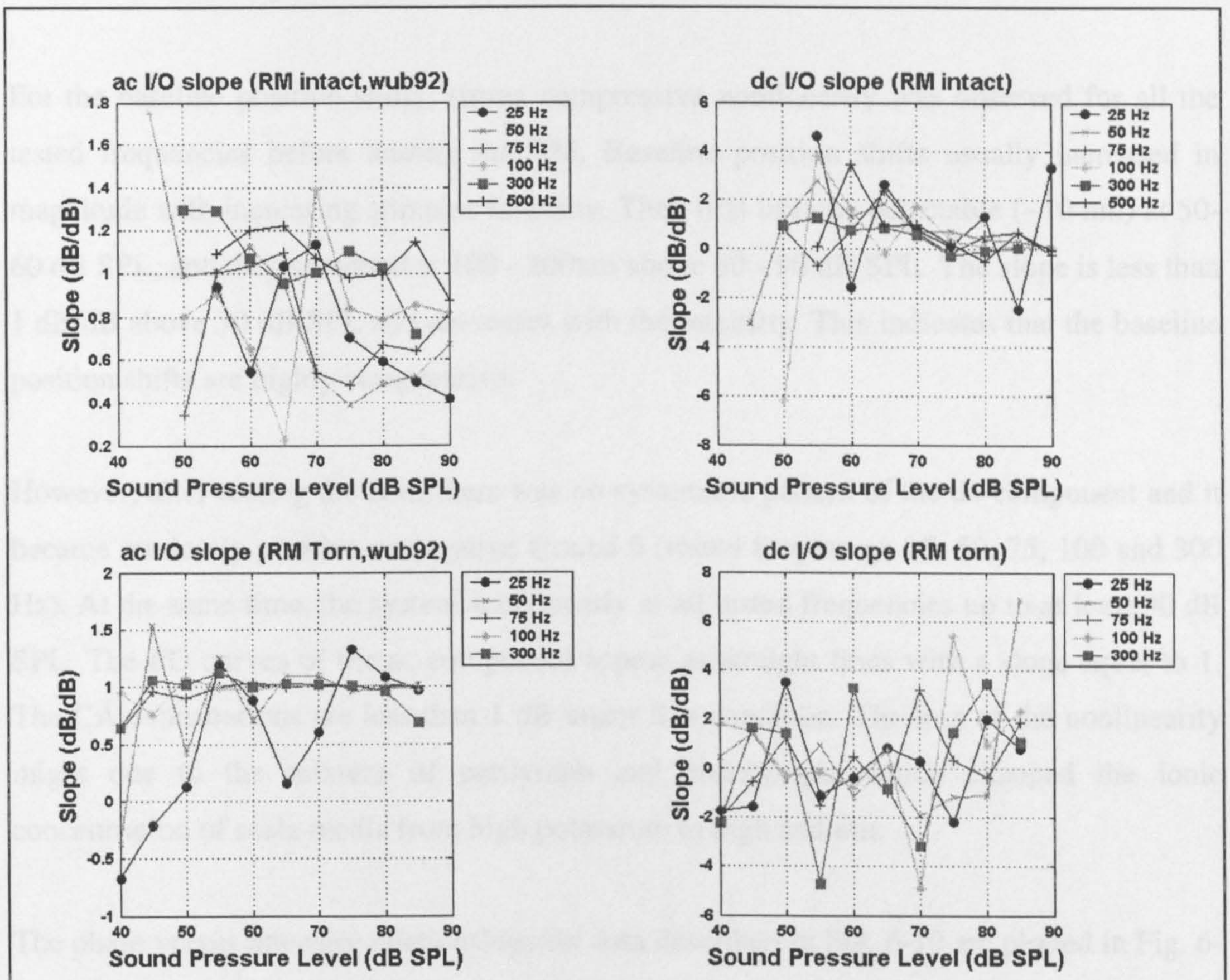

Figure 6-11 Slope of I/O curves of Fig. 6-10.

Before tearing the RM, the response amplitudes increase with sound pressure level linearly first at low intensities, and then, after certain level, the I/O curves become compressively nonlinear. The slope of the I/O curves of the oscillatory responses (i.e. ac) below 100 Hz decreases with sound pressure level. The slopes are less than 1 dB/dB above 70 dB SPL. This indicates that the system behaves compressively nonlinearly at these frequencies and at these sound pressure levels. The compressive nonlinearity seems frequency dependent, the lower the frequency is, the higher the level of compressive nonlinearity is. For the 300 Hz responses, a slope of 0.8 dB/dB was observed only at high sound pressure level (85 dB

SPL). For 500 Hz, the slopes are nearly equal to 1 at all the tested intensities. At these frequencies at moderate intensities, the cochlear partition appears to behave linearly. The cochlear amplification for 25 to 100 Hz tones is between 8.6 and 12.2 dB. For 300 and 500 Hz, the cochlear amplification is less than 4 dB.

For the baseline position shifts, strong compressive nonlinearity was observed for all the tested frequencies before tearing the RM. Baseline position shifts usually increased in magnitude with increasing stimulus intensity. They first became detectable (~10 nm) at 50-60 dB SPL, and they saturated at 100 - 200nm above 80 - 90 dB SPL. The slope is less than 1 dB/dB above 70 dB SPL and decreases with the intensity. This indicates that the baseline position shifts are highly compressive.

However, after tearing the RM, there was no systematic pattern of the dc component and it became randomly positive or negative around 0 (tested frequency: 25, 50, 75, 100 and 300 Hz). At the same time, the system acts linearly at all tested frequencies up to at least 90 dB SPL. The I/O curves of the ac component appear as straight lines with a slope equal to 1. The CA contributions are less than 1 dB under this condition. The loss of the nonlinearity might due to the mixture of perilymph and endolymph, which changed the ionic concentration of scala media from high potassium to high sodium.

The phase versus intensity relationships for data described in Fig. 6-10 are plotted in Fig. 6-12. Before tearing the RM, the phase appears to vary systematically with sound pressure level. At frequencies below 100 Hz, phase seems to increase with the sound pressure level above 55 dB SPL. Above 100 Hz, the phase increases with the sound pressure level and reaches its peak value at certain intensity and then decreases. After tearing the RM, the phase becomes relatively flat in the tested sound pressure level range. Considering the average behaviours across 8 animals, there was high-intensity-produced phase lead at low frequencies. The phase lead decreased with decreases in the nonlinearity and became flat when the system was linear. On the other hand, there was a phase lag near or above the best frequency and it seems that the phase lag increased with the stimulus frequency.

All the 8 cochleae gave similar results before and after tearing the RM, although for some of them, the baseline position shifts were not as strong as the example presented here.

Before tearing the RM, to the pure tone pips, responses from the HC present a strong baseline position shifts. Both the ac and dc components behave in a compressively nonlinear manner. However, after tearing the RM, the baseline position shifts disappeared immediately and the system acts in a linear way instead.

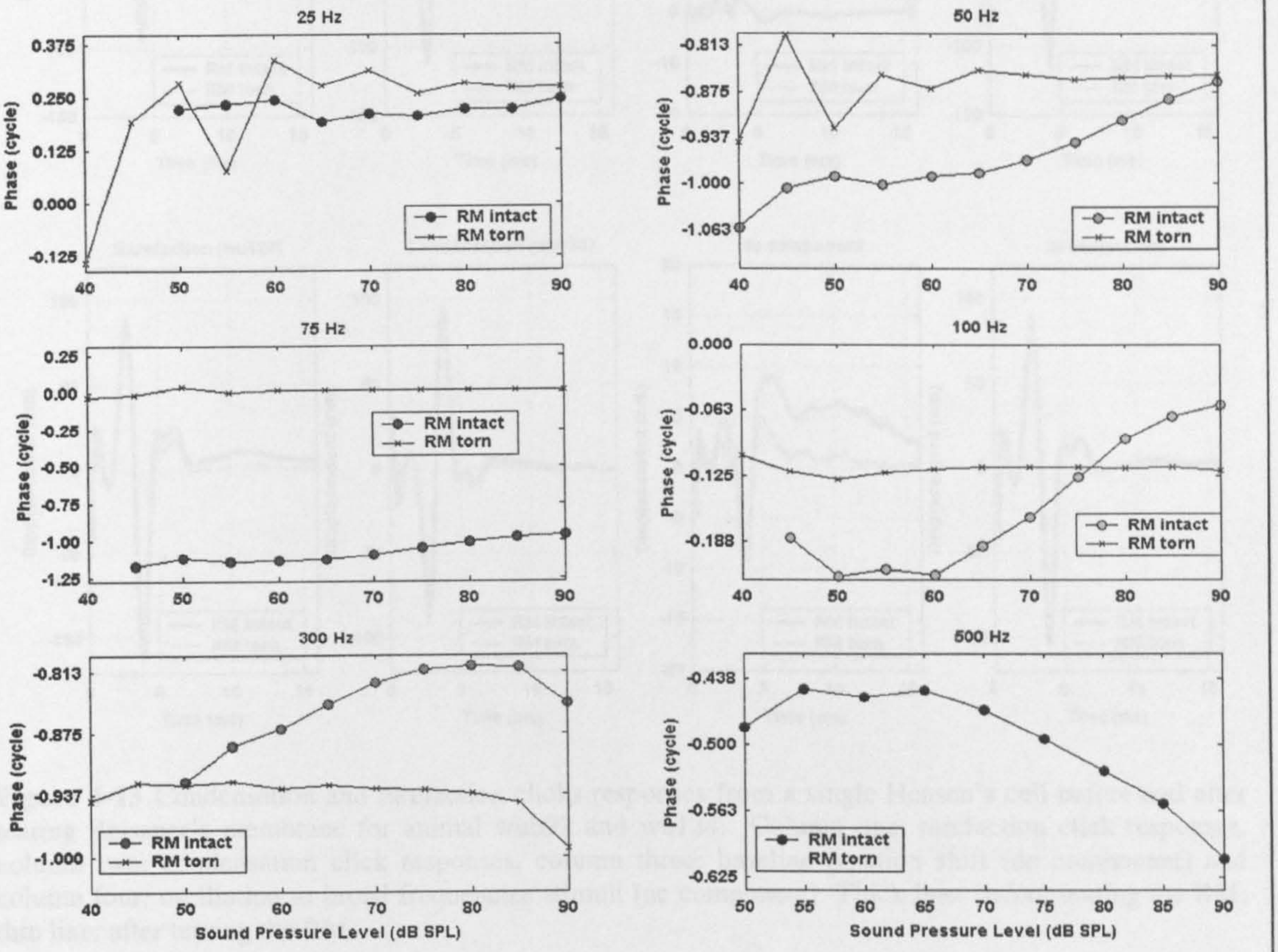

Figure 6-12 Phase of input-output functions of Fig.8. circles represent responses collected before tearing the RM. Crosses represent responses recorded after tearing the RM. Stimuli frequency is labeled in each figure.

6.3 Click-Evoked Responses

Baseline position shifts are also observed in the partitions responses to condensation and rarefaction clicks before tearing the Reissner's membrane. Fig. 6-13 shows the condensation and rarefaction click responses of a single Hensen's cells before (thick line) and after (thin line) tearing the Reissner's membrane in examples from wub92 and wu124.

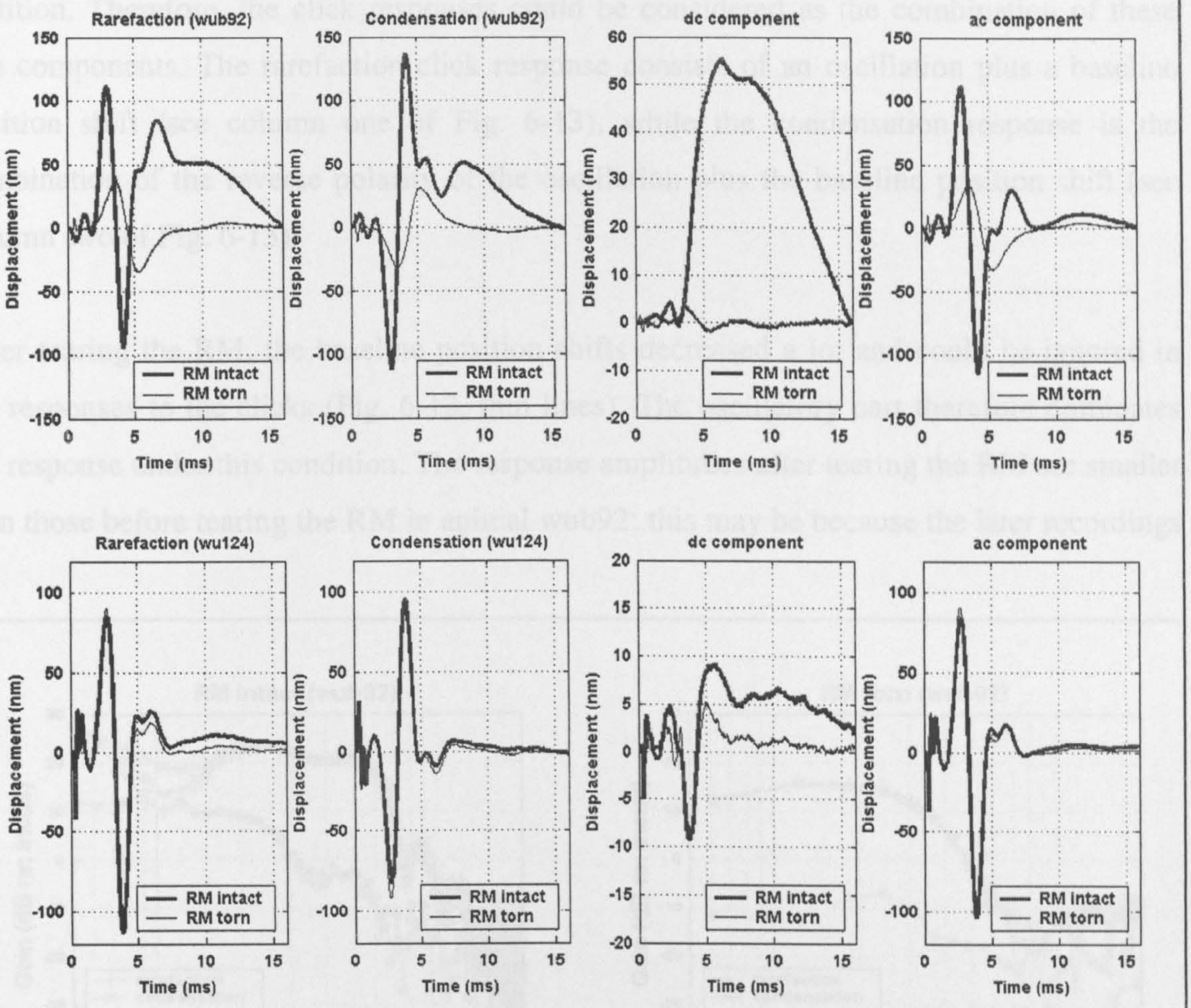

Figure 6-13 Condensation and rarefaction clicks responses from a single Hensen's cell before and after tearing Reissner's membrane for animal wub92 and wu124. Column one: rarefaction click responses, column two: condensation click responses, column three: baseline position shift (dc component) and column four: oscillation to broad frequencies stimuli (ac component). Thick line: before tearing the RM; thin line: after tearing the RM.

In the time domain, the responses could easily be separated into 'fast' and 'slow' waves, which relates to the sealing condition of the opening of the cochlea and was discussed in chapter 5. On the other hand, it appears that the waveform of the 'slow' response to the clicks contains two parts as well: positive baseline position shifts (dc component) and oscillations to a broad range frequencies in the stimuli (ac component). The baseline position shifts were manifested as response components which did not invert when the polarity of the stimulus was changed (i.e. from a rarefaction to a condensation click, see column 3 of Fig. 6-13). The oscillatory part does change with the stimuli polarity (see column 4 of Fig. 6-13). The non-inverting components oscillated on a much longer

timescale than the conventional (i.e. best-frequency related) oscillations of the apical partition. Therefore, the click responses could be considered as the combination of these two components. The rarefaction click response consists of an oscillation plus a baseline position shift (see column one of Fig. 6-13), while the condensation response is the combination of the reverse polarity of the oscillation plus the baseline position shift (see column two of Fig. 6-13).

After tearing the RM, the baseline position shifts decreased a lot and could be ignored in the responses to the clicks (Fig. 6-13, thin lines). The oscillatory part therefore dominates the response under this condition. The response amplitudes after tearing the RM are smaller than those before tearing the RM in animal wub92; this may be because the later recordings

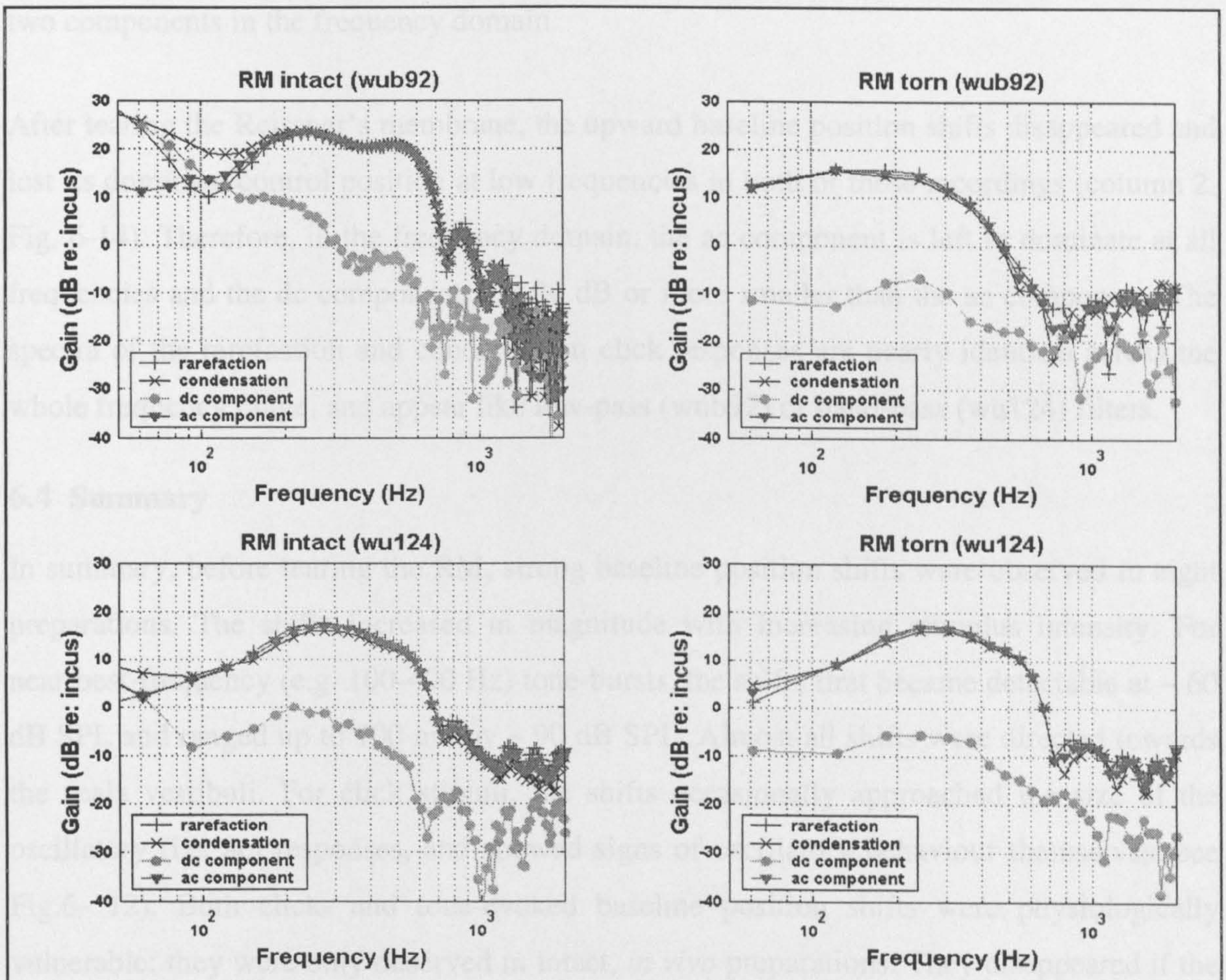

Figure 6-14 Spectral analysis of rarefaction and condensation clicks responses before and after tearing the RM. Plusses represent FFT of rarefaction click response, crosses indicates FFT of condensation click response, circles show baseline position shift (dc component) FFT result and triangles show FFT of ac component.

were collected 5 hours after the tearing of the RM, which may lead to the loss of hearing sensitivity by mixing the perilymph and endolymph.

Figure 6-14 shows the spectra of the four waveforms in Fig. 6-13, as revealed by performing a Fast Fourier Transform. Plusses, crosses, triangles and circles represent the spectra of rarefaction, condensation, oscillatory and baseline position shifts. Before tearing the RM, transfer functions of rarefaction, condensation and the oscillatory component are identical above 200 Hz. However, below 200 Hz, especially below 100 Hz, baseline position shift (circles) begin to interfere. The magnitude of dc component drops very quickly with increasing frequency and becomes ~ 15 dB less than that of the ac component just above 100 Hz. The ac component (triangles) behaves like a band-pass filter from 200 to 600 Hz. The rarefaction and condensation response spectra are the combination of these two components in the frequency domain.

After tearing the Reissner's membrane, the upward baseline position shifts disappeared and lost its dominant control position at low frequencies in both of these recordings (column 2, Fig. 6-14). Therefore, in the frequency domain, the ac component is left to dominate at all frequencies and the dc component is ~ 20 dB or more smaller than the ac component. The spectra of the rarefaction and condensation click responses are nearly identical across the whole frequency range, and appear like low-pass (wub92) or band-pass (wu124) filters.

6.4 Summary

In summary, before tearing the RM, strong baseline position shifts were observed in eight preparations. The shifts increased in magnitude with increasing stimulus intensity. For near-best-frequency (e.g. 100-400 Hz) tone-bursts, the shifts first became detectable at ~ 60 dB SPL and ranged up to 100 nm by ~ 90 dB SPL. Almost all shifts were directed towards the scala vestibuli. For click stimuli, the shifts occasionally approached the size of the oscillatory (i.e. ac) responses, and showed signs of oscillatory behaviour themselves (see Fig.6- 12). Both click- and tone-evoked baseline position shifts were physiologically vulnerable: they were only observed in intact, *in vivo* preparations. They disappeared if the scala media was disrupted (e.g. when Reissner's membrane was torn) and they disappeared *post-mortem*. The baseline position shift behaves in a highly compressive manner in the system.

Compressive nonlinearity was also observed at low frequencies above 70 dB SPL in the oscillatory response before tearing the RM. Tearing the RM appears have little effect of the ac component, the tuning and the phase show the same pattern and nearly the same displacement sensitivity as those when the RM was intact. However, tearing the RM did diminish the compressive nonlinearity of cochlear system.

6.5 Discussion

6.5.1 Nonlinearity in the apical turn of the cochlea before tearing the RM

One important feature of the present study is the observation of compressive nonlinearity in the apical turn of the cochlea before tearing the RM. This feature is considered to be related to the physiological condition of the cochlea. The nonlinearity observed in the apical turn (Cooper and Rhode 1995; Cooper and Rhode 1996; Khanna and Hao 1999) is not as strong as that of the basal cochlea (Rhode 1971; Rhode 1978; Sellick et al. 1982; Robles et al. 1986; Ruggero and Rich 1991; Cooper and Rhode 1992; Ruggero et al. 1992; Cooper 1996) and only appears in the intact, *in vivo* condition. Both of the ac and dc components contribute to the nonlinearity. The compressive nonlinearity seems only to exist in a restricted frequency range (50 – 280 Hz and 600 – 900 Hz, see Fig. 6-8). Between 280 and 600 Hz, the preparations appear to respond linearly. However, this does not mean that the cochlea does respond linearly at these frequencies. There may still be some nonlinearity, but it could be covered by some linear factor and hence cannot be expressed obviously. FFT analyses of the raw waveforms show the existence of the harmonic distortion products at almost all frequencies, although the second and the third harmonic products are 30-40 dB down compared with the first harmonic. Our FFT results are completely different from those in Khanna's (Khanna and Hao 1999) report, which shows more than 10 harmonic distortions. The reason for this is not clear.

After tearing the RM, both the strong baseline position shifts and nonlinearity in oscillatory responses disappear, even though the oscillatory responses change little.

6.5.2 Nonlinearity in phase

The low frequency phase data obtained before tearing the RM shows systematic intensity dependence (see Fig. 6-9 and Fig. 6-12). Below CF, the phase lag decreases with increasing stimulation intensity, at CF, the phase changes little with intensity, and above CF, the phase lag increases with the stimulation intensity. This observation is consistent with the mechanical phase data reported by Cooper (Cooper and Rhode 1995). However, this is inconsistent with phase data reported from low CF cochlear nerve fibres (Anderson et al. 1971; Carney and Yin 1988). In the neural data, below CF, the phase lags tend to increase with stimulation intensity, and above CF, responses tend to lead with increasing intensity. This inconsistency of the mechanical and neural phase data means that there must be additional processing at the micro-mechanical/hair cell/neural levels.

6.5.3 Sound-evoked changes in the baseline position of the cochlear partition before tearing the RM

Sound-evoked changes in the baseline position of the cochlear partition have been reported previously by several research groups (LePage 1987; LePage 1989; Brundin et al. 1992; Cooper and Rhode 1992; Cooper and Rhode 1995; Cooper and Rhode 1996; Rhode 1996), but their exact characteristics, their origins, and their importance remain issues of contention.

In the basal turn of the guinea-pig cochlea, sharply-tuned 'dc-shifts' were reported by LePage (LePage 1987; LePage 1989). These shifts included both tonic and accumulating components, and could change the baseline position of the cochlear partition by several micrometers. These characteristics were later refuted by Cooper and Rhode (Cooper and Rhode 1992; Cooper and Rhode 1995; Cooper and Rhode 1996; Rhode 1996).

In the apical turn of the guinea pig cochlea, sharply-tuned 'displacement responses' were reported by Brundin et al (Brundin et al. 1992). These responses could also change the baseline position of the partition by several micrometers. However, these responses were later refuted by Cooper and Rhode (Cooper and Rhode 1995; Cooper and Rhode 1996) and by Gummer et al. (Gummer et al. 1993).

Much smaller and less frequency dependent baseline position shifts were reported by Cooper and Rhode (Cooper and Rhode 1995; Cooper 1999) in the apical turns of the

guinea-pig and chinchilla cochlea. The result reported here provides further evidence of dc-shifts in the apical turn of the guinea-pig cochlea, and shows these shifts to be physiologically vulnerable. They were only observed in intact, *in vivo* preparations, and they disappeared reversibly during periods of anoxia. These sound-evoked shifts could be generated by the outer hair cells in the apical turn of the cochlea: the time-course, magnitude and physiological vulnerability of the shifts are certainly consistent with such an origin. Baseline position shifts may be responsible for non-interleaving neural responses (Pfeiffer and Kim 1972; Lin and Guinan 2000), as will be explained below.

6.5.4 Comparison with previous mechanical studies

The *in vivo* mechanics at the apex of the guinea pig cochlea reported here are consistent with responses at the apex of the chinchilla cochlea *in vivo* (Cooper and Rhode 1995; Cooper and Rhode 1996; Rhode 1996). Most of the recordings are from the cochlear partition with CF between 200 to 400 Hz. Without rupturing the RM, responses grow at a mildly compressive nonlinear rate (< 1dB/dB) at low frequencies so that the vibration sensitivity increases systematically with decreasing stimulus intensity. This is not consistent with the results from similar preparation which failed to detect nonlinearity in the vibration of organ of Corti (Khanna and Hao 1999; Khanna and Hao 1999). Above CF, the cochlear partition appears to behave in a linear way. However, this is not sufficient to conclude that cochlear partition vibrates linearly, or as one previous investigation suggested that a vulnerable expansive nonlinearity exists in the apical cochlea (Zinn et al. 2000).

Previous mechanical studies at the apex of the guinea pig cochleae seem to be less sensitive than those from chinchilla (Cooper and Rhode 1995; Cooper and Rhode 1996; Hao and Khanna 1996; Rhode 1996; Cooper and Rhode 1997; Zinn et al. 2000). However, in our experiment, the sensitivities at CF of single HC or TM sites are mostly more than 500 nm/Pa and the highest reaches over 3000 nm/Pa. This higher sensitivity might indicate that "how normal the cochlea was" becomes a more important issue for mechanical studies in the apex of the cochlea. After tearing the RM, the mixture of perilymph and endolymph lead to a decrease of sensitivity. On the other hand, the Q_{10} value changed little before and after tearing the RM. The Q_{10} of tuning curves in the studies was normally around 0.5-0.6, which is lower than that in many other reports. The reason for this is that apical responses appear to behave as low-pass filter in our results both before and after tearing the RM.

6.5.5 Positive feedback model

Based on the observation of compressive nonlinearity and baseline position shifts, we have proposed a positive feedback loop to understand the cochlear mechanics in the apical turn of the cochlea (**Dong and Cooper** 2001). Fig. 6-15 shows a simple model, which can replicate most of the features observed in the apical cochlear partition responses to rarefaction and condensation clicks. This model relies on positive feedback between the outer hair cells and the cochlear partition (Cooper 1998), in distinct contrast to the negative feedback hypotheses proposed by other investigators (Khanna and Hao 2000; Zinn et al. 2000).

This feedback loop contains two paths in a physiologically plausible positive feedback configuration. The first path, from filter 1 direct to the output, replicates most of the ac components in the observed responses (the mostly high frequency oscillations near the onset of the responses). The second path provides the slower oscillations and the dc response components by filtering a nonlinearly transformed (almost half-wave rectified and slightly compressed) version of filter 1's output. In the real cochlea, the second path can be

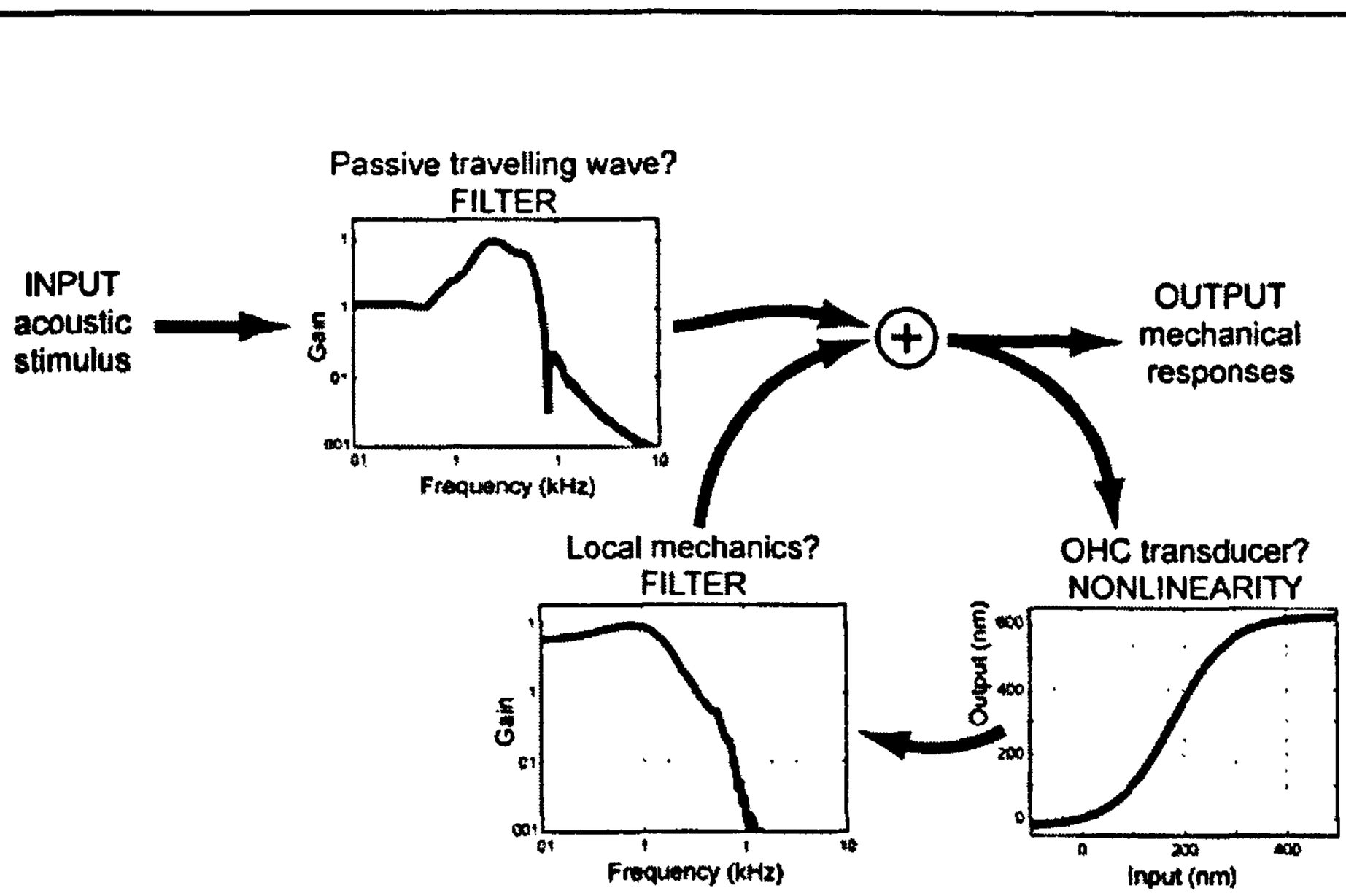

Figure 6-15 Schematic Sketch of positive feedback loop of apical turn of cochlea (diagramed by N. Cooper).

thought of as the outer hair cells, which sense the vibrations of the cochlear partition (initially driven by the output of filter 1) and transduce them nonlinearly into intracellular voltages. These intracellular responses are expected to drive some form of cellular motility (either somatic or hair-bundle based), which can, in turn, cause the cochlear partition to vibrate.

In order to test the model, incus responses to condensation and rarefaction clicks were used as the input to the model and output was compared with the responses to condensation and rarefaction responses. Fig. 6-16 allows the comparison of the calculation result of the model and real experiments. Green lines show the output of the model and the blue lines represents the experimental results. The positive feedback model provides a reasonable match to the rarefaction and condensation click responses observed in real experiments. It can account for both ac and dc components in the real cochlea. This model is capable of replicating the observed data reasonably well and none of the parameters look entirely

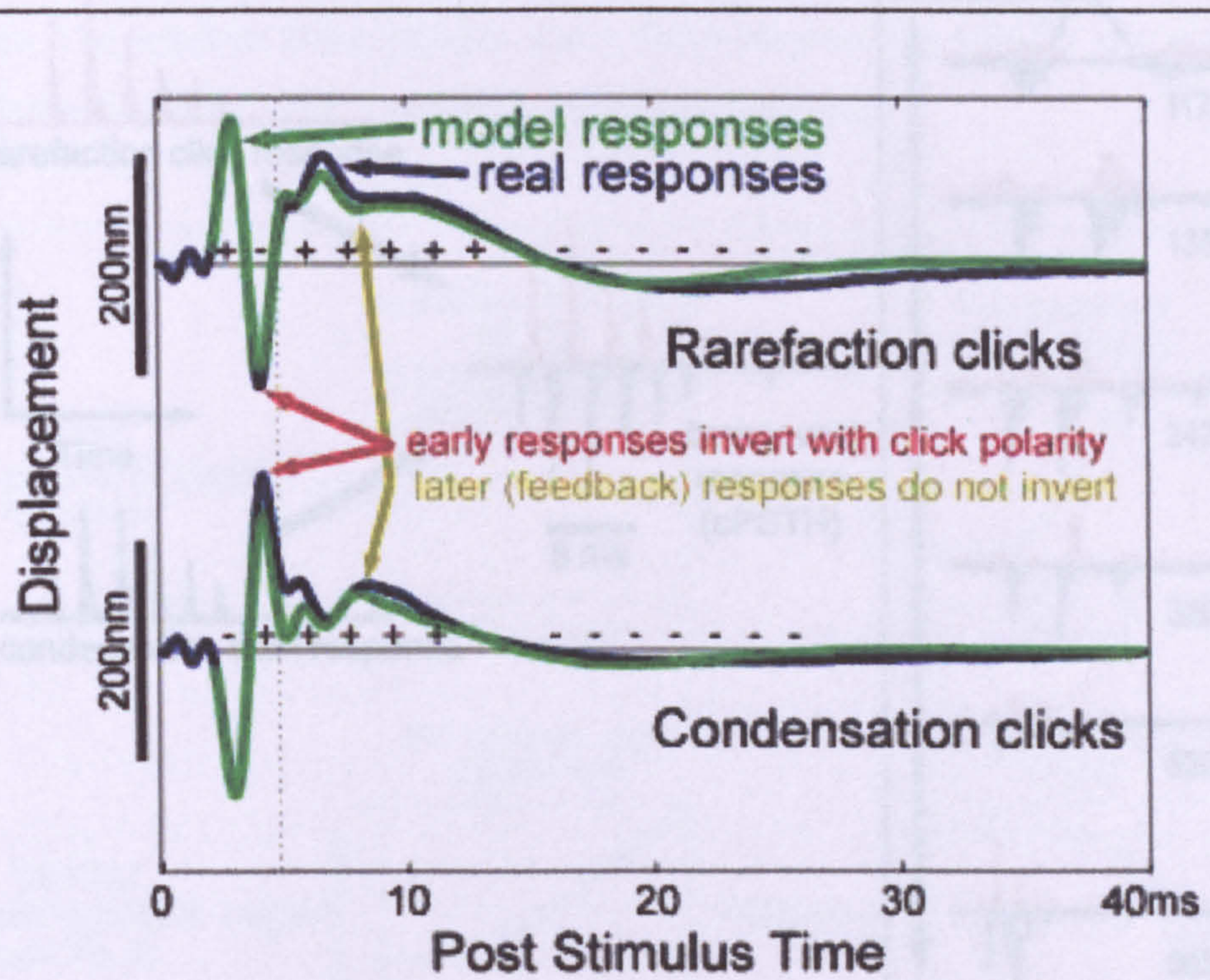

Figure 6-16 Comparison of output of model and real experiments click response. Green lines are rarefaction and condensation responses computed by the positive feedback model and blue lines show the real experimental data (diagramed by N. Cooper).

unrealistic from a physiological point of view.

After tearing the RM, the mixture of the perilymph and endolymph changed the ionic environment of the hair cells, which in turn, affects the endocochlear potential and leads to the loss of the positive feedback loop in the model. Therefore, in the responses after tearing the RM, only the ac component is detected and there are no slower oscillations & dc components contributing to the responses.

Auditory nerve fiber responses to clicks of opposite polarity generally interleave with each other quite accurately in the time domain, as shown in Figure 6-17 (left). However, a small group of fibers have non-interleaving responses, as shown in Figure 6-17 (right). The fibers with non-interleaving responses have very low characteristic frequencies (CFs), and presumably innervate the very apical regions of the cochlear partition. The non-interleaving

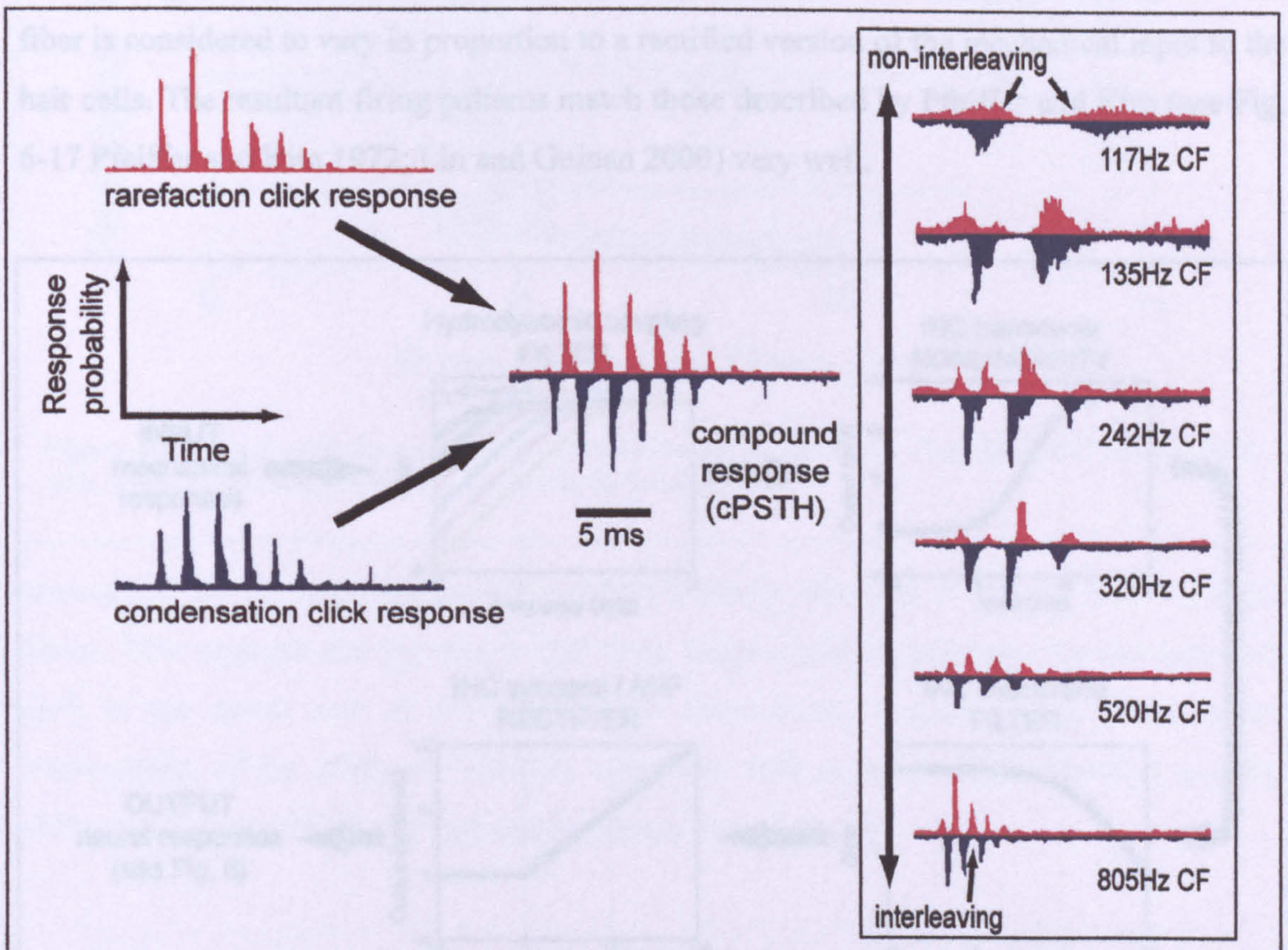

Figure 6-17 Construction of a compound post-stimulus time histogram (cPSTH). The accurate interleaving of responses to condensation and rarefaction clicks seen in most auditory nerve fibers (left). and non-interleaving to interleaving responses seen only from low-CF auditory nerve fibers (right).

decreases when the CF increases. The mechanical responses of the apical cochlear partition are quite different from those in other regions of the cochlea: sounds can evoke strong baseline position shifts in the apical turn of the cochlea (see Fig. 6-1 and 6-2). The following part is to explain how these baseline position shifts might be generated, and to consider whether they might account for the non-interleaving neural responses.

Signal processing continues in the cochlea that the output of the positive feedback model (Fig. 6-15 and 6-16) will excite the hair cells to change mechanical signals into electronic signals. Fig. 6-18 shows a simple signal-processing model for the inner hair cells and auditory nerve fiber synapses in the cochlea. Using the real experimental rarefaction and condensation click responses, the output from the positive feedback loop, (see Fig. 6-16) as the mechanical input to excite the model's inner hair cells, non-interleaving compound post-stimulus time histogram (cPSTH) were predicted when the cut-off frequency of the inner hair cell's high-pass filter was low (e.g. f_c<100Hz, Fig. 6-19). The degree of non-interleaving decreased as the cut-off frequency increased. The firing probability of each fiber is considered to vary in proportion to a rectified version of the mechanical input to the hair cells. The resultant firing patterns match those described by Pfeiffer and Kim (see Fig. 6-17 Pfeiffer and Kim 1972; Lin and Guinan 2000) very well.

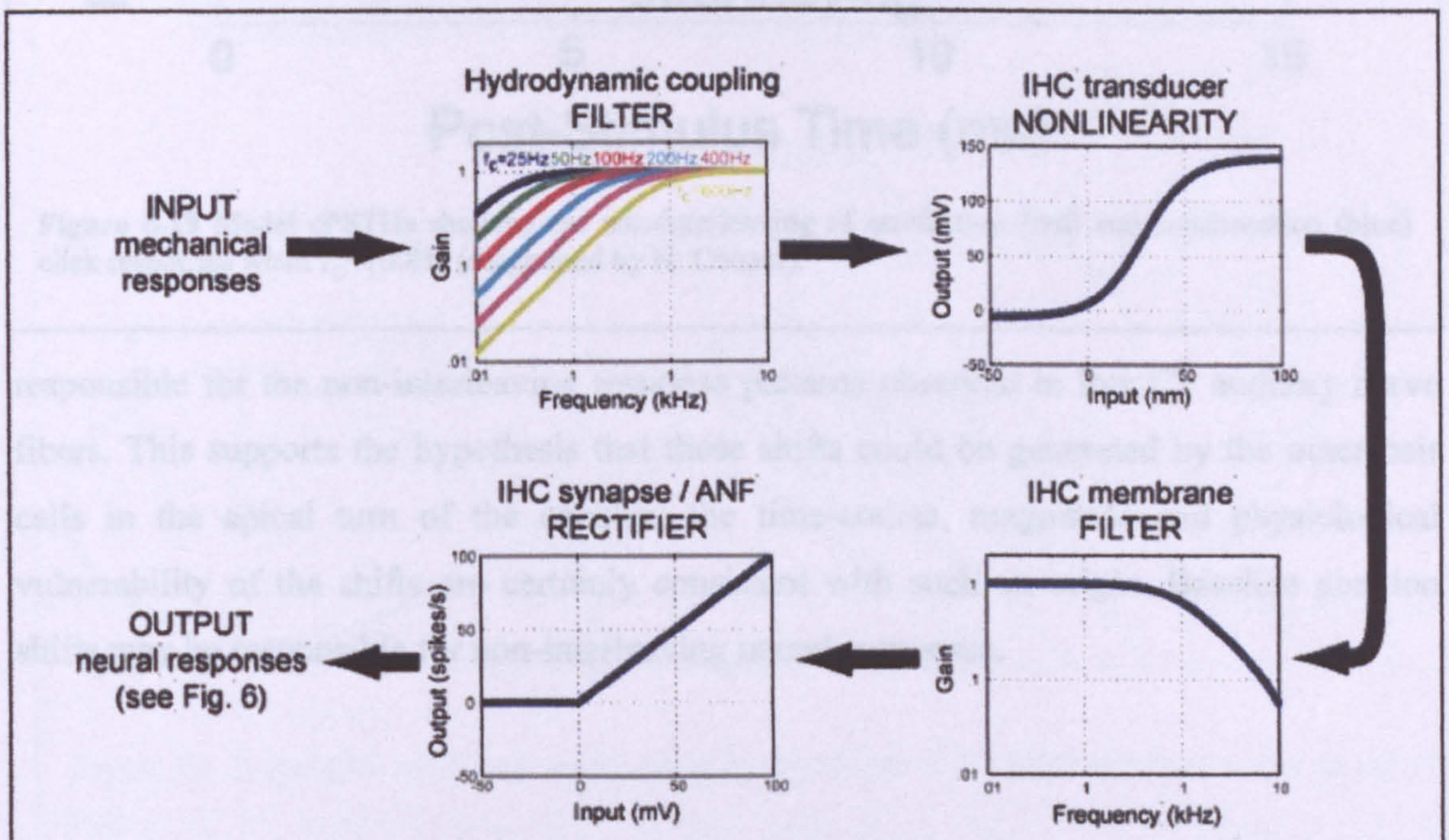

Figure 6-18 Signal processing model for the inner hair cells and auditory nerve fiber synapses in the cochlea (diagramed by N. Cooper).

These modeling studies show that baseline position shifts on the cochlear partition could result from positive feedback between the partition and the outer hair cells, and could be

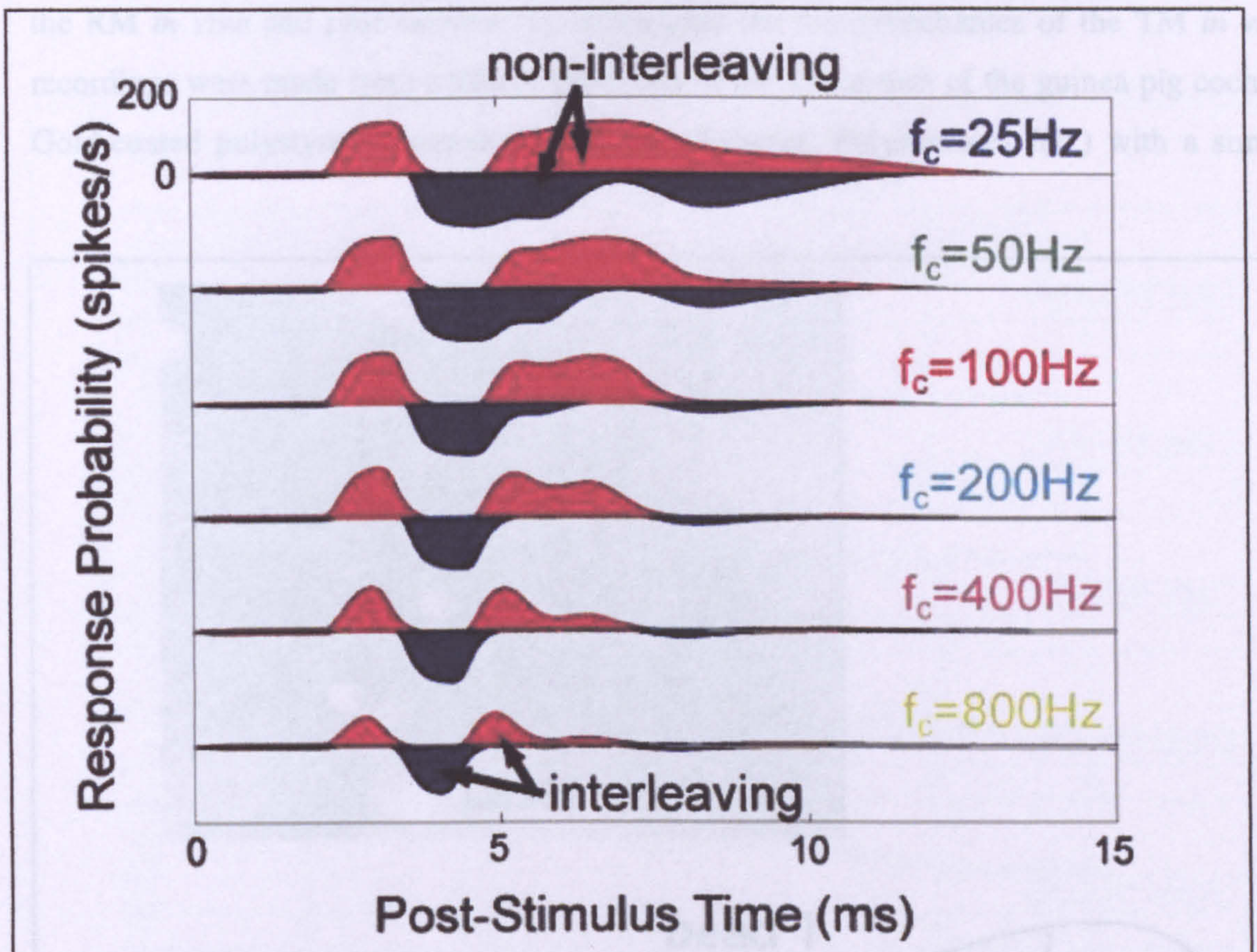

Figure 6-19 Model cPSTHs showing the non-interleaving of rarefaction (red) and condensation (blue) click responses when f_c<100Hz (diagramed by N. Cooper).

responsible for the non-interleaving response patterns observed in low CF auditory nerve fibers. This supports the hypothesis that these shifts could be generated by the outer hair cells in the apical turn of the cochlea: the time-course, magnitude and physiological vulnerability of the shifts are certainly consistent with such an origin. Baseline position shifts may be responsible for non-interleaving neural responses.

Chapter 7 Tectorial membrane responses to sound

7.1 Introduction

This chapter compares the sound-evoked responses of TM to that of the HC after tearing the RM *in vivo* and *post mortem*. To investigate the micromechanics of the TM *in vivo*, recordings were made from cochlear partitions in the apical turn of the guinea pig cochlea. Gold-coated polystyrene microbeads (25 μm diameter; Polysciences Inc.) with a similar

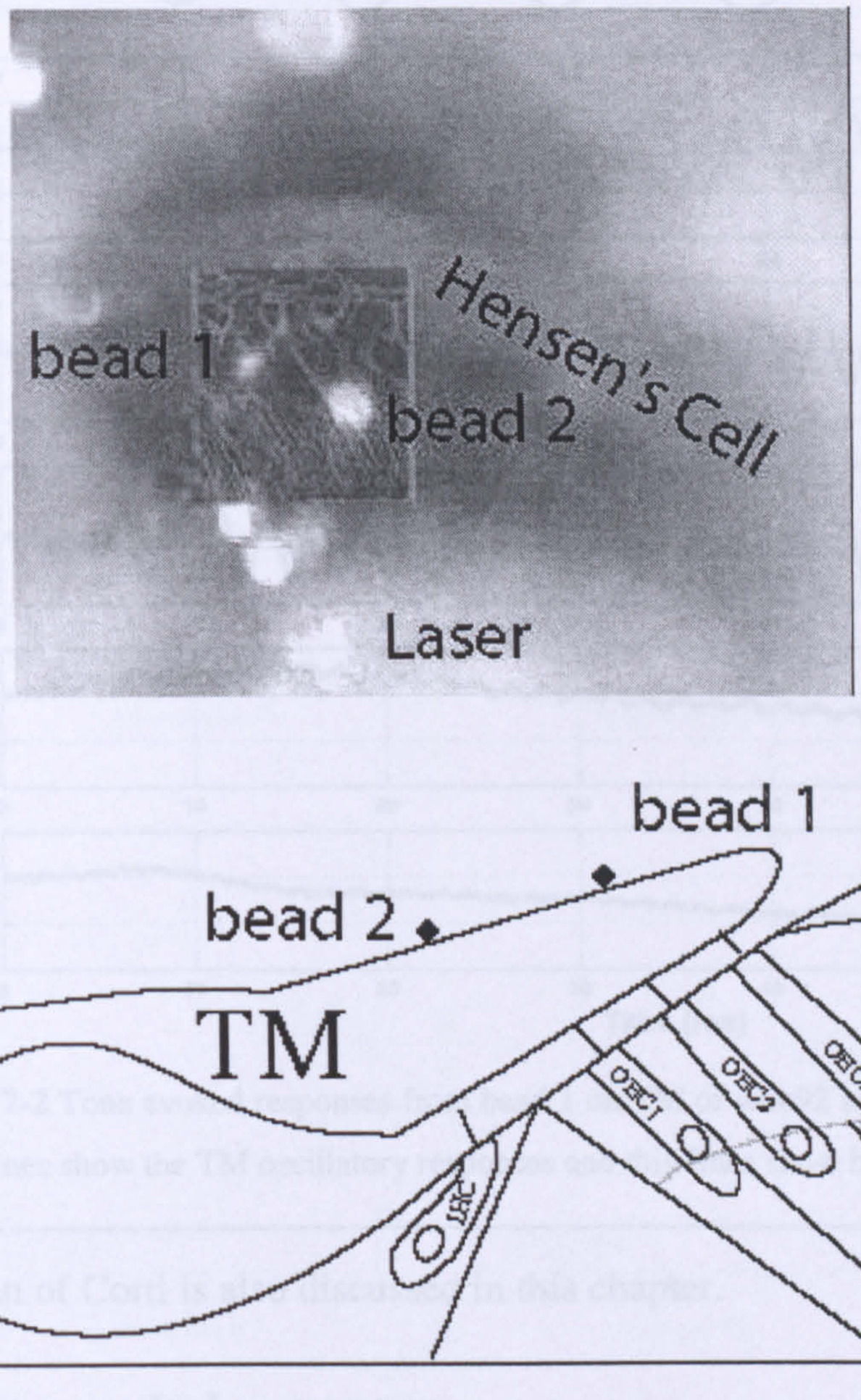

Figure 7-1 Preparation of animal wub92. Bead 1 was on top of the OHC and bead 2 was on top of the IHC.

density to that of water have to be introduced into the scala media via a small tear in Reissner's membrane (RM). These beads settled on the TM to enhance the reflectivity of TM (rupturing Reissner's membrane effects were discussed in Chapter 6). The initial opening of the cochlea was covered and/or resealed using a glass coverslip and high-vacuum grease to minimize the opening effects of the cochlea (discussed in Chapter 5). Tone bursts and click stimuli were used in this study. The effect of introducing beads into

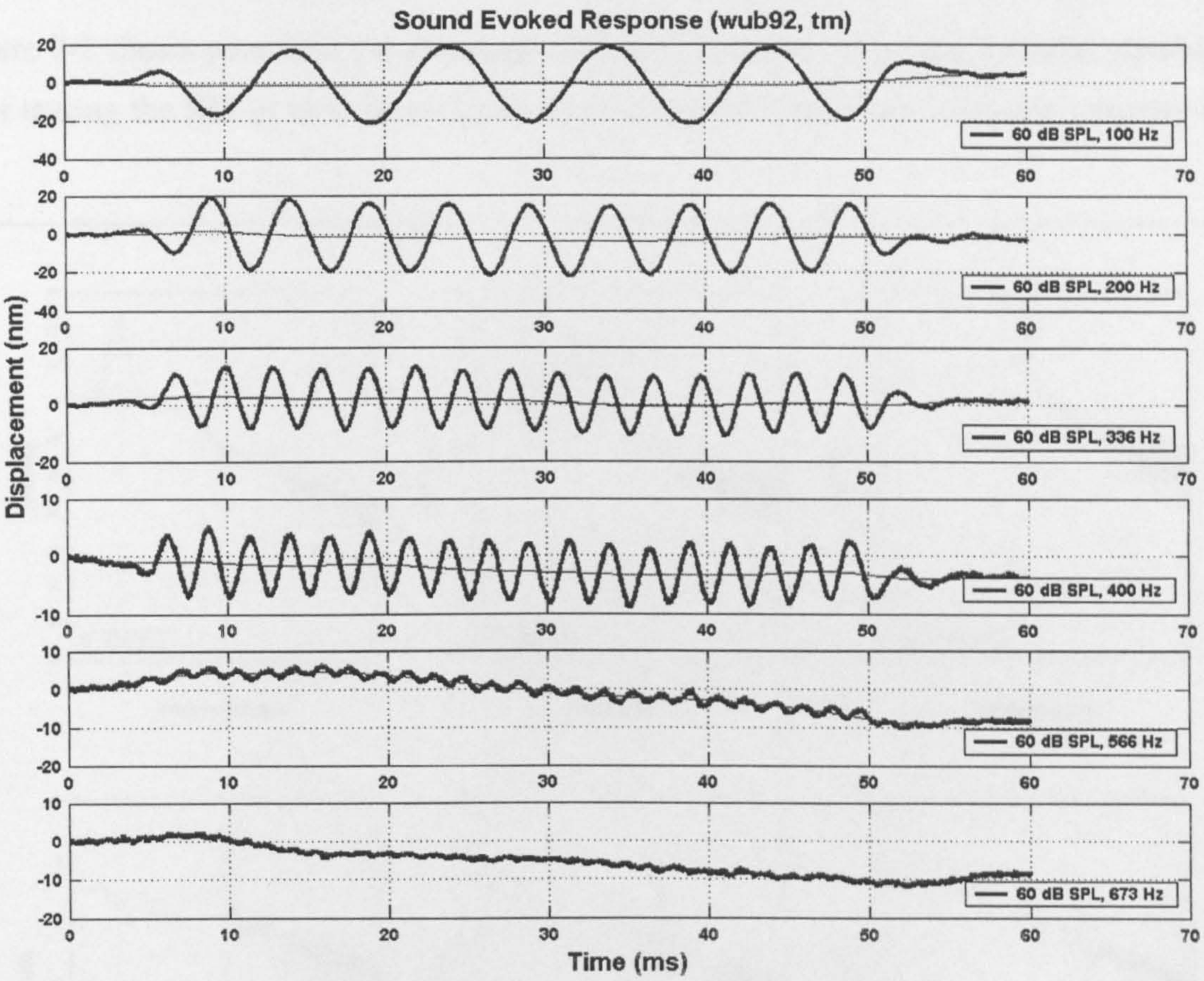

Figure 7-2 Tone evoked responses from bead 1 on TM of wub92 after tearing the Reissner's membrane.. Thick lines show the TM oscillatory responses and thin lines show baseline position shifts.

the organ of Corti is also discussed in this chapter.

7.2 Tone-evoked responses

A total of 42 animals contribute similar substantial data. One example is chosen to highlight this chapter. For this animal, two gold-coated polystyrene microbeads were

successfully introduced into the scala media and settled on the TM. One bead was above the OHCs, the other was above the IHCs. For this preparation, the band of Hensen's cell was shining and easily recognized from other cellular cochlear structures. The bead positions were 17-17.5 mm away from the stapes of the guinea pig cochlea. The photo of the preparation is shown in Figure 7-1 with a schematic figure showing the cross section of the Organ of Corti. The fibres of the TM are also shown in the figure by attaching another photo copied from Lim's review (Lim 1980).

7.2.1 Responses waveforms

Figure 7-2 shows pure tone pip responses collected from bead 1 on the tectorial membrane after tearing the RM *in vivo*. Waveforms were averaged 8 times and stimulus intensity was

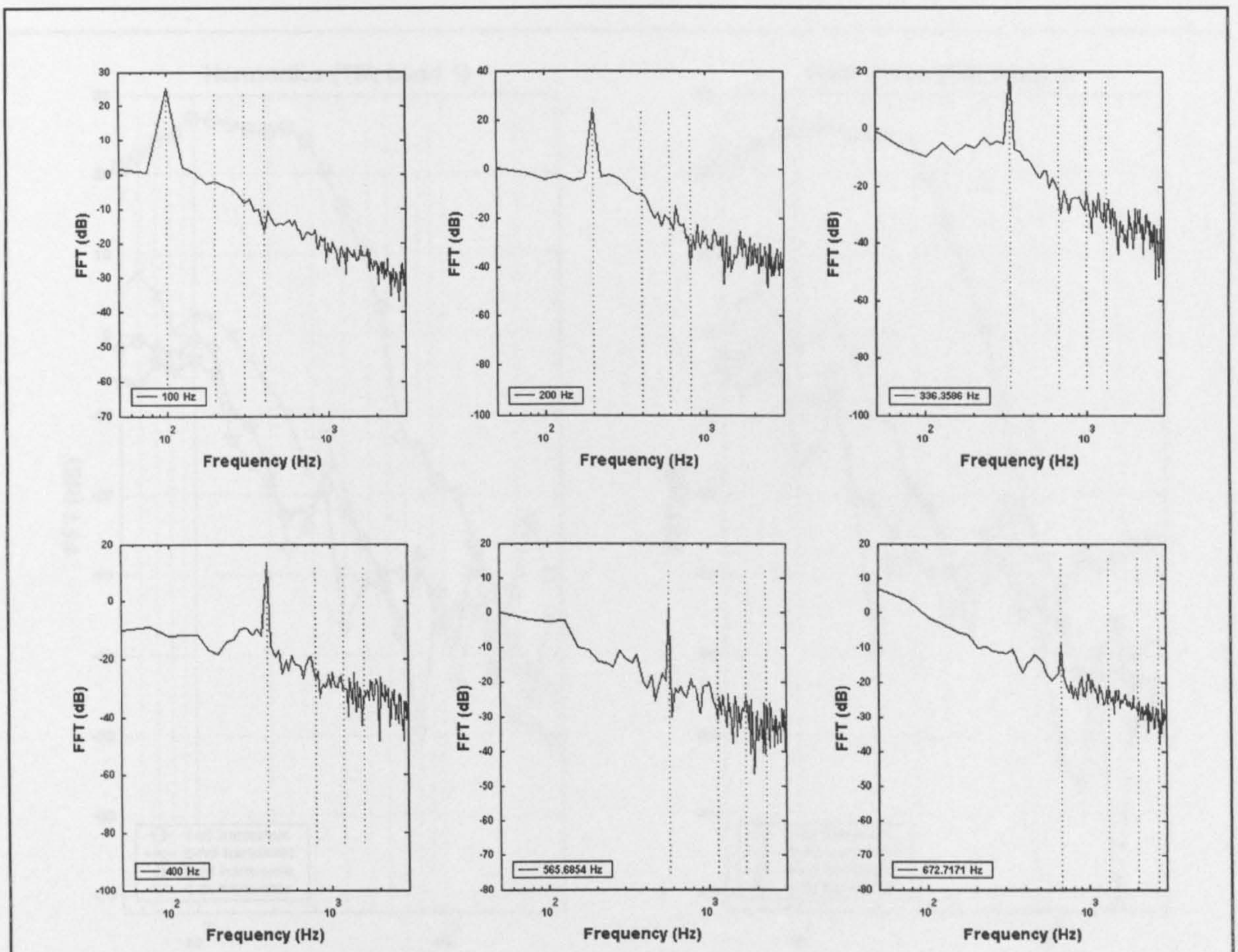

Figure 7-3 FFT results of responses raw waveforms of bead 1 on TM. Dotted lines show the positions of the first, second, third and forth harmonic position.

60 dB SPL. Only a selected series of frequencies (100, 200, 336, 400, 566 and 673 Hz) from a wide band of tested frequencies (50 to 2 kHz) are shown in the figure. Thick lines show the raw response waveforms and thin lines show the baseline position shifts. These shifts were uncovered using Butterworth low-pass filters to filter the original waveforms. There are no obvious systematic baseline position shifts observed in TM's responses.

The FFTs of these waveforms are shown in Figure 7-3. The first harmonics of the responses are more than 20-40 dB higher than the second, third and fourth harmonics (dotted lines). It is obvious that the first harmonic dominates the TM's response to tone bursts and therefore the responses can be considered as sinusoidal.

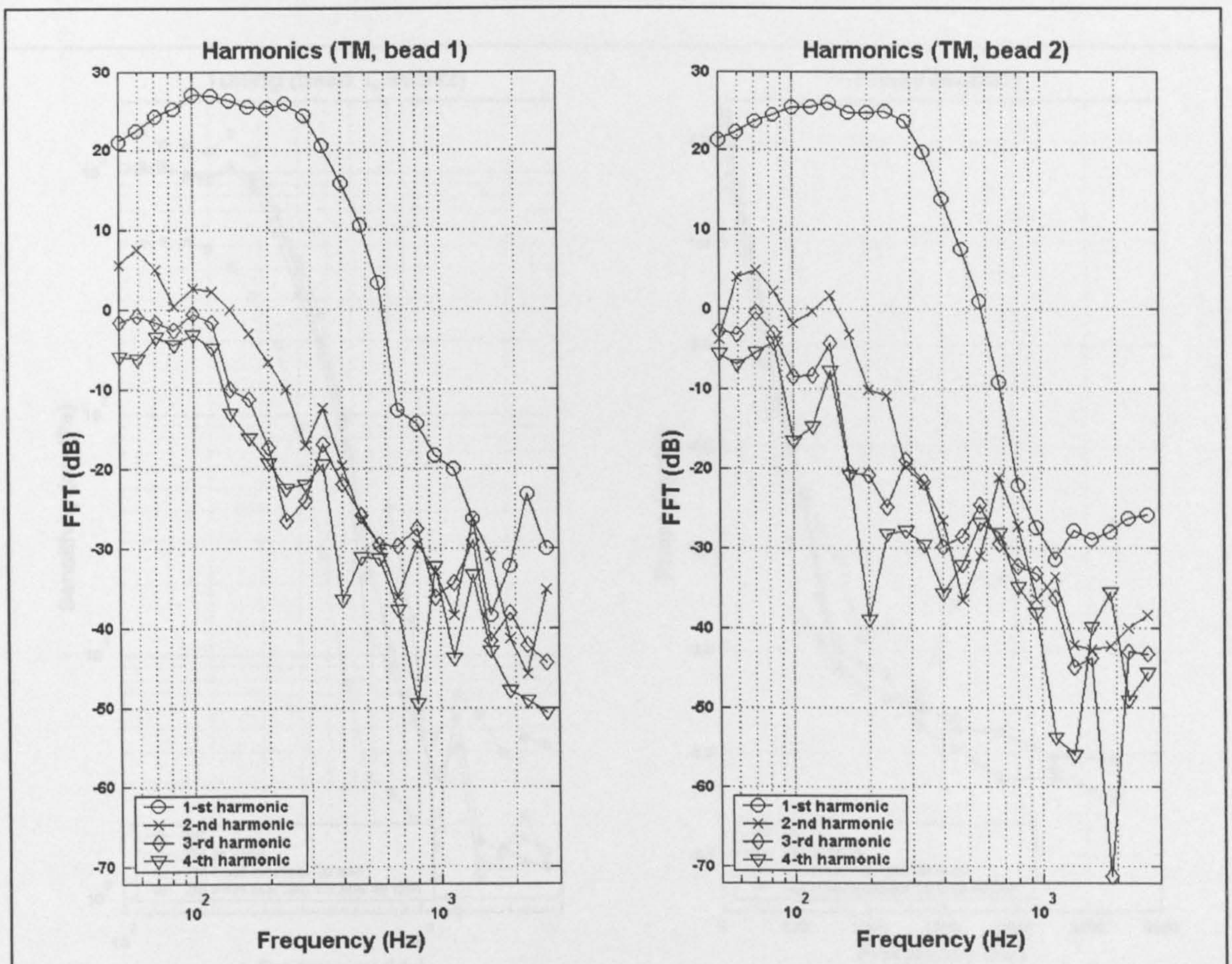

Figure 7-4 Harmonic analyses of responses to pure tone pips of bead 1 and 2 on TM.

TM responses to pure tone pips were studied frequency by frequency for bead 1 and bead 2. The harmonic products of first to fourth order were calculated and shown in Fig. 7-4. Even after tearing the RM, the first harmonic is more than 20 dB higher than all the other harmonics, no matter where the recording position was. It is obvious the first harmonic dominates the tuning characteristic up to 1000 Hz. The second, third and fourth harmonics decrease with increasing frequency across the whole range studied. Therefore, we can assume that the responses of TM to tone bursts are sinusoidal.

7.2.2 Tuning curves

Responses to pure tone pips of bead 1 and bead 2 were studied frequency by frequency at different times in this preparation and are shown in Figure 7-5 and 7-6. Recordings from a

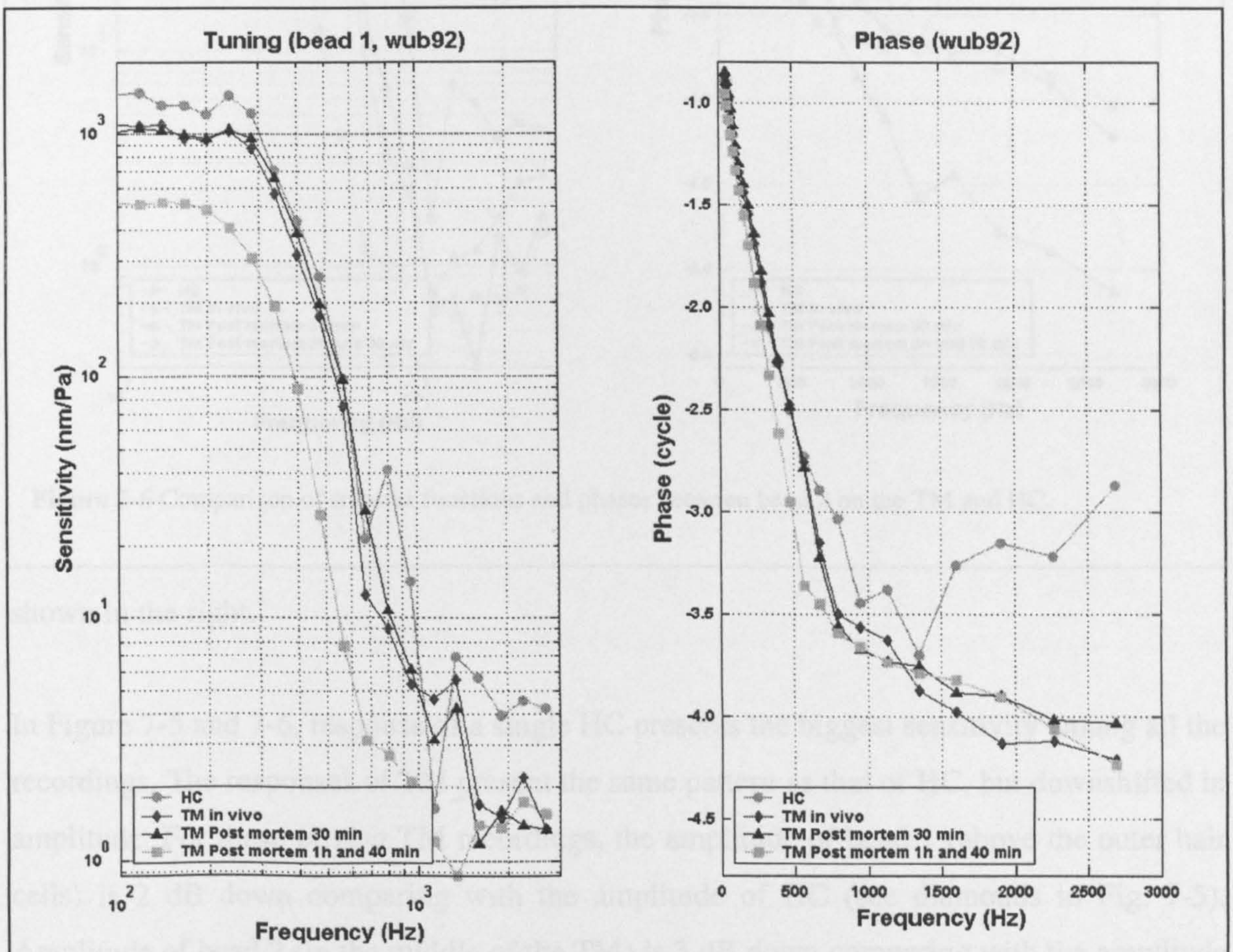

Figure 7-5 Comparison of transfer functions and phases between bead 1 on the TM and HC.

single HC near bead 1 are also plotted in both figures for comparison to the TM responses. Responses of the single HC were collected after tearing the RM *in vivo* and are shown as circles in the figures. The tuning curves are displayed in the left and relative phase data are

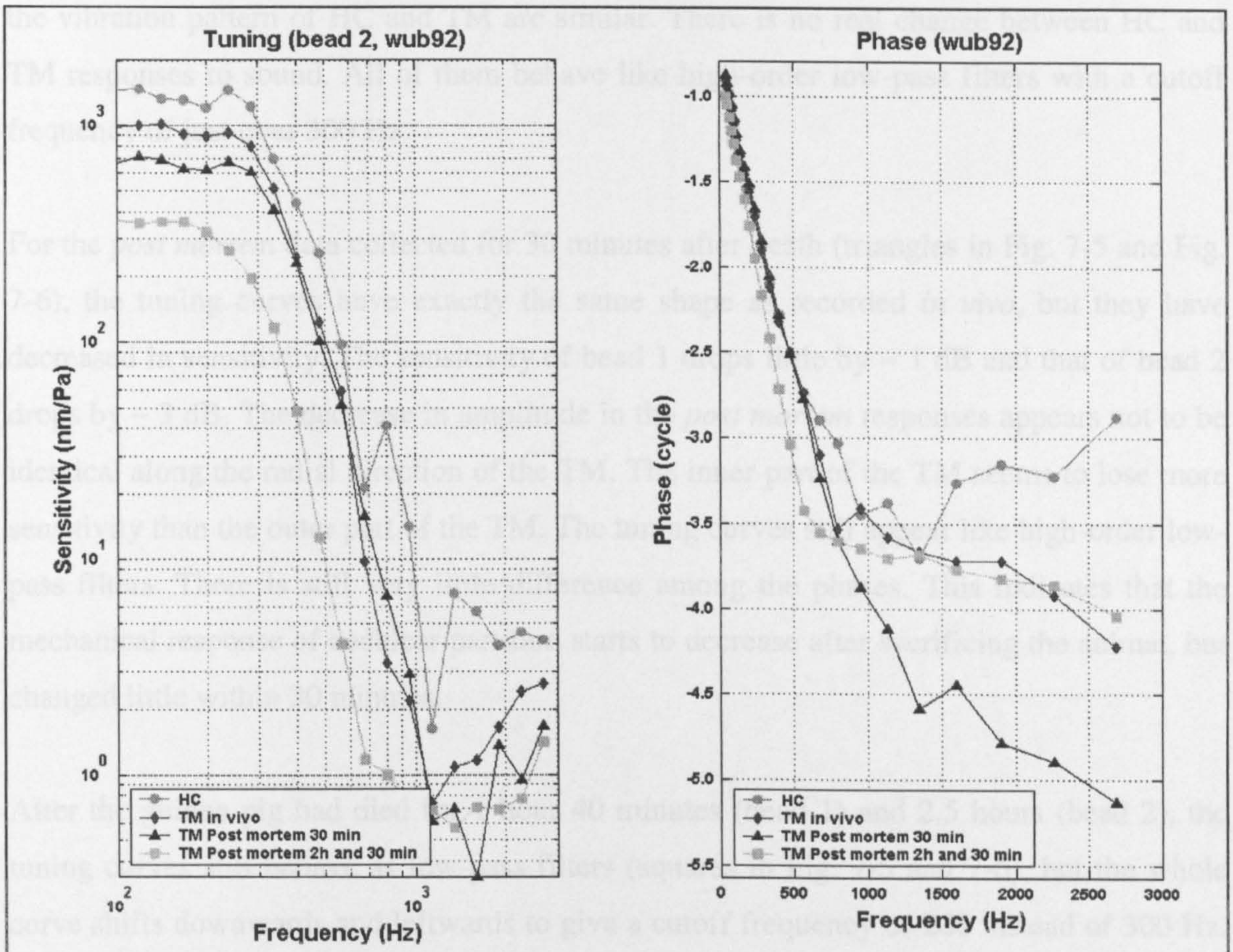

Figure 7-6 Comparison of transfer functions and phases between bead 2 on the TM and HC.

shown in the right.

In Figure 7-5 and 7-6, response of a single HC presents the biggest sensitivity among all the recordings. The responses of TM present the same pattern as that of HC, but downshifted in amplitude. For these *in vivo* TM recordings, the amplitude of bead 1 (above the outer hair cells) is 2 dB down comparing with the amplitude of HC (see diamonds in Fig. 7-5). Amplitude of bead 2 (in the middle of the TM) is 3 dB down comparing with the amplitude of the HC (see diamonds in Fig. 7-6). This indicates that amplitudes of sound-induced vibration change with the recording locations. In the organ of Corti, the outer edge of the

HC band has the highest response amplitude, while, the inner locations respond to stimuli with lower amplitude at the same sound pressure level. The response phases of bead 1 and 2 *in vivo* are nearly identical to that of HC (right of Fig. 7-5 and 7-6). The response phase lag increases monotonically with an almost constant slope up to 4 cycles. This suggests that the vibration pattern of HC and TM are similar. There is no real change between HC and TM responses to sound. All of them behave like high-order low-pass filters with a cutoff frequency of just over 300 Hz.

For the *post mortem* data collected for 30 minutes after death (triangles in Fig. 7-5 and Fig. 7-6), the tuning curves have exactly the same shape as recorded *in vivo*, but they have decreased in sensitivity. The sensitivity of bead 1 drops little by ~ 1 dB and that of bead 2 drops by ~ 3 dB. The decrease in amplitude in the *post mortem* responses appears not to be identical along the radial direction of the TM. The inner part of the TM seems to lose more sensitivity than the outer part of the TM. The tuning curves still appear like high-order low-pass filters. There is still very little difference among the phases. This indicates that the mechanical response of cochlear partition starts to decrease after sacrificing the animal, but changed little within 30 minutes.

After the guinea pig had died for 1 hour 40 minutes (bead 1) and 2.5 hours (bead 2), the tuning curves still behave as low-pass filters (squares in Fig. 7-5 and 7-6), but the whole curve shifts downwards and leftwards to give a cutoff frequency of 200 instead of 300 Hz. Comparing with the HC's tuning curve *in vivo* (circles) and earlier *post mortem* (triangles), there is an extra decrease at least of 6 dB in amplitude. The sensitivity of bead 1 is still higher than that of bead 2. The phases at the three locations no longer match up very closely; there is additional lag of –150 degrees at bead 1 and –248 degrees at bead 2 across a wide frequency range. Nonetheless, the recordings appear quite stable regardless of the drop in amplitude and slight change in phase.

7.2.3 Input-output function

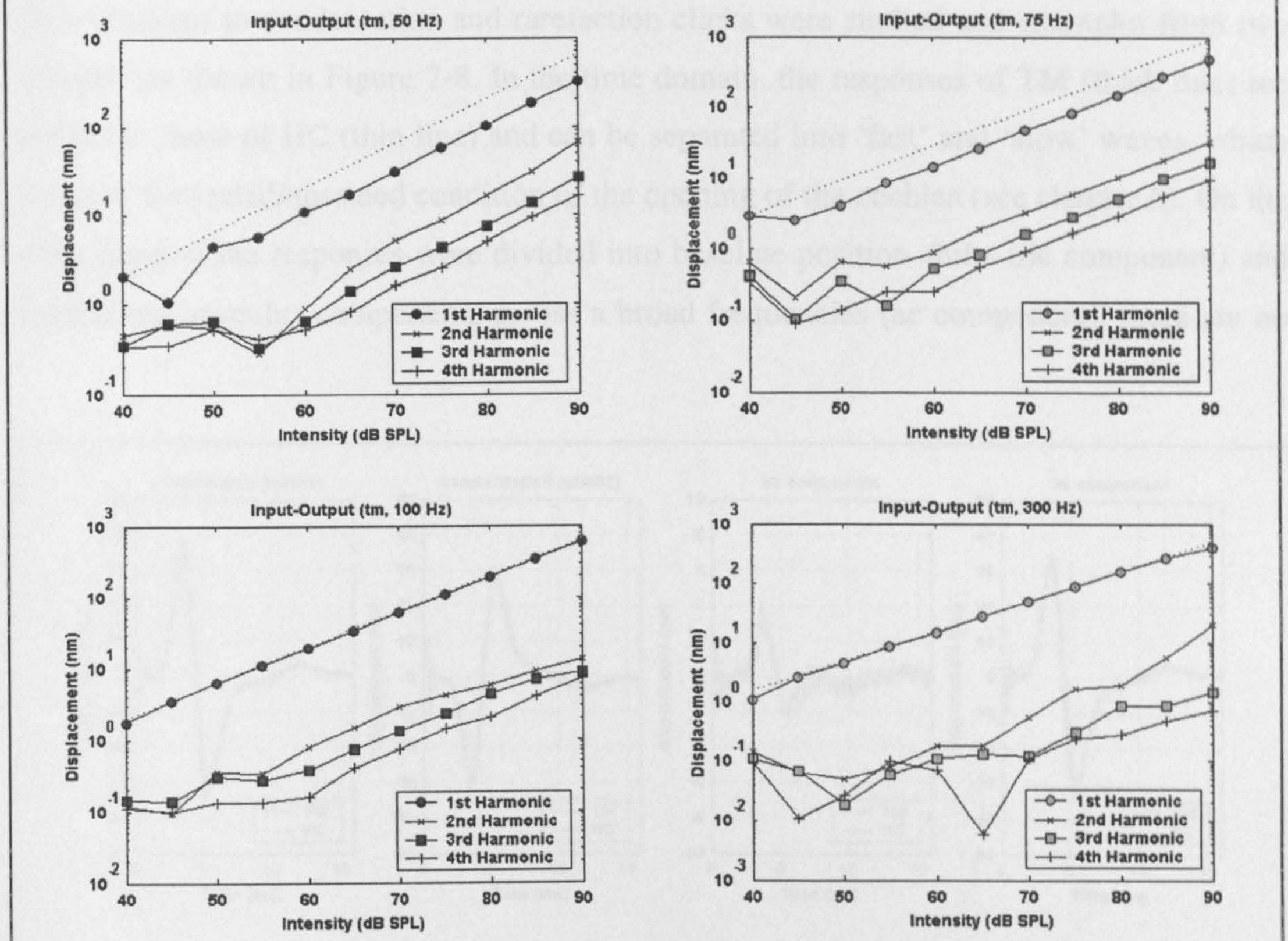

Figure 7-7 Input – output function of TM *in vivo*. Dotted line shows a linear relationship of response and stimulus intensity with a slope of 1 dB/dB.

The input-output functions of TM responses of bead 1 to tone bursts were studied at 50, 75, 100 and 300 Hz in this preparation *in vivo*. Amplitude of response is plotted as a function of stimulus intensity. The harmonics were also analyzed and are shown in the Figure 7-7. The dotted line shows a linear relationship between amplitude and intensity with a 1 dB/dB growth rate. It is obvious that the amplitude of the first harmonic component grows linearly with the stimuli intensity and dominates the responses at all the tested frequencies. The distortion products are much smaller than the first harmonic and increase with the stimulus intensity as well. Therefore, after tearing the RM, we can say that the TM vibrates in an almost linear way to pure tone pip stimuli (see chapter 6).

7.3 Click – evoked responses

TM responses to condensation and rarefaction clicks were studied and examples from two animals are shown in Figure 7-8. In the time domain, the responses of TM (thick line) are similar to those of HC (thin line) and can be separated into 'fast' and 'slow' waves, which relate to the sealed/unsealed condition of the opening of the cochlea (see chapter 5). On the other hand, if the responses were divided into baseline position shifts (dc component) and oscillations stimulus components across a broad frequencies (ac component), there are no

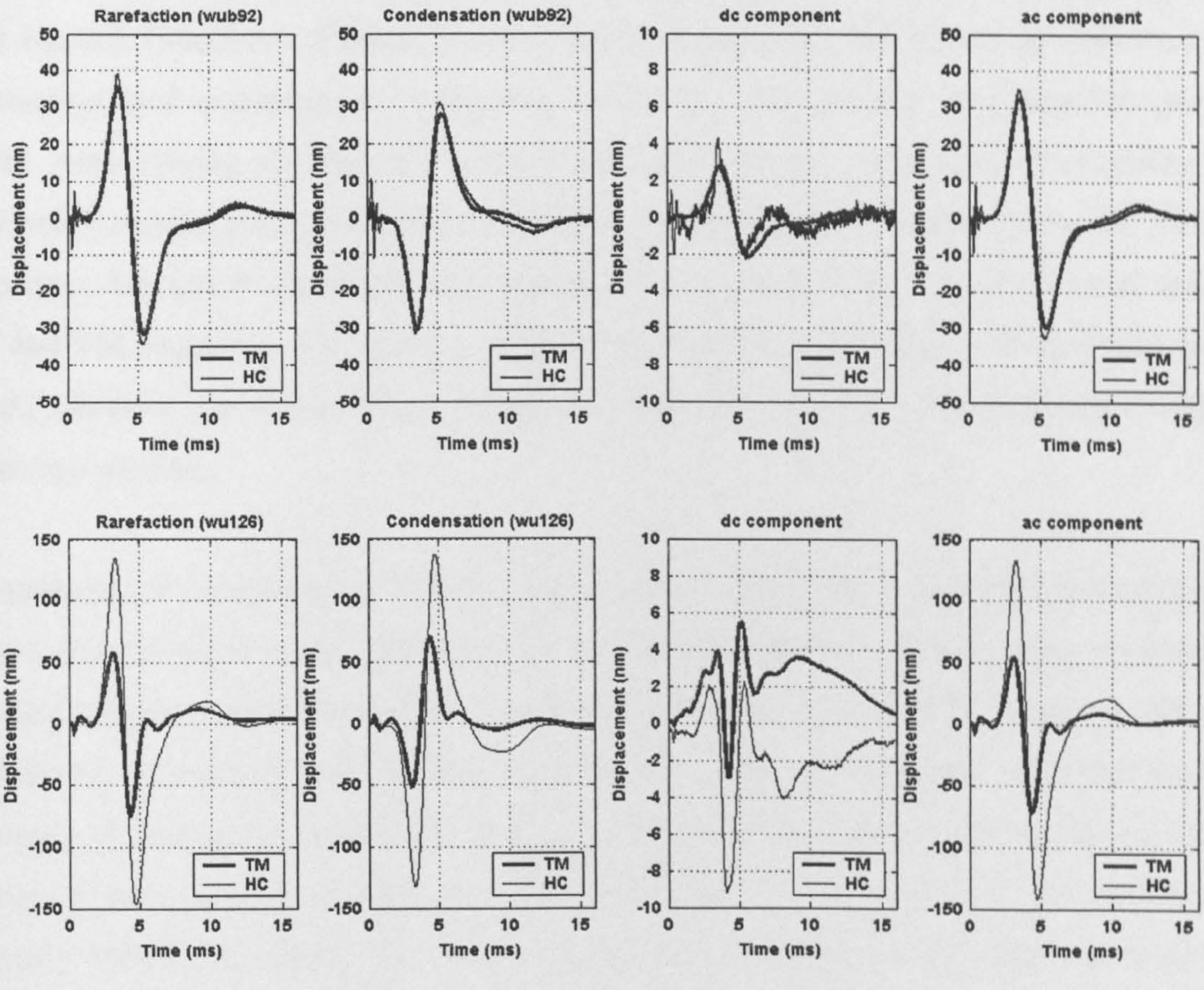

Figure 7-8 Comparison of condensation and rarefaction clicks responses of HC (RM was torn) and TM. Column one: rarefaction click responses, column two: condensation click responses, column three: baseline position shift (dc component) and column four: oscillation to broad frequencies stimuli (ac component). Thick line: response of single bead firmly attached the TM; thin line: response of a single HC after tearing the RM.

positive baseline position shifts either in the responses of the HC (RM torn) or in the responses of the TM. Therefore, the oscillatory components dominate the responses under this condition. The responses of HC and TM are nearly identical in animal wub92, but have a huge difference in amplitude in animal wu126. This might be because that the responses in animal wub92 were collected at around the same time, whereas, the TM responses in animal wu126 were recorded 3 hours after the recording of HC's responses. Therefore, the decrease of amplitude may be due to the time course, perhaps due to the mixing of perilymph and endolymph, which led to changes in the ionic environment of the organ of Corti.

Figure 7-9 shows the spectra of the four waveforms in Fig. 7-8, as revealed by performing a Fast Fourier Transform. Plusses, crosses, triangles and circles represent the spectra of the rarefaction and condensation responses, oscillatory components and baseline position shifts. After tearing the RM, the transfer functions for the rarefaction, condensation and oscillatory components are identical across the whole frequency range both for HC and TM responses. The baseline position shift spectra (circles) lie more than 20 dB down in both the HC and TM responses. The spectra of the rarefaction and condensation click responses are nearly identical across the whole frequency range and present a low-pass filter shape in these two animals.

In summary, the responses of the TM to the sound stimuli (pure tone pips and clicks) are very similar to those of HC after tearing the RM. No obvious variation was detected. No baseline position shifts were observed across the tested range of frequencies. The TM vibrates in a linear way. The amplitude of the response increases with the stimulus intensity. At any given sound pressure level, the amplitude varies with frequency and the tuning of the response behaves as a low-pass filter if the opening of the cochlea was properly sealed (see chapter 5). The first harmonic component of the responses dominates across the whole range of frequencies tested. The second, third and fourth harmonic components are also observed in TM's responses, but more than 20 dB below that of the first order component. The amplitude of the TM response is normally lower than that of a single HC and also varies with the relative radial position in the TM. The amplitude of response collected from the outer edge of the TM is higher than that from the inner part of the TM. The amplitude of the response also decreases *post mortem*. However, there is only

a little change within 30 minutes of the animal death. The TM responses to rarefaction and condensation clicks can be separate into 'fast' and 'slow' components in the time domain. The spectra of the condensation and rarefaction responses are nearly identical and act as low-pass filters in the frequency domain.

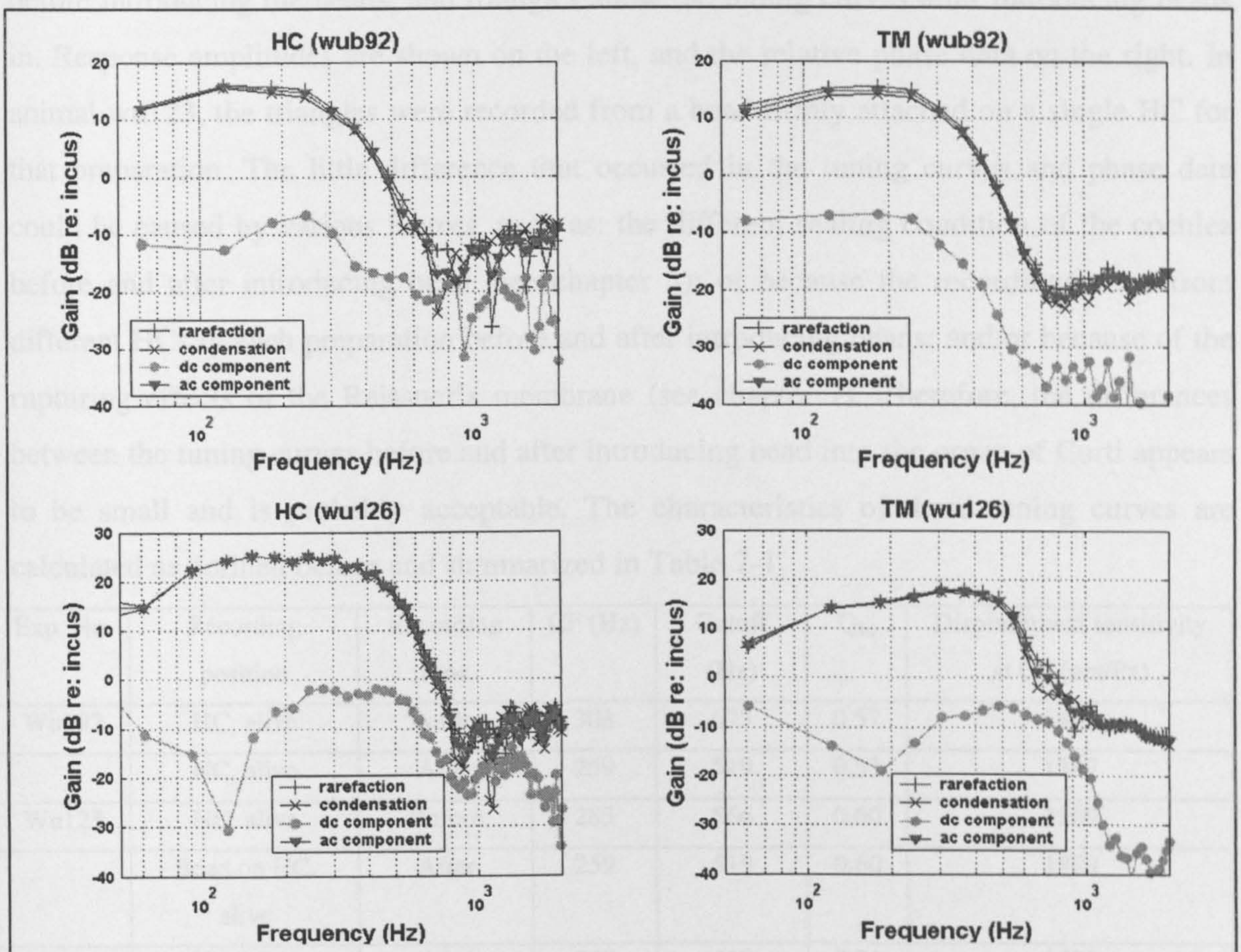

Figure 7-9 Spectra analysis of rarefaction and condensation clicks responses of HC and TM after tearing the RM. Pluses represents FFT of rarefaction click response, crosses indicates FFT of condensation click response, circles show baseline position shift (dc component) FFT result and triangles show FFT of ac component.

7.4 Mass load of bead on TM

The gold-coated polystyrene microbeads (15 or 25 μm diameter) used in the present experiments have a mean density range of 1.05 to 1.1 $g.cm^{-3}$. Is it possible that this could

increase the mass load of the tectorial membrane during the sound delivery procedure so that the beads change the function of the tectorial membrane? This question is simply answered by comparing tuning curves of single HC responses before and after introducing the beads into the organ of Corti. Fig. 7-10 shows four examples of the effects of adding a bead to the HC tuning curves *in vivo*. Circles in this figure show a single HC tuning curve before introducing the beads, and triangles show the tuning curves after introducing beads in. Response amplitudes are shown on the left, and the relative phase data on the right. In animal wu123, the triangles were recorded from a bead firmly attached on a single HC for that preparation. The little difference that occurred in the tuning curves and phase data could be caused by various factors, such as: the different sealing condition of the cochlea before and after introducing bead (see chapter 5); or because the recordings were from different HCs in each preparation before and after introducing beads; and/or because of the rupturing effects of the Reissner's membrane (see chapter 7). Therefore, the differences between the tuning curves before and after introducing bead into the organ of Corti appears to be small and is probably acceptable. The characteristics of these tuning curves are calculated as defined before and summarized in Table 7-1.

Exp. No.	Recording position	Recording time	CF (Hz)	Cutoff (Hz)	Q_{10}	Displacement sensitivity at CF (nm/Pa)
Wub92	HC, alive	Before	308	673	0.57	1486
	HC, alive	After	259	519	0.57	1347
Wu123	HC, alive	Before	283	566	0.60	1209
	Bead on HC, alive	After	259	519	0.60	1889
	HC, alive	After	308	519	0.71	1522
Wu125	HC, alive	Before	519	951	0.62	333
	HC, alive	After	366	800	0.57	663
Wu126	HC, alive	Before	336	617	0.66	2857
	HC, alive	After	283	566	0.62	3239

Table 7-1 Characteristics of tuning curves in Figure 7-10 before and after introducing beads into the organ of Corti.

The results of this study are therefore consistent with previous studies of the effects of beads on cochlear mechanics (Khanna et al. 1998; Cooper 1999). The beads used in our study can follow the motion of the organ of Corti (see example of wu123 in Figure 7-10), and do not add more mass load on the organ of Corti.

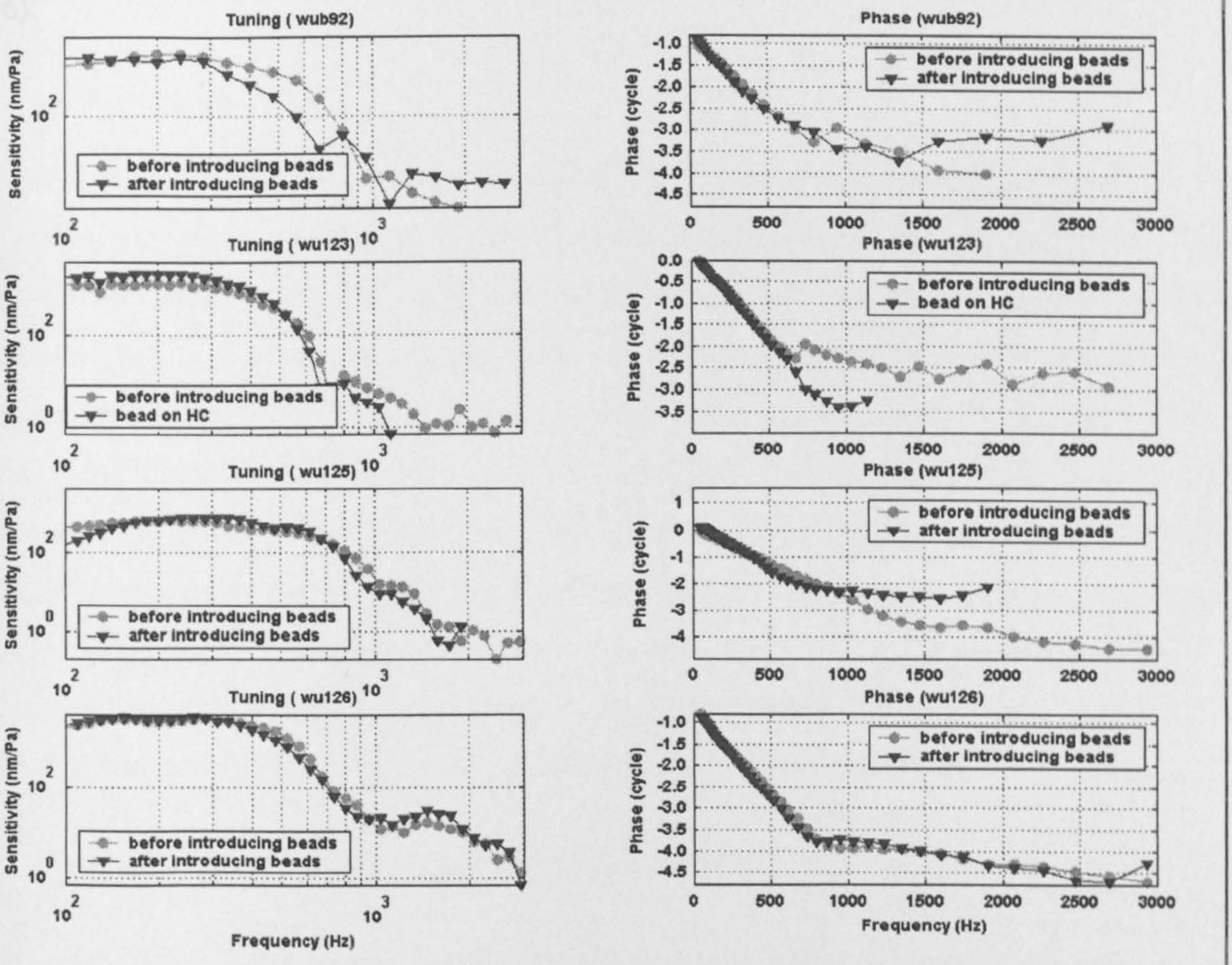

Figure 7-10 Single HC tuning curves before and after introducing bead onto the cochlear partition *in vivo*.

7.5 Discussion

The responses of TM are similar to those of the HCs, although the maximum vibration amplitude is always seen at the Hensen's. The amplitude of TM is 2-3 dB lower than that of HC. This is consistent with the previous study, where the vibration amplitude at the HCs was about 6 dB or more higher than that at the outer hair cells (Khanna et al. 1989; Ulfendahl et al. 1996). Only minor differences can be observed in the responses measured radially across the TM. The phase responses of the TM at the inner hair cells and at the outer hair cells are very similar (Khanna et al. 1989; Khanna et al. 1989; Ulfendahl et al. 1996). The main difference between the tuning curves is the vibration amplitude which increases when moving from the inner hair cell region to the outer edge of the Hensen's

cells (Khanna et al. 1989; Khanna et al. 1989; Cooper and Rhode 1996; Ulfendahl et al. 1996).

Chapter 8 Tectorial membrane vibration in 3-dimensional space

8.1 Introduction

This chapter investigates the vibration modes of the TM *in vivo* in three-dimensional space. A three-dimensional (3-D) reconstruction technique was developed using our interferometer system combined with a two-axis goniometer system (see chapter 3). This system allows us to detect vibrations in three orthogonal directions by using different viewing angles. Recordings were made from cochlear partitions in the apical turn of the guinea pigs cochlea both *in vivo* and *post mortem*. Single gold-coated polystyrene microbeads (25 μm diameter; Polysciences Inc.) with a similar density to that of water were introduced into the scala media via small tear in Reissner's membrane (RM). These beads were firmly attached on the TM and enhance the reflectivity of TM (see Chapter 6 and 7). The initial opening of the cochlea was resealed/covered using a glass coverslip and high-vacuum grease to minimize the opening effects of the cochlea (see Chapter 5).

8.2 Repeatability of recordings from bead on the TM

In the experiments the zero position for the goniometer ($\theta = \theta_o$, $\phi = \phi_o$) corresponds to an observation direction, which allows an approximately equal and symmetric variation in observation angle both in θ and ϕ. In practice, the observed bead is focused in the middle of the field of view, so that both goniometers can be varied by a minimum of ± 20° in each direction without losing sight of the bead.

The total recording time for each observed point, including recording and adjustments of the observation angle was 30 – 40 minutes. Each set of data was collected as fast as possible. This was necessary in order to minimize possible changes with time in the frequency response of the observed point. Responses to pure tone pips were normally saved with frequency from 50 to 2000 Hz in steps of ¼ oct. and from at least 5 different viewing angles. Repeated measurements were thus necessary to monitor any changes in the responses with time. The repeated measurements at the zero position were made at the beginning, middle, and the end of each set of measurements, typically at ~ 15-20 minute intervals.

Fig. 8-1 displays such repeatability recordings of bead 1 and 2 in the *in vivo* TM preparation described earlier in chapter 7 (wub92). In each figure, the 3 sets of responses were collected at ~20 minute intervals at 60 dB SPL. Response amplitudes and phases were plotted as a function of frequency from 50 to 2000 Hz in 1/4 oct. step. The circles represent recordings of the beads at the beginning of the measurements and serve as the criteria to compare the later recordings with. The diamonds were collected 20 minutes later from the same beads by returning the goniometers to the zero position. The triangles were recorded from the same bead at the end of the measurements, another 20 minutes later. There is little

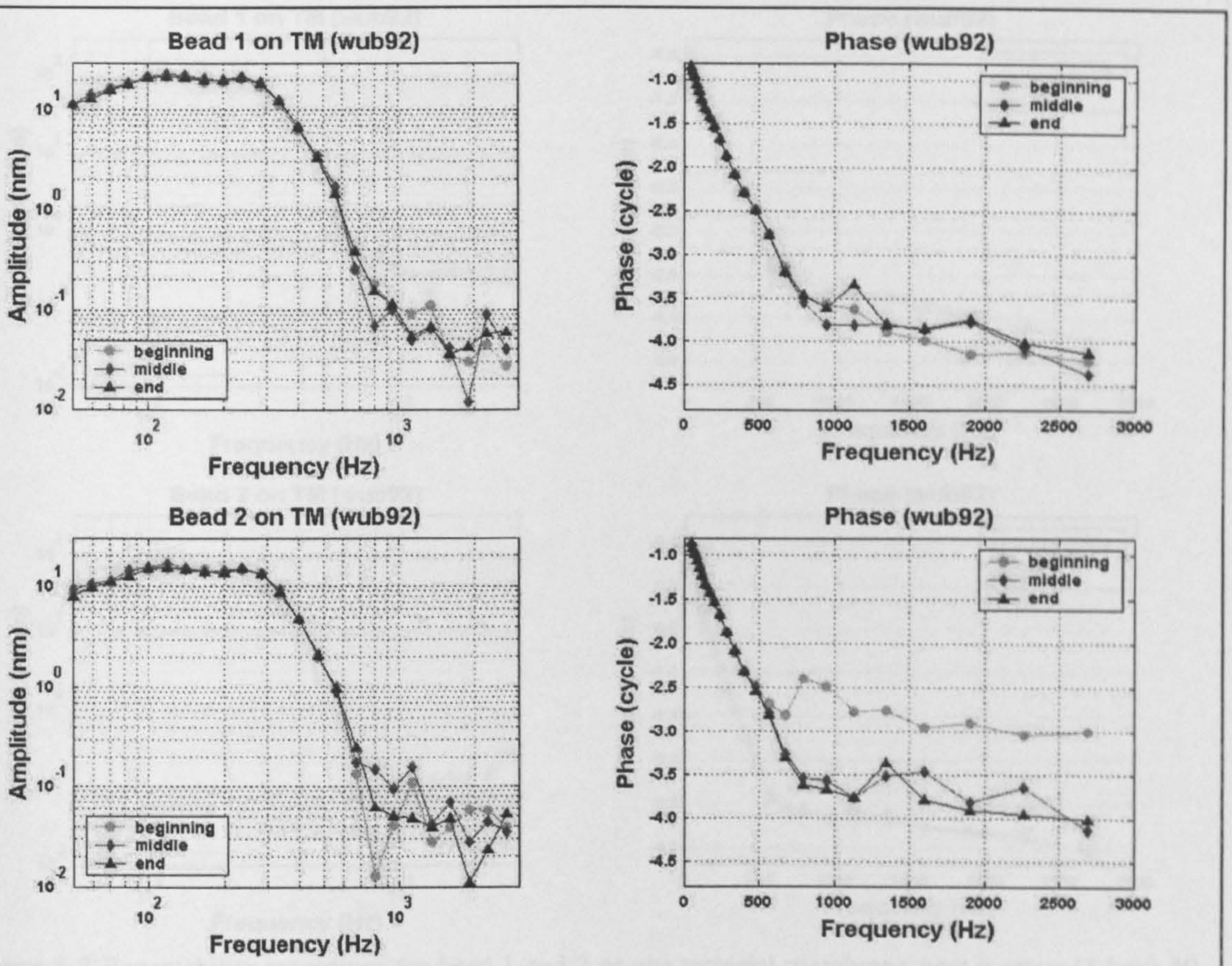

Figure 8-1 Repeatability recordings of bead 1 and 2 on tectorial membrane *in vivo*. Responses were collected every ~20 minutes at 60 dB SPL. Response amplitudes and phases were plotted as a function of frequency from 50 to 2000 Hz in 1/4 oct. step. Circles represent recordings of the beads at the beginning of the measurements. Diamonds were collected 20 minutes later from the same bead by returning the goniometers to the zero position. Triangles were recorded from the same bead in the end of the measurements, another 20 minutes later. The left column shows the tuning curves. The right column shows phase data.

variation in either amplitude or phase. The amplitude variation was within 1 dB below 500 Hz, but larger above this frequency. This is because the actual amplitudes of the responses are very low in the high-frequency tails of the tuning curves. The phases of the responses varied very little below 500 Hz in this preparation. Therefore, the responses from beads on tectorial membrane appear quite stable, or at least changed little during the measurements.

In the *post mortem* recordings, the repeatability of the measurements at the same two beads appeared lower than that observed *in vivo*. Changes with time occurred both in amplitude

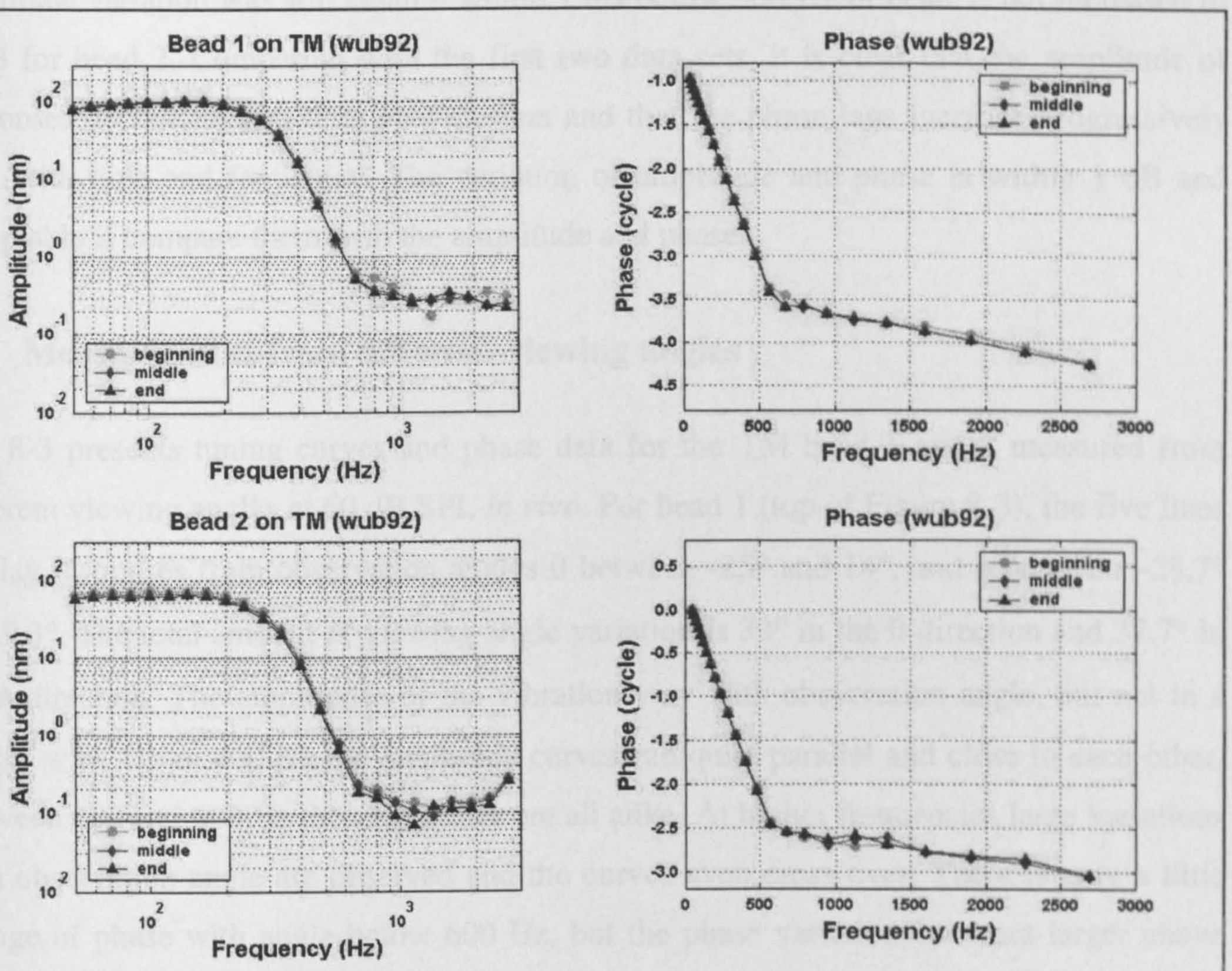

Figure 8-2 Repeatability recordings for bead 1 and 2 on the tectorial membrane *post mortem* (1 hour 40 minutes and 2 hour 20 minutes). Responses were collected every ~15 minutes at 80 dB SPL. Response amplitudes and phases were plotted as a function of frequency from 50 to 2000 Hz in 1/4 oct. steps. Circles represent recordings of the beads at the beginning of the measurements. Diamonds were collected 15 minutes later from the same bead by returning the goniometers to the zero position. Triangles were recorded from the same bead, at zero position, in the end of the measurements, another 15 minutes later. The left column shows the tuning curves of these responses. The right column shows phase data.

and in phase. Figure 8-2 shows the repeatability recordings of the two beads *post mortem*. Recordings of bead 1 were collected around 1 hour and 40 minutes *post mortem* (top of Figure 8-2). Recordings of bead 2 were collected around 2 hours and 20 minutes *post mortem* (bottom of Figure 8-2). Responses were collected every ~15 minutes at 80 dB SPL, covering frequencies from 50 to 2000 Hz in 1/4 oct. step. Circles represent recordings of the beads at the beginning of the measurements and serve as the criteria to compare later the recordings with. Diamonds were collected 10/15 minutes later from the same bead by returning the goniometers to the zero position. Triangles were recorded from the same bead, at zero position, at the end of the measurements, another 10/15 minutes later. The amplitude variation was still small – within 1 dB below 500 Hz of bead 1, but increased to 2 dB for bead 2. Comparing with the first two data sets, it is clear that the amplitude of responses decreases with time *post mortem* and that the phase lags increase progressively both with time and frequency. The variation of amplitude and phase is within 1 dB and acceptable if compare them with the amplitude and phase.

8.3 Measurements from different viewing angles

Fig. 8-3 presents tuning curves and phase data for the TM bead 1 and 2 measured from different viewing angles at 60 dB SPL *in vivo*. For bead 1 (top of Figure 8-3), the five lines display responses from observation angles θ between -25° and 14°, and ϕ between –28.7° and 9.3°. The total amount of viewing angle variation is 39° in the θ direction and 37.7° in the ϕ direction. The amplitudes of the vibration vary with observation angle, but not in a simple way. Up to 400 Hz the amplitude curves run quite parallel and close to each other. Between 400 and 600 Hz the amplitudes are all alike. At higher frequencies large variations with observation angle are observed and the curves even cross over. There is only a little change of phase with angle below 600 Hz, but the phase variation becomes larger above that frequency.

The bottom of Fig. 8-3 presents tuning curves and phases for bead 2 on the TM of the same preparation measured from 5 different viewing angles at 60 dB SPL *in vivo*. These five lines display responses from observation angles θ between -30° and 10°, and ϕ between –30° and 6°. The total amount of viewing angle variation is 40° in the θ direction and 36° in the ϕ direction. The amplitude seems to separate to two groups and varies with observation

angle. Up to 400 Hz the amplitude curves run quite parallel and close to each other. Between 400 and 600 Hz the amplitudes are very similar. At higher frequencies large variations with observation angle are observed and the curves even cross over. Again, there is only a little change of phase with angle below 600 Hz, but the phase variation becomes

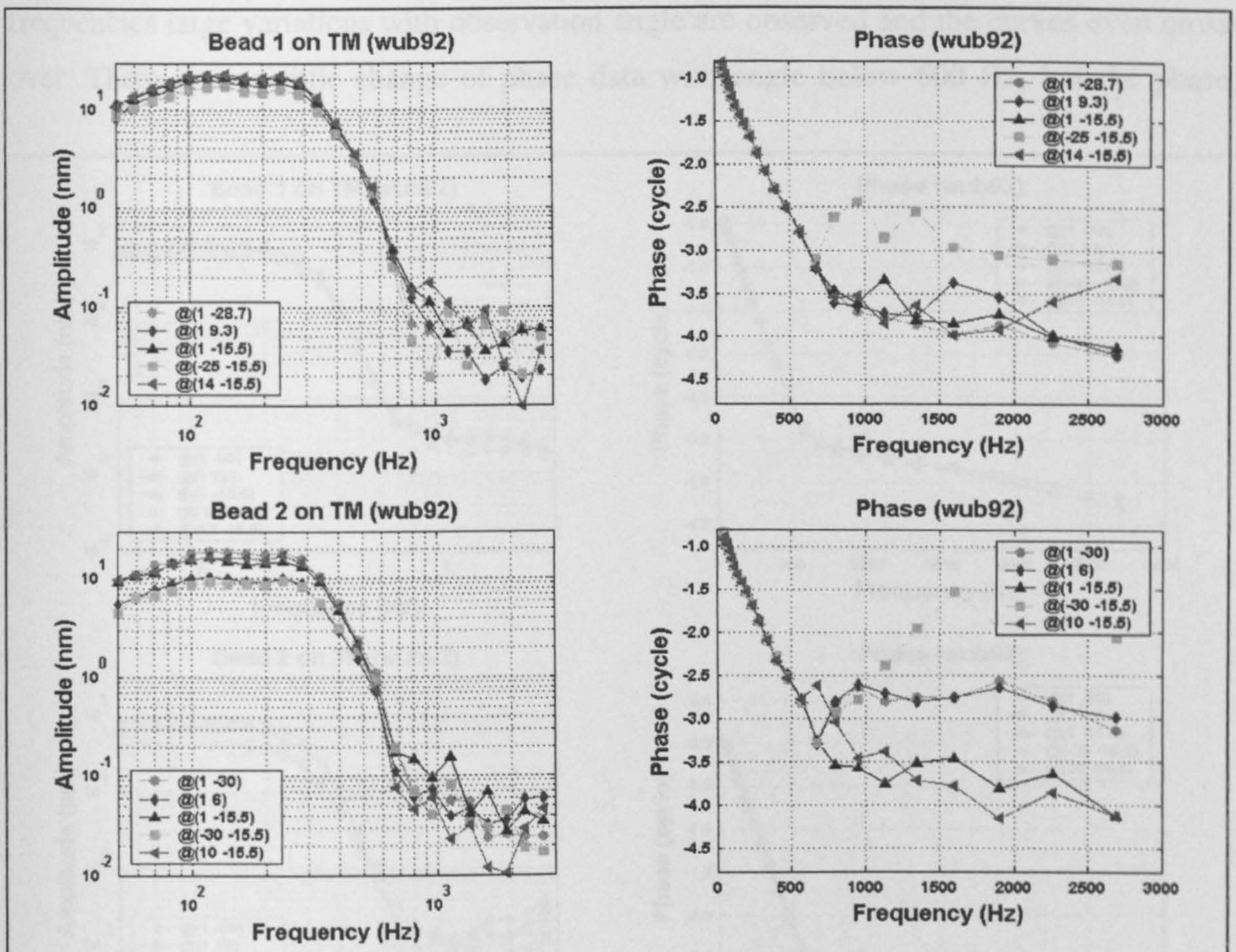

Figure 8-3 Tuning curves and phase of bead 1 and 2 on the TM measured from 5 different viewing angles at 60 dB SPL *in vivo*. The five lines display responses from observation angles labeled in the figure. The total amount of viewing angle variation is 39° in the θ direction and 37.7° in the ϕ direction for bead 1, and 40° in the θ direction and 36° in the ϕ direction for bead 2. Legends show the viewing angles of each measurement at θ and ϕ directions.

larger above that frequency.

Fig. 8-4 presents tuning curves and phases for bead 1 and 2 on the TM measured from 5 different viewing angles at 80 dB SPL *post mortem* (died 1 hour 40 minutes ago for bead 1 and died 2 hour 20 minutes ago for bead 2). For these two beads, the five lines display

responses from observation angles θ between -30° and 10°, and ϕ between –30° and 10°. The total amount of viewing angle variation is 40° in the θ direction and 40° in the ϕ direction. For both bead 1 and bead 2, the amplitudes of vibration vary with observation angle, but not in a simple way. Up to 350 Hz the amplitude curves run quite parallel and close to each other. Between 400 and 700 Hz the amplitudes are all alike. At higher frequencies large variations with observation angle are observed and the curves even cross over. There is only little change of phase data with angle below 600 Hz, but the phase

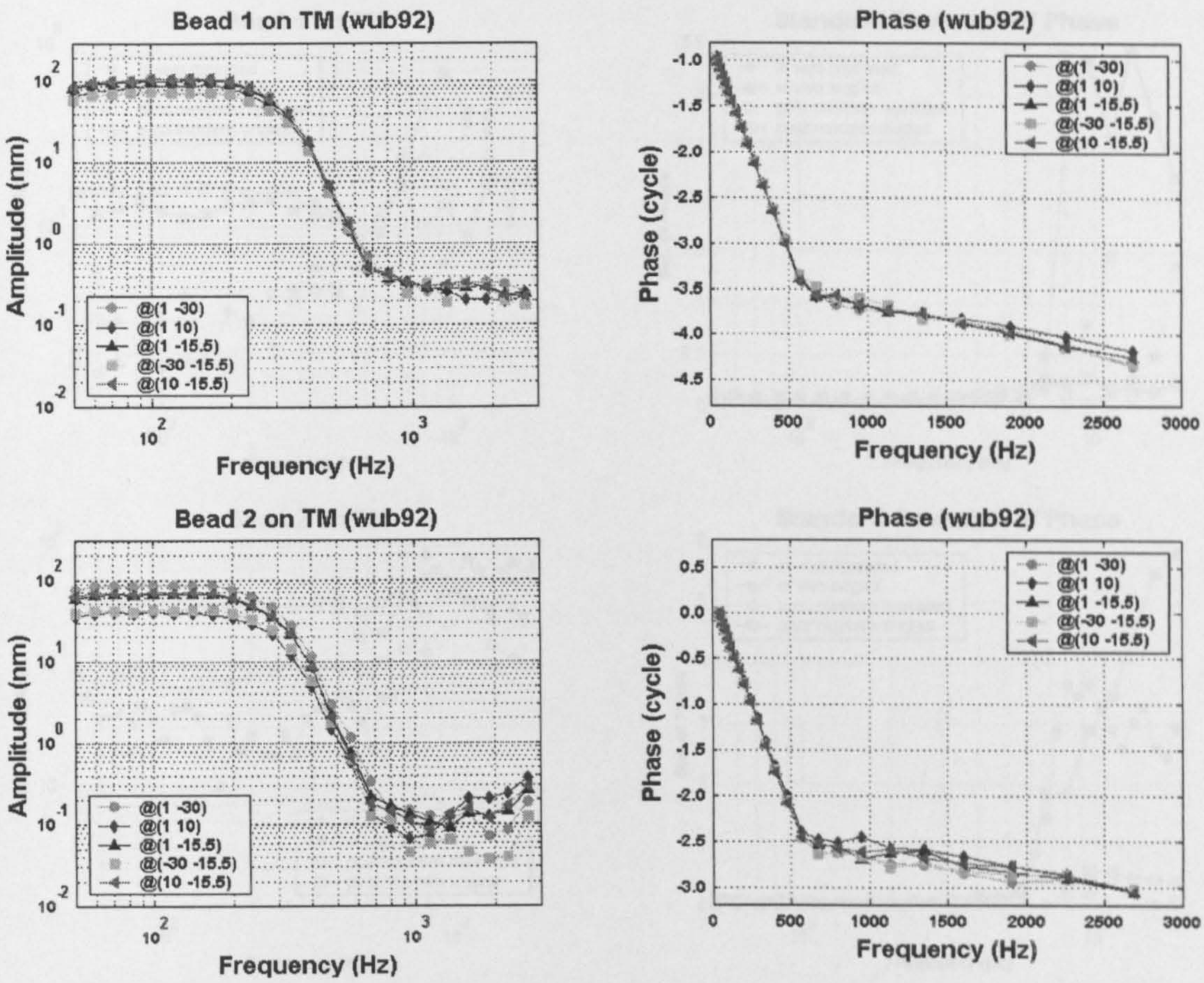

Figure 8-4 Tuning curves and phase of bead 1 and 2 on the TM measured from 5 different viewing angles at 80 dB SPL *post mortem*. The five lines display responses from observation angles θ between -30° and 10°, and ϕ between –30° and 10°. The total amount of viewing angle variation is 40° in the θ direction and 40° in the ϕ direction. Legends show the viewing angles of each measurement at θ and ϕ directions.

variation becomes larger above that frequency.

Recordings from other preparations provide similar results. The tuning curves recorded from different viewing angles were nearly always similar to each other. They are all shaped like low-pass filters up to a certain frequency (350 Hz for this example) *in vivo* and *post mortem*. There was a clear difference among the amplitudes for different viewing angles, but the phase changed very little with the recording angle at low frequencies. In order to show whether the variations of amplitude and phase with viewing angle are significant or not, relative standard deviations (std.) of the amplitudes and standard deviations (std.)

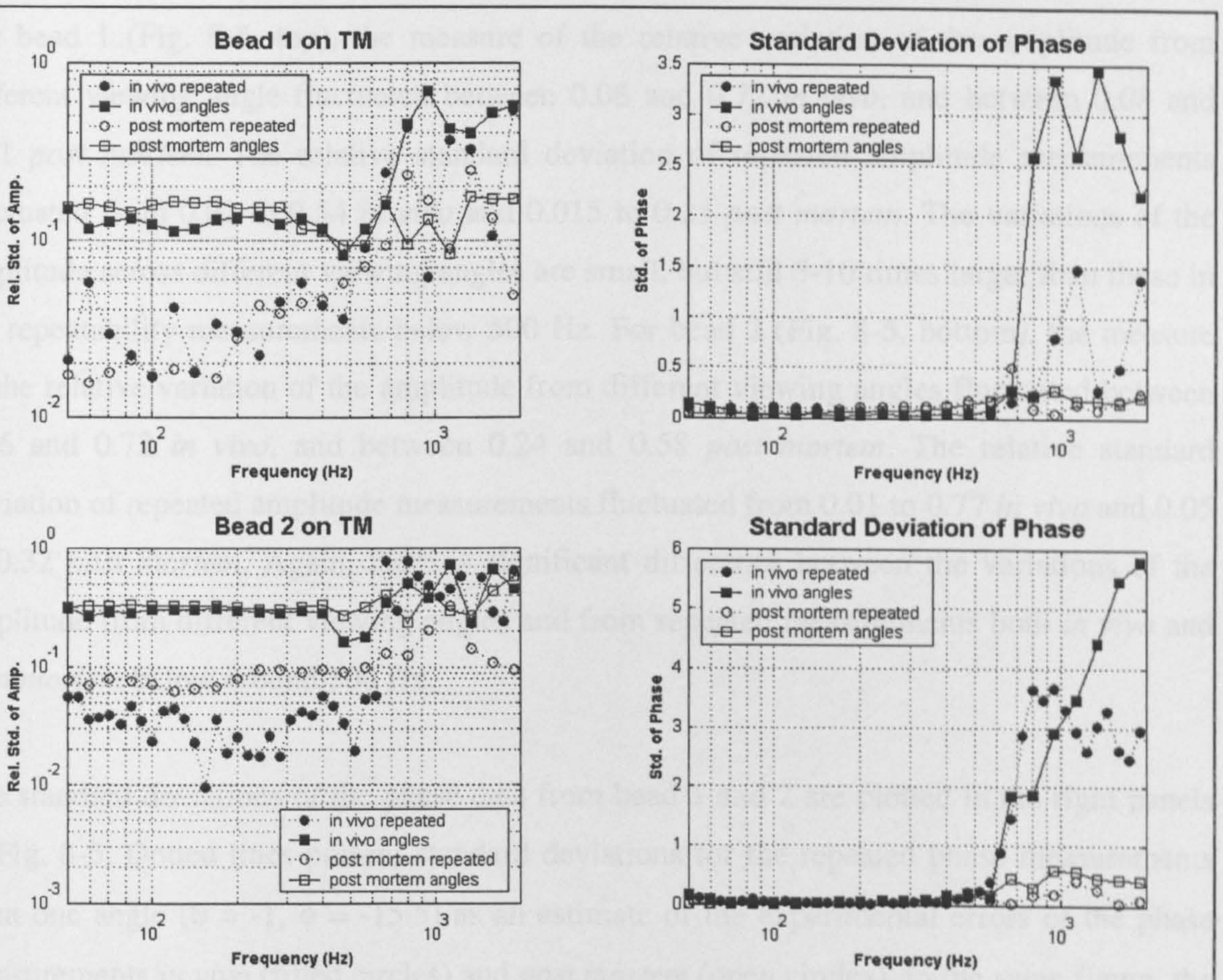

Figure 8-5 Standard deviation of amplitude (left) and phase (right). Standard deviations (std.) of amplitude ('relative' standard deviation equals standard deviation divided by the mean value) and phase of the observed point (beads 1 and 2 on the TM, in wub92) are calculated frequency by frequency. Dotted lines represent measurement repeatablility as an estimate of the experimental error *in vivo* and *post mortem*. Squares are the standard deviation of the amplitude and phase of responses measured from different viewing angles *in vivo* and *post mortem*.

phases for each observed point (bead 1 and 2 on TM) were calculated frequency by frequency and are shown in Fig. 8-5.

The dotted lines in Fig. 8-5 represent the standard deviations of repeated amplitude measurements relative to the mean amplitudes. This provides an estimate of the relative experimental error of the amplitude measurements *in vivo* (filled circles) and *post mortem* (open circles) in the left of Fig. 8-5. The relative standard deviations of the response amplitudes measured from different viewing angles are shown as solid lines *in vivo* (filled squares) and *post mortem* (open squares).

For bead 1 (Fig. 8-5, top), the measure of the relative variation of the amplitude from different viewing angle fluctuated between 0.08 and 0.72 *in vivo*, and between 0.08 and 0.21 *post mortem*. The relative standard deviation of repeated amplitude measurements fluctuated from 0.02 to 0.54 *in vivo* and 0.015 to 0.25 *post mortem*. The variations of the amplitude across different viewing angles are small, but still 5-10 times larger than those in the repeatability measurements below 500 Hz. For bead 2 (Fig. 8-5, bottom), the measure of the relative variation of the amplitude from different viewing angles fluctuated between 0.16 and 0.72 *in vivo*, and between 0.24 and 0.58 *post mortem*. The relative standard deviation of repeated amplitude measurements fluctuated from 0.01 to 0.77 *in vivo* and 0.05 to 0.32 *post mortem*. Again, there is significant difference between the variations of the amplitude from different viewing angles and from repeated measurements both *in vivo* and *post mortem* below around 500 Hz.

The standard deviations of the phase data from bead 1 and 2 are plotted in the right panels of Fig. 8-5. Dotted lines present standard deviations for the repeated phase measurements from one angle ($\theta = -1$, $\phi = -15.5$) as an estimate of the experimental errors of the phase measurements *in vivo* (filled circles) and *post mortem* (open circles). In the same figure, the standard deviation of the response phases measured from different viewing angles are plotted as squares *in vivo* (filled squares) and *post mortem* (open squares). The standard deviation of the phase is stable and nearly constant for all the cases discussed here below about 600 Hz, indicating that the phase of the response changed little either in the repeated recordings, or in the responses measured from different viewing angles. Calculations for other preparations gave similar results, indicating that the accuracy of the measurement is sufficiently good enough to measure the changes associated with changing the viewing angles of the object.

8.4 Transfer Functions for three orthogonal components

A right-handed coordinate system is used to describe the three-dimensional vibration of a point on the TM. The coordinate system is shown in Fig. 8-6 together with a sketch of the organ of Corti. The z-axis corresponds to the usual observation direction. The x-y plane corresponds approximately to the plane of the BM, while the x-z and y-z planes correspond to radial and longitudinal cross sections of the partition, respectively. If the preparation were perfectly aligned along the interferometer axis, the z component would represent up-and-down transverse motion, while radial and longitudal directions could be defined in x-y plane. However, it was not possible to align the preparations perfectly along the interferometer axis in the time available to do these experiments, and it is obviously impossible to know the precise direction of the motion of the bead on the TM before measuring it. Therefore, every case has to be explained individually with the help of the

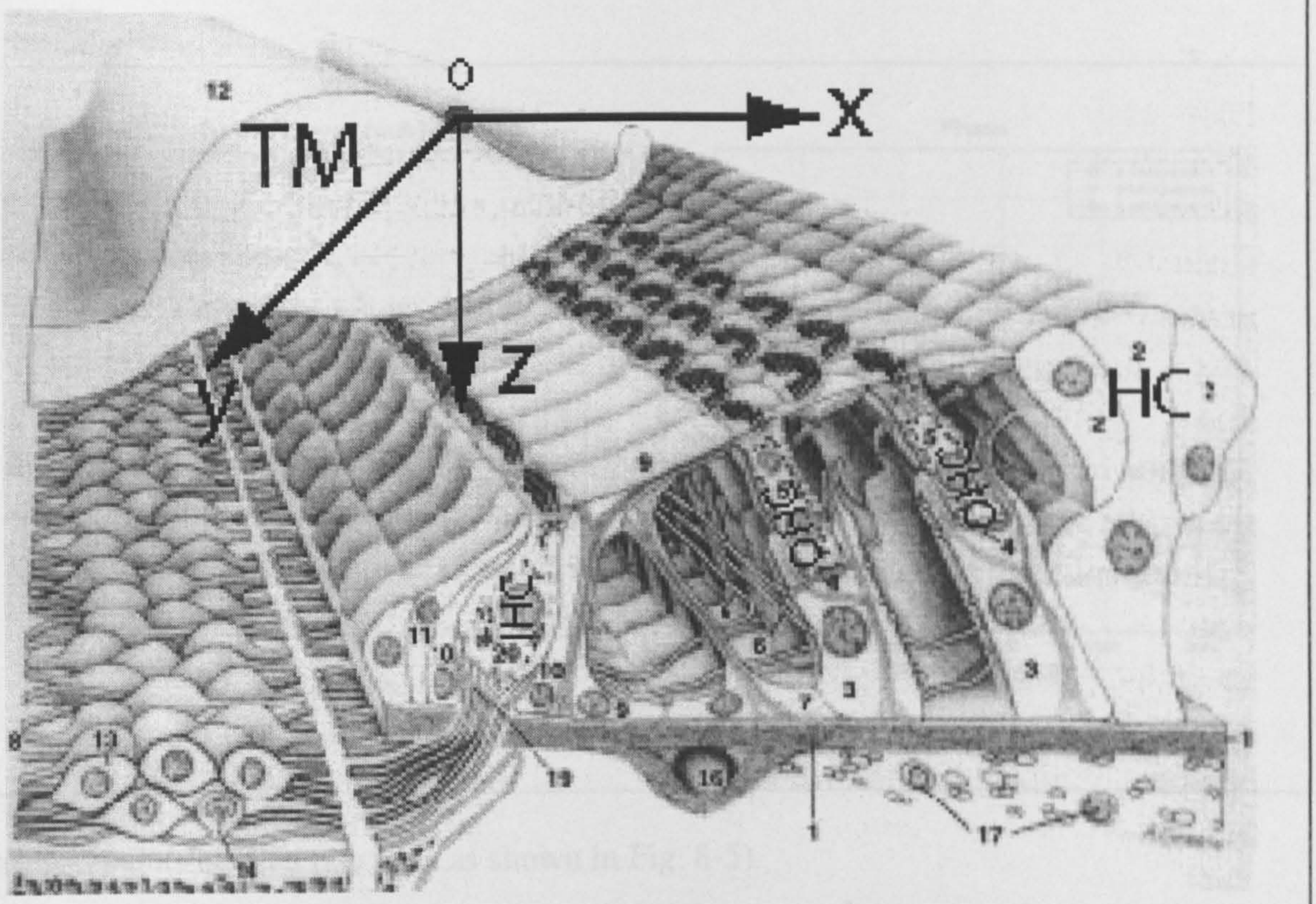

Figure 8-6 Right-handed coordinate system and the relationship with the organ of Corti. The z-axis corresponds to the usual observation direction (Modified from Fig. 2-2 of Cochlea, 1996).

photographs taken in each experiment.

The amplitude and phase for the three orthogonal components of the TM's motion were calculated according to the 3-dimensional reconstruction technique described in the methods section (chapter 3). Fig. 8-7 shows three reconstructed orthogonal components of the amplitude and phase of bead 1 on the TM *in vivo*. Circles, triangles and diamonds represent x, y and z component, respectively. For bead 1, the amplitudes in the x and y directions are almost equal to each other below the cutoff frequency. However, the z component is 3 times bigger than the other two components in this frequency range, which means the major vibration was directed along the z direction. Above 800 Hz, the x and y direction components are higher than the z direction, which means the x and y components come to be predominant for these frequencies. However, in this frequency range, the amplitudes of the three orthogonal components are nearly 30-40 dB less than the peak value, which probably means this region is unimportant for hearing, and the measurements may even be unreliable (remember that this is the region where the repeatability of the measurements is relatively poor as shown in Fig. 8-5).

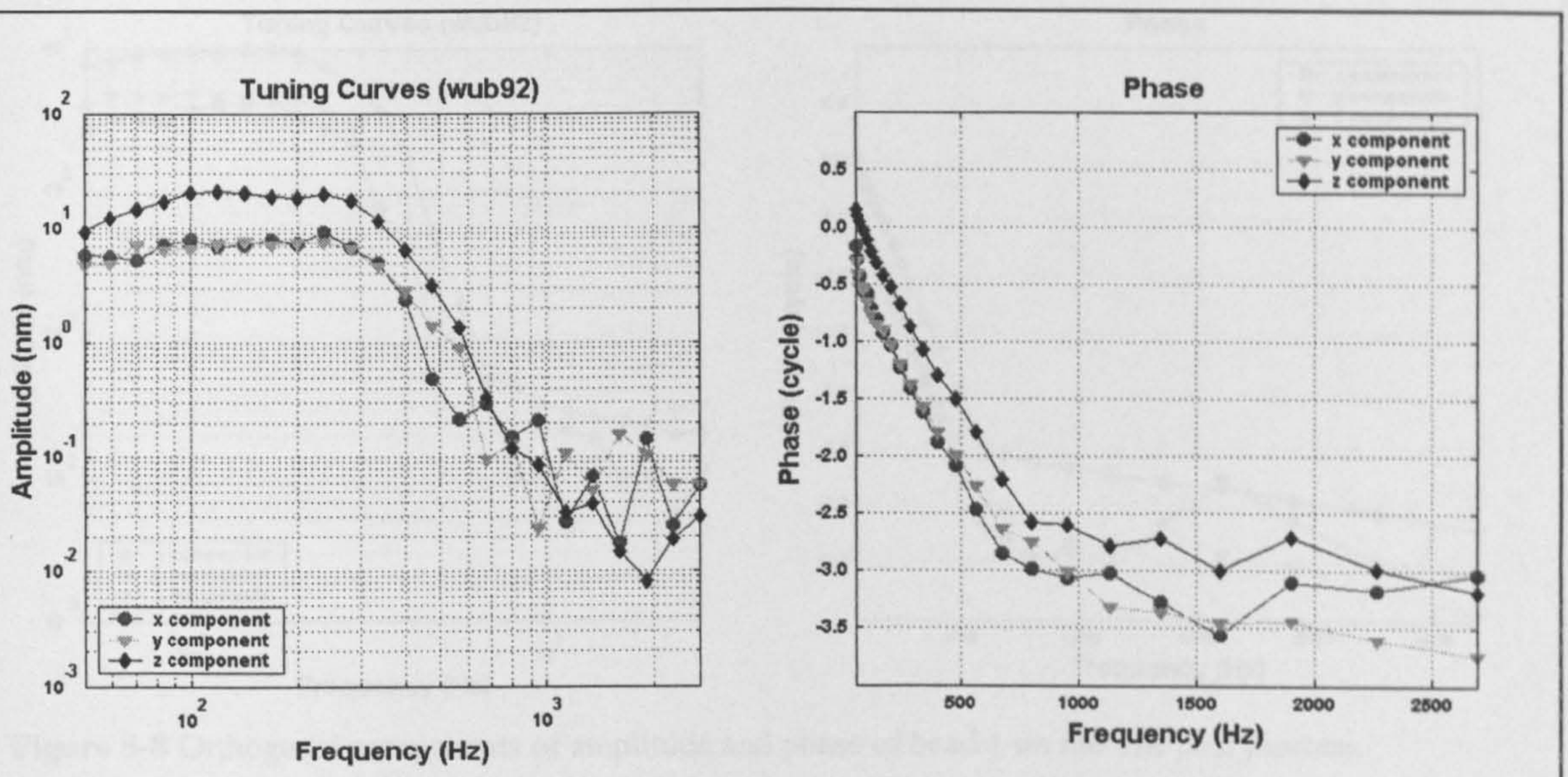

Figure 8-7 Orthogonal components of amplitude and phase for bead 1 on the TM *in vivo*.

Phase information for the three orthogonal components is displayed in the right panel of Fig. 8-7. The x and y components are nearly in phase up to 400 Hz, but the z component

vibrates in anti-phase in the same region. This indicates the paths of the observed point in 3-D space are straight lines for these frequencies. Above this frequency, the phase difference among x y and z components varies with the frequency and becomes more complicated. This means that the path of the observed point in 3-dimensional space became more complicated than the straight line, more likely to be an ellipse.

Figure 8-8 displays the three orthogonal components reconstructed from *post mortem* data of bead 1. Comparing this figure to that of *in vivo* data (Fig. 8-7). The z component (diamonds) dominates across nearly the whole frequency range and it is 2 times larger than the x (circles) and y (triangles) components up to 500 Hz. On the other hand, below 300 Hz, the x and y components are nearly in phase, but the z component is in anti-phase to these two components. This means that bead 1 still moves mainly in the transverse up-and-down direction after the animal died and the vibration paths in 3-D space are straight lines below 300 Hz. Above this frequency, the x and y components develop additional phase lags

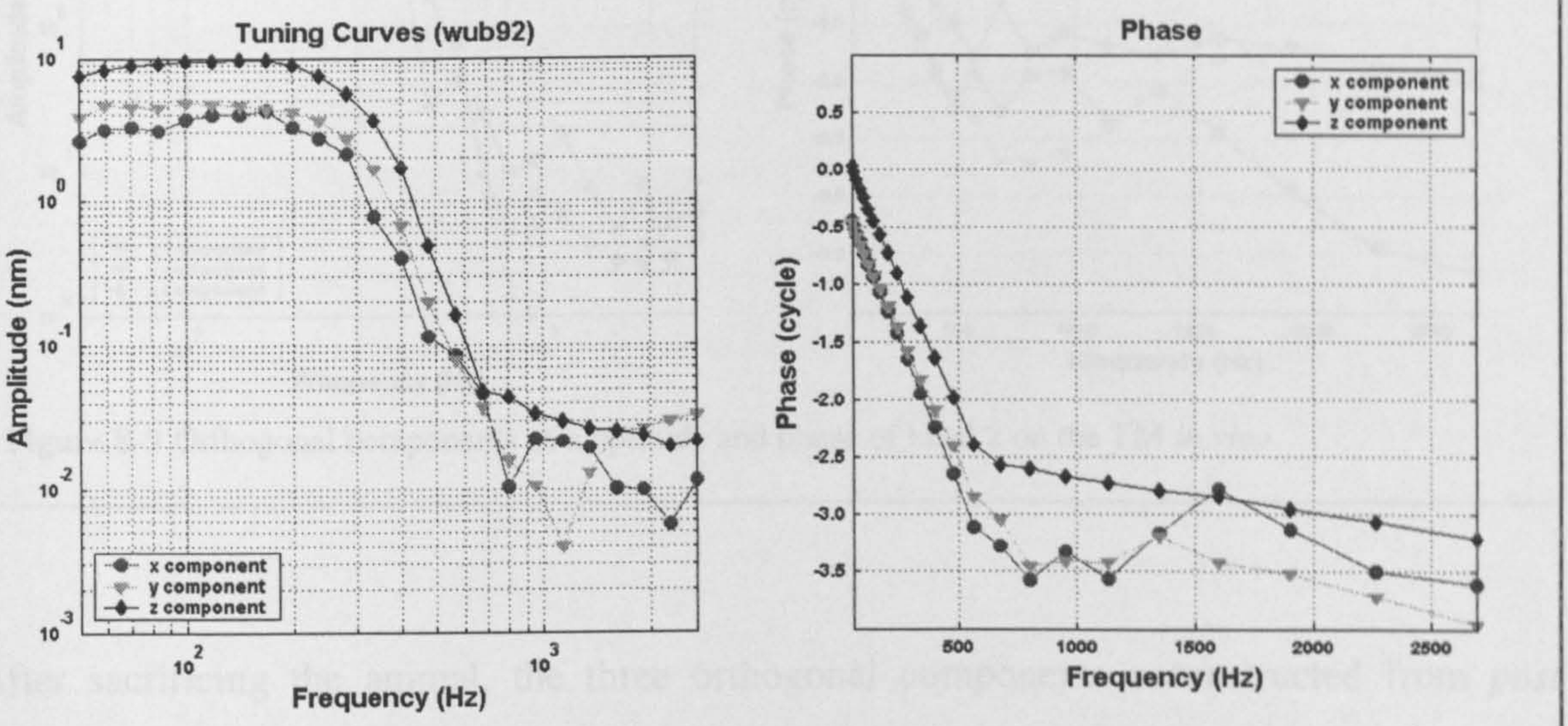

Figure 8-8 Orthogonal components of amplitude and phase of bead 1 on the TM *post mortem*.

when compared with z direction and bead 1 moves along elliptical paths instead.

Figure 8-9 shows the three orthogonal components of bead 2 on the TM *in vivo*. Circles, triangles and diamonds represent the x, y and z component, respectively. For this example, the y component has the largest amplitude among the three orthogonal components. The domination of the y component lasts up to 400 Hz and then the three orthogonal components cross each other and make the vibration mode of the observed point more complicated. The three orthogonal components vibrate in phase (or in anti-phase) up to 500 Hz. All these results show that bead 2 on the TM *in vivo* moves along a straight line inclined towards the longitudinal (y) direction up to 500 Hz. Above this frequency, the vibration mode may change to follow an elliptical path and the direction may change as well.

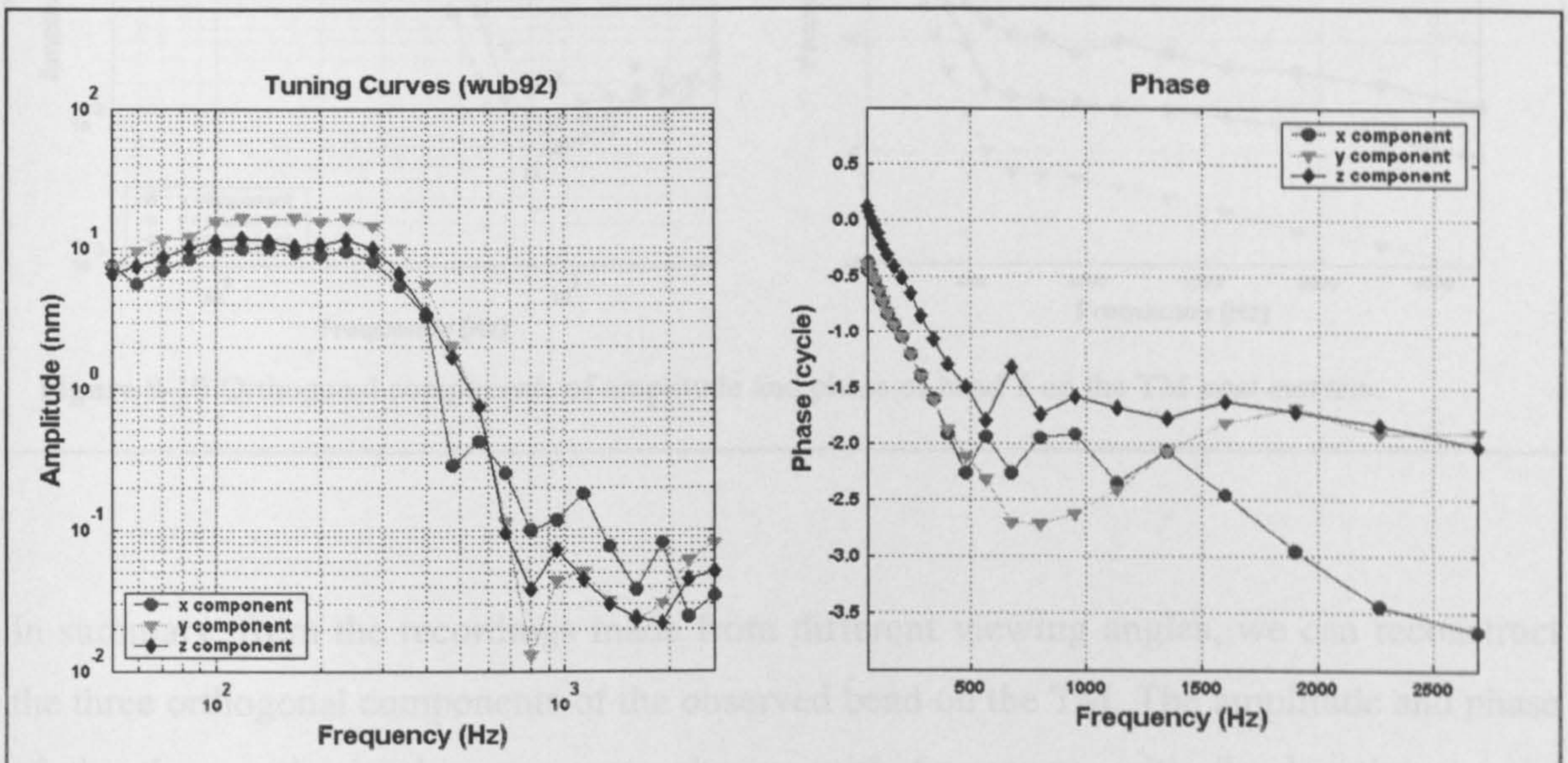

Figure 8-9 Orthogonal components of amplitude and phase of bead 2 on the TM *in vivo*.

After sacrificing the animal, the three orthogonal components reconstructed from *post mortem* data of bead 2 are plotted in Fig. 8-10 with same symbols as used in Fig. 8-9. Comparing this figure to that of *in vivo* data (Fig. 8-9), the y component (triangles) dominates over nearly the whole frequency range and it is 2 or 3 nm higher than the z (diamonds), or x (circles) components. The x direction has the lowest amplitude. For the phase data, the three orthogonal components are nearly in phase (or in anti-phase) up to 500 Hz. The phase difference among the three components increases after that frequency.

Therefore, for bead 2 on the TM, after the animal had died for 2 hours and 20 minutes, the reconstructed motion appears to follow a straight-line path up to 500 Hz, and changes its path into ellipse afterwards. The straight-line path appears to align with the y-axis in this case, just as it did *in vivo*.

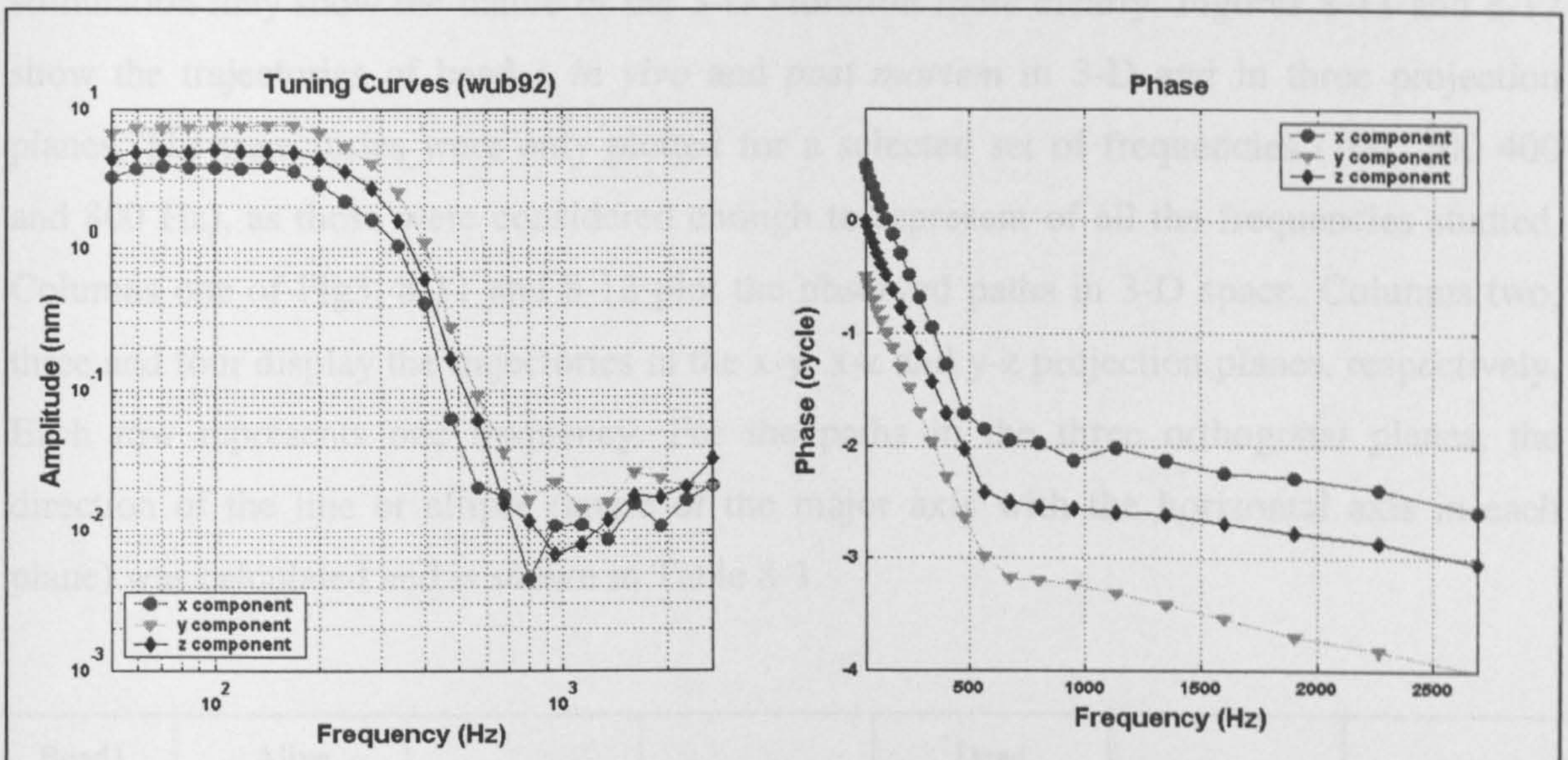

Figure 8-10 Orthogonal components of amplitude and phase of bead 2 on the TM *post mortem*.

In summary, from the recordings made from different viewing angles, we can reconstruct the three orthogonal components of the observed bead on the TM. The amplitude and phase of the three orthogonal components change with frequency, with the location on the tectorial membrane and also with the cochlear condition (alive or dead). These results clearly provide enough information to describe the path of the observed points in three-dimensional space at least for frequencies below the cochlear partition's cut-off frequency. However, it is clearly necessary to study every point individually in order to build up a whole picture of the tectorial membrane's motion.

8.5 Vibration paths in three-dimensional space

8.5.1 Vibration of Bead 1 on TM

Plotting the paths of observed points on the TM during one period of the sine-wave stimulation may show the nature of the 3-D vibration more clearly. Figures 8-11 and 8-12 show the trajectories of bead 1 *in vivo* and *post mortem* in 3-D and in three projection planes. The trajectories were only plotted for a selected set of frequencies (100, 200 400 and 800 Hz), as those were considered enough to represent of all the frequencies studied. Columns one of Fig3. 8-11 and 8-12 plot the observed paths in 3-D space. Columns two, three and four display the trajectories in the x-y, x-z and y-z projection planes, respectively. Each row represents one frequency. For the paths in the three orthogonal planes, the direction of the line or ellipse (angle of the major axis with the horizontal axis in each plane) was calculated and is shown in Table 8-1.

Bead1	Alive			Dead		
	x-y plane	x-z plane	y-z plane	x-y plane	x-z plane	y-z plane
Frequency (Hz)	Angle-x (degree)	Angle-x (degree)	Angle-y (degree)	Angle-x (degree)	Angle-x (degree)	Angle-y (degree)
100	39	-69	-72	52	-69	-63
200	46	-68	-68	52	-70	-65
400	51	-72	-66	66	-79	-69
800	15	-38	41	60	77	76

Table 8-1 Ellipse or line direction in the three orthogonal projection planes for bead 1 *in vivo* and *post mortem.*

Results at 100 and 200 Hz represent the vibration pattern of bead 1 in the low frequency region of the transfer function. At 100 Hz *in vivo*, bead 1, moves mainly along the z direction in a thin elliptical path. The path changes into a slanting line after the animal died (Fig. 8-12). In the x-y projection plane, bead 1 moves along an elliptical path with the long

radius directed 39° away from the x direction *in vivo*. Its path becomes a line tilting at an angle of 52° *post mortem*. Vibrations in the x and y directions are more in phase *post mortem* than that *in vivo*. The x and y components are only half as large as the z component. In the x-z projection plane, the vibration direction is the same *in vivo* and *post mortem*. The path is also a thin ellipse with its major motion along z direction. In the y-z plane, the ellipse becomes thinner after the animal died and tilts towards the y-axis a further

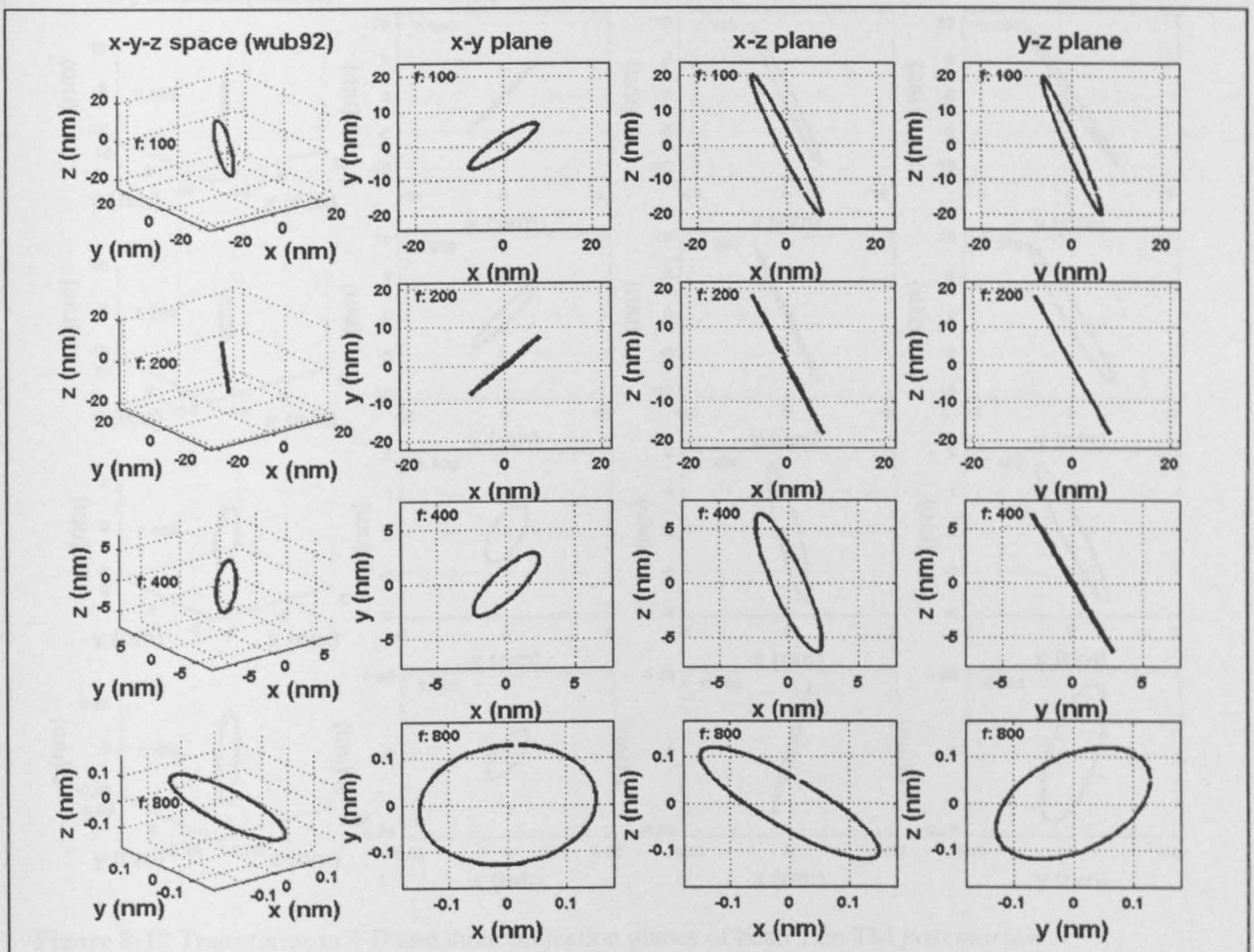

Figure 8-11 Trajectories in 3-D space and three projection planes of bead 1 on TM *in vivo*.

10° degrees.

At 200 Hz, the x, y and z components all move in phase (anti-phase), resulting in linear paths in 3-D space and in all the three projection planes *in vivo*. All the paths stay nearly the same as *in vivo* after the animal died, although they do become slightly more elliptical.

At 400 Hz, in the region where the transfer function falls with a steep slope, bead 1 moves in nearly the same direction as it does at 200 Hz, but on a slightly more elliptical path. The y and z components of its motion move nearly in/anti phase, but the x component is not. Moreover, the amplitude of the vibration drops to one-fourth of the amplitude at 200 Hz. Still the major component of the motion is in the z direction.

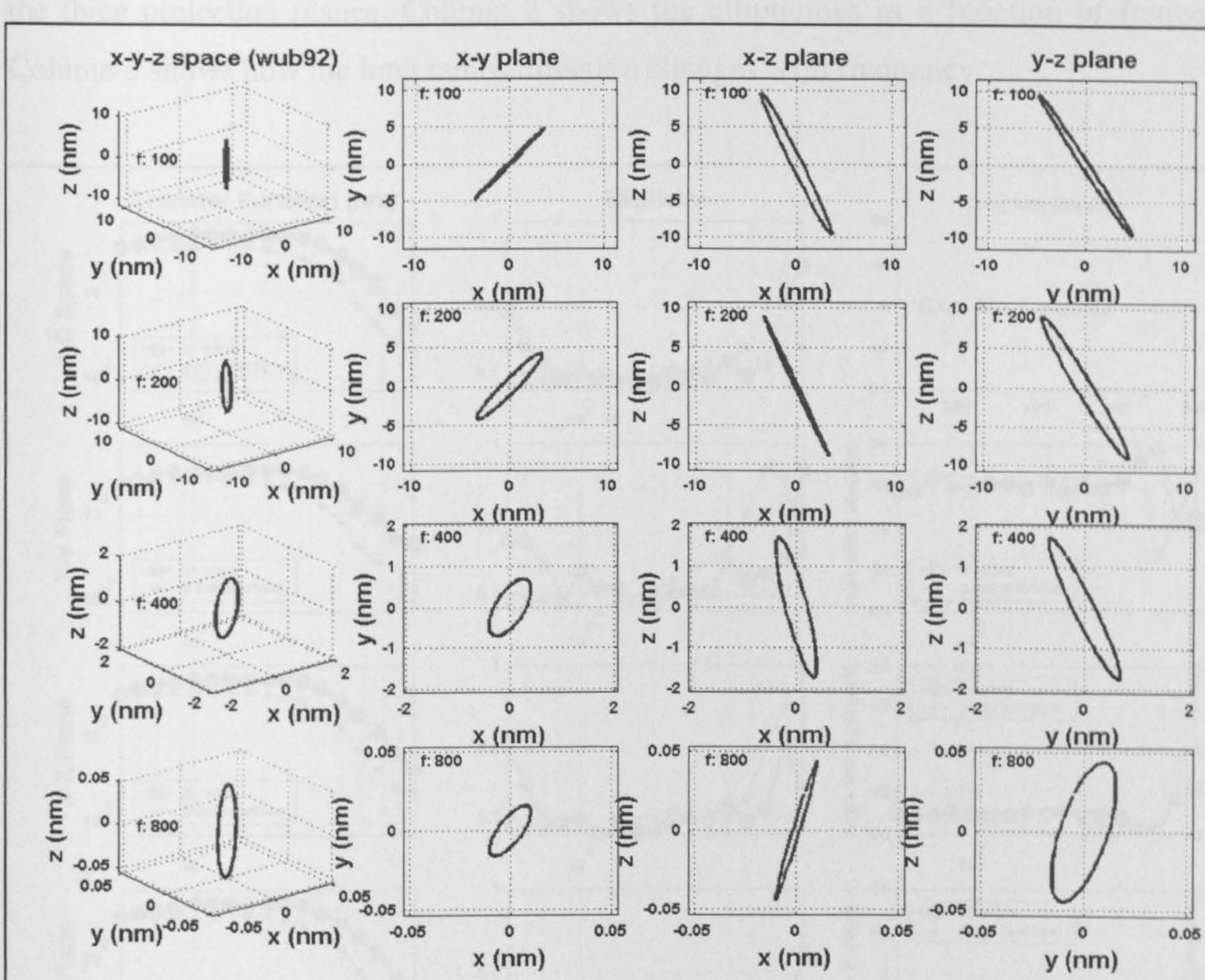

Figure 8-12 Trajectories in 3-D and three projection planes of bead 1 on TM *post mortem*.

However, at 800 Hz, in the high-frequency tail region of the transfer function, bead 1 moves in a more circular way and in a quite different direction. The amplitude in each direction is only 1/200 of that of 200 Hz.

In order to show the vibration pattern of bead 1 more systematically, the ellipticities and long radius directions for every ellipse in 3-D space and the three projection planes were

calculated frequency by frequency up to 800 Hz. The ellipticity was defined as the ratio of the short radius divided by the long radius. The long radius direction was defined as the angle with the horizontal axis in each plane and represents the direction of the line or ellipse. The calculation results are plotted frequency by frequency in Fig. 8-13. The big circles represent the results *in vivo* and small circles stand for the *post mortem* results. The first column compares the transfer functions *in vivo* and *post mortem* in 3-D space and in the three projection planes. Column 2 shows the ellipticities as a function of frequency. Column 3 shows how the long radius direction changes with frequency.

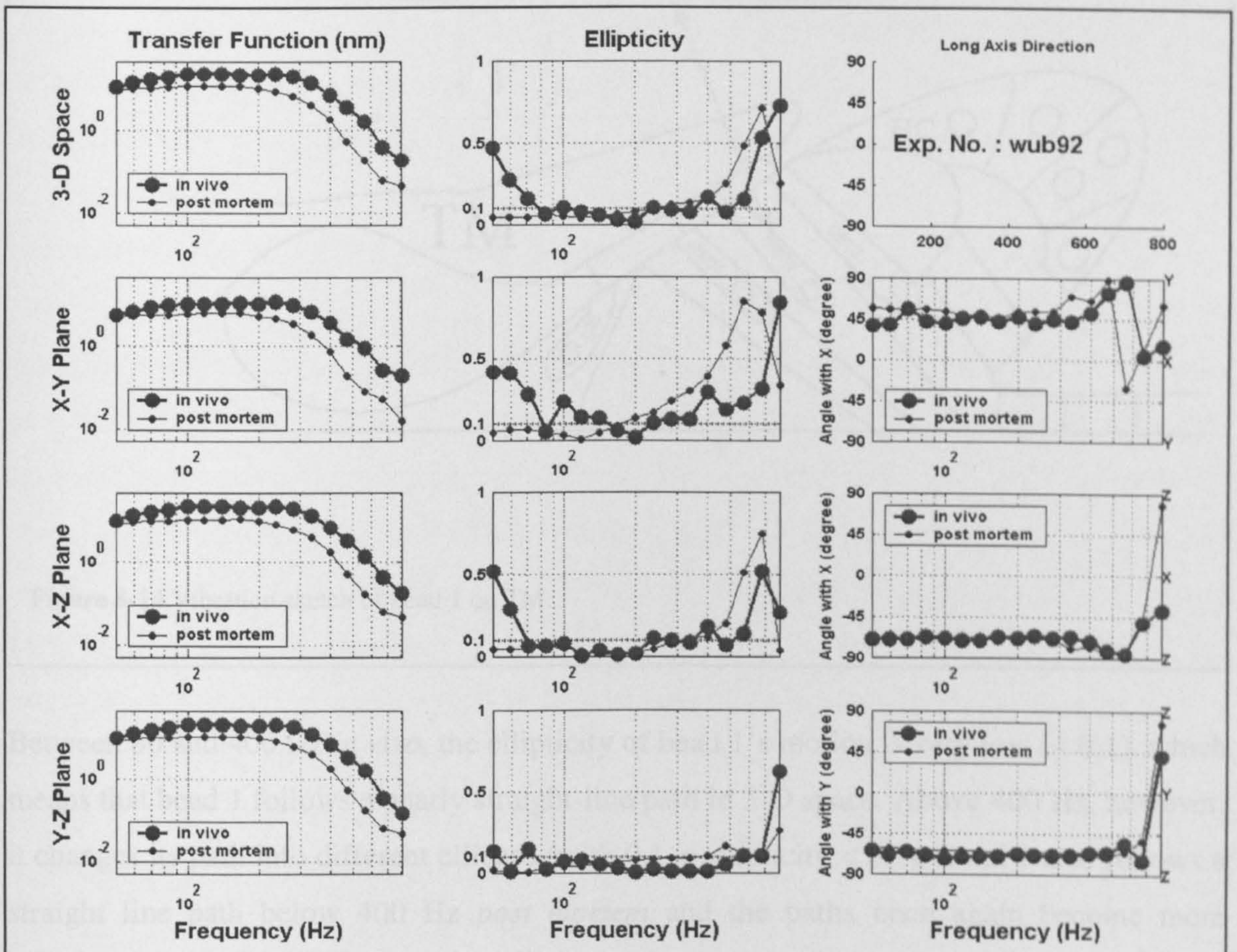

Figure 8-13 Characteristics of bead 1 vibration pattern *in vivo* and *post mortem*.

The transfer functions in 3-D space and in the three projection planes all look like high-order low-pass filters, with cutoff frequencies of ~300 Hz *in vivo* and ~200 *post mortem*. The *post mortem* amplitudes are all lower than the *in vivo* data. The amplitude difference between the *in vivo* and *post mortem* data increases with increasing frequency.

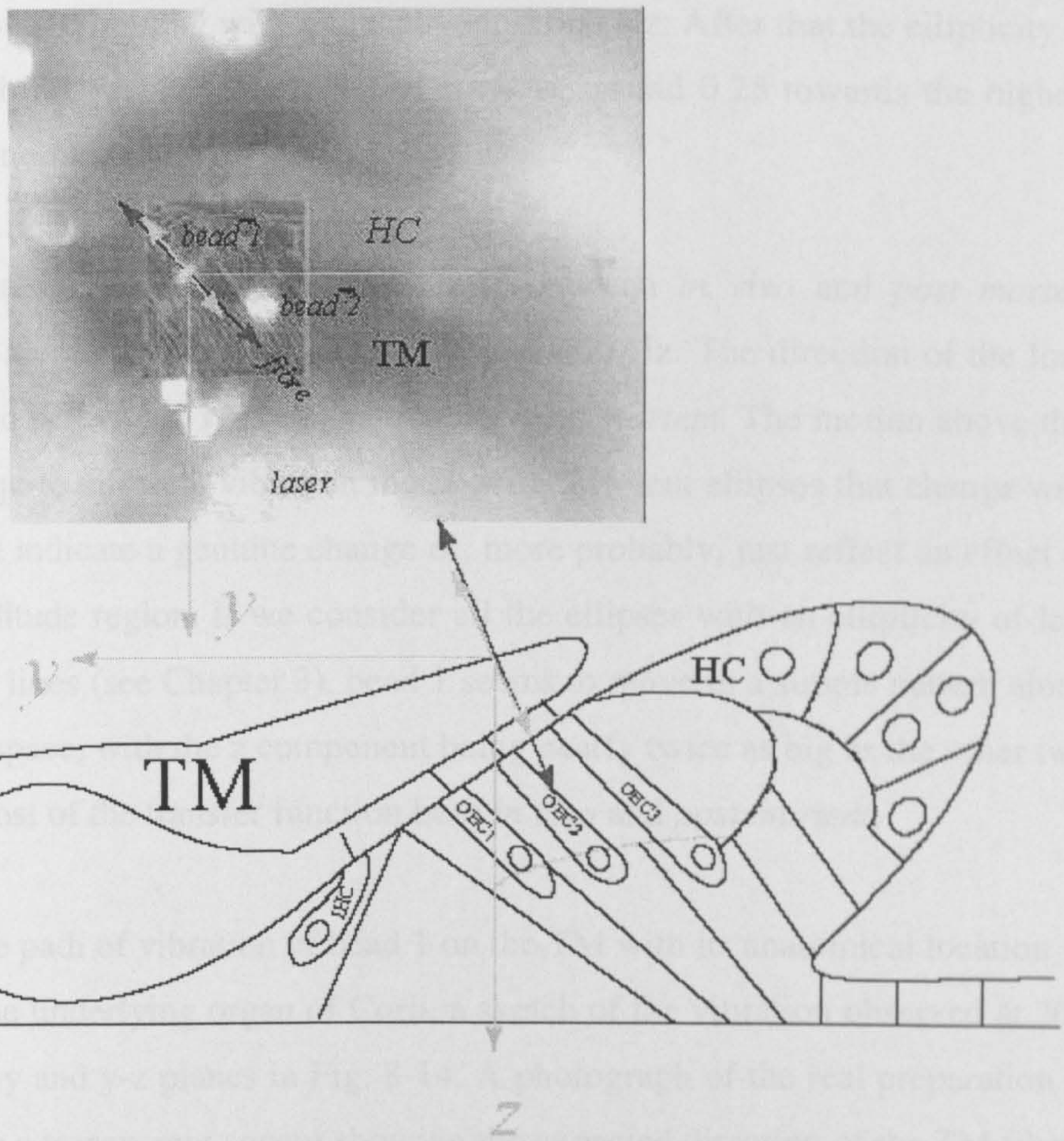

Figure 8-14 Vibration sketch of bead 1 on TM.

Between 80 and 400 Hz *in vivo*, the ellipticity of bead 1's motion is very low (< 0.1), which means that bead 1 follows a nearly straight-line path in 3-D space. Above 400 Hz, however, it changes its path into different ellipses (with 0.1 < ellipticity < 0.7). Bead 1 also follows a straight line path below 400 Hz *post mortem* and the paths once again become more elliptical above that frequency. Tracing the path of bead 1 in different projection planes, it is interesting to see that below 400 Hz, it moves along a straight line (ellipticity < 0.1) both in x-z and y-z planes along the same direction *in vivo* and *post mortem*. Above 400 Hz, in these two planes, bead 1 follows different elliptical paths and it seems that its long radius changes towards the horizontal axis of each plane. However, there is no simple pattern found with frequency both in ellipticity and in long radius direction. In the x-y plane, bead 1 generally follows thin elliptical paths below 400 Hz in the same direction *in vivo*. After

the animal died, bead 1 follows a straight-line path below 80 Hz and changes its path to an ellipse with an increasing ellipticity with frequency until 600 Hz. After that the ellipticity of its path decreases with increasing frequency and stays at around 0.25 towards the highest frequencies (not shown in Fig. 8-13).

In summary, the vibration of bead 1 changes little between *in vivo* and *post mortem* conditions. It follows an almost straight-line path below 400 Hz. The direction of the long radius stays unchanged below 400 Hz both *in vivo* and *post mortem*. The motion above this frequency presents a quite different vibration mode, with different ellipses that change with frequency. This might indicate a genuine change or, more probably, just reflect an effect of noise in the low amplitude region. If we consider all the ellipses with an ellipticity of less than 0.1 to be straight lines (see Chapter 3), bead 1 seems to move in a simple pattern along a straight line in 3-D space, with the z component being nearly twice as big as the other two components across most of the transfer function both *in vivo* and *post mortem*.

In order to connect the path of vibration of bead 1 on the TM with its anatomical location and the structure of the underlying organ of Corti, a sketch of the vibration observed at 200 Hz is plotted in the x-y and y-z planes in Fig. 8-14. A photograph of the real preparation is shown on the top with a transparent square showing the expected direction of the TM fibres in the apical turn of the cochlea. The observed bead formed the origin of the right-hand coordinate system. The bottom panel of Fig. 8-14 shows the expected cross section of the preparation. The origin of the y-z plane is aligned to the location of the recording bead. The direction of vibration of bead 1 is represented by a red-two-arrow-line *in vivo* and cyan-two-arrow-line *post mortem*. It is interesting to see that in the x-y plane, bead 1 moves along the direction of the TM fibres instead of in a pure radial direction. This is true both *in vivo* and *post mortem*. In the y-z plane, bead 1 vibrated almost perpendicularly to the expected plane of the reticular lamina both *in vivo* and *post mortem*. This vibration pattern fits bead 1 for frequencies less than 400 Hz. Above 400 Hz, the vibration direction is changed and the paths become difficult to describe as discussed earlier. Moreover, as the vibration amplitudes were nearly 200 times lower above 400 Hz, these paths are thought to be out of the interesting frequency range for this recording location.

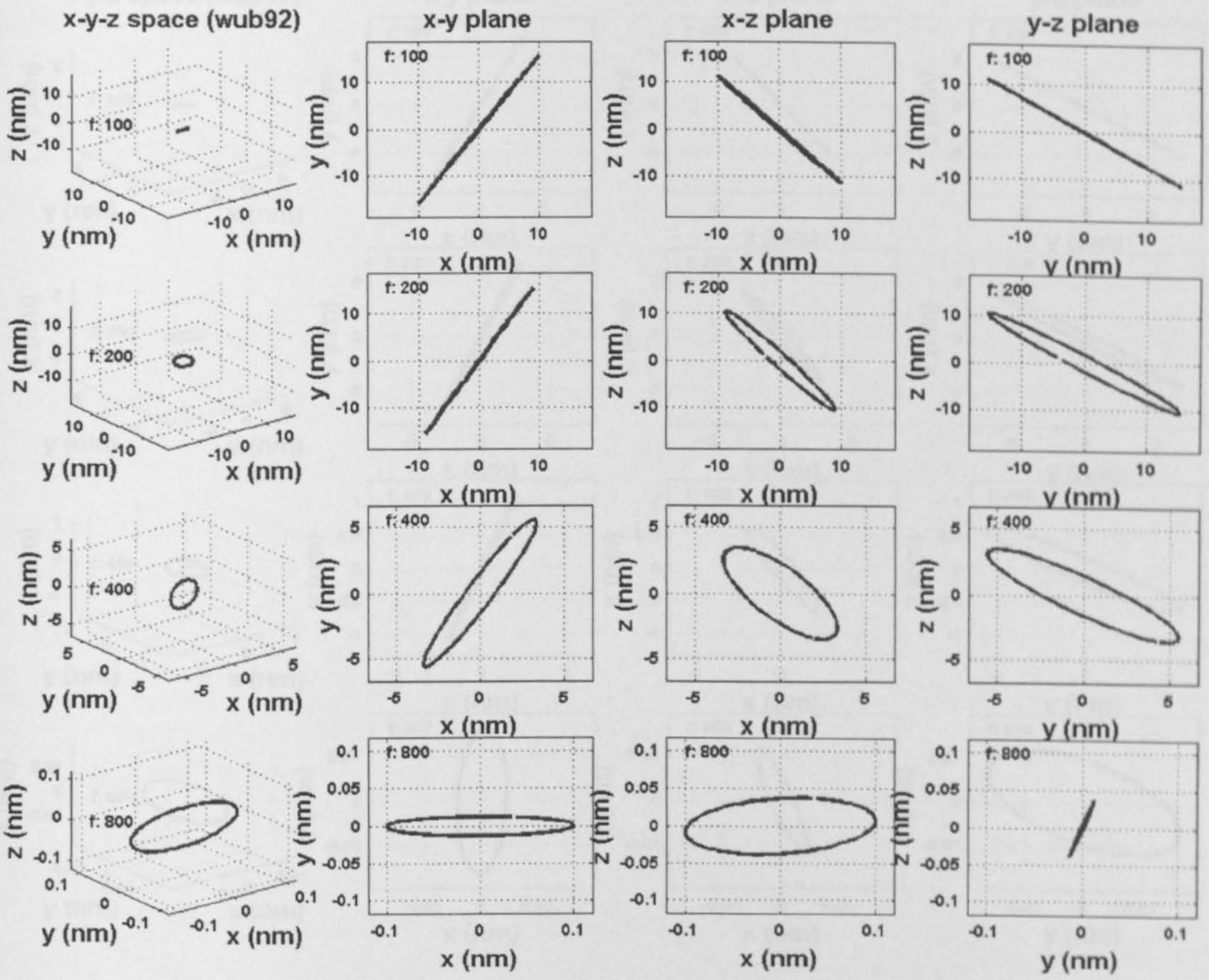

Figure 8-15 Trajectories in 3-D space and three projection planes of bead 2 on TM *in vivo*.

8.5.2 Vibration of Bead 2 on TM

Figure 8-15 and 8-16 show the trajectories of bead 2 in 3-D and in three projection planes *in vivo* and *post mortem*. As before, examples at 100, 200 400 and 800 Hz are plotted. In these two figures, column one plots the path in 3-D space. Column two, three and four display the trajectories in x-y, x-z and y-z projection planes, respectively. Frequency values are labeled at the corner of each subfigure. The direction of the path in the three orthogonal planes was calculated as before and is shown in Table 8-2.

For those frequencies in the pass-band of the transfer function, e.g. 100 and 200 Hz, bead 2 moves along a slanting line in the 3-D space and three projection planes both *in vivo* and *post mortem* (Fig. 8-15 and Fig. 8-16). In contrast with bead 1, the maximum vibration of

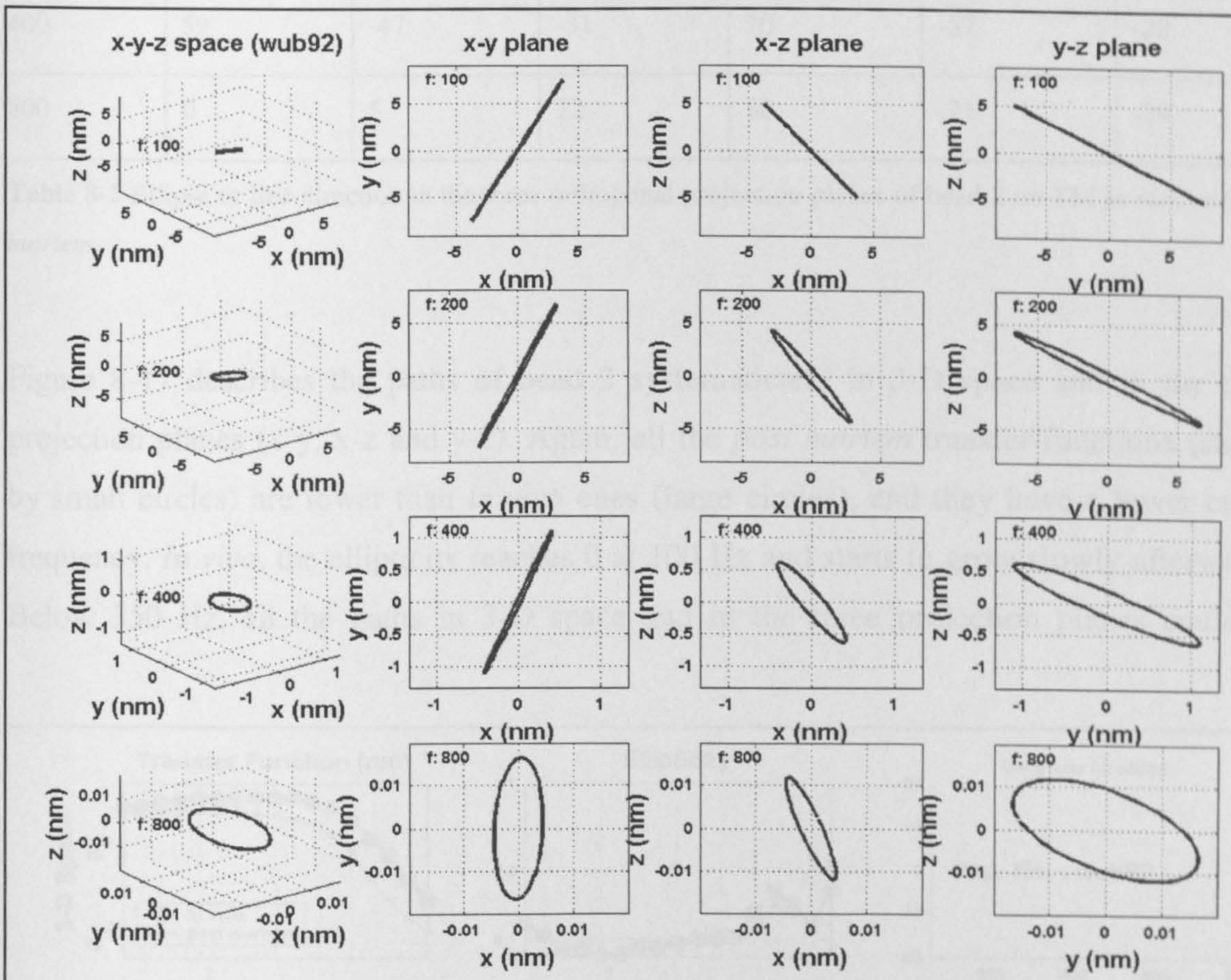

Figure 8-16 Trajectories in 3-D space and three projection planes of bead 2 on TM *post mortem*.

bead 2 occurs in the y instead of z direction. The vibration pattern changed into ellipse at 400 Hz, but kept the same direction as at low frequencies. The vibration becomes more complex at 800 Hz, but at a very small magnitude compared with the low frequencies.

Bead2	Alive			Dead		
	x-y plane	x-z plane	y-z plane	x-y plane	x-z plane	y-z plane
Frequency (Hz)	Angle-x (degree)	Angle-x (degree)	Angle-y (degree)	Angle-x (degree)	Angle-x (degree)	Angle-y (degree)
100	57	-49	-36	63	-53	-34
200	60	-50	-34	67	-57	-33

400	59	-47	-31	70	-57	-28
800	0	5	72	88	-71	-29

Table 8-2 Ellipse or line direction in the three orthogonal projection planes of bead 2 on TM *in vivo* and *post mortem*.

Figure 8-17 describes the paths of bead 2 systematically in 3-D space and in the three projection planes (x-y, x-z and y-z). Again, all the *post mortem* transfer functions (shown by small circles) are lower than *in vivo* ones (large circles), and they have a lower cutoff frequency. *In vivo*, the ellipticity reaches 0 at 100 Hz and starts to grow slowly afterwards. Below 350 Hz, all the paths in 3-D space and in the three projection planes could be

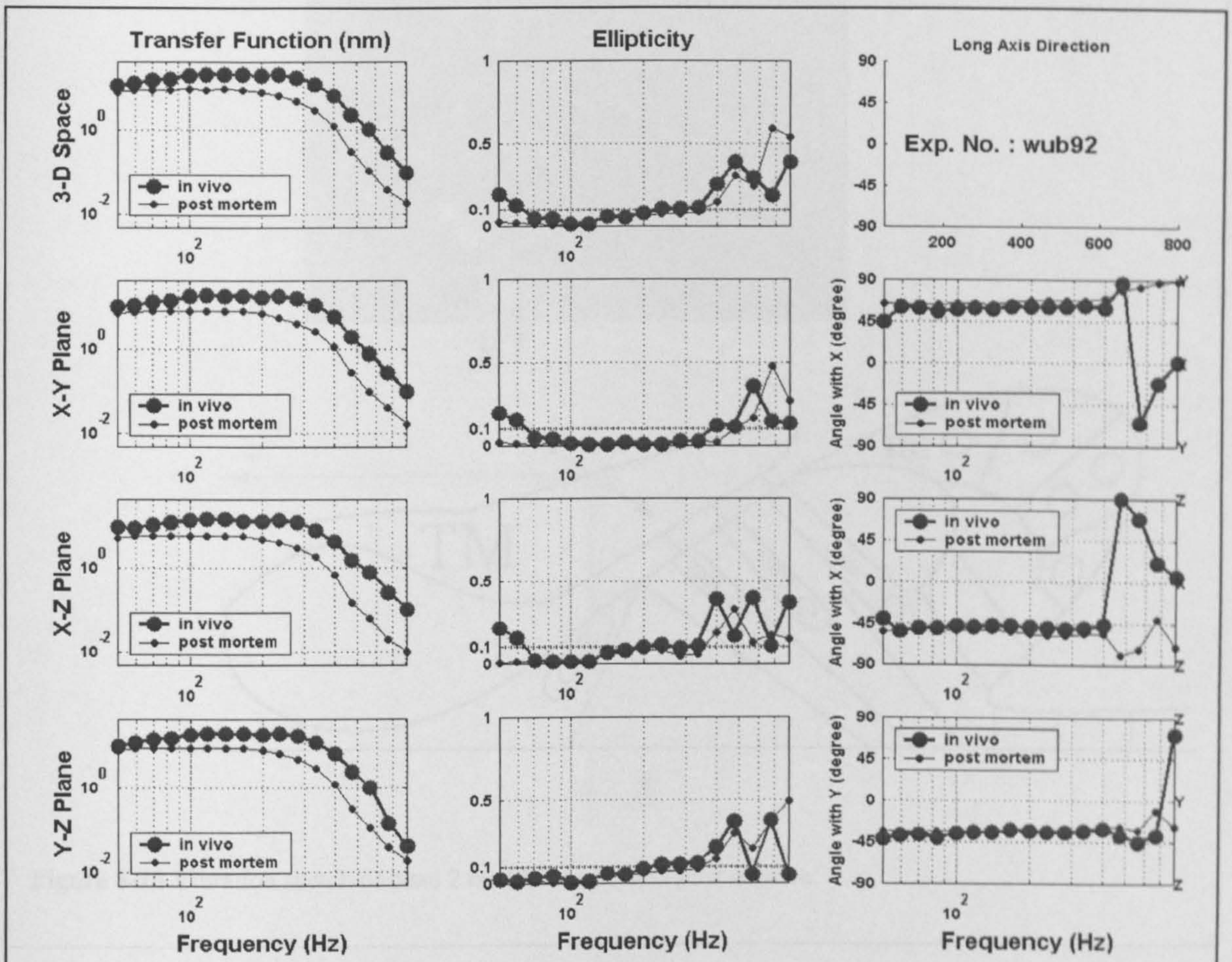

Figure 8-17 Characteristics of bead 2 vibration pattern *in vivo* and *post mortem*.

considered as slanting lines, since their ellipticities are less than 0.1. Above 350 Hz, the ellipticities become larger but more irregular, which indicates that the paths change into different ellipses. The long radius direction changes little *in vivo* and *post mortem* below 400 Hz, but after that it changes with frequency.

In spite of the changing vibration magnitudes, the vibrations of bead 2 hardly changed in their pattern at all *in vivo* and *post mortem*. The paths follow slanting straight lines below 350 Hz and then change into ellipses. The direction of the long radius stays the same below 400 Hz both *in vivo* and *post mortem* and becomes irregular above that frequency.

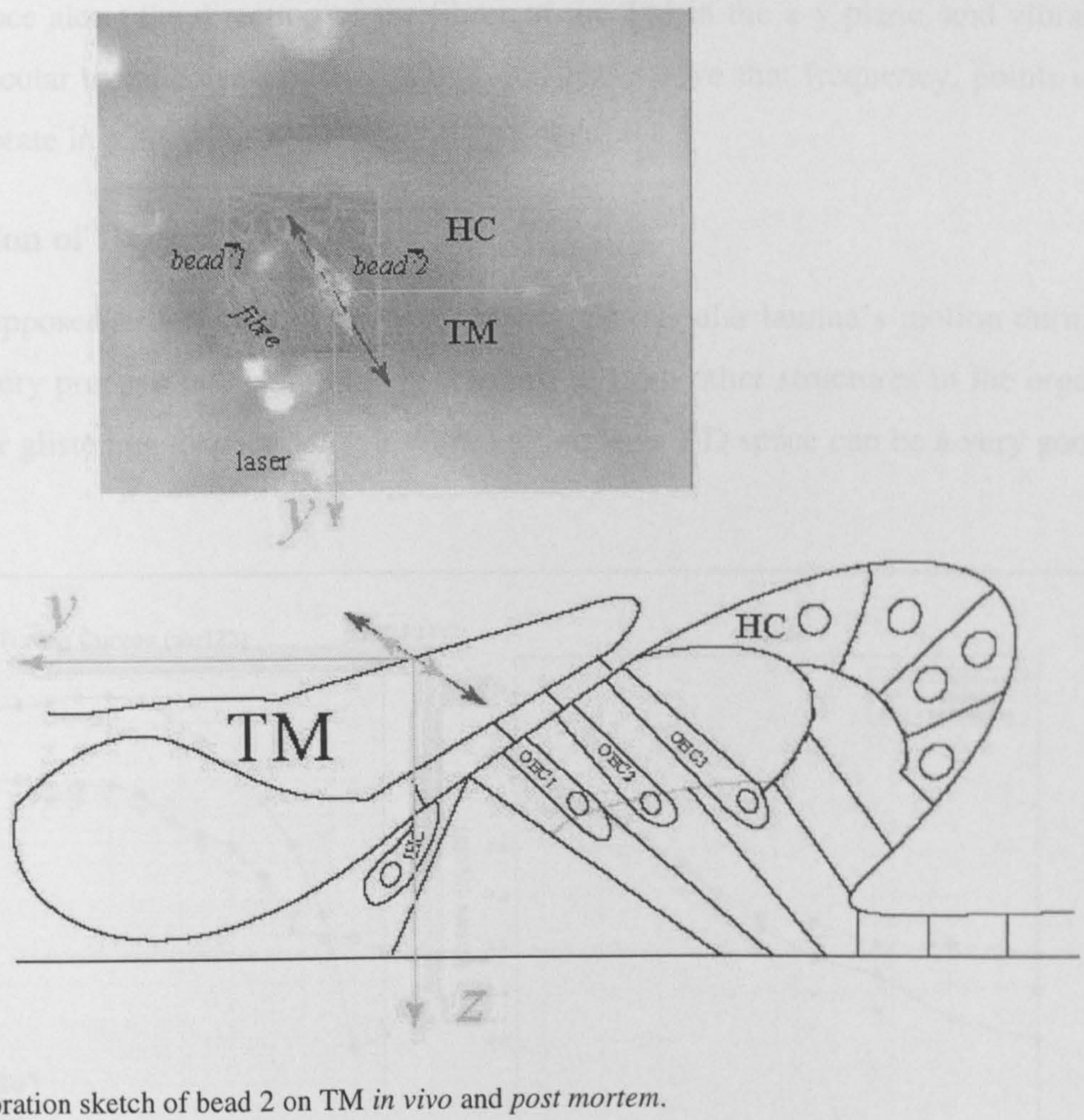

Figure 8-18 Vibration sketch of bead 2 on TM *in vivo* and *post mortem*.

To visualize the vibration of bead 2 in the organ of Corti, Figure 8-18 shows a sketch of the vibration mode of bead 2 *in vivo* and *post mortem*. Being in the middle position of the TM,

bead 2 moves almost perfectly along the lines of the TM's fibres in the x-y plane (Fig. 8-18). Even though the vibration direction changed slightly after sacrificing the animal, the vibration is still approximately along the direction of the TM's fibre in the apical turn of the cochlea. In the y-z plane, bead 2 moves in a direction slightly away from the direction perpendicular to the reticular lamina. Bead 2 vibrates in this pattern to all the sound stimuli below 350 Hz, but it changed into elliptical vibration above that. It appears that the middle part of the TM mainly moves along TM's fibre direction to shear the stereocilia of the outer hair cells.

In summary, from this particular example, the points on the TM vibrate in three-dimensional space along the direction of the fibres of the TM in the x-y plane, and vibrate nearly perpendicular to reticular lamina below ~ 400 Hz. Above that frequency, points on the TM may vibrate in a different way.

8.5.3 Vibration of HC

The HCs are supposed to follow the basilar membrane or reticular lamina's motion during the sound delivery process and can be easily recognized from other structures in the organ of Corti by their glistening droplets. Their vibration mode in 3-D space can be a very good

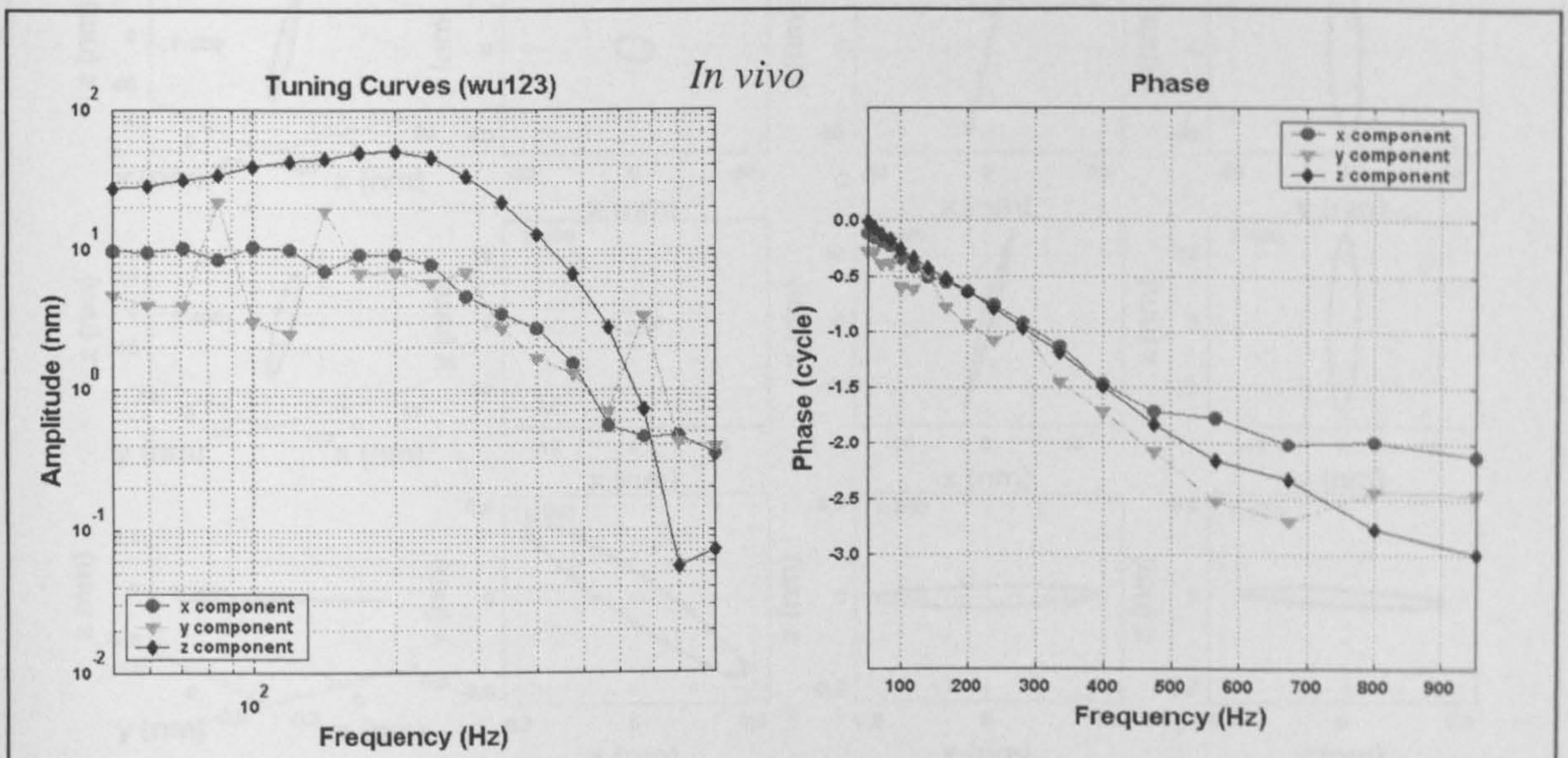

Figure 8-19 Orthogonal components of amplitude and phase of HC vibration (wu123) *in vivo*.

example in understanding the vibration of TM because the TM only covers the sensory cells in the organ of Corti.

To investigate the vibration of the HC, one bead was introduced deliberately onto a HC in one preparation (wub123). The experiment was performed in the same way as the studies of the TM. According to the method described before, 5 measurements from observation angles θ between –23.5° and 14°, and ϕ between –18° and 11.9° were collected within 30 minutes *in vivo*. The characteristic frequency was 238 Hz, with Q_{10} equal to 0.61. The three orthogonal components of the bead motion are plotted in Fig. 8-19. It is clear that the z component dominates up to 600 Hz in this preparation and it is nearly as 5 times as big as the x or y component. The x and z components have nice low-pass filter tuning curves, but the tuning of the y component was quite irregular *in vivo*.

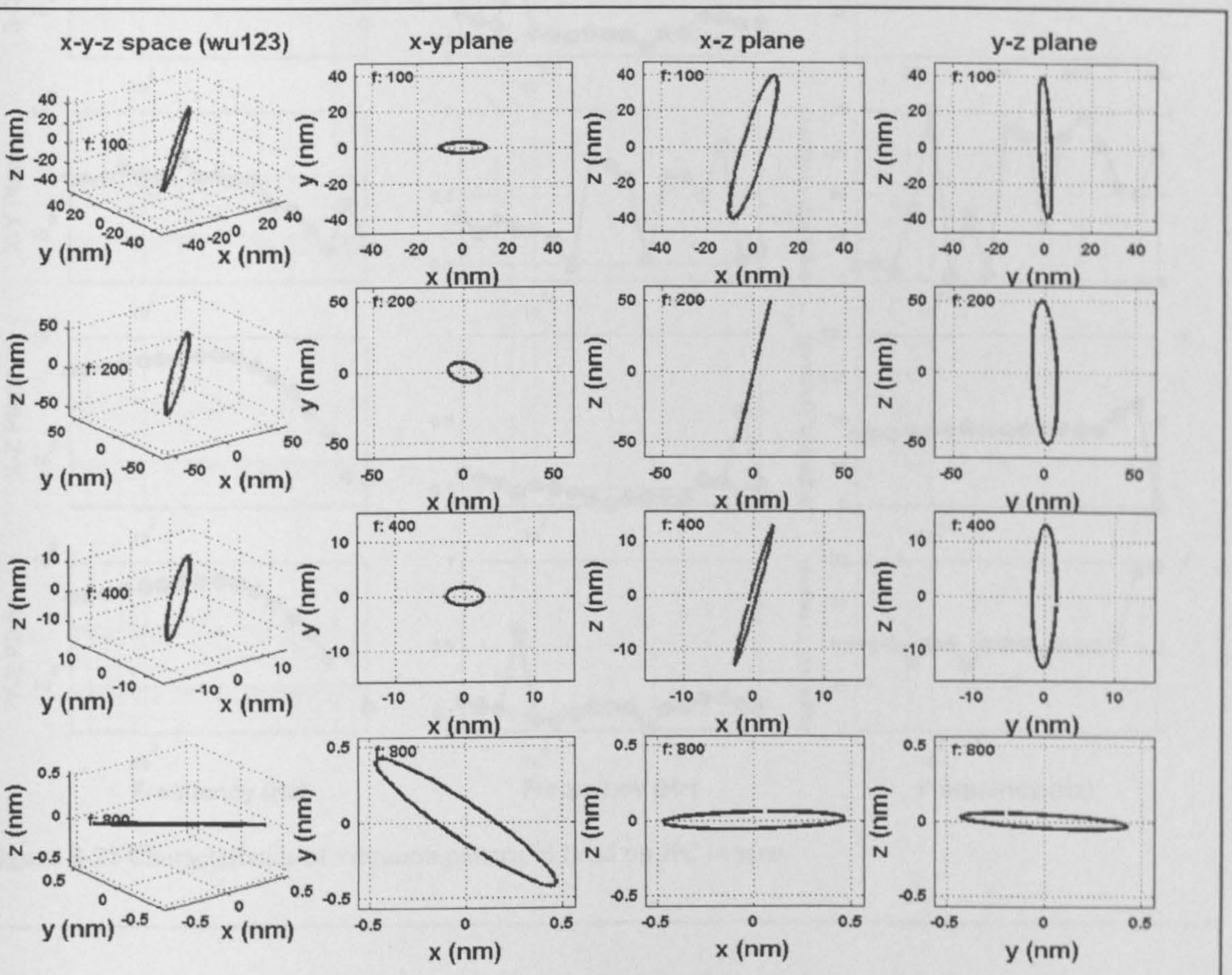

Figure 8-20 Trajectories in 3-D space and three projection planes of bead on HC *in vivo*.

Fig. 8-20 shows the vibration paths of this bead in three-dimensional space and in three orthogonal projection planes for a series of selected frequencies. It is obvious that both in x-y and y-z planes, the paths are very thin ellipses with their long radius almost along the z direction for 100, 200 and 400 Hz. In the x-y plane, the path is only a small ellipse with the long radius nearly in y direction. Therefore, for 100, 200 and 400 Hz, the bead on HC nearly vibrates in the same direction; along very thin elliptical paths, with the major motion being in z direction. At 800 Hz, the path changed totally, from a vertical ellipse into a horizontal one, with the major vibration at ~45°from the x and y axes.

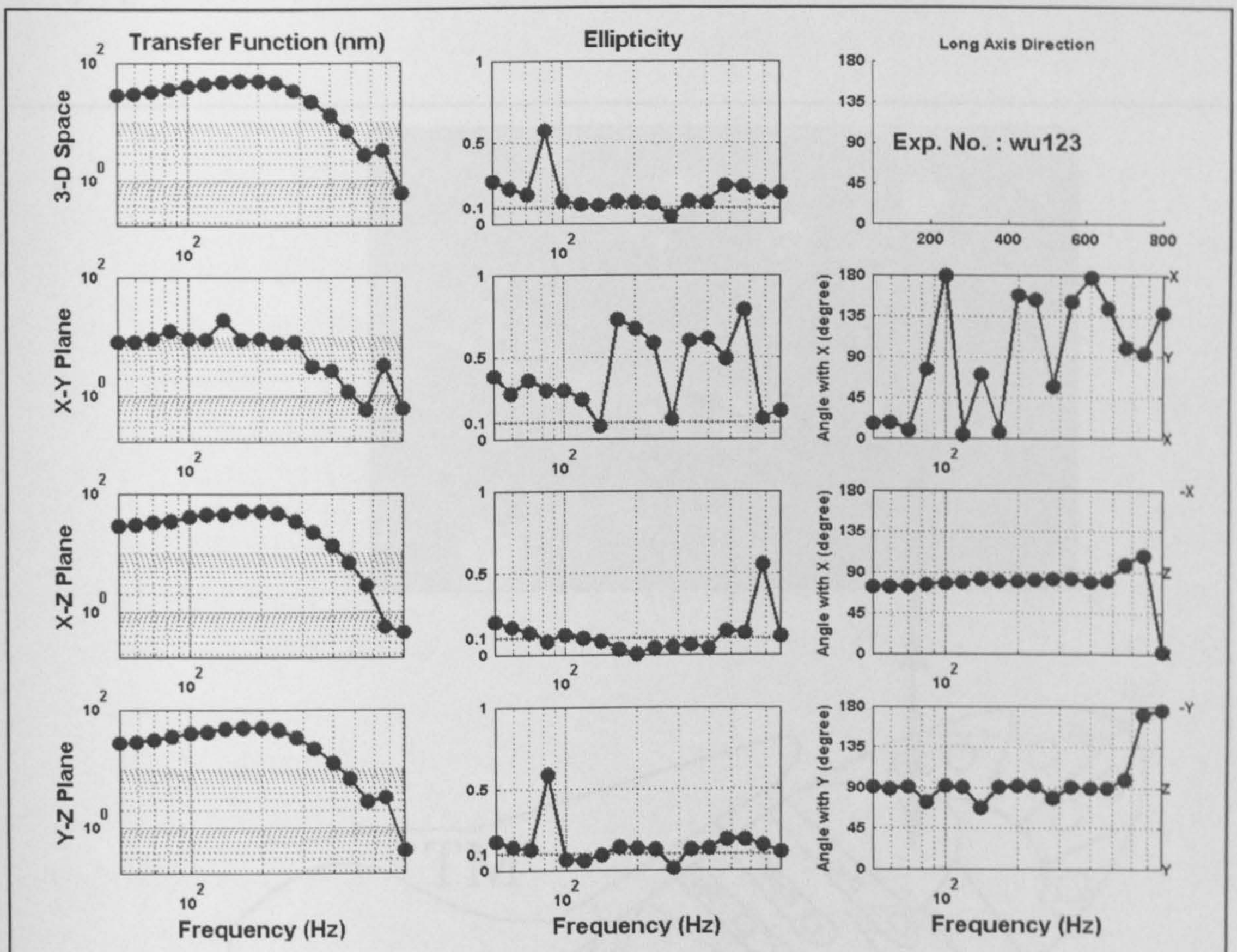

Figure 8-21 Characteristics of vibration pattern of bead on HC *in vivo*.

Figure 8-21 describes the characteristics of the elliptical paths of the HC bead *in vivo* frequency by frequency. The first column shows the transfer function of the bead in 3-D space, and in the x-y, x-z and y-z planes. The second column displays the ellipticity of each path in 3-D space, and in the x-y, x-z and y-z planes. The third row shows the long radius direction in the x-y, x-z and y-z planes. Generally speaking, the paths in the x-z, y-z and three-dimensional space can be considered as straight lines between 100 to 400 Hz (ellipticity around 0.1). The direction of the paths in the x-z and y-z planes is almost in line with the z axis. For the frequencies below 100 and above 400 Hz, the paths are still thin ellipses (ellipticity less than 0.25) except for two special points. The paths in the x-y plane are much wider ellipses with changeable directions, because the x and y components are nearly equal.

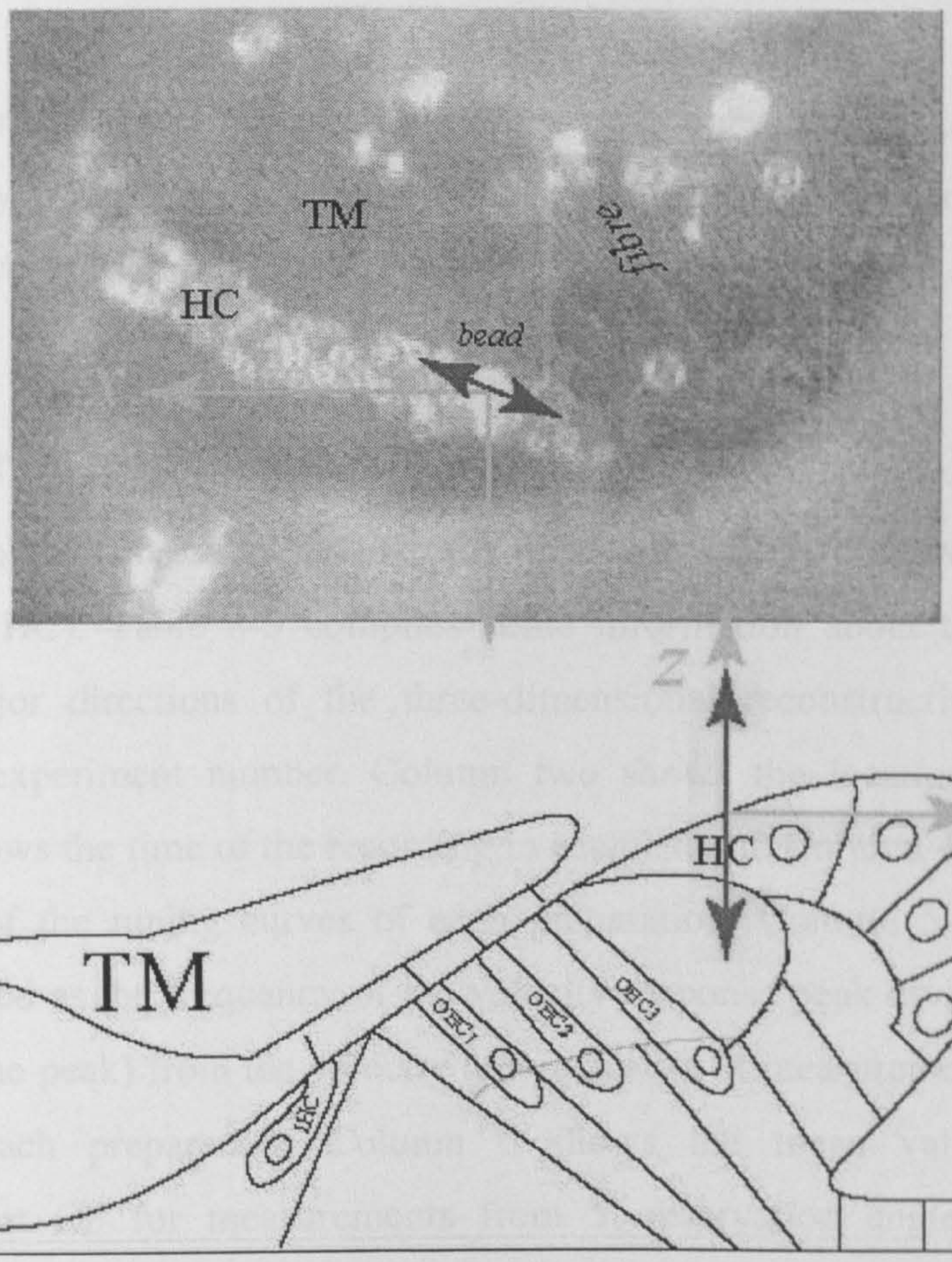

Figure 8-22 Sketch of vibration of observed bead on HC *in vivo*. Red two-head arrow line represents the vibration direction in each plane.

A sketch of the vibration path at 200 Hz is shown in Fig. 8-22 to help the visualization of the vibration mode for the bead on the HC *in vivo*. The top background picture of the organ of Corti was taken from the experiment. The glistening HC band is standing out in an arch shape in this preparation. The direction of the TM fibre was shown in the figure by pasting another photo of the TM from the apical turn of a guinea pig cochlea. The observed bead was centered in the coordinate system and the x, y and z directions are labeled by pink arrows in the figure. In the x-y plane, according to the calculations above, the recorded bead moves along a thin elliptical path at 200 Hz with only 1/5 of the amplitude of z component. The vibration direction in this plane may vary with frequency, but with small amplitude. In the y-z plane, for nearly all frequencies, the observed bead moves along the z direction, which means that it mainly moves in up-and-down and follows the expected vibration of the basilar membrane.

Therefore, it would appear that the HCs move in a very simple way in the organ of Corti during the sound delivery procedure. The HCs mainly follow the basilar membrane's motion, but they may move very slightly around their resting (x-y) position on the surface of the organ of Corti.

8.5.4 TM vibration for all preparations

In total 42 animals contributed substantial data for the three-dimensional reconstruction of the vibration of TM (or HC). Table 8-3 compiles some information about the various preparations and the major directions of the three-dimensional reconstruction results. Column one shows the experiment number. Column two shows the location for each preparation. Column 3 shows the time of the recording in each animal. Column 4 shows the characteristic frequency of the tuning curves of each preparation. Column 5 shows the averaged Q_{10} value (defined as the frequency of the velocity response peak divided by the bandwidth 10 dB below the peak) from the velocity tuning curves of measurements from 5 observation angles in each preparation. Column 6 shows the mean value of the displacement sensitivity at CF for measurements from 5 observation angles of each preparation. Column 7 gives information on the major direction of the reconstructed vibration paths in three-dimensional space. Column 8 provides phase information from the three-orthogonal components of the reconstructed motion.

Exp.No.	ids	condition	CF (Hz)	Q_{10}	Displacement sensitivity at CF (nm/Pa)	Major direction around CF	In/anti phase components around CF
*wu126	tm3	alive	336	0.7	1308	z	y,z
	tm5	died, 30 min	336	0.6	608	z	x.z
wu125	tm3	alive	336	0.51	238	z	x,z
	tm4	died, 1 min	336	0.51	248	z	x,z
wu124	tm3	died, 2h	200	0.46	313	z	x,y,z
*wu123	hc7	alive	238	0.61	1762	z	x,z
	hc9	alive	238	0.67	956	z	x,z
wu122	tm2	died, 2h + 30 min	283	0.74	267	z (~x)	x,y,z
wu121	tm2	died, 2h	168		59	z	y,z
*wu120	tm2	alive	476	0.79	558	z (~x, ~y)	x,z
	tm3	died, 10 min	476	0.74	728	z	x,z
*wu119	tm1	alive	283	0.51	648	z	x,z
	tm3	alive	283	0.51	579	z	x,z
	tm6	died, 30 min	238	0.49	297	z (~x)	x,z
*wu116	tm2	alive	400	0.69	585	z	y,z
	tm3	alive	336	0.71	159	z (~x)	y,z
	tm5	died, 30 min	336	0.69	227	z (~x)	y,z
wu114	bead2	alive	283	0.75	153	z	x,y,z
	bead4	died, 30 min	238	0.6	26	z	x,y,z
Wu113	tm3	alive	400	0.76	101	z	y,z
	tm5	died, 5 min	476	0.82	109	z	x,y,z
*wu112	tm3	alive	336	0.68	1213	z	x,z
	tm5	alive	336	0.51	1612	z	x,y,z
	tm6	died, 30 min	336	0.6	850	z	x,z
wu111	tm1	alive	283	0.59	469	y (~x, ~z)	y,z
	tm3	died, 30 min	283	0.61	304	z	x,y,z
*wu110	bead2	alive	336	0.63	729	z	x,y
	bead3	died, 10 min	336	0.63	608	z	x,y
*wu109	tm2	alive	283	0.69	632	z	x,y
	tm3	alive	283	0.69	647	z	x,y

	tm4	alive	283	0.63	671	z	x,y
	tm5	died, 20 min	283	0.63	630	z (~x)	x,y,z
wu108	tm2	died, 2h	336	1.14	18	x	x,z
wu106	tm2	died, 3h	476	1.38	112	z	x,y,z
wu105	bead2	died, 2h + 40 min	400	0.82	212	z	x,y,z
wu104	tm2	died, 4 min	400	0.59	215	z	x,y,z
	tm3	died, 1h + 10 min	566	0.67	126	z	x,y
wu103	tm1	died, 3h + 30 min	283	0.75	21	z	y,z
*wu102	hc3	died, 10 min	336	0.61	518	y	y,z
	rm1	died, 1h	238	0.5	221	z	x,z
wu101	tm4	died, 1h + 10 min	238	0.63	460	z	x,z
	tm5	died, 2h	238	0.63	212	x	x,z
wu100	tm1	died 1h	283	0.59	331	z	y,z
	tm2	died, 2h	238	0.53	354	z	x,z
*wub99	tm1	died, 1h	252	0.52	531	z	y,z
wub98	tm1	dying	400	0.79	295	z	x,y,z
	tm2	died, 40 min	400	0.9	216	z	x,y,z
*wub97	tm1	died, 1h	238	0.52	724	z	x,y,z
	rm1	died, 2h + 30 min	238	0.54	418	z	x,y,z
wub96	tm1	dying	400	0.84	227	z (~x)	x,z
	tm2	died, 40 min	336	0.86	157	z (~x)	x,z
	tm3	died, 2h + 30 min	283	0.6	96	z	x,y,z
wub95	tm1	died, 2h	200	0.59	44	y	x,y,z
	tm2	died, 2h	238	0.59	28	z	x,z
	tm4	died, 5h + 10 min	200	0.58	119	z (~x)	x,y,z
wub94	tm1	died, 1h	400	0.89	147	z	x,y,z
	tm2	died, 1h + 40 min	400	0.94	65	z	y,z
*wub93	tm1	alive	336	0.58	835	y (~z)	x,y
	tm3	died, 1h +	336	0.76	479	z (~y)	x,y,z

		20 min					
*wub92	tm2	alive	283	0.7	874	z	x,y,z
	tm6	died, 1h + 30 min	200	0.48	455	z	x,y,z
	tm3	alive	283	0.69	616	y	x,y,z
	tm7	died, 2h	200	0.57	268	y	x,y,z
wub91	tm2	alive	400	0.79	30	z	y,z
	tm4	died, 1h + 50 min	200	0.52	187	z	x,y,z
*wub89	tm4	died, 1 min	336	0.71	667	z	
*wub87	tm2	alive	336	0.58	959	z	x,z
	tm3	alive	336	0.61	853	z	y,z
	tm4	alive	283	0.48	606	z	y,z
	tm5	died, 5 min	283	0.52	587	z	x,y,z
	tm6	died, 1h + 20 min	336	0.67	501	z (~x)	x,z
	tm7	died, 35 min	336	0.75	250	z	y,z
	tm8	died, 35 min	283	0.6	444	z	
wub85	tm1	alive	400	0.87	105	y (~z)	x,y,z
	tm4	alive	336	0.87	29	y (~z)	x,y,z
	tm5	died, 5h	336	0.86	2	y (~z)	x,y,z
*wub84	tm2	died, 1h	200	0.43	693	z	y,z
	tm3	died, 2h	200	0.4	711	z	y,z
	tm4	died, 3h+10 min	168	0.45	336	z	x,y,z
*wub83	tm6	died, 50 min	476	0.83	940	x	x,y,z
	tm7	died, 1h + 30 min	476	0.62	600	z	x,y,z
	hc1	died, 2h + 20 min	400	0.5	486	x	x,y,z
	tm8	died, 3h	400		359	z	y,z
	tm9	died, 3h + 50 min	400		225	z	x,y,z
wub68	tm2	died, 2h + 15 min	400	0.74	146	x (~z)	y,z
wub67	tm2	died, 5h + 15 min	238	0.51	231	z	x,y,z

wub58	tm1	died, 1h +40 min	951		10	z	y,z
	tm3	died, 2h + 25 min	951		25	z	x,z
	tm2	died, 3h	200		65	z	y,z
*wub57	tm1	died, 1h + 20 min	200	0.39	702	z	x,y,z
	tm2	died, 3h	283	0.76	42	z	x,y,z
	tm4	died, 4h	200	0.49	83	z (~y)	x,z
wub52	tm1	died, 1h	283	0.41	463	y	x,y,z
	tm2	died, 1h + 30 min	283	0.61	708	z	x,y,z
	tm3	died, 2h	200	0.35	229	z	x,y,z
	tm4	died, 2h + 30min	200	0.4	66	z	x,y,z
	tma	died, 4h + 30 min	283	0.89	76	z	x,y,z
	tmb	died, 4h + 30 min	283	0.88	65	z	x,y,z
	tm5	died, 5h + 20 min	283	0.47	87	z	x,y,z
	tm6	died, 6h	283	0.77	93	z	x,y,z
	tmc	died, 6h + 30 min	283	0.93	36	z	

Table 8-3 Calculations for 42 animals which provided data for the three-dimensional reconstruction of the vibration of TM/HC.

Among all the preparations, 18 examples (labeled with a '*' in Table 8-3) provide data with the initial displacement sensitivity above 500 nm/Pa. These are the preparations which we believe to give the most reliable results. The displacement sensitivity always decreased after the animals died. Three-dimensional reconstruction results show that for almost all the preparations, no matter whether the data were collected from *in vivo* or *post mortem*, the basic motion of the observed bead on TM/HC is along z direction. This means that the TM and HC's mainly move up-and-down, following the expected vibration pattern of the basilar membrane (see Fig. 8-6). Among the three orthogonal components of the reconstructed motion, at least 2 components are moving in/anti phase. This means that the

projection of the vibration path in that plane is a straight line. Therefore we can come to the conclusion that the TM moves in a rather simple way, nearly along a straight line in three-dimensional space with the major component of its motion in an up-and-down direction. There is no obvious indication of a second vibration mode in the TM vibrations in three-dimensional space.

8.6 Discussion

The three-dimensional reconstruction technique that we used has been modified from that described by Decraemer (Decraemer et al. 1994). It is used to reconstruct the vibration in three-dimensional space from one-dimensional measurements. It provides insight into the 3-D motion of the observed point based on the setup of interferometer recording system with a two-axis goniometer. It works well for the mathematical and ideal vibrator (loudspeaker) models discussed in chapter 3. The opening of the cochlea was made as big as possible while keeping the helicotrema and scala media intact, so that bigger viewing angles could be achieved in every preparation. For most of the preparations, the viewing angles could change by nearly 40° in each direction. This range is sufficient to overcome the limitation of the small viewing angles, which might lead to imprecise results in the reconstruction technique. However, for the beads studied on the tectorial membrane, it was not possible to align the preparations perfectly during the measurements, or to set the z direction exactly perpendicular to the basilar membrane in the original position before the measurements were made. Therefore, we could not provide exact details of the direction of the vibration with respect to the geometry of the organ of Corti as well as Hemmert et al. (Hemmert et al. 2000) did. However, by taking care to set up each preparation in the beginning, the result of the major motion of the observed point on the TM combined with the picture of the organ of Corti is enough to show the major function of the TM in 3-D space.

The technique used here provides the possibility to study the vibrations of the organ of Corti *in vivo* as well as *post mortem* and keeps the organ of Corti in an integrated working condition. The mixture of the perilymph and the endolymph hardly changed the tuning shape of the cochlear partition, but it does change the whole system into a linear system (discussed in chapter 6). This is nearly the best we can do to study the cochlear mechanics

in near normal conditions. Even though the temporal-bone preparation (Hemmert et al. 2000) has some advantage for studying cochlear mechanisms, all of the recordings are from *in vitro* conditions and these are hard to compare with the *in vivo* results.

The present measurements indicate that at frequencies below the cutoff value, the vibration of the TM in response to pure-tone pips occurs along almost rectilinear paths along the z direction. It seems that the TM at these frequencies moves in a simple way, following the vibration of the organ of Corti, rather than possessing an additional vibration mode, resonating in the radial direction (Zwislocki 1979; Allen 1980; Gummer et al. 1996; Hemmert et al. 2000). For the frequencies above the cut-off value, the motion appears to change into some form of ellipse and became more complicated, but with much smaller amplitudes. No significant difference between the tuning curve shapes of HCs and the TM further confirmed that the organ of Corti moves as an integrated unit during the sound delivery. This conclusion is consistent with the results of Ulfendahl (Ulfendahl et al. 1995), and does not support modern theories that the TM resonates to form a second filter inside the cochlea.

Chapter 9 Conclusion

Summarizing some of the most interesting findings in this thesis may produce a more complete picture of the cochlear mechanics of the apical turn *in vivo* and the function of the tectorial membrane.

Firstly, the direct approach to the apical turn of the cochlea *in vivo* can be done with little hearing loss, but the whole process has to be approached with extreme care. The more extensive surgery does not cause any damage to the hearing although it may temporarily change the local blood supply of the brain. Opening the bulla from the ventral side appears easy to perform during the approach, but *it causes hearing* losses in the most sensitive range of frequencies for the guinea-pig. However, opening the bulla does not affect the hearing in the low frequency range we are interested in. Opening the cochlea is the most delicate step during the procedure, and this may cause local hearing damage directly from the opening. This local hearing loss can be avoided by taking great care and keeping Reissner's membrane and helicotrema intact. Tearing the RM does not seem to cause an immediate hearing loss. However, further hearing losses develop progressively after tearing the RM, possibly due to the mixture of the perilymph and endolymph which will change the ionic concentration of the scala media. Therefore, the experiments in the apical turn of the cochlea have to be performed as quickly as possible.

Secondly, the opening of the cochlea does affect the mechanics in some way. The most striking feature is the introduction of an artifact known as the fast component into the mechanics. The fast component is highly correlated to the opening condition. The fast component can be as big in amplitude as 2/3 of that of the slow traveling wave in an open cochlea, and it extends over 2 ms so that it merges with the slow wave. Therefore, in an open cochlea, the interacting of the fast and the slow component can lead to a remarkable notch in the tuning curve. The fast component can be avoided by making a mechanical sealing of the cochlea. Under sealed conditions, the fast component can be as small as only 4% of that of the slow wave, it finishes within 2 ms, and it can be easily separated from the slow component in the time domain. Therefore, we can imagine that in the real cochlea, there is no fast wave traveling along the cochlear partition. It is the slow wave which

transfers the mechanical energy to excite the cochlea partition and which is the source of the micromechanics of the cochlea.

Thirdly, strong baseline position *shifts were* observed in the intact cochleae *in vivo*. This provides evidence that distinguished the apex from the basal part of the cochlea. The sound-evoked responses in the apex of the cochlea consist of both baseline position shifts (dc component) and oscillatory responses (ac component). The baseline position shifts are always towards the scala vestibuli. They are highly compressive and saturate at high stimulus intensity (80-90 dB SPL). Their displacement sensitivities can be as high as that of the oscillatory responses. And they are physiological vulnerable, since they disappear after tearing the RM and *post mortem*. The baseline position shifts are supposed to be responsible for the non-interleaving feature observed in the low-frequency nerve fibers.

Fourthly, weak compressive nonlinearity was observed in the oscillatory responses of the apex when the scala media was intact. The strongest compressive nonlinearity occurred at low frequencies (25, 50 and 75 Hz). The tuning curves of the oscillatory responses *in the* apex behave as low-pass filters rather than band-pass in the basal of the cochlea with the Q_{10} value of 0.5-0.6 under sealed condition. The experimental recordings fit the positive feedback model very well. This suggests that the apical turn of the cochlea acts in the same way as the basal turn of the cochlea in delivery sound to the cochlear partition. There are not two cochleae in one cochlear tube.

Fifthly, tearing the RM causes the loss of the baseline position shifts as well as the compressive nonlinearity in the oscillatory responses. Therefore, after tearing the RM, recordings are all collected in a linear system. The tectorial membrane responses are nearly the same as that of the HCs recorded under the same condition apart from with lower amplitude. A radial gradient in amplitude has been observed in the cochlear partition response to sound. The HCs present the highest response in amplitude, while the inner part of the tectorial membrane presents lower response in amplitude. It seems that the responses can be kept stable within half hour after *post mortem* and then decrease with time. Imagining that the tectorial membrane could be measured directly in an intact cochlea, the baseline position shifts and compressive nonlinear oscillatory responses should be observed as well.

Finally, the organ of Corti moves in three-dimensional space as an integrated unit. The HCs move mainly transversely, simply following the expected pattern of the basilar membrane's motion. The heads of the HCs seem to move around their resting positions, but the maximum amplitude is only 1/4 of that of the transverse amplitude. This is probably due to the dragging of the viscous force produced by of the fluid's movements between the tectorial membrane and the reticular lamina. The tectorial membrane overlying the OHCs is moving in a similar pattern as the HCs, with its motion mainly along the transverse direction, nearly perpendicular to the reticular lamina plane. The radial motion is nearly along the direction of the tectorial membrane's 'radial' fibres. The part of the tectorial membrane on top of the IHCs appears to move less in the transverse direction than that of the radial direction. The radial motion is still along the fibers' direction of the TM. Supposing this difference due to the motility of the OHCs. The elongation and contraction of the OHCs may enhance the driving force of the basilar membrane, so that the TM in this region mainly moves transversely in the same time when the TM deflecting the stereocilia of the OHCs. Without the OHCs's motility and less driven force from the basilar membrane in the IHC's region, the TM mainly fulfills the shearing motion relative to the reticular lamina to excite the sensory cells instead. This description of the vibration mode of the organ of Corti in three-dimensional space does not support that the TM resonates to forms a second filter inside the cochlea.

In conclusion, the present study has sheds a light on the cochlear mechanics of the apex, especially on the function of the TM *in vivo*. It is sincerely hoped that these studies may act to inspire further research on the cochlear mechanics *in vivo*.

Reference

Abbas, P. J. and M. P. Gorga (1981). "AP responses in forward-masking paradigms and their relationship to responses of auditory-nerve fibers." J Acoust Soc Am 69(2): 492-9.

Abnet, C. C. and D. M. Freeman (2000). "Deformations of the isolated mouse tectorial membrane produced by oscillatory forces." Hear Res 144(1-2): 29-46.

Allen, J. B. (1980). "Cochlear micromechanics--a physical model of transduction." J Acoust Soc Am 68(6): 1660-70.

Anderson, D. J.et al. (1971). "Temporal position of discharges in single auditory nerve fibers within the cycle of a *sine*-wave stimulus: frequency and intensity effects." J Acoust Soc Am 49(4): Suppl 2:1131+.

Bohne, B. A. and C. D. Carr (1985). "Morphometric analysis of hair cells in the chinchilla cochlea." J Acoust Soc Am 77(1): 153-8.

Brown, M. C.et al. (1983). "Cochlear inner hair cells: effects of transient asphyxia on intracellular potentials." Hear Res 9(2): 131-44.

Brown, M. C.et al. (1983). "Anesthesia and surgical trauma: their influence on the guinea pig compound action potential." Hear Res 10(3): 345-58.

Brown, M. C.et al. (1983). "The temperature dependency of neural and hair cell responses evoked by high frequencies." J Acoust Soc Am 73(5): 1662-70.

Brownell, W. E.et al. (1985). "Evoked mechanical responses of isolated cochlear outer hair cells." Science 227(4683): 194-6.

Brundin, L.et al. (1992). "The tuned displacement response of the hearing organ is generated by the outer hair cells." Neuroscience 49(3): 607-16.

Brundin, L.et al. (1992). "Sound induced displacement response of the guinea pig hearing organ and its relation to the cochlear potentials." Hear Res 58(2): 175-84.

Bruns, V.et al. (1988). "Inner ear structure and electrophysiological audiograms of the subterranean mole rat, Spalax ehrenbergi." Hear Res 33(1): 1-9.

Butler, R. A., Konishi, T., and Fernandez, C. (1960). "Temperature coefficients of cochlear potentials." Am. J. Physiol. 199: 688 - 692.

Cabezudo, L. M. (1978). "The ultrastructure of the basilar membrane in the cat." Acta Otolaryngol 86(3-4): 160-75.

Carney, L. H. and T. C. Yin (1988). "Temporal coding of resonances by low-frequency auditory nerve fibers: single-fiber responses and a population model." J Neurophysiol 60(5): 1653-77.

Cheatham, M. A. and P. Dallos (1994). "Stimulus biasing: a comparison between cochlear hair cell and organ of Corti response patterns." Hear Res 75(1-2): 103-13.

Cody, A. R. and I. J. Russell (1988). "Acoustically induced hearing loss: intracellular studies in the guinea pig cochlea." Hear Res 35(1): 59-70.

Cooper, N. P. (1996). Mid-band sensitivity notches in apical cochlear mechanics. Diversity in Auditory Mechanics., World Scientific, Singapore: 298-304.

Cooper, N. P. (1996). "Two-tone suppression in cochlear mechanics." J Acoust Soc Am 99(5): 3087-98.

Cooper, N. P. (1998). "Harmonic distortion on the basilar membrane in the basal turn of the guinea-pig cochlea." J Physiol 509(Pt 1): 277-88.

Cooper, N. P. (1999). "An improved heterodyne laser interferometer for use in studies of cochlear mechanics." J Neurosci Methods 88(1): 93-102.

Cooper, N. P. (1999). "Vibration of beads placed on the basilar membrane in the basal turn of the cochlea." J Acoust Soc Am 106(6): L59-64.

Cooper, N. P. and W. S. Rhode (1992). "Basilar membrane mechanics in the hook region of cat and guinea-pig cochleae: sharp tuning and nonlinearity in the absence of baseline position shifts." Hear Res 63(1-2): 163-90.

Cooper, N. P. and W. S. Rhode (1992). "Basilar membrane tonotopicity in the hook region of the cat cochlea." Hear Res 63(1-2): 191-6.

Cooper, N. P. and W. S. Rhode (1995). "Nonlinear mechanics at the apex of the guinea-pig cochlea." Hear Res 82(2): 225-43.

Cooper, N. P. and W. S. Rhode (1996). "Fast travelling waves, slow travelling waves and their interactions in experimental studies of apical cochlear mechanics." Audit. Neurosci 2: 289-299.

Cooper, N. P. and W. S. Rhode (1997). "Mechanical responses to two-tone distortion products in the apical and basal turns of the mammalian cochlea." J Neurophysiol 78(1): 261-70.

Cooper, N. P.et al. (1993). "Cochlear nerve fiber responses to amplitude-modulated stimuli: variations with spontaneous rate and other response characteristics." J Neurophysiol 70(1): 370-86.

Dallos, P. (1973). "The Auditory Periphery." Academic Press, New York: 228-288.

Dallos, P. (1986). "Neurobiology of cochlear inner and outer hair cells: intracellular recordings." Hear Res 22: 185-98.

Dallos, P.et al. (1972). "Cochlear inner and outer hair cells: functional differences." Science 177(46): 356-8.

Dallos, P. and M. A. Cheatham (1976). "Compound action potential (AP) tuning curves." J Acoust Soc Am 59(3): 591-7.

Dallos, P. and M. A. Cheatham (1976). "Production of cochlear potentials by inner and outer hair cells." J Acoust Soc Am 60(2): 510-2.

Dallos, P.et al. (1974). "Cochlear mechanics, nonlinearities, and cochlear potentials." J Acoust Soc Am 55(3): 597-605.

Dallos, P. and J. D. Durrant (1972). "On the derivative relationship between stapes movement and cochlear microphonic." J Acoust Soc Am 52(4): 1263-5.

Dallos, P. and B. N. Evans (1995). "High-frequency motility of outer hair cells and the cochlear amplifier." Science 267(5206): 2006-9.

Dallos, P.et al. (1978). "Behavioral, compound action potential, and single unit thresholds: relationship in normal and abnormal ears." J Acoust Soc Am 64(1): 151-7.

Dallos, P.et al. (1972). "Cochlear summating potentials. Descriptive aspects." Acta Otolaryngol Suppl 302: 1-46.

Dallos, P. and C. Y. Wang (1974). "Bioelectric correlates of kanamycin intoxication." Audiology 13(4): 277-89.

Dancer, A. and R. Franke (1980). "Intracochlear sound pressure measurements in guinea pigs." Hear Res 2(3-4): 191-205.

Davis, H., Deatherage, B.H., Eldredge, D.H.. Smith, C.A. (1958). "Summating potentials of the cochlea." Am. J. Physiol. 195: 251 - 261.

Davis, H. (1965). "A model for transducer action in the cochlea." Cold Spring Harb Symp Quant Biol 30: 181-90.

Davis, H. (1983). "An active process in cochlear mechanics." Hear Res 9(1): 79-90.

de Boer, E. (1996). Mechanics of the Cochlea: Modeling Effects. The Cochlea. P. Dallo , Popper, A.N., Fay, R.R. New York, Springer-Verlag: 258-317.

Decraemer, W. F.et al. (1994). "A method for determining three-dimensional vibration in the ear." Hear Res 77(1-2): 19-37.

Dong, W. and N. P. Cooper (2001). Modeling baseline position shifts on the cochlear partition as the basis of non-interleaving click responses in the auditory nerve. 2001 ARO MidWinter Meeting.

Dragsten, P. R.et al. (1976). "Light-scattering heterodyne interferometer for vibration measurements in auditory organs." J Acoust Soc Am 60(3): 665-71.

Echteleler, S. M., Fay, R.R. and Popper, A.N. (1994). Structure of the Mammalian Cochlea. Comparative Hearing: Mammals. R. R. Fay, Popper, A.N. New York, Springer-Verlag. 4: 134-171.

Edge, R. M.et al. (1998). "Morphology of the unfixed cochlea." Hear Res 124(1-2): 1-16.

Eggermont, J. J. (1974). "The temperature dependency of cochlear adaptation and masking in the guinea pig." Audiology 13(2): 147-61.

Evans, E. F. (1972). "The frequency response and other properties of single fibres in the guinea-pig cochlear nerve." J Physiol 226(1): 263-87.

Frank, G.et al. (1999). "Limiting dynamics of high-frequency electromechanical transduction of outer hair cells." Proc Natl Acad Sci U S A 96(8): 4420-5.

Freeman, D. M.et al. (1994). "The osmotic response of the isolated tectorial membrane of the chick to isosmotic solutions: effect of Na+, K+, and Ca2+ concentration." Hear Res 79(1-2): 197-215.

Geisler, D. C. (1998). From sound to synapse - physiology of the mammalian ear. New York, Oxford University Press.

Gorga, M. P. and P. J. Abbas (1981). "Forward-masking AP tuning curves in normal and in acoustically traumatized ears." J Acoust Soc Am 70(5): 1322-30.

Gummer, A. W.et al. (1993). Micromechanics of cellular structures in the mammalian cochlea: Auditory and electrical stimulation. Great Yarmouth, England, Pergamon.

Gummer, A. W.et al. (1996). "Resonant tectorial membrane motion in the inner ear: its crucial role in frequency tuning." Proc Natl Acad Sci U S A 93(16): 8727-32.

Hao, L. F. and S. M. Khanna (1996). "Reissner's membrane vibrations in the apical turn of a living guinea pig cochlea." Hear Res 99(1-2): 176-89.

Harris, D. M. and P. Dallos (1979). "Forward masking of auditory nerve fiber responses." J Neurophysiol 42(4): 1083-1107.

Harrison, R. V. (1981). "Rate-versus-intensity functions and related AP responses in normal and pathological guinea pig and human cochleas." J Acoust Soc Am 70(4): 1036-44.

Harrison, R. V.et al. (1981). "AP tuning curves from normal and pathological human and guinea pig cochleas." J Acoust Soc Am 69(5): 1374-85.

Harvey, D. and K. P. Steel (1992). "The development and interpretation of the summating potential response." Hear Res 61(1-2): 137-46.

Hasko, J. A. and G. P. Richardson (1988). "The ultrastructural organization and properties of the mouse tectorial membrane matrix." Hear Res 35(1): 21-38.

Heffner, R.et al. (1971). "Behavioral measurements of absolute and frequency-difference thresholds in guinea pig." J Acoust Soc Am 49(6): 1888-95.

Hemmert, W.et al. (2000). "Characteristics of the travelling wave in the low-frequency region of a temporal-bone preparation of the guinea-pig cochlea." Hear Res 142(1-2): 184-202.

Hemmert, W.et al. (2000). "Three-dimensional motion of the organ of Corti." Biophys J 78(5): 2285-97.

Henson, M. M.et al. (1982). "The cells of Boettcher in the bat, Pteronotus p. parnellii." Hear Res 7(1): 91-103.

Henson, M. M.et al. (1983). "Sustentacular cells of the organ of Corti--the tectal cells of the outer tunnel." Hear Res 10(2): 153-66.

Holley, M. C. (1996). Outer Hair Cell Motility. The Cochlea. P. Dallo , Popper, A.N., Fay, R.R. New York, Springer-Verlag: 386-434.

Holley, M. C. and J. F. Ashmore (1988). "A cytoskeletal spring in cochlear outer hair cells." Nature 335(6191): 635-7.

Hoshino, T. (1974). "Relationship of the tectorial membrane on the organ of Corti. A scanning electron microscope study of cats and guinea pigs." Arch Histol Jpn 37(1): 25-39.

Hoshino, T. (1976). "Attachment of the inner sensory cell hairs to the tectorial membrane. A scanning electron microscopic study." ORL J Otorhinolaryngol Relat Spec 38(1): 11-8.

Hoshino, T. (1977). "Contact between the tectorial membrane and the cochlear sensory hairs in the human and the monkey." Arch Otorhinolaryngol 217(1): 53-60.

Hoshino, T. (1981). "Imprints of the inner sensory cell hairs on the human tectorial membrane." Arch Otorhinolaryngol 232(1): 65-71.

Hudspeth, A. J. and D. P. Corey (1977). "Sensitivity, polarity, and conductance change in the response of vertebrate hair cells to controlled mechanical stimuli." Proc Natl Acad Sci U S A 74(6): 2407-11.

Johnsson, L. G.et al. (1979). "Bilateral cochlear implants: histological findings in a pair of temporal bones." Laryngoscope 89(5 Pt 1): 759-62.

Johnstone, B. M.et al. (1986). "Basilar membrane measurements and the travelling wave." Hear Res 22: 147-53.

Johnstone, J. R.et al. (1979). "CAP threshold and single unit thresholds." J Acoust Soc Am 65(1): 254-257.

Johnstone, J. R.et al. (1979). "Cochlear action potential threshold and single unit thresholds." J Acoust Soc Am 65(1): 254-7.

Khalkhali-Ellis, Z.et al. (1987). "Glycoconjugates of the tectorial membrane." Hear Res 25(2-3): 185-91.

Khanna, S. M.et al. (1989). "Changes in cellular tuning along the radial axis of the cochlea." Acta Otolaryngol Suppl 467: 163-73.

Khanna, S. M. and L. F. Hao (1999). "Nonlinearity in the apical turn of living guinea pig cochlea." Hear Res 135(1-2): 89-104.

Khanna, S. M. and L. F. Hao (1999). "Reticular lamina vibrations in the apical turn of a living guinea pig cochlea." Hear Res 132(1-2): 15-33.

Khanna, S. M. and L. F. Hao (2000). "Amplification in the apical turn of the cochlea with negative feedback." Hear Res 149(1-2): 55-76.

Khanna, S. M. and D. G. Leonard (1982). "Basilar membrane tuning in the cat cochlea." Science 215(4530): 305-6.

Khanna, S. M.et al. (1989). "Mechanical tuning characteristics of outer hair cells and Hensen's cells." Acta Otolaryngol Suppl 467: 139-44.

Khanna, S. M.et al. (1989). "Modes of cellular vibration in the organ of Corti." Acta Otolaryngol Suppl 467: 183-8.

Khanna, S. M.et al. (1998). "Vibration of reflective beads placed on the basilar membrane." Hear Res 116(1-2): 71-85.

Khanna, S. M.et al. (1989). "Measurement of optical reflectivity in cells of the inner ear." Acta Otolaryngol Suppl 467: 69-75.

Kiang (1965). "Discharge patterns of single fibers in the cat's auditory nerve." Research Monograph No. 35 (MIT, Cambridge, MA).

Kiang, N. Y. and E. C. Moxon (1974). "Tails of tuning curves of auditory-nerve fibers." J Acoust Soc Am 55(3): 620-30.

Kiang, N. Y.et al. (1967). "Shapes of tuning curves for single auditory-nerve fibers." J Acoust Soc Am 42(6): 1341-2.

Killick, R.et al. (1995). "Molecular cloning of chick beta-tectorin, an extracellular matrix molecule of the inner ear." J Cell Biol 129(2): 535-47.

Killick, R. and G. P. Richardson (1997). "Antibodies to the sulphated, high molecular mass mouse tectorin stain hair bundles and the olfactory mucus layer." Hear Res 103(1-2): 131-41.

Kimura, R. S. (1966). "Hairs of the cochlear sensory cells and their attachment to the tectorial membrane." Acta Otolaryngol 61(1): 55-72.

Kimura, R. S. (1975). "The ultrastructure of the organ of Corti." Int Rev Cytol 42: 173-222.

Kossl, M. and I. J. Russell (1995). "Basilar membrane resonance in the cochlea of the mustached bat." Proc Natl Acad Sci U S A 92(1): 276-9.

Kraus, H.et al. (1973). "[Interferometric measurements of the density in the aging of the basilar and tectorial membrane of the guinea pig]." Arch Klin Exp Ohren Nasen Kehlkopfheilkd 204(2): 115-21.

Kraus, H. J. and K. Aulbach-Kraus (1981). "Morphological changes in the cochlea of the mouse after the onset of hearing." Hear Res 4(1): 89-102.

Kronester-Frei, A. (1978). "Ultrastructure of the different zones of the tectorial membrane." Cell Tissue Res 193(1): 11-23.

Kronester-Frei, A. (1979). "The effect of changes in endolymphatic ion concentrations on the tectorial membrane." Hear Res 1(2): 81-94.

Kronester-Frei, A. (1979). "Localization of the marginal zone of the tectorial membrane in situ, unfixed, and with in vivo-like ionic milieu." Arch Otorhinolaryngol 224(1-2): 3-9.

Kros, C. J. (1996). Hair Cell Physiology. The Cochlea. P. Dallo , Popper, A.N., Fay, R.R. New York, Springer-Verlag: 318-385.

Kros, C. J.et al. (1992). "Mechano-electrical transducer currents in hair cells of the cultured neonatal mouse cochlea." Proc R Soc Lond B Biol Sci 249(1325): 185-93.

Le Page, E. L. and B. M. Johnstone (1980). "Nonlinear mechanical behaviour of the basilar membrane in the basal turn of the guinea pig cochlea." Hear Res 2(3-4): 183-9.

Legan, P. K.et al. (2000). "A targeted deletion in alpha-tectorin reveals that the tectorial membrane is required for the gain and timing of cochlear feedback." Neuron 28(1): 273-85.

Legan, P. K.et al. (1997). "The mouse tectorins. Modular matrix proteins of the inner ear homologous to components of the sperm-egg adhesion system." J Biol Chem 272(13): 8791-801.

LePage, E. L. (1987). "Frequency-dependent self-induced bias of the basilar membrane and its potential for controlling sensitivity and tuning in the mammalian cochlea." J Acoust Soc Am 82(1): 139-54.

LePage, E. L. (1989). "Functional role of the olivo-cochlear bundle: a motor unit control system in the mammalian cochlea." Hear Res 38(3): 177-98.

Liberman, M. C. and W. Y. Gao (1995). "Chronic cochlear de-efferentation and susceptibility to permanent acoustic injury." Hear Res 90(1-2): 158-68.

Lim, D. J. (1972). "Fine morphology of the tectorial membrane. Its relationship to the organ of Corti." Arch Otolaryngol 96(3): 199-215.

Lim, D. J. (1980). "Cochlear anatomy related to cochlear micromechanics. A review." J Acoust Soc Am 67(5): 1686-95.

Lim, D. J. (1986). "Functional structure of the organ of Corti: a review." Hear Res 22: 117-46.

Lim, D. J. and M. Anniko (1985). "Developmental morphology of the mouse inner ear. A scanning electron microscopic observation." Acta Otolaryngol Suppl 422: 1-69.

Lin, T. and J. J. Guinan, Jr. (2000). "Auditory-nerve-fiber responses to high-level clicks: interference patterns indicate that excitation is due to the combination of multiple drives." J Acoust Soc Am 107(5 Pt 1): 2615-30.

Mammano, F. and J. F. Ashmore (1995). "A laser interferometer for sub-nanometre measurements in the cochlea." J Neurosci Methods 60(1-2): 89-94.

Manley, G. A. and B. M. Johnstone (1974). "Middle-ear function in the guinea pig." J Acoust Soc Am 56(2): 571-6.

Margolis, R. H.et al. (1992). "Tympanic electrocochleography: normal and abnormal patterns of response." Audiology 31(1): 8-24.

McMullen, T. A. and D. C. Mountain (1985). "Model of d.c. potentials in the cochlea: effects of voltage-dependent cilia stiffness." Hear Res 17(2): 127-41.

Meyer zum Gottesberge, A. M. and S. Tsujikawa (1993). "Glycerol effect on the guinea pig tectorial membrane." Eur Arch Otorhinolaryngol 250(2): 88-91.

Munyer, P. D. and B. A. Schulte (1991). "Immunohistochemical identification of proteoglycans in gelatinous membranes of cat and gerbil inner ear." Hear Res 52(2): 369-78.

Murugasu, E. and I. J. Russell (1996). "The effect of efferent stimulation on basilar membrane displacement in the basal turn of the guinea pig cochlea." J Neurosci 16(1): 325-32.

Naftalin, L. (1976). "The peripheral hearing mechanism: a biochemical and biological approach." Ann Otol Rhinol Laryngol 85(1 Pt 1): 38-42.

Narayan, S. S.et al. (1998). "Frequency tuning of basilar membrane and auditory nerve fibers in the same cochleae." Science 282(5395): 1882-4.

Nedzelnitsky, V. (1980). "Sound pressures in the basal turn of the cat cochlea." J Acoust Soc Am 68(6): 1676-89.

Neely, S. T. and D. O. Kim (1986). "A model for active elements in cochlear biomechanics." J Acoust Soc Am 79(5): 1472-80.

Nuttall, A. L. and D. F. Dolan (1996). "Steady-state sinusoidal velocity responses of the basilar membrane in guinea pig." J Acoust Soc Am 99(3): 1556-65.

Nuttall, A. L.et al. (1997). "Basilar membrane velocity noise." Hear Res 114(1-2): 35-42.

Nuttall, A. L.et al. (1981). "Does loud sound influence the intracochlear oxygen tension?" Hear Res 5(2-3): 285-93.

Olson, E. S. (1998). "Observing middle and inner ear mechanics with novel intracochlear pressure sensors." J Acoust Soc Am 103(6): 3445-63.

O'Neill, M. P. and A. Bearden (1995). "Laser-feedback measurements of turtle basilar membrane motion using direct reflection." Hear Res 84(1-2): 125-38.

Orman, S. and A. Flock (1983). "Active control of sensory hair mechanics implied by susceptibility to media that induce contraction in muscle." Hear Res 11(3): 261-6.

Patuzzi, R. (1996). Cochlear Micromechanics and Macromechanics. The Cochlea. P. Dallo , Popper, A.N., Fay, R.R. New York, Springer-Verlag. 8: 186-257.

Patuzzi, R. and P. M. Sellick (1983). "The alteration of the low frequency response of primary auditory afferents by cochlear trauma." Hear Res 11(2): 125-32.

Patuzzi, R. B. and G. K. Yates (1987). "The low-frequency response of inner hair cells in the guinea pig cochlea: implications for fluid coupling and resonance of the stereocilia." Hear Res 30(1): 83-98.

Patuzzi, R. B.et al. (1989). "Changes in cochlear microphonic and neural sensitivity produced by acoustic trauma." Hear Res 39(1-2): 189-202.

Patuzzi, R. B.et al. (1989). "The origin of the low-frequency microphonic in the first cochlear turn of guinea-pig." Hear Res 39(1-2): 177-88.

Pfeiffer, R. R. and D. O. Kim (1972). "Response patterns of single cochlear nerve fibers to click stimuli: descriptions for cat." J Acoust Soc Am 52(6): 1669-77.

Preyer, S.et al. (1994). "Frequency response of mature guinea-pig outer hair cells to stereociliary displacement." Hear Res 77(1-2): 116-24.

Prieto, J. J.et al. (1990). "Localization of anionic sulfate groups in the tectorial membrane." Hear Res 45(3): 283-93.

Recio, A.et al. (1998). "Basilar-membrane responses to clicks at the base of the chinchilla cochlea." J Acoust Soc Am 103(4): 1972-89.

Rhode, W. S. (1971). "Observations of the vibration of the basilar membrane in squirrel monkeys using the Mossbauer technique." J Acoust Soc Am 49(4): Suppl 2:1218+.

Rhode, W. S. (1974). "Measurement of vibration of the basilar membrane in the squirrel monkey." Ann Otol Rhinol Laryngol 83(5): 619-25.

Rhode, W. S. (1978). "Some observations on cochlear mechanics." J Acoust Soc Am 64(1): 158-76.

Rhode, W. S. (1980). "Cochlear partition vibration--recent views." J Acoust Soc Am 67(5): 1696-703.

Rhode, W. S., and Cooper, N.P. (1996). "Nonlinear mechanics in the apical turn of the chinchilla cochlea in vivo." Auditory Neurosci 3: 101-121.

Rhode, W. S. and C. D. Geisler (1967). "Model of the displacement between opposing points on the tectorial membrane and reticular lamina." J Acoust Soc Am 42(1): 185-90.

Richardson, G. P.et al. (1987). "Polypeptide composition of the mammalian tectorial membrane." Hear Res 25(1): 45-60.

Robles, L.et al. (1976). "Transient response of the basilar membrane measured in squirrel monkeys using the Mossbauer effect." J Acoust Soc Am 59(4): 926-39.

Robles, L. and M. A. Ruggero (2001). "Mechanics of the mammalian cochlea." Physiol Rev 81(3): 1305-52.

Robles, L.et al. (1986). "Basilar membrane mechanics at the base of the chinchilla cochlea. I. Input-output functions, tuning curves, and response phases." J Acoust Soc Am 80(5): 1364-74.

Robles, L.et al. (1991). "Two-tone distortion in the basilar membrane of the cochlea." Nature 349(6308): 413-4.

Robles, L.et al. (1997). "Two-tone distortion on the basilar membrane of the chinchilla cochlea." J Neurophysiol 77(5): 2385-99.

Rose, C. and T. F. Weiss (1988). "Frequency dependence of synchronization of cochlear nerve fibers in the alligator lizard: evidence for a cochlear origin of timing and non- timing neural pathways." Hear Res 33(2): 151-65.

Rosowski, J. J. (1994). Outer and Middle Ears. Comparative Hearing: Mammals. R. R. a. P. Fay, A.N. New York, Springer Ver-lag. 4: 172-248.

Ross, M. D. (1974). "The tectorial membrane of the rat." Am J Anat 139(4): 449-81.

Roth, B. and V. Bruns (1992). "Postnatal development of the rat organ of Corti. I. General morphology, basilar membrane, tectorial membrane and border cells." Anat Embryol 185(6): 559-69.

Ruggero, M. A. (1992). "Responses to sound of the basilar membrane of the mammalian cochlea." Curr Opin Neurobiol 2(4): 449-56.

Ruggero, M. A. and N. C. Rich (1991). "Application of a commercially-manufactured Doppler-shift laser velocimeter to the measurement of basilar-membrane vibration." Hear Res 51(2): 215-30.

Ruggero, M. A. and N. C. Rich (1991). "Furosemide alters organ of corti mechanics: evidence for feedback of outer hair cells upon the basilar membrane." J Neurosci 11(4): 1057-67.

Ruggero, M. A.et al. (1997). "Basilar-membrane responses to tones at the base of the chinchilla cochlea." J Acoust Soc Am 101(4): 2151-63.

Ruggero, M. A.et al. (1990). "Middle-ear response in the chinchilla and its relationship to mechanics at the base of the cochlea." J Acoust Soc Am 87(4): 1612-29.

Ruggero, M. A.et al. (1992). "Two-tone suppression in the basilar membrane of the cochlea: mechanical basis of auditory-nerve rate suppression." J Neurophysiol 68(4): 1087-99.

Ruggero, M. A.et al. (1992). "Basilar membrane responses to two-tone and broadband stimuli." Philos Trans R Soc Lond B Biol Sci 336(1278): 307-14; discussion 314-5.

Russell, I. J. and M. Kossl (1992). "Modulation of hair cell voltage responses to tones by low-frequency biasing of the basilar membrane in the guinea pig cochlea." J Neurosci 12(5): 1587-601.

Russell, I. J. and K. E. Nilsen (1997). "The location of the cochlear amplifier: spatial representation of a single tone on the guinea pig basilar membrane." Proc Natl Acad Sci U S A 94(6): 2660-4.

Russell, I. J. and P. M. Sellick (1978). "Intracellular studies of hair cells in the mammalian cochlea." J Physiol 284: 261-90.

Russell, I. J. and P. M. Sellick (1983). "Low-frequency characteristics of intracellularly recorded receptor potentials in guinea-pig cochlear hair cells." J Physiol 338: 179-206.

Saito, H. and J. F. Daly (1970). "Quantitative analysis of acid mucopolysaccharides in the normal guinea pig cochlea." Acta Otolaryngol (Stockh) 69(5): 333-40.

Santi, P. A.et al. (1990). "Ultrastructure of proteoglycans in the tectorial membrane." J Electron Microsc Tech 15(3): 293-300.

Sellick, P. M.et al. (1982). "Measurement of basilar membrane motion in the guinea pig using the Mossbauer technique." J Acoust Soc Am 72(1): 131-41.

Sellick, P. M.et al. (1982). "Modulation of responses of spiral ganglion cells in the guinea pig cochlea by low frequency sound." Hear Res 7(2): 199-221.

Sellick, P. M. and I. J. Russell (1980). "The responses of inner hair cells to basilar membrane velocity during low frequency auditory stimulation in the guinea pig cochlea." Hear Res 2(3-4): 439-45.

Shah, D. M.et al. (1995). "The osmotic response of the isolated, unfixed mouse tectorial membrane to isosmotic solutions: effect of Na+, K+, and Ca2+ concentration." Hear Res 87(1-2): 187-207.

Silman, S. (1984). The Acoustic Reflex: Basic Principles and Clinical Applications, New York: Academicc Press.

Slepecky, N. B. (1996). Structure of the Mammalian Cochlea. The Cochlea. P. Dallo, Popper, A.N., Fay, R.R. New York, Springer-Verlag. 8: 44-129.

Slepecky, N. B.et al. (1992). "Type II and type IX collagen form heterotypic fibers in the tectorial membrane of the inner ear." Matrix 12(1): 80-6.

Slepecky, N. B.et al. (1992). "Electron-microscopic localization of type II, IX, and V collagen in the organ of Corti of the gerbil." Cell Tissue Res 267(3): 413-8.

Slepecky, N. B.et al. (1992). "Localization of type II, IX and V collagen in the inner ear." Acta Otolaryngol 112(4): 611-7.

Smith, C. A. (1968). "Ultrastructure of the organ of Corti." Adv Sci 24(122): 419-33.

Spicer, S. S. and B. A. Schulte (1994). "Ultrastructural differentiation of the first Hensen cell in the gerbil cochlea as a distinct cell type." Anat Rec 240(2): 149-56.

Spoendlin, H. (1971). "Primary structural changes in the organ of Corti after acoustic overstimulation." Acta Otolaryngol (Stockh) 71(2): 166-76.

Steel, K. (1980). "The proteins of normal and abnormal tectorial membranes." Acta Otolaryngol 89(1-2): 27-32.

Steel, K. P. (1983). "Donnan equilibrium in the tectorial membrane." Hear Res 12(2): 265-72.

Steel, K. P. (1983). "The tectorial membrane of mammals." Hear Res 9(3): 327-59.

Steel, K. P. (1985). Composition and properties of the mammals' tectorial membrane. In auditory Biochemistry. D. G. Drescher. New York, Raven Press.

Steel, K. P. (1986). Tectorial membrane. Neurobiology of hearing: The cochlea. D. W. Altschuler, Hoffman and Robbin, R.P. New York, Raven Press: 139-148.

Strelioff, D. and A. Flock (1984). "Stiffness of sensory-cell hair bundles in the isolated guinea pig cochlea." Hear Res 15(1): 19-28.

Sugiyama, S.et al. (1992). "Ultrastructural localization and semiquantitative analysis of glycoconjugates in the tectorial membrane." Hear Res 58(1): 35-46.

Tasaki, I. (1954). "Nerve impulses in individual auditory nerve fibers of guinea pig." J. Neurophysiol. 17: 97-122.

Teas, D. C., Eldredge, D.H. and Davis, H. (1962). "Cochlear responses to acoustic transients. An interpretation of whole nerve action potentials." J. Acoust. Soc. Am 24: 1431-1459.

Thalmann, I. (1993). "Collagen of accessory structures of organ of Corti." Connect Tissue Res 29(3): 191-201.

Thalmann, I.et al. (1986). "Collagen--the predominant protein of the tectorial membrane." ORL J Otorhinolaryngol Relat Spec 48(2): 107-15.

Thalmann, I.et al. (1987). "Composition and supramolecular organization of the tectorial membrane." Laryngoscope 97(3 Pt 1): 357-67.

Thalmann, R. and I. Thalmann (1987). "Role of amino acids in the inner ear with special reference to tectorial membrane." Adv Otorhinolaryngol 37: 5-10.

Tilanus, C. C.et al. (1992). "Effects of anoxia on the cochlear summating potential in the guinea pig." Eur Arch Otorhinolaryngol 249(1): 12-5.

Tsuprun, V. and P. Santi (1996). "Crystalline arrays of proteoglycan and collagen in the tectorial membrane." Matrix Biol 15(1): 31-8.

Tsuprun, V. and P. Santi (1997). "Ultrastructural organization of proteoglycans and fibrillar matrix of the tectorial membrane." Hear Res 110(1-2): 107-18.

Ulfendahl, M. (1997). "Mechanical responses of the mammalian cochlea." Prog Neurobiol 53(3): 331-80.

Ulfendahl, M.et al. (2001). "Structural relationships of the unfixed tectorial membrane." Hear Res 151(1-2): 41-47.

Ulfendahl, M.et al. (1996). "Mechanical response characteristics of the hearing organ in the low- frequency regions of the cochlea." J Neurophysiol 76(6): 3850-62.

Ulfendahl, M.et al. (1996). "Mechanical response characteristics of the hearing organ in the low-frequency regions of the cochlea." J Neurophysiol 76(6): 3850-62.

Ulfendahl, M.et al. (1995). "Shearing motion in the hearing organ measured by confocal laser heterodyne interferometry." Neuroreport 6(8): 1157-60.

van Deelen, G. W. and G. F. Smoorenburg (1986). "Electrocochleography for different electrode positions in guinea pig." Acta Otolaryngol 101(3-4): 207-16.

van Emst, M. G.et al. (1998). "The generation of DC potentials in a computational model of the organ of Corti: effects of voltage-dependent K+ channels in the basolateral membrane of the inner hair cell." Hear Res 115(1-2): 184-96.

von Bekesy, G. (1960). Experiments in Hearing, Robert E. Krieger Publishing Company, New York.

Voss, S. E.et al. (1996). "Is the pressure difference between the oval and round windows the effective acoustic stimulus for the cochlea?" J Acoust Soc Am 100(3): 1602-16.

Weaver, S. P. and L. Schweitzer (1994). "A radial gradient of fibril density in the gerbil tectorial membrane." Hear Res 76(1-2): 1-6.

Weiss, T. F. and D. M. Freeman (1997). "Equilibrium behavior of an isotropic polyelectrolyte gel model of the tectorial membrane: effect of pH." Hear Res 111(1-2): 55-64.

Willemin, J. F.et al. (1988). "Heterodyne interferometer for submicroscopic vibration measurements in the inner ear." J Acoust Soc Am 83(2): 787-95.

Wilson, J. P. and J. R. Johnstone (1975). "Basilar membrane and middle-ear vibration in guinea pig measured by capacitive probe." J Acoust Soc Am 57(3): 705-23.

Wright, A. (1984). "Dimensions of the cochlear stereocilia in man and the guinea pig." Hear Res 13(1): 89-98.

Yates, G. K.et al. (1992). "Mechanical preprocessing in the mammalian cochlea." Trends Neurosci 15(2): 57-61.

Yates, G. K. a. J., B.M. (1979). Measurement of basiliar membrane movement. Auditory Investigation: The Scientific and Technological Basis. H. A. Beagley, Oxford: Clarendon: 418-30.

Zenner, H. P. (1986). "K+-induced motility and depolarization of cochlear hair cells. Direct evidence for a new pathophysiological mechanism in Meniere's disease." Arch Otorhinolaryngol 243(2): 108-11.

Zenner, H. P.et al. (1985). "Reversible contraction of isolated mammalian cochlear hair cells." Hear Res 18(2): 127-33.

Zheng, X. Y.et al. (1997). "Evidence that inner hair cells are the major source of cochlear summating potentials." Hear Res 113(1-2): 76-88.

Zinn, C.et al. (2000). "Evidence for active, nonlinear, negative feedback in the vibration response of the apical region of the in-vivo guinea-pig cochlea." Hear Res 142(1-2): 159-83.

Zwislocki, J. J. (1979). "Tectorial membrane: a possible sharpening effect on the frequency analysis in the cochlea." Acta Otolaryngol 87(3-4): 267-9.

Zwislocki, J. J. (1980). "Theory of cochlear mechanics." Hear Res 2(3-4): 171-82.

Zwislocki, J. J. (1988). "Mechanical properties of the tectorial membrane in situ." Acta Otolaryngol 105(5-6): 450-6.

Zwislocki, J. J. and L. K. Cefaratti (1989). "Tectorial membrane. II: Stiffness measurements in vivo." Hear Res 42(2-3): 211-27.

Zwislocki, J. J. and E. J. Kletsky (1979). "Tectorial membrane: a possible effect on frequency analysis in the cochlea." Science 204(4393): 639-41.

Appendix

Introduction

The original aim of this project also included determining the effects of the tectorial membrane's mass and stiffness in cochlear mechanics. I planned to expose *in vitro* tectorial membrane to various ionic media (e.g. to various concentrations of Ca^{++}), which are known to induce structural changes (e.g. mass/ stiffness/shape changes), as well to antibodies, which are more or less specific to the membrane's constituent proteins. Some of these antibodies are expected to alter the stiffness of the membrane through their ability to cross-link their target proteins; this prediction will be tested using an excised tectorial membrane preparation before it is used in intact cochleae. In order to change the tectorial membrane's mass, as well as its stiffness, the antibodies will be conjugated with gold particles of various sizes. Light (and possibly electron-) microscopy will be used to determine the extent of antibody and/or gold labeling.

In order to investigate the effects of mass and stiffness of TM to the cochlear mechanics, two hybridoma cell lines (17W and 14G) were developed by Dr. Holley's group, which produce IgM class antibodies that bind selectively to the mammalian tectorial membrane. These antibodies were raised against the tectorial membrane of the guinea pigs which supposed could be better for cross-linking and stiffening the TM because they are large, made of 5 immunoglobulin molecules. These antibodies were used to cross-link the tectorial membrane *in vitro*, but limited by *in vivo* measurements.

Methods and Materials

Culture media

1. Preparation of culture media (MEM comes in a bottle)
   - Warm HAT Growth Medium in 37° C water bath for 15 minutes
   - Put DOMA-DRIVE in room temperature for 15 minutes
   - HAT Growth Medium for Hybridomas mix with 10% DOMA-DRIVE

Cell culture

2. Thaw frozen cells: (M17, and 14G)
   - Immerse the frozen cells quickly into the 37° C water bath until it melted.
   - Swab the outside of each vial with 70% ethanol before opening under sterile conditions in a laminar flow hood.
   - Transfer the content of the vial into a 15-ml centrifuge plastic tube with 10 ml pre-warmed, pre-prepared MEM
   - Suck up for several times to make it into suspension
3. Centrifuge the cells at about 1000g for 3 minutes at room temperature. Discard the supernatant. This wash will get rid off the freezing media.
4. Re-suspend the cell pellet into 5 ml MEM, suck up-and-down for several times so that the cells distribute evenly.
5. Transfer into a 24-well culture plates with the concentration of each well diluted half in turn.

. First well	the original suspension	
. Second well	1 ml original suspension	+ 1 ml MEM
. Third well	1 ml second suspension	+ 1 ml MEM
. Nth well	1 ml (N-1) suspension	+ 1 ml MEM

6. Incubate at 37° C for 2 days until cells are 80% confluent.
7. Refresh the medium when the suspension color changes from orange to yellow
8. Immunisation and Screening, if the tectorial membrane is labeled, then
9. Colony cells
   - Counting Cells
     - ➢ Suck up-and-down for several times for the selected cell well
     - ➢ Transfer them to a 15-ml plastic tube
     - ➢ Sample 10 µl to the counting plate and count cells by averaging 6 subunit numbers (cells/ml)
   - Dilute the cells until reach 1 cell/ml, 10 cells/ml and 100 cells/ml in 10 ml MEM
   - Transfer to 96-well plates for the three different concentration, respectively, 100 µl /well, incubate in 37° C for 3 days
   - Put the rests into three 25 cm^2 vented cap flasks, incubate in 37° C for 3 days
10. Immunisation and Screening, if the tectorial membrane is labeled, then
11. Collect supernatant
    - Transfer the supernatant from each flask to a 50 ml centrifuge tube when the suspension color changes from orange to yellow
    - Centrifuge the cells at about 1000g for 3 minutes at room temperature
    - Transfer supernatant to a new tube
    - Add 1:100 NaN_3 (for *in vitro* experiment)
    - Keep the supernatant in 4°C or -20°C fridge for future use.
12. Freeze cells
    - Prepare the freezing media in a cryo-tube. Label the tube with the cell line name, passage number and date (Freezing medium: FCS + 10% DMSO)
    - Shake the chosen 25 cm^2 vented cap flasks on the desk so that the cells detached the surface of the flask
    - Transfer the suspension to a sterile 50 ml centrifuge tube
    - Centrifuge the cells at about 1000g for 3 minutes at room temperature

- Remove the supernatant to the original flask
- Re-suspend the cells in 4 ml freezing medium and pipet up-and-down many times
- Divided 4 ml suspension into two 2-ml pre-prepared cryo-tube
- The optical freezing rates is 1C/min. Place the vial of cells in a freezing container and place it overnight at -80°C fridge, and then transfer to liquid nitrogen tank (-196°C)

Media and plastics

HAT Growth Medium for Hybridomas	ISL
Doma Drive :	ISL
FCS: Foetal Calf Serum:	Gibco BRL
DMSO: Dimethyl Sulphoxide	Sigma
MEM Alpha Media	Gibcobrl
NaN_3: Sodium azide	BDH

Molecular weight 65.01, made from 0.5 g power NaN_3 diluted into 50 ml sterile water, keep in 4°C or -20°C freezer, for a long time keeping

25 cm^2 vented cap flasks	Falcon
24-well culture plates	Falcon
96 wells tissue culture dish	Falcon
15 ml plastic centrifuge tube	Falcon
50 ml plastic centrifuge tube	Falcon
cryo-tube	Simport

Dissection of the Organ of Corti

Adult guinea pigs (300 – 350 g) were killed by cervical dislocation and their temporal bones were removed. The bullae were opened in MEM saline, the cochlea spirals removed and the organs of Corti isolated from the basilar membrane by microdissection. The organs of Corti were removed into another container with MEM Alpha Medium or PBS and sucked up-and down for a few times to dissociate the tissue. One drop of the resultant suspension was placed into each well of gelatin-coated multiwell slides, and allowed to dry.

Immunisation and Screening

(1). Place a drop of cold acetone into each well and left for approximate 30 seconds to precipitate out the protein. Leave it dry in air for 5 minutes. (Acetone kept in freezer part of fridge.)
(2). Draw a circle round every well with a DAKO pen lightly (also kept in fridge), this is to avoid the samples and medium cross contaminating.
(3). Rehydrate with MEM saline -- one drop on each well.
(4). Place slides in box with damp tissue underneath to ensure slides do not dry out.

(5). Remove MEM saline from each well in turn replacing with 1st antibody samples. Avoid touching the bottom of wells.
(6). Then left the samples in fridge (4° C) overnight.
(7). Remove samples from wells, wash wells with MEM saline three times.
(8). Remove MEM saline and replace with 2nd antibody Antimouse IgM FITC & TRITC conjugates 4μl in 1 ml MEM saline.
(9). Place samples in dark at room temperature for approximately 2.5hours.
(10). Rinse well with MEM saline three times.
(11). Remove all MEM saline and replace with one drop of Vectorshield (mounting medium for fluorescence) in each well and cover carefully with a large cover slip. Avoid trapping bubbles.
(12). Ready for examination on microscope.

MEM saline:

Alpha medium: GIBCOBRI
PBS: Phosphate Buffered Saline OXOID
Dissolve 1 tablet in 100 ml distilled water and autoclave at 115°C for 10 minutes, PH = 7.3 (approx.) (for in vitro diagnostic use)
Anti-mouse lgM: SIGMA
(μ-chain specific), FITC conjugate, antibody developed in goat
normally 4 μl lgM diluted in 1 ml MEM saline
Vectashield: VECTOR
H-1000, (Mounting medium for fluorescence), stored at 4°C
Vector Laboratories, Inc.
DAKO pen: DAKO
Aceton: BDH

Results and discussion

Supernatents from the two hybridoma cell lines (17W and 14G) were screened on guinea pig tectorial membrane preparation as described in the method. The antibodies were visualised with goat-anti-mouse immunoglobulins conjugated with fluorescein isothiocyanate (FITC). The fibrous layer of tectorial membrane has been clearly stained and shown in Fig. 1. The limbal, middle and marginal zones can be easily distinguished from the staining. Most of the fibres of tectorial membrane radiate outwards from the inner zone, but a few longitudinal fibres are also seen. It appears that the fibres density is higher in the limbal zone.

The necessary timing of the primary antibody staining on the TM was studied. It shows that, for clear and stable staining, at least half an hour was needed for these *in vitro* preparations, whose proteins has been nicely fixed. However, it raises some difficulties to

use these antibodies to affect the TM's physical properties *in vivo*. The uncertainty is no matter how to introduce the antibody into the scala media, the circulation of perilymph and endolymph is always diluting the concentration of the induced antibody. In the same time, not only the mixture of perilymph and endolymph has altered the ionic environment of the TM, but also the suspension, which carries the antibody. Due to TM is extremely sensitive to its ionic environment and the cochlear condition changing with time, it is difficult to find

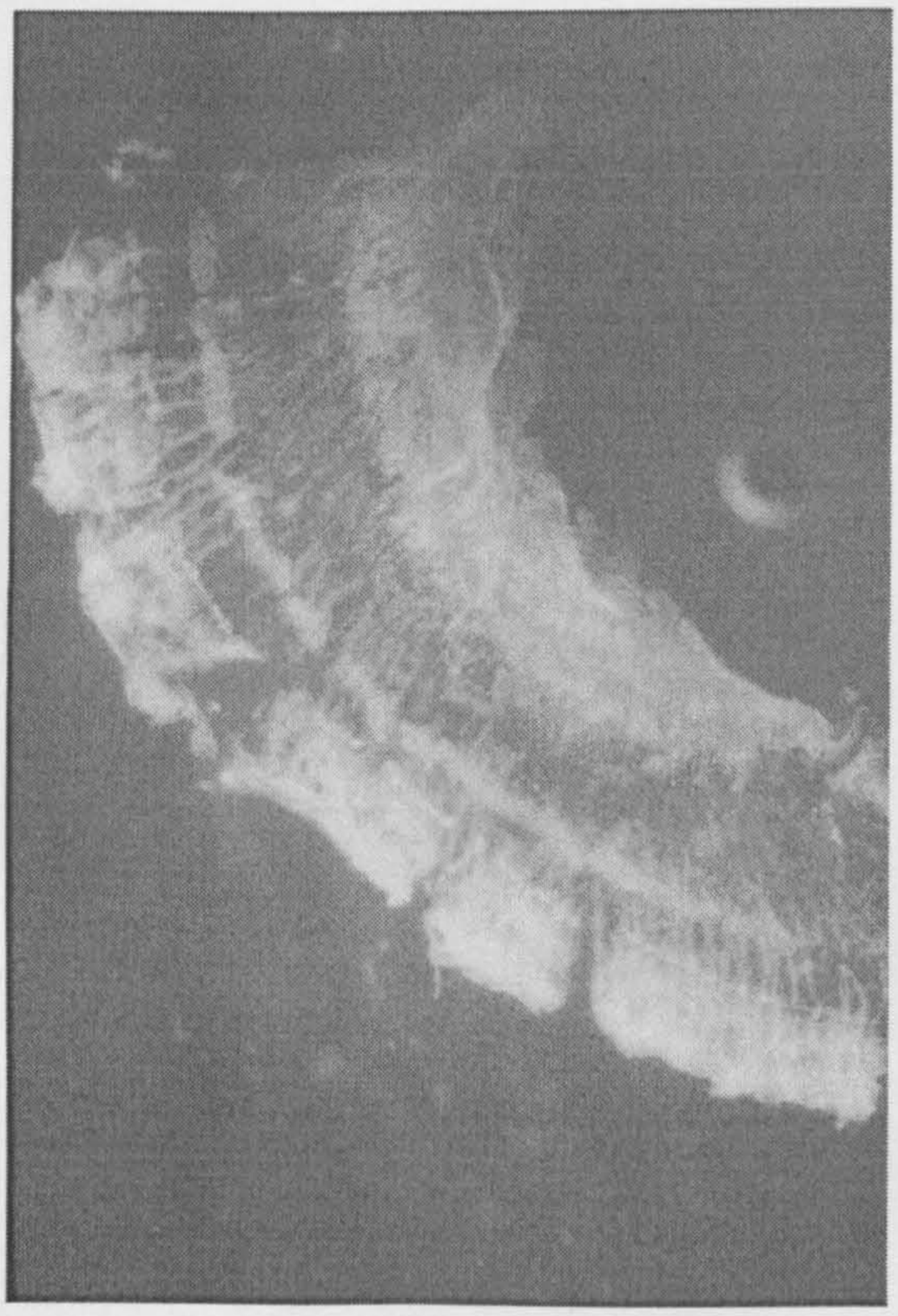

Figure a Tectorial membrane of guinea-pig.

the major factor responsible for altering the TM's physical properties and as a direct result, the mechanical responses to sound stimuli has been changed.

Another difficulty is that it is difficult to maintain the cochlear condition in good condition in present technique for going though all the procedures concerning all the factors involved in varying the mechanical responses to sound stimuli of TM in one animal.

As a conclusion the selective antibodies has been raised and successfully stained on the tectorial membrane of *in vitro* preparations. It has been found difficult to perform on *in vivo* preparations under present technique. It could be done with an improved technique in the near future.